TTI: 0-6715

Texas A&M Transportation Institute

Interaction between Drilled Shaft and Mechanically Stabilized Earth (MSE) Wall: Technical Report

Technical Report 0-6715-1

Cooperative Research Program

TEXAS A&M TRANSPORTATION INSTITUTE
COLLEGE STATION, TEXAS

in cooperation with the
Federal Highway Administration and the
Texas Department of Transportation
http://tti.tamu.edu/documents/0-6715-1.pdf

Technical Report Documentation Page

1. Report No.	2. Government Accession No.	3. Recipient's Catalog No.
FHWA/TX-15/0-6715-1		

4. Title and Subtitle	5. Report Date
INTERACTION BETWEEN DRILLED SHAFT AND MECHANICALLY STABILIZED EARTH (MSE) WALL: TECHNICAL REPORT	Published: April 2017
	6. Performing Organization Code
7. Author(s)	8. Performing Organization Report No.
Jean-Louis Briaud, Marcelo Sanchez, Mohammad Aghahadi, Gang Bi, Jie Huang	Report 0-6715-1
9. Performing Organization Name and Address	10. Work Unit No. (TRAIS)
Texas A&M Transportation Institute College Station, Texas 77843-3135	
	11. Contract or Grant No.
	Project 0-6715
12. Sponsoring Agency Name and Address	13. Type of Report and Period Covered
Texas Department of Transportation Research and Technology Implementation Office 125 E. 11th Street Austin, Texas 78701-2483	Technical Report: September 2012–August 2015
	14. Sponsoring Agency Code

15. Supplementary Notes

Project performed in cooperation with the Texas Department of Transportation and the Federal Highway Administration.

Project Title: Interaction between Drilled Shaft and Mechanically Stabilized Earth (MSE) Wall

URL: http://tti.tamu.edu/documents/0-6715-1.pdf

16. Abstract

Drilled shafts are being constructed within the reinforced zone of mechanically stabilized earth (MSE) walls especially in the case of overpass bridges where the drilled shafts carry the bridge deck or traffic signs. The interaction between the drilled shaft and the MSE wall is not well known and not typically incorporated into the design. As part of the research project, a full-scale test was conducted in 2012 at Texas A&M University.

The test was performed on an MSE wall where the backfill material was clean sand and the soil reinforcement was made of metal strips. Also two real projects were instrumented during construction, and data were gathered for one year. A numerical model was used and calibrated against the results of the three full-scale cases. Then a sensitivity analysis was performed and 64 numerical cases were modeled to understand the effect of different parameters on the interaction between the MSE wall and the drilled shaft. The data from the simulations, the full-scale test results, and the monitoring of the real site were processed, and a modification of the current guidelines was proposed for the case where there is a drilled shaft subjected to a horizontal load in the reinforced zone of the MSE wall. A design chart is presented to take into account the additional pressure on the wall created by the drilled shaft.

17. Key Words	18. Distribution Statement
Drilled Shaft, MSE Wall, Interaction, Full-Scale Test, Numerical Modeling	No restrictions. This document is available to the public through NTIS: National Technical Information Service Alexandria, Virginia http://www.ntis.gov

19. Security Classif.(of this report)	20. Security Classif.(of this page)	21. No. of Pages	22. Price
Unclassified	Unclassified	200	

Form DOT F 1700.7 (8-72) Reproduction of completed page authorized

INTERACTION BETWEEN DRILLED SHAFT AND MECHANICALLY STABILIZED EARTH (MSE) WALL: TECHNICAL REPORT

by

Jean-Louis Briaud
Research Engineer
Texas A&M Transportation Institute

Marcelo Sanchez
Research Engineer
Texas A&M Transportation Institute

Mohammad Aghahadi
Graduate Student
Texas A&M Transportation institute

Gang Bi
Graduate Student
Texas A&M Transportation Institute

Jie Huang
Research Engineer
University of Texas – San Antonio

Report 0-6715-1
Project 0-6715
Project Title: Interaction between Drilled Shaft and Mechanically Stabilized Earth (MSE) Wall

Performed in cooperation with the
Texas Department of Transportation
and the
Federal Highway Administration

Published: April 2017

TEXAS A&M TRANSPORTATION INSTITUTE
College Station, Texas 77843-3135

DISCLAIMER

This research was performed in cooperation with the Texas Department of Transportation (TxDOT) and the Federal Highway Administration (FHWA). The contents of this report reflect the views of the authors, who are responsible for the facts and the accuracy of the data presented herein. The contents do not necessarily reflect the official view or policies of the FHWA or TxDOT. This report does not constitute a standard, specification, or regulation. The engineer in charge of this part of the project was Dr. Jean-Louis Briaud, P.E. (Texas, #48690).

ACKNOWLEDGMENTS

This project was conducted in cooperation with TxDOT and FHWA. The director of the project was Kevin Pete. Other members of the project monitoring committee from TxDOT were Dina Dewane, John Delphia, Bryan Esmaili-Doki, Marcus Galvan, Taya Retterer, and Sean Yoon. The authors thank them for their support during this project. The authors are also grateful to Mojdeh Pajouh and Kelsey McCoy for their help in proofreading the manuscript.

TABLE OF CONTENTS

Page

LIST OF FIGURES

Page

LIST OF TABLES

Page

CHAPTER 1:
INTRODUCTION

BACKGROUND

Mechanically stabilized earth (MSE) walls have been widely used since 1970. They consist of four main parts: 1) wall panels, 2) soil reinforcements, 3) backfill material, and 4) natural soil. The working mechanism of this kind of wall is to dissipate the pressure that would otherwise exist on the wall to the soil reinforcements. The reinforcement transfers this pressure to the surrounding soil by friction.

The wall panels are usually standard concrete panels, about 5 ft by 5 ft. The soil reinforcement may have different geometries and can be made up of different materials. The more common reinforcement is metal strips, metal grids, geogrids, and geosynthetics. The backfill material is usually granular materials such as clean sand or crushed rock. Fine backfill materials are typically not used. MSE walls can be built on different natural soils. The obvious limitation is that the natural soils must be able to carry the weight of the wall while keeping the settlement within an acceptable range.

In some projects, a drilled shaft may have to be placed within the MSE wall. If the drilled shaft is in the reinforced zone of the wall, it interacts with the wall. This can potentially cause some problems for the wall. The drilled shafts that are used in this kind of project are usually horizontally loaded, resulting in additional pressure on the wall panels.

MOTIVATION

Some previous research has been conducted to quantify the effect of a horizontally loaded drilled shaft on an MSE wall, but the existing research was focused on MSE walls reinforced with geogrids and geosynthetics. To the researchers' knowledge, in MSE walls with metallic reinforcement, no test has been performed and no design method has been proposed for drilled shafts. The first goal of this research is to understand the interaction between horizontally loaded drilled shafts and MSE walls with metallic strips and/or grids as soil reinforcements. A second goal is to propose guidelines for designing the MSE wall reinforcement when a horizontally loaded drilled shaft is in the reinforced zone. The third goal is to study the behavior

of metal strips and their performance as soil reinforcements, including the impact of an increase in the number of ribs per foot of strip.

OBJECTIVES

The main objectives of this research are to:

- Study the effect of horizontally loaded drilled shafts on the pressure distribution, on the wall panels, and on the load in the reinforcement.
- Understand the effect of the MSE wall on the horizontal capacity and the deformation of the drilled shaft.
- Explore the effect of different parameters of the MSE wall and the drilled shaft (e.g., wall and shaft geometries, distance between wall and shaft, and soil parameters) on the pressure distribution on the panels, on the load in the reinforcement, and on the capacity of the drilled shaft.
- Propose guidelines for designing the reinforcement of an MSE wall with horizontally loaded drilled shafts in the reinforced zone based on the geometry and soil parameters of the project.
- Study the friction mechanism of metal strips in the MSE wall and investigate the effect of the strip bumps (e.g., number, shape, and arrangement) on the strip soil friction factor.

ACTIVITIES

To achieve the objectives stated above, a number of tasks were performed:

- Study the state of the art in this field, including typical problems occurring in real projects because of bad designs associated with the lack of information on MSE walls with horizontally loaded drilled shafts in the reinforced zone.
- Carry out a full-scale loading test at the Texas A&M University (TAMU) Riverside Campus. Design and construct the wall and the drilled shaft. Design and install the instrumentation necessary to gather data required for this research.
- Monitor two real Texas Department of Transportation (TxDOT) projects to study the behavior of two MSE walls under real conditions and at actual scale. Instrumentation was also designed and installed for both projects.

- Perform laboratory tests (triaxial tests) on the backfill material and in-situ tests (pressuremeter tests [PMTs] and pocket penetrometer tests) on the backfill material and the natural soil to obtain soil properties useful in numerical modeling.
- Calibrate the 3D numerical model against the full scale measured data.
- Model the TxDOT projects being monitored.
- Perform sensitivity analyses to study the effect of different factors (e.g., wall and shaft geometries, distance between wall and shaft) on the performance of the MSE wall with the explicit aim of preparing design guidelines.
- Process the data from the sites and from the numerical modeling to propose design guidelines.

ACCOMPLISHMENTS

The accomplishments of this study include:

- The full-scale load test at the TAMU Riverside Campus was performed successfully. The pressure on the wall panel, the displacement of the drilled shaft and of the wall, and the load in the soil reinforcements were collected.
- Two real projects in Bastrop and Salado, Texas, were instrumented and monitored. The Bastrop project was monitored for 18 months and the Salado project for 5 months.
- Constitutive models for the soil and the strips were calibrated using independent small-scale tests. These models were used in the 3D simulations.
- Laboratory and in-situ tests were performed on the backfill materials and on the natural soils. The parameters obtained from these tests were used in the numerical modeling.
- 3D numerical models of the full-scale test and the real projects were developed and calibrated. The validation of the numerical models was very satisfactory, as the simulation outputs and experimental results showed very good agreement. This indicates that the models selected for the soil, fill, wall, and strips (alongside the associated constitutive laws) are appropriate to study this problem.
- A total of 64 MSE wall simulations models were prepared to investigate how different wall geometries, shaft geometries, and soil parameters affect the performance of the MSE wall-shaft system.

- Actual strips were modeled in 3D. Both the shape of the bumps and their quantity per unit length were studied to see their effects on the friction factor. A graph summarizing the influence of the number of bumps and the bump geometry versus friction factor was developed in this report.
- Data from numerical models were processed to study the effect of each parameter on the pressure distribution on the panels.
- A new design method was proposed for designing MSE walls with horizontally loaded drilled shafts placed inside the MSE wall.

REPORT ORGANIZATION

This report is composed of seven chapters. Chapter 1 is an introduction to the research performed. Chapter 2 focuses on the literature review and previous work in this field. The instrumentation used in those studies and their main results are discussed.

Chapter 3 covers the design of the instrumentation for the full-scale test at the TAMU Riverside Campus and for the real TxDOT projects. The measurements to be made and the different devices available to measure these parameters are also discussed in this chapter. Chapter 4 presents the full-scale test and monitoring of the real projects. Instrumentation, construction, and monitoring results are discussed in this chapter.

Chapter 5 is related to the numerical study. This chapter discusses 3D models of the TAMU loading test and of the two real projects. Comparison between the results from the numerical models and the TAMU full-scale test is presented in this chapter. The numerical model of the pullout tests for obtaining the strip parameters to be used in the MSE wall model is also shown in Chapter 5. The last part of this chapter is related to the parametric study.

Data processing and the proposed design method are the main components of Chapter 6. The current design method for MSE walls according to American Association of State Highway and Transportation Officials (AASHTO) (2010) are presented in this chapter. Based on the results from the loading tests, monitoring, and numerical study, a new design guideline is proposed for the case where a drilled shaft is horizontally loaded in the MSE wall. Chapter 7 compiles the main conclusions of this report and suggestions for possible future research in this area.

CHAPTER 2:
LITERATURE REVIEW

INTRODUCTION

This research is aimed at gaining a better understanding of the interaction between MSE walls and drilled shafts placed in the body of the MSE wall. MSE walls have been used widely since 1970 because of their low cost and easy construction (Koerner and Soong, 2001). Each year around 9,000,000 ft^2 of MSE wall are constructed in Texas (Berg et al., 2009). In Texas, they have become the dominant retaining wall type, accounting for more than 80 percent of the TxDOT retaining walls based on statistical data collected between August 1, 2006, and June 20, 2007 (Figure 1) (Chen et al., 2007). The data also show that MSE walls are among the least expensive retaining wall types with a unit cost (i.e., cost per unit front area) equal to one half of the drilled shaft and soil nails walls and only one third of the tie-back walls (Chen et al., 2007).

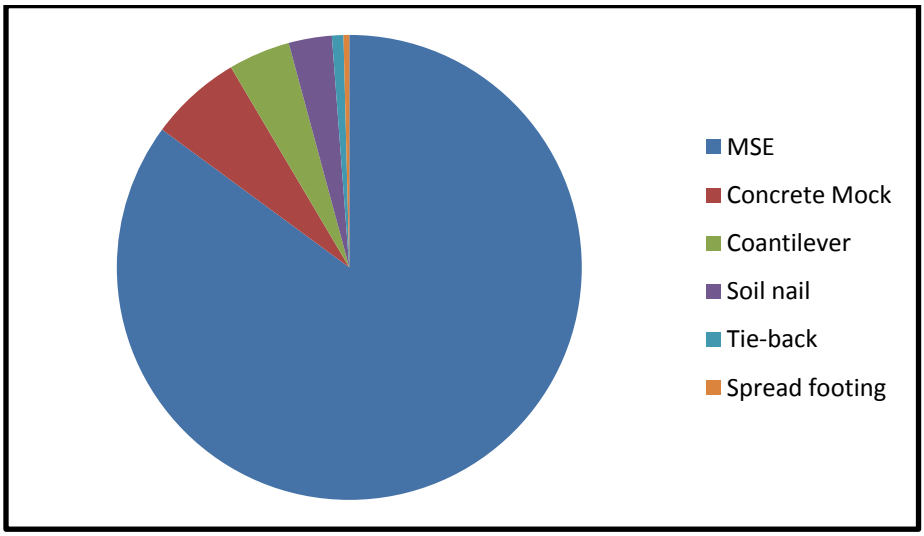

Figure 1. Retaining Walls Used by TxDOT from August 1, 2006, through June 20, 2007 (Modified from [Chen et al., 2007]).

Drilled shafts have been constructed in MSE walls within the reinforced zone. They are designed to carry both lateral and vertical loads. They are usually constructed, among other cases, in overpass bridges and to support traffic signs. The lateral loads applied to these structures are due to traffic load (e.g., vehicles braking), wind loads, and deck movement in bridges. In most cases, the interaction between MSE walls and drilled shafts is not considered since they are usually too far away from the front of the wall to have any influence on each other.

However, on occasion, drilled shafts and MSE walls are relatively close and their interactions have to be considered.

The U.S. highway system has been experiencing major maintenance across the nation in recent years. According to the Federal Highway Administration (FHWA) data (Christopher et al., 1990), a large percentage of the maintenance and reconstruction budget went to roadway widening. Due to right-of-way issues, the drilled shafts are more and more frequently constructed within the footprint of the MSE walls (Figure 2). A good example is that during roadway widening the drilled shafts often have to invade into the reinforced zone of an MSE wall to support bridge abutments. The interaction between the drilled shafts and the MSE wall is inevitable and has to be addressed appropriately in the design and construction.

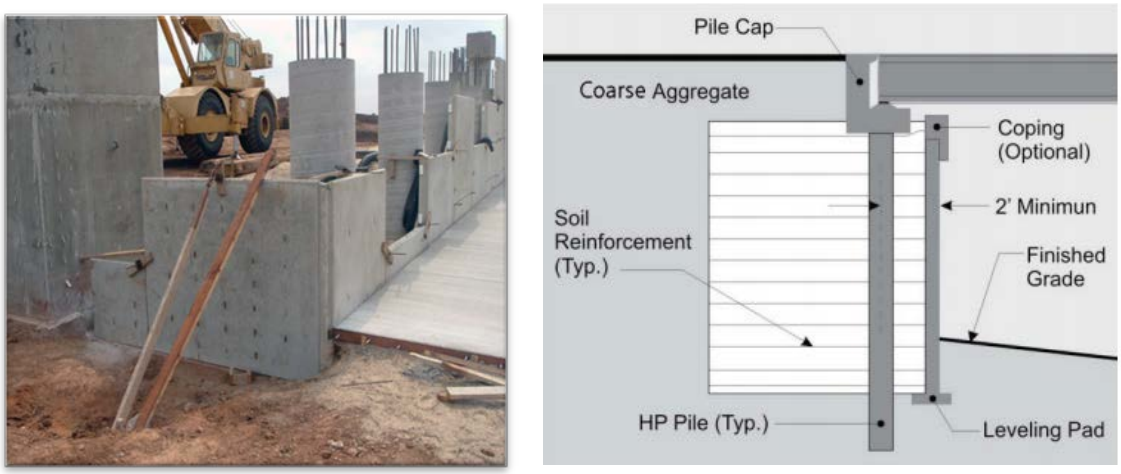

(a) **(b)**

Figure 2. Drilled Shafts within MSE Wall: (a) Construction of Drilled Shaft behind MSE Wall, and (b) Drilled Shafts behind MSE Wall Supporting Bridge Abutment (after Anderson and Brabant, 2005).

CURRENT PRACTICE

As mentioned in the previous section, the common practice is to design the MSE wall and the drilled shaft separately without considering any interaction between them (Huang et al., 2013). Bearing in mind that the reinforced wall and backfill material are not considered when designing the drilled shaft, it is possible to anticipate that shafts are generally over-designed (Pierson, 2008).

A good understanding of the interaction between drilled shafts and MSE walls will allow an optimal design of these two geotechnical structures and may also prevent possible global and

local failures of the MSE wall. This research has been done after observing serious damage of wall panels located within the vicinity of drilled shafts in a number of projects in Texas. Previous studies in this area reported in the literature include both experimental and numerical investigations. Some recent studies have focused on numerical modeling of the MSE wall with different types of reinforcements (Abdelouhab et al., 2011), 2D and 3D modeling of reinforced embankments (Bergado and Teerawattanasuk, 2008), modeling of pullout test on soil nail (Zhou et al., 2011), lateral loads induced by temperature change in the shaft and how these loads are transferred from the shaft to the MSE wall (Arenas, 2010), and modeling of MSE walls (Gerber and Cummins, 2009; Suksiripattanapong et al., 2012; Tanchaisawat et al., 2008).

Other studies have concentrated on the behavior of metal strips, including load prediction in the strips (Bathurst et al., 2009; Miyata and Bathurst, 2012), pullout test on steel grid reinforcements (Bergado et al., 1992), effect of reinforcement on the soil behavior (Jewell, 1980), pullout test on metal strips (Johnson, 2013), effect of reinforcement on horizontal displacement of MSE wall (Kibria et al., 2014), and pullout resistance factor for MSE wall reinforcement (Lawson et al., 2013).

Other studies were found on the effect of backfill on wall movements (Hossain et al., 2011), the design and performance of a tall MSE wall (Stuedlein et al., 2010), the analysis of soil-pile interaction in abutment (Khodair and Hassiotis, 2005), the bearing capacity of MSE walls (Leshchinsky et al., 2012), the proposal of a procedure for estimating active earth pressures on the wall (Ahmadabadi and Ghanbari, 2009), and the study of the effect of pile driving in the reinforced zone of MSE walls (Berg and Vulova, 2007).

In previous investigations looking at the interaction between drilled shafts and MSE walls, the reinforcement used in the tests was geogrid and/or geosynthetics. For example, a full-scaled test on an MSE wall with geogrid sheets was performed by the Kansas Department of Transportation (KDOT) (Pierson et al., 2009). The instrumentation and monitoring of MSE walls have been a crucial component of previous studies in this field (e.g., Stuedlein et al., 2010 and Kibria et al., 2014). In previous studies, the analyses of the field tests were generally supported by numerical simulations (Hatami and Bathurst, 2005; Huang et al., 2011; Huang et al., 2013). However, after an exhaustive review of the open literature, no studies were found that related the interaction between drilled shafts and MSE walls with metal strips.

A novel contribution of this report will be the study of the interaction between drilled shafts and MSE walls involving metallic strips. This is not a problem that is very well known, but it needs to be addressed in order to provide precise guidelines for a safe and economical design of MSE walls involving drilled shafts. To better understand the interaction between MSE walls and drilled shafts, this research combines experimental and numerical studies. The experimental investigation includes the study of different laboratory and in-situ tests, a large-scale field loading test of an MSE wall subjected to increasing horizontal loads on a drilled shaft placed inside the MSE wall mass until failure, and the monitoring of two actual MSE walls with embedded drilled shafts. The modeling activities include the numerical analyses of different components of the problem, such as the simulation of the in-situ tests, laboratory pullout tests, and a series of numerical analyses associated with the modification of the guidelines. Reinforcement with metal strips provides tensile strength to the soil mass. The presence of strips improves the overall mechanical properties of the soil (Abdelouhab et al., 2011). For the internal stability analysis, the common method is based on the verification of the strip tensile force and adherence or bond capacity at the soil-strip interface (AASHTO 2010). The study reported herein benefited from the pullout tests on metal strips performed at Texas Tech University (Lawson et al., 2013). Those tests have been used to calibrate the FLAC-3D cable model adopted in the numerical analysis to simulate the strips.

The major reason for neglecting the influence of the MSE wall on the horizontal and vertical capacity of the drilled shaft is that it is likely a conservative approach. However, the MSE wall design does not account for the additional lateral pressure induced by the drilled shaft. Consequently, drilled shafts are always over-designed with unduly embedment depth (Figure 3), and the MSE walls are often under-designed (Pierson, 2008). Figure 3 presents some of the failure modes that have been observed in real constructed structures. The other failure modes have been observed in research projects when the drilled shaft was loaded to extreme situations.

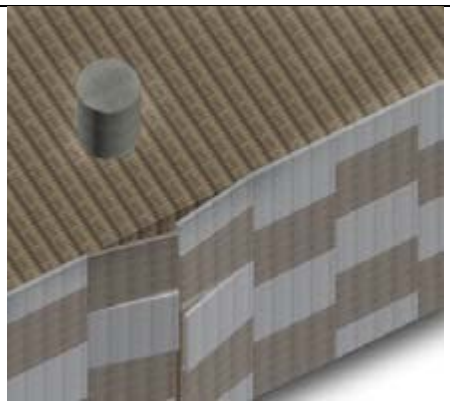

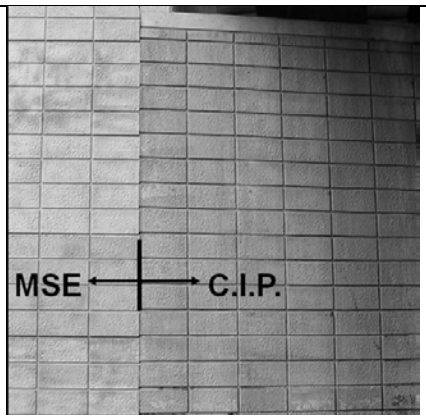

Dislocation or pop out of panel finish
(photo: modified from Berg et al., 2009)

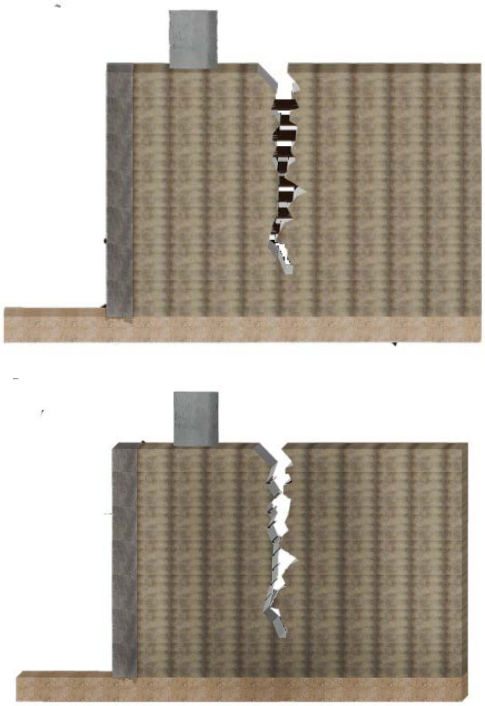

Rupture/pullout of the reinforcement
(photo: courtesy of J. Han and R. L. Parsons)

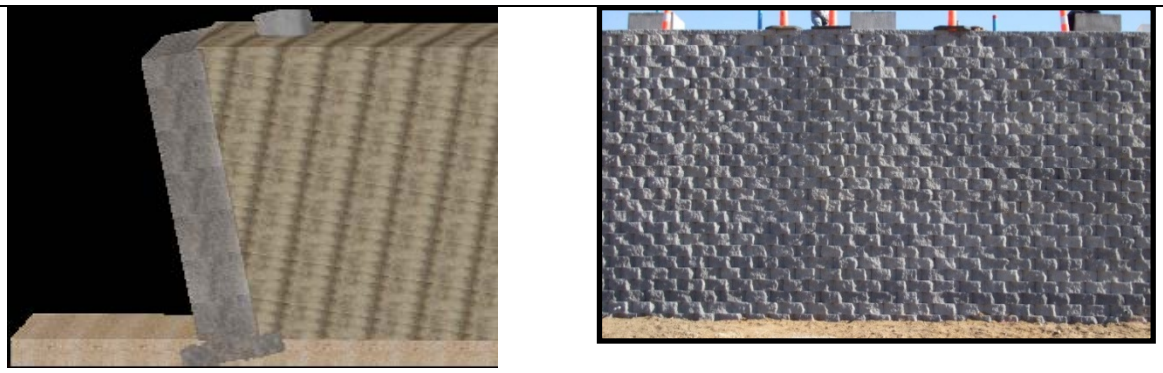

Excessive MSE wall deflection
(photo: courtesy of J. Han and R. L. Parsons)

Figure 3. Failure Modes of MSE Wall.

The design guidelines of AASHTO (2010) and FHWA (Berg et al., 2009) do not address the drilled shafts and MSE wall interaction. The FHWA manual suggests a conceptual lateral earth pressure diagram induced by laterally loaded drilled shaft (Figure 4). The conceptual earth pressure distribution is essentially a trapezoidal/triangular distribution. However, because of the lack of experimental data and evidence that can support this design, the manual does not provide details on how to determine the magnitude of the lateral earth pressure distribution.

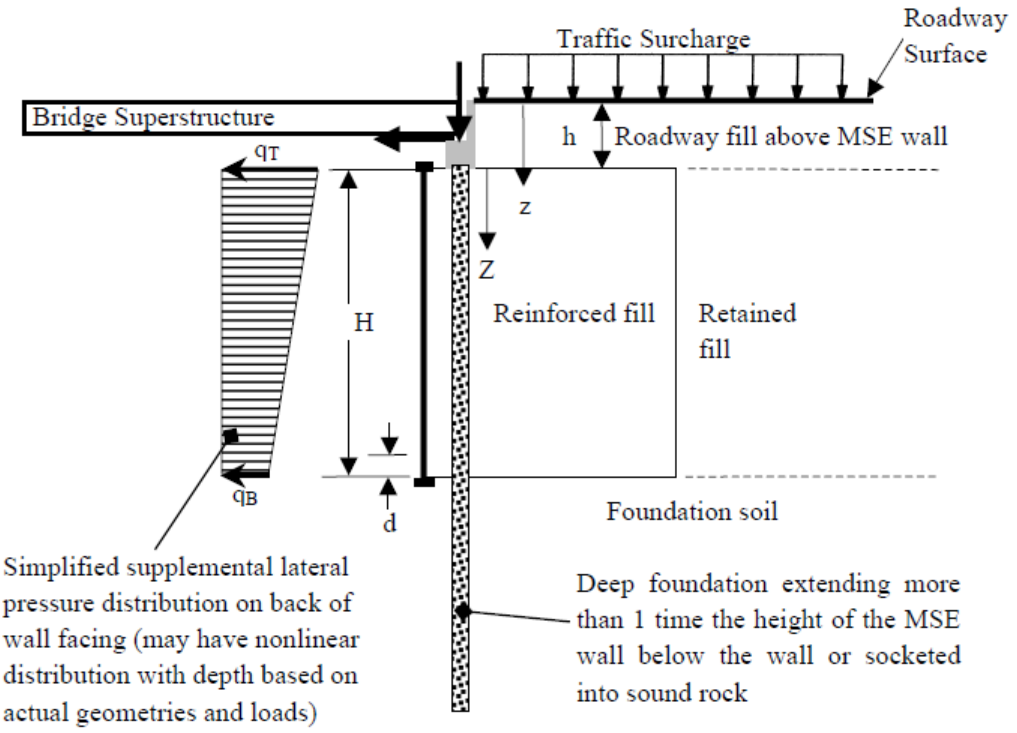

Figure 4. Lateral Earth Pressure Induced by Laterally Loaded Drilled Shaft (Berg et al., 2009).

Besides the interaction between drilled shafts and MSE walls, the drilled shafts can act as an obstruction for the placement of the MSE wall reinforcement (Figure 5[a]). In this case, the reinforcement has to be interrupted, laterally shifted, or skewed (Figure 5[b]). The presence of the drilled shafts also affects proper compaction, particularly if the space between the drilled shafts and MSE wall facing is limited. These problems associated with the presence of the drilled shafts close to the MSE wall could trigger some of the observed distresses.

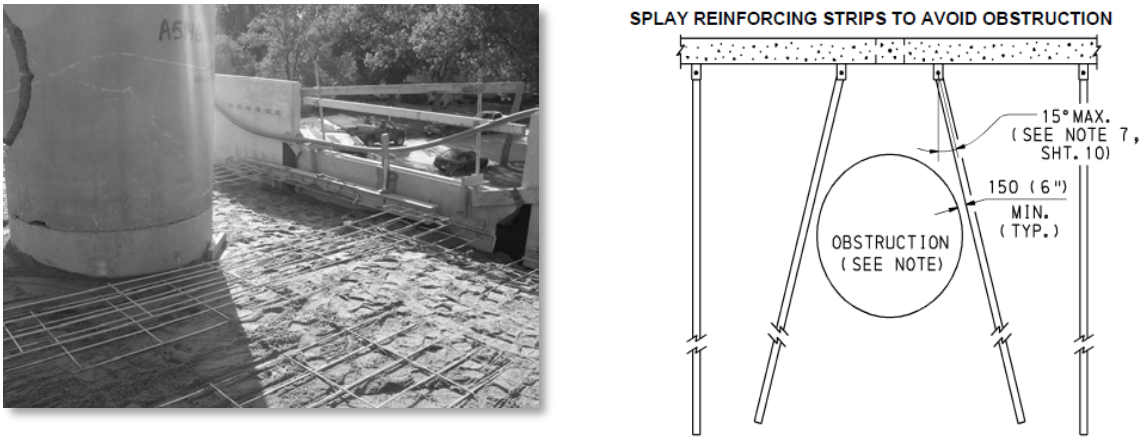

(a) **(b)**

Figure 5. Conflict of Shafts and Reinforcement: (a) Construction Obstruction; (b) Rearrangement of Reinforcement (Berg et al., 2009).

The MSE wall could load the drilled shaft; this load can be the result of small movements of the MSE wall backfill, sliding and overturning of MSE wall, reinforcement relaxation, and seismic effects. However, distress of drilled shafts due to the imposed load from the MSE wall has yet to be reported, and no research related to this problem has been published.

CURRENT RESEARCH STATUS

To properly address the interaction between drilled shafts/piles and MSE walls, KDOT and the Utah Department of Transportation (UDOT) have sponsored independent research programs (Pierson et al., 2009, Rollins et al., 2013). These are the only published research projects on this topic. Figure 6 presents a summary of the KDOT and UDOT research projects.

KDOT Research

Objectives:

To investigate the MSE wall resistance to the lateral load on a drilled shaft, assess the possibility of using the resistance to shorten the required drilled shaft length in the design, and develop general design guideline.

MSE wall type:

A 20' high and 140' long geogrid reinforced modular block wall

Deep foundation type:

Multiple drilled shafts of 36" in diameter

Research outline:

The research included full-scale testing and numerical modeling. The full-scale test recorded the load-deflection of multiple drilled shafts, which were of different length and located at different distances from the front of the MSE wall. The numerical modeling investigated the effects of different factors on the capacity of the shafts.

Outcomes:

- Ultimate capacity of multiple drilled shafts.
- Service limit considering different allowable deflection.
- The minimum spacing to avoid group effect.
- The effect of different factors (i.e., backfill material, reinforcement, and MSE wall facing unit) on capacity.

UDOT Research

Objectives:

To investigate the passive resistance of the backfill soil if a pile cap is loaded laterally and parallel to the length of the MSE wall. This loading condition would tend to occur during a seismic event.

MSE wall type:

Precast panel with metallic grids reinforcement

Deep foundation type:

Driven piles with a cap

Research outline:

The pile cap was loaded laterally and parallel to the length of the wall under static, cyclic, and dynamic loading conditions. The deflection and applied loads were monitored.

Outcomes:

- Passive force-deflection curves.
- Assessments of current methods used to develop the passive force-deflection curve.
- The performance of the MSE wall under such conditions.

Figure 6. Studies on the Interaction between MSE Walls and Drilled Shafts.

RESEARCH OUTCOMES OF KDOT AND UDOT RESEARCH

KDOT Research

A 20-ft high and 140-ft long MSE test wall was built inside the southwest clover of the IH-435/Leavenworth road interchange in Kansas (Pierson, 2008). The MSE wall was a geogrid reinforced modular block wall. Multiple drilled shafts of a 36 in. diameter were built behind the MSE wall. The 120 ft long MSE wall was divided into 6 test sections plus two wing wall sections at the ends (Figure 7). Among 6 test sections, one test section was 45-ft in width, which was designed to test a group of three shafts situated 72 in. from the MSE wall facing to investigate the group effect. Each of the remaining five sections had one drilled shaft constructed behind it. The drilled shaft was situated 36 in., 72 in., 72 in., 108 in., and 144 in. away from the MSE wall facing. One of two shafts situated 72 in. from the MSE wall facing was shorter than the rest, with only 15-ft embedment depth into the MSE wall backfill, and the rest were fully embedded (20 ft) into the MSE wall backfill. Each section was tested separately. Slip joints were installed between the adjacent test sections to minimize the influence between them. The MSE wall facing and the drilled shafts were extensively instrumented with slope inclinometers, linear variable differential transducers (LVDTs), tell tales, earth pressure cells, strain gauges, photogrammetry targets to monitor the deflections of the drilled shafts and the MSE wall facing, sensors to measure the increases in lateral earth pressure, and geogrid strains (Pierson et al., 2010).

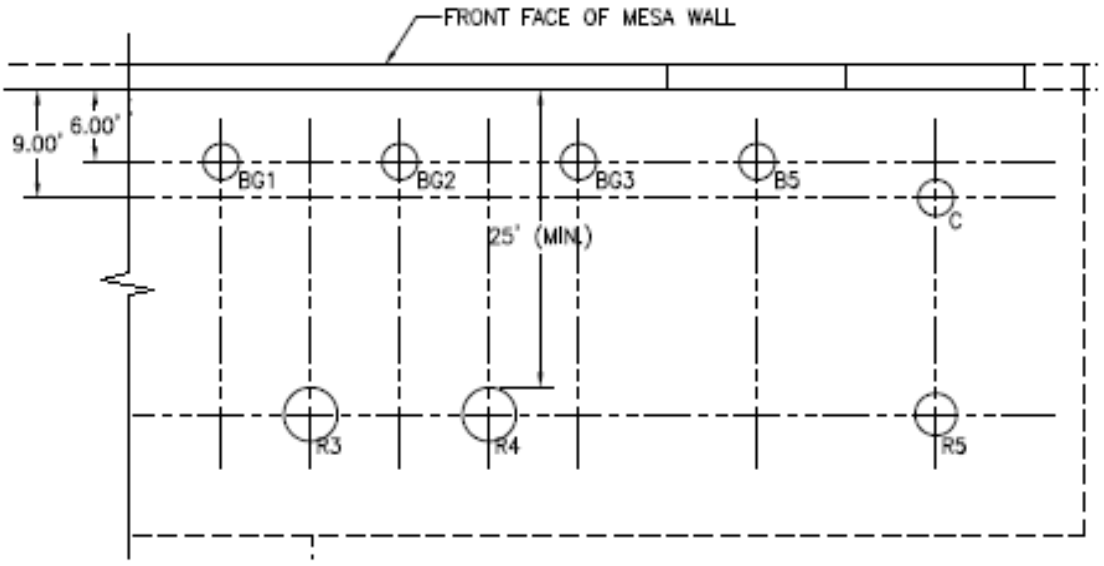

Figure 7. Plan View of MSE Test Wall and Shafts (Pierson, 2008).

The shafts were laterally loaded by hydraulic jack toward the wall facing using a displacement control mode (Figure 8[a] and [b]). The load-deflection curves of the shafts, including group shafts, were recorded. Researchers carried out a numerical simulation to examine the influence of the following factors on the capacity of the drilled shaft: different reinforcement types, quality of the backfill material, and different MSE wall facing units.

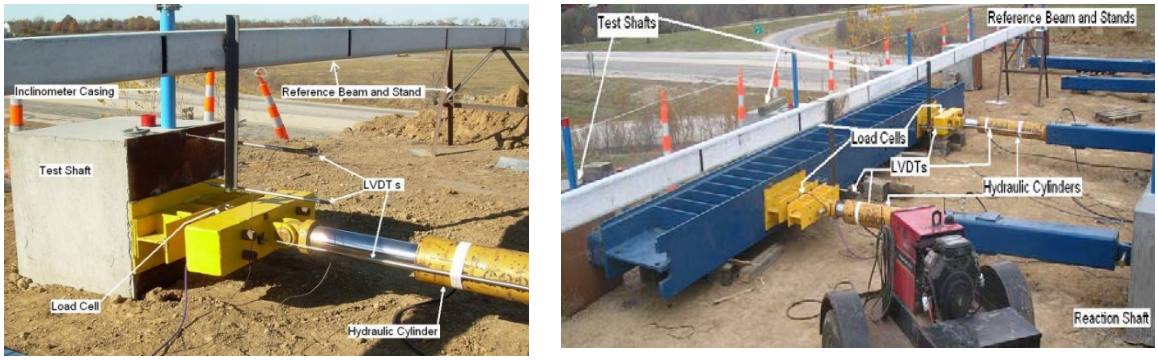

(a) **(b)**

Figure 8. Full-Scale Tests: (a) Single Shaft and (b) Group Shafts.

Based on the test data obtained, a design chart was developed (Figure 9) that can be used to determine the drilled shaft capacity at the allowable deflection and the given drilled shaft locations. An empirical equation was also proposed to calculate the minimum spacing between piles to avoid group effect, as shown in Eq. (2.1) (Pierson, 2008):

$$W_{influence} = 1.47 D_w + 6.23 \quad (2.1)$$

Where $W_{influence}$ is the minimum spacing between shafts to avoid group effect [ft], and D_w is the distance from the MSE wall [ft].

If the actual drilled shaft spacing is less than $W_{influence}$ calculated from Eq. (2.1), a linear reduction factor was suggested. The reduced factor to account for the group effect is shown in Eq. (2.2):

$$P_{group} = \frac{P_{single} S_s}{W_{influence}} \quad (2.2)$$

Where P_{single}, P_{group} are the capacity of single and one group shafts, respectively, and S_s is distance from the MSE wall [ft].

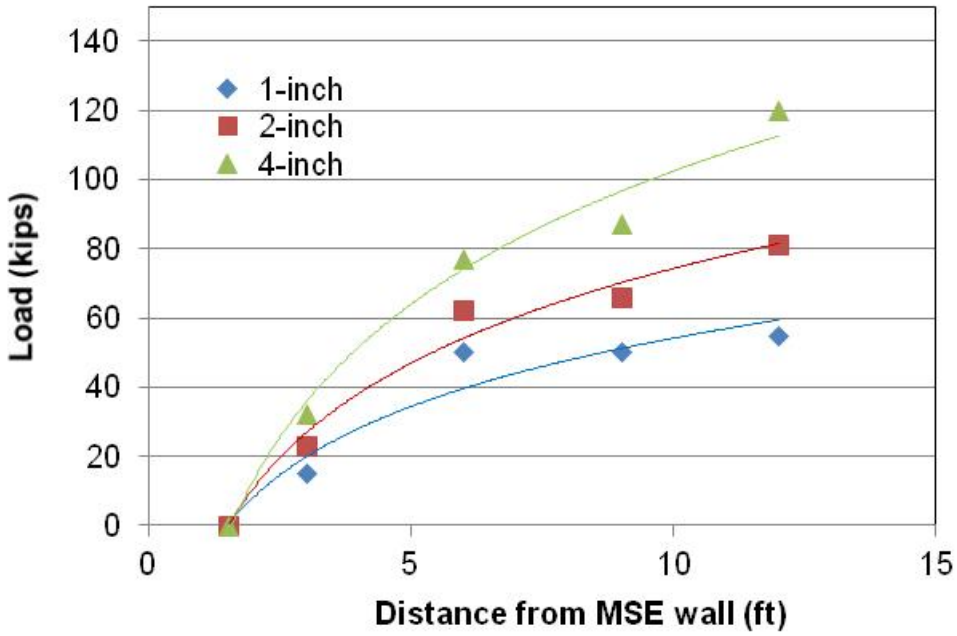

Figure 9. Design Chart for Drilled Shaft.

Numerical modeling of the interaction between the drilled shaft and MSE wall were carried out by Huang et al. (2011), Pierson (2008), and Pierson et al. (2010). Based on the numerical modeling results, Pierson (2008) ranked the influence of geogrid reinforcement, backfill material, MSE wall facing, and height on the drilled shaft capacity in descriptive terms, namely high, medium, and low. The only factor that received a rating of high influence was the reinforcement. The other factors (e.g., backfill material, MSE wall facing, and height) have either medium or low effect on the drilled shaft capacity.

UDOT Research

When the bridge abutment is subjected to seismic acceleration, the piles can be forced toward the backfill behind the abutment. The backfill behind the abutment may be bounded by MSE walls on the sides (Figure 10). The load-deflection curve and the performance of MSE walls under seismic loading were to be determined. The UDOT research project (Rollins et al., 2013) was planned to obtain the load-deflection curves, evaluate the current design methods, and examine the effect of the passive force on the MSE wall.

The research encompassed one large-scale load test on the driven piles with a cap. Figure 10 and Figure 11 present illustrations of the test setup. The pile cap was loaded with two actuators, which were backed by two reaction shafts. The applied load and the corresponding

deflection were monitored. The passive force and deflection curve were obtained and compared with current design methods (Figure 12). Due to the effect of the loaded piles, the lateral earth pressure on the MSE wall could increase significantly, which could lead to excessive deflection or even failure.

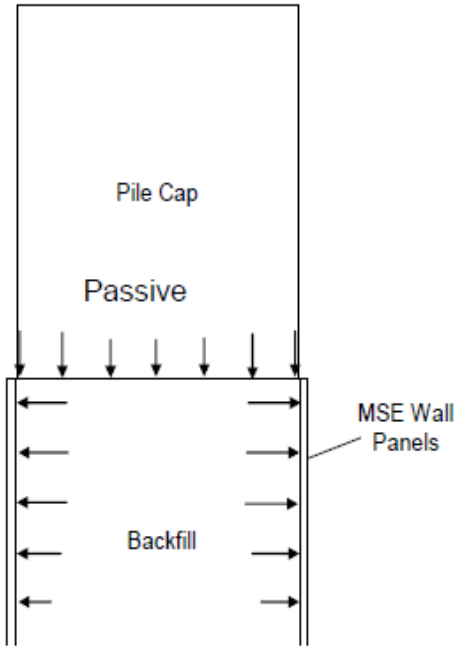

Figure 10. Conceptual Sketch of UDOT Research (Rollins et al., 2013).

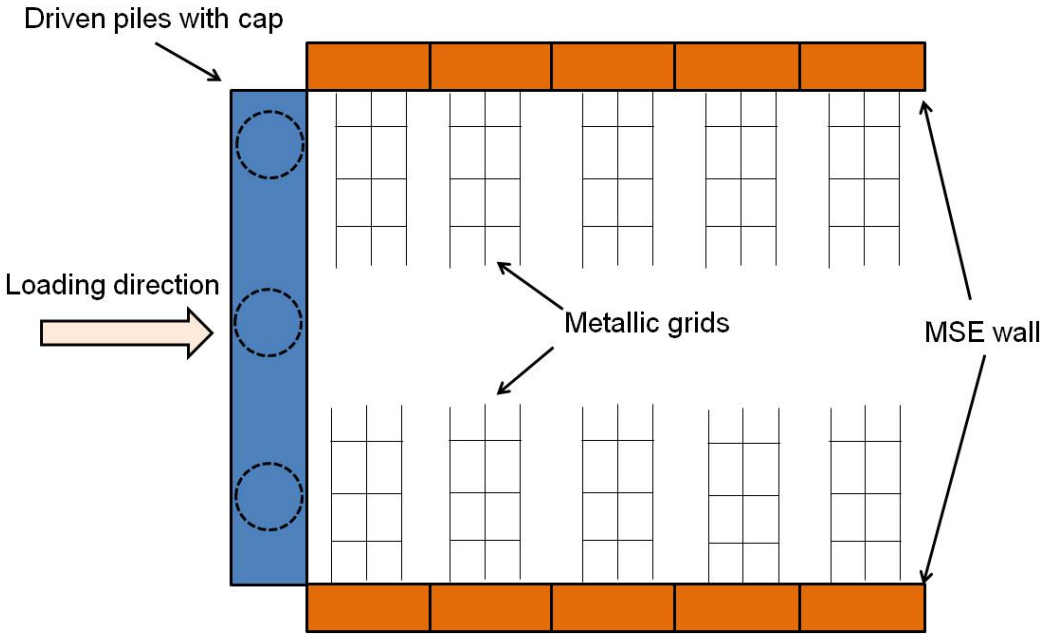

Figure 11. Test Setup.

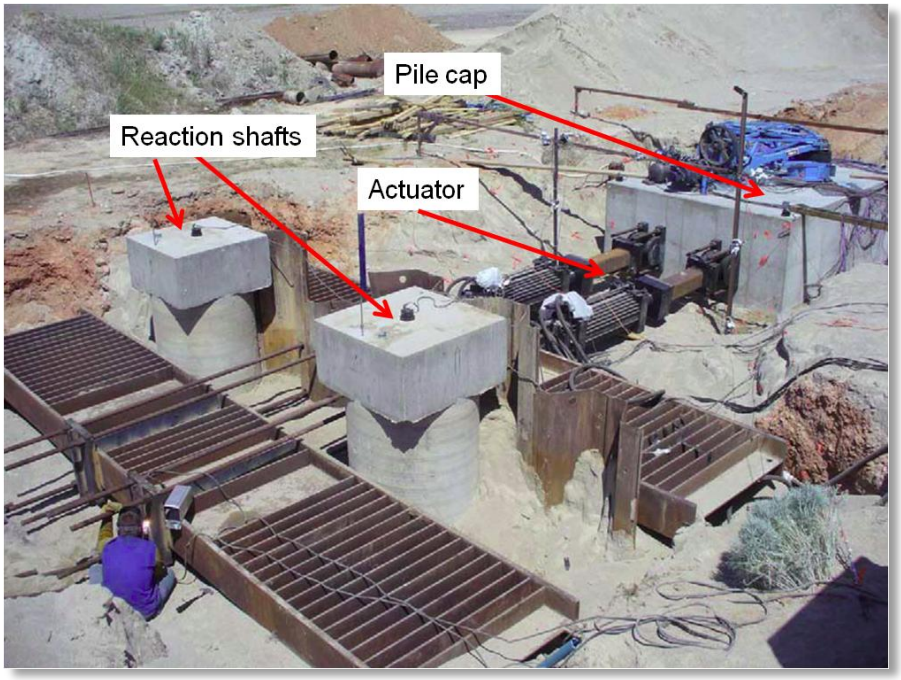

Figure 12. Field Tests (Rollins et al., 2013).

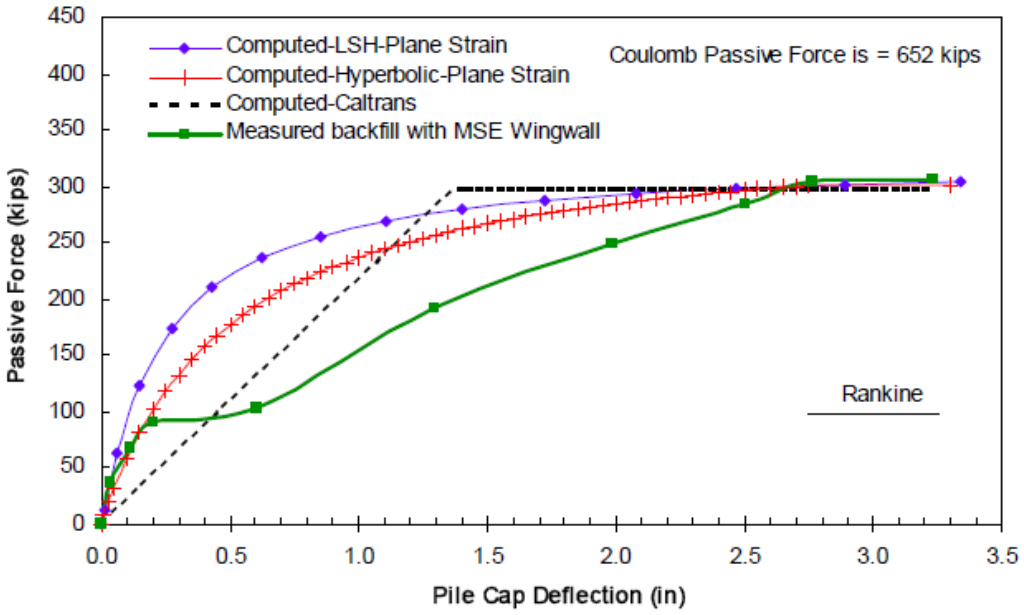

Figure 13. Passive Force-Deflection Curves (Rollins et al., 2013).

Instrumentation of KDOT and UDOT Research

Both KDOT and UDOT research projects used extensive instrumentation for data acquisition. Table 1 summarizes the typical types of instrumentations. The instrumentation in

Table 1, with the exception of survey and Light Detection and Ranging (LIDAR), has been used either in KDOT or UDOT research projects. Survey and LIDAR, which are popular in remote sensing, have been increasingly used to measure movement for engineering purposes (Laefer et al., 2009). In Chapter 3, the advantages and disadvantages of the instrumentation in Table 1 are discussed when considering their application in this study.

Table 1. Commonly Used Instrumentations.

Horizontal movement	Slope inclinometer
	LVDT
	Tell tale
	Photogrammetry
	Survey
	String potentiometer
	LIDAR
Strain	Strain gauge
Earth pressure	Earth pressure cell
Load	Load cell

OTHER BACKGROUND INFORMATION

Besides the published reports, papers, and presentations, communications with engineers from different state departments of transportation (DOTs) were maintained during this report. The major pieces of information collected from the DOTs are:

- None of the state DOTs have a rational design method to account for the interaction between MSE walls and drilled shafts.
- All engineers expressed interest in the investigation related to the interaction between MSE walls and drilled shafts. Most of the engineers considered that such a research was important and necessary.
- A few engineers considered that the interaction between MSE wall and drilled shaft was a trivial issue, at least for the design in their state.
- None of engineers were able to provide details of their practice on building MSE wall with drilled shafts, including compaction details and any repair measure for distressed MSE walls.

CONCLUSION

MSE walls are widely used to support bridge abutment, and in some cases, the interaction between the drilled shaft and the MSE wall can be problematic. Some studies have been performed on the interaction between MSE walls with drilled shafts, but the soil reinforcement in these studies are geosynthetics and geogrids. There are no proposed design guidelines that came out of these studies.

In this research, the main focus is on MSE walls with metal strips and metal grids. A design guideline is proposed at the end to overcome the failure problem of MSE walls with drilled shafts in the reinforced zone.

Instrumentation design for the full-scale test and the two monitoring project sites are discussed in the next chapter.

CHAPTER 3:
INSTRUMENTATION DESIGN

INSTRUMENTATION USED IN PREVIOUS WORKS

The first step in this study was to check previous work that was reported in Chapter 2. In recent years, there were other somewhat similar studies to the one proposed in this report, but the type of MSE wall reinforcement to be used in this research and the tests protocols were different. For all intents and purposes, the main outcomes of these previous studies are not applicable to the MSE walls project in Texas. This is because they do not involve metallic reinforcement, which is the most popular reinforcement used by TxDOT for its designs. These previous studies have impacted our research, making it possible to learn what kind of instrumentation worked well and which to adopt for the tests and monitoring deliberated in this study. For example, a total of seven types of instrumentations were successfully used in the KDOT project: strain gauges, earth pressure cells, load cells, LVDTs, slope inclinometers, tell tales, and photogrammetry targets.

The strain gauges were installed to measure the strain developed in the reinforcements. At each location, the strain gauges were installed on the upper and lower surfaces of the reinforcement to compensate for bending. To protect the strain gauges, they were encased in a flexible plastic tube.

The earth pressure cells were installed to measure the increase of the earth pressure induced by the laterally loaded drilled shaft. Figure 14 shows the installation adopted for the earth pressure cells. To provide an even surface between the MSE wall facing and the earth pressure cell, a masonry block was placed at the interface (Figure 14). To protect the earth pressure cell from compaction damage, a sandbag was placed between the earth pressure cell and the granular backfill material.

Load cells and LVDTs were installed at the head of the drilled shafts (Figure 15). The load cell was used to monitor the force applied at the head of the drilled shaft. LVDTs were installed to monitor deflection of the drilled shaft head. The LVDT reading was used as a reference for the slope inclinometer readings in case the bottom of the slope inclinometer had moved. LVDTs were also installed to monitor the relative movement between the test shaft and the reaction shaft (Pierson et al., 2009).

Figure 14. Installation of Earth Pressure Cells (Pierson et al., 2009).

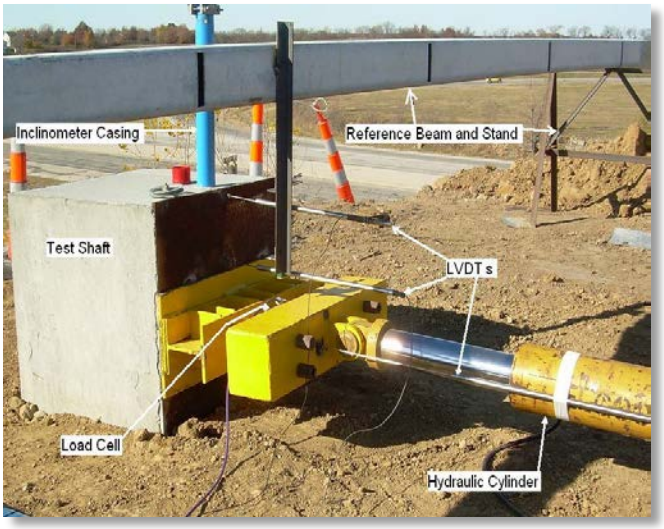

Figure 15. Installation of Load Cells and LVDTs (Pierson et al., 2009).

The tell-tales were installed to monitor the movement of the backfill material relative to the MSE wall facing. The tell-tales were arranged to measure the backfill movement in front of and also surrounding the drilled shaft. The slope inclinometers were installed at each test shaft, reaction shaft, and also at selected locations in the MSE wall. The casing of the slope inclinometers was terminated at the bottom of the drilled shaft. The bottom of the slope inclinometers cannot be treated as a fixed end since it may move during the loading. The slope inclinometer readings were adjusted based on the shaft head deflection provided by the LVDT (Pierson et al., 2009).

The movement of the MSE wall facing during loading was monitored by photogrammetry. Figure 16 shows the photogrammetry targets. Each target had a 6-in. long black portion, which provides a reference for movement. A tripod was fixed with a 10 megapixel digital single lens reflex camera to capture the images of the wall facing targets at a designated time. The images were then restored into AutoCAD. Using each target's 6-in. scale, the MSE wall facing movement was established by comparing the photo taken before and after each loading stage (Pierson et al., 2009).

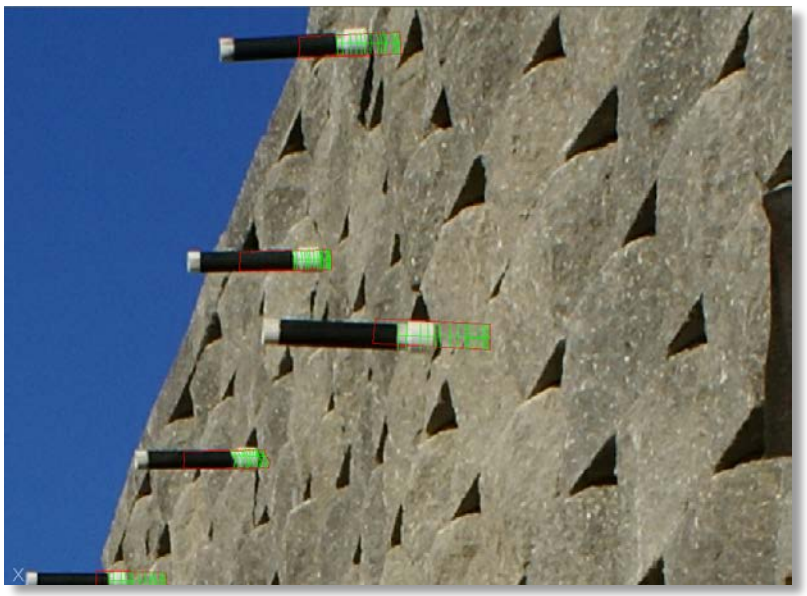

Figure 16. Installation of Photogrammetry Targets (Pierson et al., 2009).

In summary, a total of four different devices were used to monitor the deflection. Table 2 summarizes the advantages and disadvantage of these instruments. This discussion is based on the instruments' application to monitoring the movements of the drilled shaft and the MSE wall, meaning the conclusions may not be valid for other applications. The load cell was used to monitor the applied load. Since the load cell has certain dimensions, an even and smooth contact surface is required. Strain gauges need to survive the construction, especially the compaction of the granular materials. Protection measures are necessary and earth pressure cells need to survive the construction as well. The earth pressure cell requires good contact between the backfill material and the face of the cell. Obtaining reliable earth pressure monitoring data is a challenge, especially in granular materials. Engineers always face the dilemma that the compaction can easily damage the cells and that any protection measures for compaction may undermine the contact between the cell and the backfill material.

Table 2. Comparison of Different Displacement Monitoring Instrumentations.

	Advantages	Disadvantages
Slope inclinometer	• Easy to implement • Provide continuous profile • Not susceptible to environmental deterioration • Damage can be easily detected • Easy to monitor multiple points on the same vertical line	• Need a fixed end or reference point with known displacement • Need access for monitoring personnel • Need time to acquire each set of reading
LVDT	• Most accurate • Need reference beams • Costly if multiple points to be monitored	• Susceptible for environmental deterioration • Not suitable for long-term monitoring • Need access to the instrumentation
Tell tale	• Easiest to use • Cheap	• Least accurate • Subject to construction damage • Need access to acquire readings
Photogrammetry	• Easy to implement • Low cost • Time saving. Monitor multiple points at the same time • No access to the monitored points is need. Can monitor the displacement from a distance away from the monitored objects	• Need a scale reference • Need clear view of the monitoring object • Need photo process software to analyze the photo

PARAMETERS MEASURED

The final goal of the instrumentation was to gather experimental data that would allow researchers to better understand the problem, calibrate the numerical model, and ultimately recommend guidelines. The actual sites provide real world situations. In addition, the National Geotechnical Experimentation Site (NGES) site afforded the luxury of controlled loading conditions and the possibility of loading to failure. For those purposes the following parameters were measured:

1. Deflection of drilled shafts.
2. Deflection of MSE wall panels.
3. Earth pressure at the back of MSE wall panels.
4. Earth pressure at the front of drilled shafts.
5. Strain in MSE wall reinforcement and in drilled shafts.

Shaft and Wall Deflection

To track the deflection of the shaft and wall panels, both inclinometers and tiltmeters were used in this study. On one hand, inclinometer readings allow for a continuous profile of the deflection versus depth at a certain time (time of reading). Because these readings are generally taken manually, a limited number of profile deflections is obtained. On the other hand, tiltmeters provide an automatic and continuous monitoring of the wall or shaft inclination but at a limited number of points (i.e., where the tiltmeters are placed). In this research, two tiltmeters were used on the shaft and another two on the wall. Deflections of the shaft and wall panels are an important parameter in numerical analysis, so researchers decided to use both inclinometers and tiltmeters for this project.

Earth Pressure

There was a need to know the earth pressure at the back of the wall and in front of the shaft, so researchers used earth pressure cells. The backfill material used in this research was clean sand and crushed rock. As explained above, they could cause some problems for pressure cells, resulting in imprecise data. A type of pressure cells that is working well with granular materials was adopted in this study. The working mechanism and how it overcomes typical problems associated with earth pressure cells will be discussed in the next chapter. Pressure cells were installed near the top of the height of the shaft and of the wall.

Load in Reinforcements

By measuring the strains in the wall reinforcement, the load carried can be calculated. The strains can be measured using strain-gauges at specific positions of the reinforcement. The total number of monitoring positions is limited by the number of channels in the data logger. Preliminary numerical analyses (explained in Chapter 4) indicated that the force in the

reinforcement due to the horizontal load on the drilled shaft in the bottom 2/3 of the wall is small, so all strain gauges were installed in the top 1/3 of the wall.

Data Acquisition System

The experimental data provided by the different sensors were collected with a data logger. Two data loggers were used for the full-scale test at the Riverside Campus. As for the actual projects, only one data logger was used. The inclinometer was read manually. Figure 17 and Figure 18 show sketches of the instrumentation.

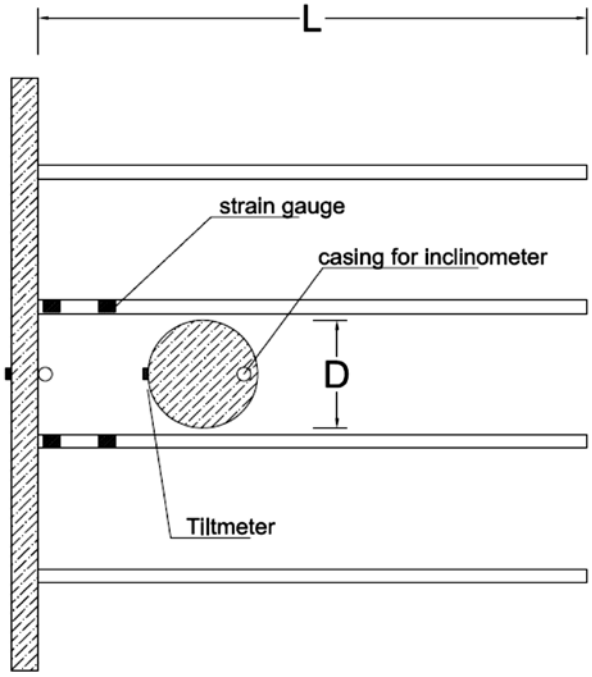

Figure 17. Schematic Representation of Instrumentation (Plan View).

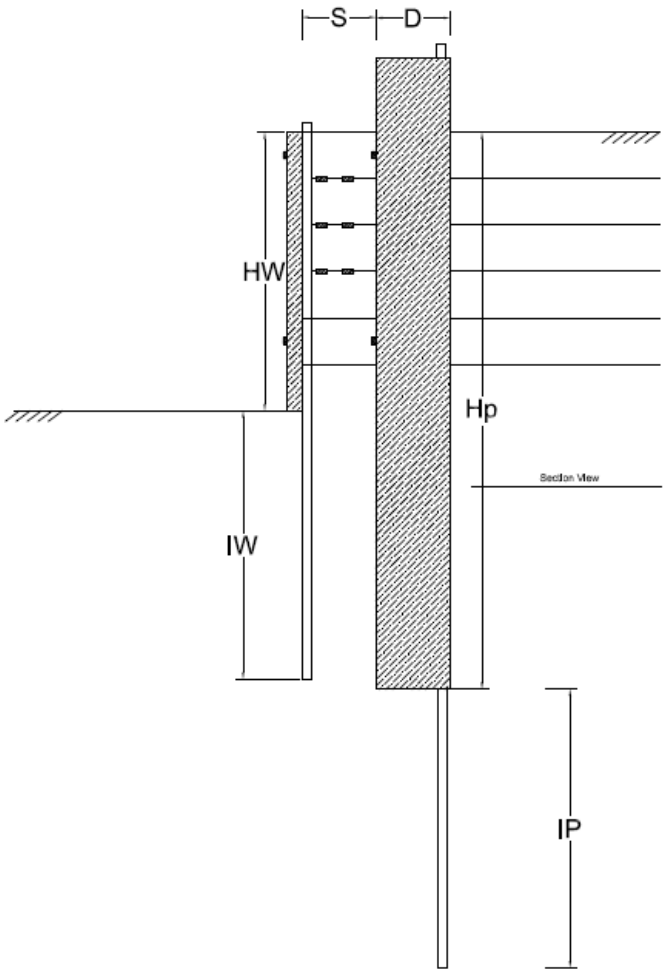

Figure 18. Schematic Representation of Instrumentation (Cross Section View).

Power Supply

Power is needed for the data acquisition system. There was a power supply at the Riverside Campus, but not at the two TxDOT actual sites. Solar panels were installed to provide the required power.

ADOPTED INSTRUMENTATION

This section introduces all of the instruments that were used in this research. They were selected to measure displacements, deformations, and stresses. For each instrument a general description is presented, followed by their main advantages and disadvantages. Afterward, the data acquisition system is presented, respectively.

For all the electronic devices that can be used in this research, there are two different functional systems that can be selected. The traditional one, also known as a voltage based system, and a relatively new system that is based on vibrating wires.

In the traditional one, the parameters to be measured are relayed via the gauge base (electrical insulation) to the resistance wire or foil in the gauge. As a result, the fine wire (or foil) experiences a variation in electrical resistance. This variation is exactly proportional to the parameter. For example, a strain-gauge is constructed by bonding a fine electric resistance wire, or photographically etched metallic resistance foil, to an electrical insulation base using an appropriate bonding material and attaching the gauge leads.

In the vibrating wire system, the resonant frequency of vibration of a tensioned steel wire is dependent on the strain or tension in the wire. This fundamental dependency is used in a variety of configurations for the measurement of strain, load, force, pressure, temperature, and tilt. Vibrating wire sensors are well known for their long-term stability. The advantage of vibrating wire sensors over more conventional types mainly lies in the sensor output, which is a frequency rather than a voltage. Frequencies can be transmitted over long cables (e.g., >2000 m) without appreciable degradation of the signal caused by variations in cable resistance, which can arise from water penetration, temperature fluctuations, contact resistance, or leakage. This factor results in sensors that are convenient for long-term measurements in adverse environments and exhibit good long-term stability.

In this study, researchers decided to use instruments based on the conventional system (i.e., voltage base system). Different reasons supported this decision and are as follows:

- Vibrating wire is a relatively new method; the majority of the previous projects undertaken at TAMU were instrumented with sensors based on the voltage method.
- Technicians are more familiar with this method.
- The price for instrumentations based on vibrating wires is much higher. In some cases, it is about three or four times higher than the conventional types.
- It is also recommended to use a single method for all of the devices in a particular project. Otherwise, two (or more) separate data acquisition systems will be necessary (i.e., for the voltage based gauges and another for the vibrating wire ones). To use two different kinds of data acquisition systems in a single project may create difficulties.

Tiltmeter

The tiltmeter is an instrument used for measuring inclination. Its output is determined by the mass distribution of the earth since it responds to the local acceleration of gravity (*g*). This instrument is sometimes called inclinometer, particularly if its range of measurement is large. The response of the instrument is determined by the direction of *g* relative to its orientation.

The principles of operation can be illustrated with common tools of carpentry. Consider a static plumb bob, which would constitute a spherical pendulum if the system were dynamic. The plumb bob orients itself along the direction of *g*, defining the local vertical. Alternatively, a fluid bubble, contained by a tube, will determine one of the locus of directions, orthogonal to *g*, which constitutes the local level. Figure 19 shows the tiltmeter used in this project.

Figure 19. Tiltmeter Used in the Project.

Inclinometer

Inclinometer is a device used to measure the angle of a slope. In this project, it was used to measure the vertical deflection of the wall and of the shaft.

There are many differences between an inclinometer and a tiltmeter. Perhaps the more relevant one is that an inclinometer gives the deformation profile at a specific time (e.g., at the end of the reading) for the whole depth of the inclinometer casing. In contrast, the tiltmeter gives

the deflection at a specific point but for the whole time of analysis, allowing continuous monitoring. The main components of an inclinometer are:

- Inclinometer casing: the inclinometer casing is permanently installed in a borehole that passes along the wall and shaft.
- Portable traversing probe: the traversing inclinometer probe is the standard device for surveying the casing. It is economical since it can be carried from site to site. The traversing probe obtains a complete profile because it is drawn from the bottom to the top of the casing.
- Portable readout: a portable readout is used to record the surveys obtained with the portable probe. Advanced readouts store readings in solid-state memory, eliminating pencil, paper, and transcription errors. It also simplifies transferring the data to a computer for processing.

Figure 20 presents the main components of the inclinometer device. The existing inclinometer was calibrated following the protocol indicated by the manufacturer company (Slope Indicator). First, the casing was placed in an approximately vertical position. Second, the probe was inserted into the casing and the initial inclination was read. Next, a known displacement was applied to the top of the casing while holding the bottom of the casing. A new reading was taken with the inclined casing. Then, by a simple calculation, the change in the angle was obtained. Therefore, the change in the reading could be easily related to the change in the angle. For a more precise calibrating factor, the procedure can be done using more points.

The calibration factor for the existing inclinometer is 0.297. The inclinometer was calibrated every three months.

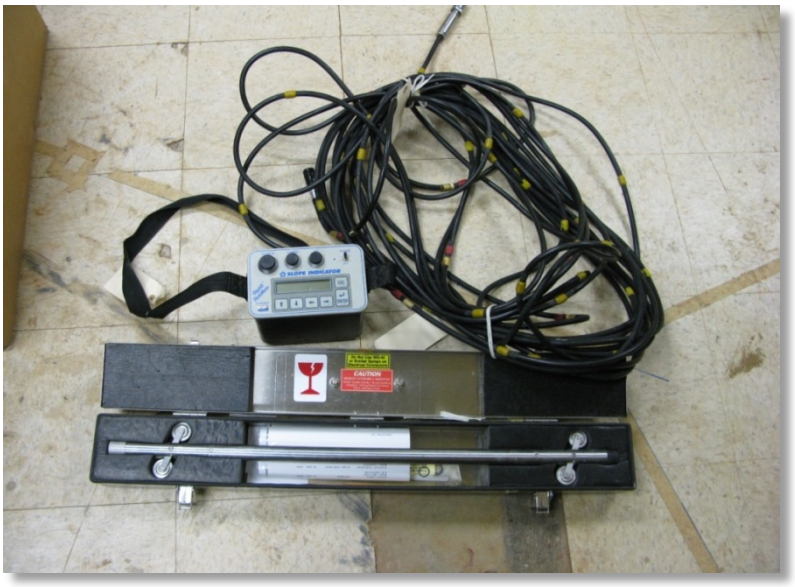

Figure 20. Inclinometer.

Photogrammetry

Photogrammetry may be defined as a technique used to obtain reliable information from physical objects and the environment. This is done through a process of recording, measuring, and interpreting aerial and terrestrial photographs. In a sense, the word photogrammetry may be analyzed in two parts: “photo-” meaning picture and “-grammetry” meaning measurement. The fundamental principle used by photogrammetry is triangulation by taking photographs from at least two different locations (the so-called lines of sight). These lines of sight are mathematically intersected to produce the 3D coordinates of the points of interest (Figure 21).

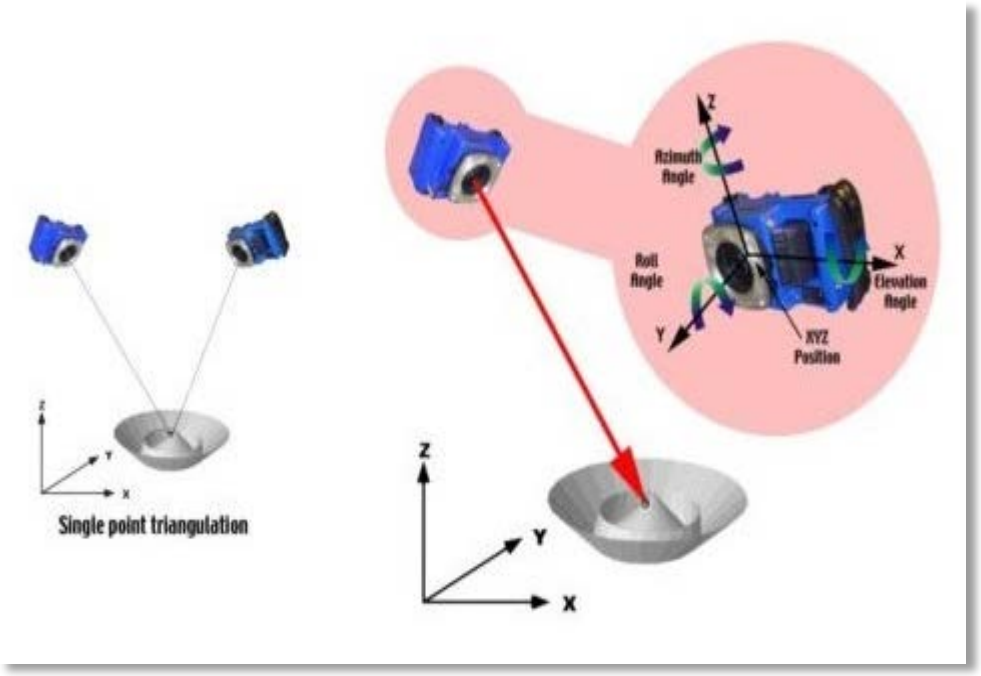

Figure 21. Photogrammetry.

Pressure Cells

Earth pressure cells, sometimes also called total pressure cells or total stress cells, are designed to measure stresses in soils or the pressure of soil on structures. Pressure cells will respond not only to soil pressures, but also to ground water pressures and pore water pressure, which is why “total pressure” or “total stress” are more appropriate terms.

From previous works dealing with granular material, it was very hard to obtain reasonable results from pressure cells. In this study, special care was taken to gather quality results from this instrument. This is explained later on in Chapter 4.

The earth pressure cells described here are the hydraulic type. Two flat plates are welded together at their periphery and are separated by a small gap filled with a hydraulic fluid. The earth pressure squeezes the two plates together, building up the pressure inside the fluid. If the plates are flexible enough (i.e., if they are thin enough relative to their lateral extent), then at the center of the plate, the supporting effect of the welded periphery is negligible, and at the center of the cell, the external soil pressure is exactly balanced by the internal fluid pressure.

Strain Gauges

Strain gauges are widely used for physical force measurements in mechanical, ocean, aerospace, and civil engineering, as well as the architecture, automobiles, and medical science fields. Strains are measured to determine the degree of deformation induced by the mechanical loads. By knowing the elastic modulus of the material being studied, it is possible to determine both the stress and the forces acting on the instrumented element.

There are a number of ways to measure strain mechanically and electrically, but the vast majority of stress measurement is carried out using strain gauges because of their superior measurement characteristics.

External force applied to a material generates physical deformation and a change in electrical resistance of the instrument material. When this material is glued onto the test specimen via electrical insulation, the material produces an electrical resistance change that corresponds to the deformation. Strain gauges consist of electrical resistance material and measure strains proportional to the change in resistance.

When strains are generated in a test specimen, a strain gauge is attached to it and the strain is relayed via the gauge base (electrical insulation) to the resistance wire or foil in the gauge. As a result, the fine wire (or foil) experiences a variation in electrical resistance that is proportional to the strain. There are many different manufacturers and different models of foil strain-gauges. The main differences between them are related to the way in which they are glued on the surface. The lead wire can be preinstalled or not and may also have a different range of electrical resistance. Based on the experiences from previous projects at TAMU, TML-FLA-5 strain gauges were chosen for this specific study.

Calibration

The first step for installing a strain gauge is to clean the surface and make it shiny by using sandpaper. Figure 22(a) and (b) show the main first steps followed to glue the strain-gauge to the metallic strips used in this study. First, coarse sandpaper was used to prepare the surface, and then progressively finer ones were used to polish the strip surface. When the strip surface was clean and polished, acetone was applied for the final treatment.

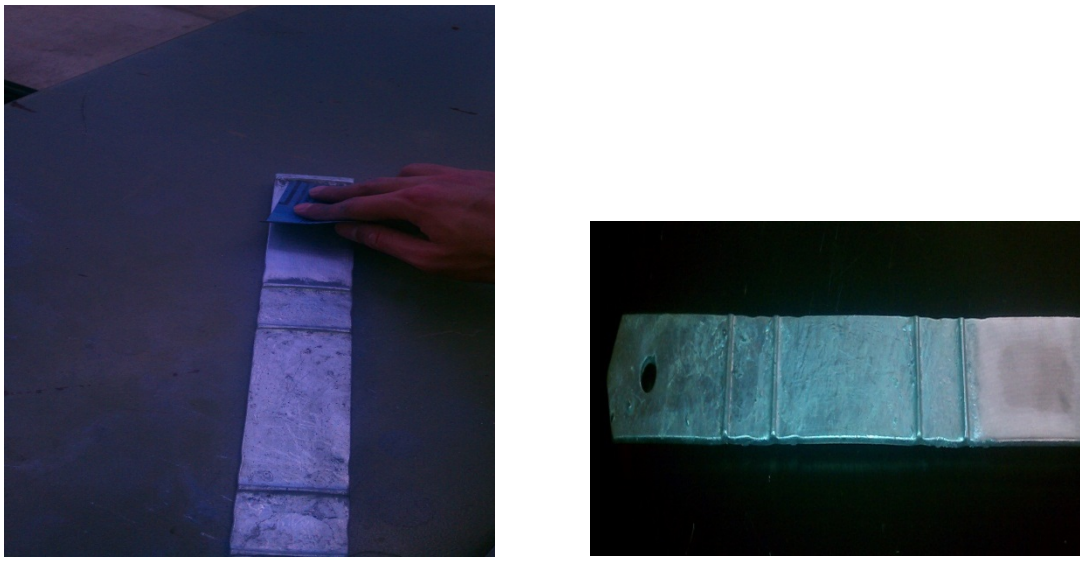

(a) (b)

Figure 22. Clean The Strip Surface by Sandpaper.

Once the surface was ready, the strain gauge was placed on the target position and a band tape was used to fix it temporarily. Super glue was then put on the target position and the strain gauge was rolled back to it (Figure 23).

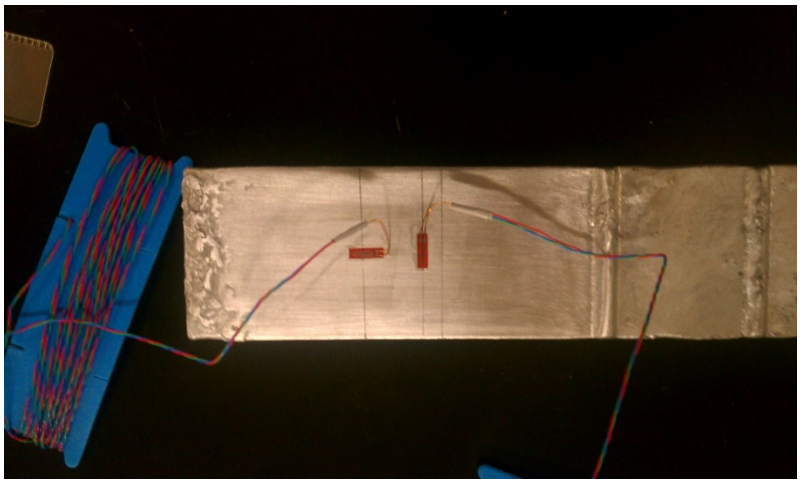

Figure 23. Installed Strain Gauges.

Once the strain gauge was installed, the lead wires were connected to the data logger. Then one side of strip was fixed, and in steps, some weights were applied to the other end (Figure 24). The maximum weight was 46.7 kg, and the strip was then unloaded. By knowing the strip material and its modulus of elasticity, the strain gauges could be easily calibrated.

Figure 24. Testing Strip with Strain Gauges.

The gauge factor 2.11 was tested (the one in the catalog). As it is shown in Figure 25, the results are acceptable.

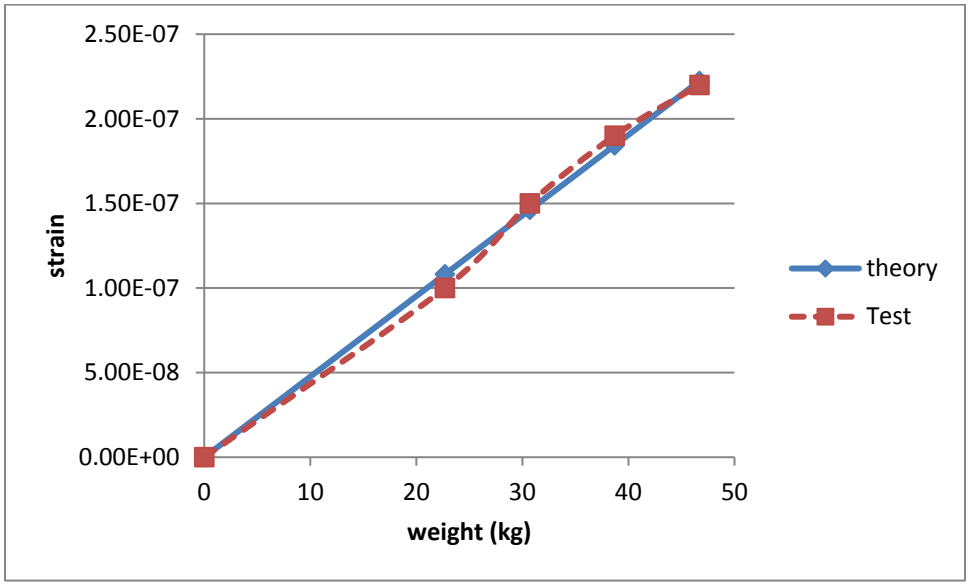

Figure 25. Calibration Results.

Data Acquisition System

The data acquisition system is used to read the data from the instruments and save them. The main components of this system are: data logger, solar panel, and battery. They are introduced below.

Data Logger

The data logger adopted in this project is a Campbell Scientific CR1000 (Figure 26). The experience at TAMU in previous projects with this type of system was very good, so it was selected for this study.

Some of the benefits of this device are:

- Serial communications with serial sensors and devices supported via I/O port pairs. It supported all of the devices used in this project.
- Compatible with channel expansion peripherals allowing for the expansion of the system. By default, it has 16 channels. It is possible to expand it to 32 if necessary.

Figure 26. CR1000 Data Logger.

Solar Panel

In this study, a Campbell Scientific SP10-10W solar panel was used for a power supply (Figure 27). It supplies electrical power when AC power is unreliable, expensive, or unavailable.

Battery

A Campbell Scientific PS100 rechargeable power supply was used in this study (Figure 28). The PS100 provides a 12-VDC, 7-Ahr rechargeable power supply. The rechargeable battery can be charged from alternating currents or from an external solar panel.

Figure 27. SP10-10W Solar Panel.

Figure 28. PS100 Rechargeable Power Supply.

CONCLUSION

Instrumentation design was performed based on the required information for the full-scale test at the TAMU Riverside Campus and for the monitoring of the two TxDOT actual sites. The most important limitation was the number of channels in the data logger. For the full-scale test, two data loggers were used and a total of 20 channels collected data. For the monitoring at actual sites, one data logger was used for each site and 15 channels collected data.

The types of devices were selected according to the required precision and durability. Durable devices were needed, especially for monitoring the two actual sites because they were designed to collect data for about 16 months. The full-scale test and the monitoring of the actual sites are discussed in detail in the next chapter.

CHAPTER 4:
FIELD STUDIES – TESTS AND MONITORING

INTRODUCTION

This chapter focuses on the monitoring and testing of the MSE wall at the field sites. Monitoring was planned for two actual sites that were selected by TxDOT and the load test carried out at TAMU-NGES. One of the actual projects selected by TxDOT was in Bastrop. The data on this project were collected from December 2013 until August 2015. The second project selected by TxDOT was in Salado. This project was delayed, and data were collected from January 2015 to August 2015.

At the TAMU-NGES, a full-scale loading test was carried out on a new MSE wall. This experiment measured the interaction between the drilled shaft and the MSE wall under actual conditions. The drilled shaft, MSE wall, and other components used during the loading test were designed and constructed by TTI personnel. The instrumentation used to gather all the data required by this research was designed and installed by the research team, as was the loading protocol.

The main objective of this research is to study the interaction between MSE walls and drilled shafts subjected to horizontal loads. In particular, the research focuses on the effect of an applied horizontal load to the drilled shaft on:

- The drilled shaft displacement.
- The wall displacement.
- The additional pressure on the wall.
- The additional force developed in the soil reinforcements and its distribution at different positions.

This chapter is organized as follows: the second section is related to the full-scale test at NGES, which also introduces details associated with the wall, the drilled shaft, and the materials and devices used for gathering the data. The loading protocol, test preparation, performance, and results are also discussed in this section. The third and fourth sections discuss the real MSE walls at the Bastrop and Salado monitoring sites, describing the installation of different devices on the walls and drilled shafts. The data collected from these sites are also presented in the third and fourth sections, respectively.

FULL-SCALE LOADING TEST

Overview

This part focuses on the different components of the loading test.

Wall Detail

The test was carried out on a new MSE wall constructed at the TAMU Riverside Campus. This wall was part of a much longer wall built for a National Cooperative Highway Research Program project that studied the impact of a tractor trailer on a barrier located on top of the wall. The length of the wall is 90 ft, and its height is 7.5 ft (Figure 29).

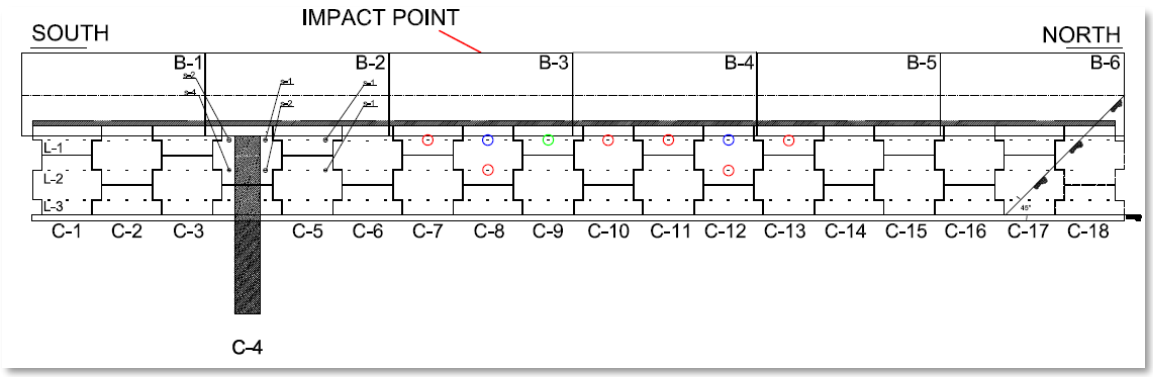

Figure 29. Wall Detail.

The panels for the wall were donated to the project by the Reinforced Earth Company (RECO). Each panel has six ties for strips (two rows and three columns). The height of the panel is 4 ft 10 in. The total height of the MSE wall consisted of one and a half panels. Figure 30 shows details of the panel.

These panels are not designed for significant lateral pressure from the soil or additional pressure caused by horizontal loading of a nearby drilled shaft; they contain minimum reinforcement (Berg et al., 2009). A shallow strip footing is first constructed to transfer the vertical load from the panels to the soil (Berg et al., 2009).

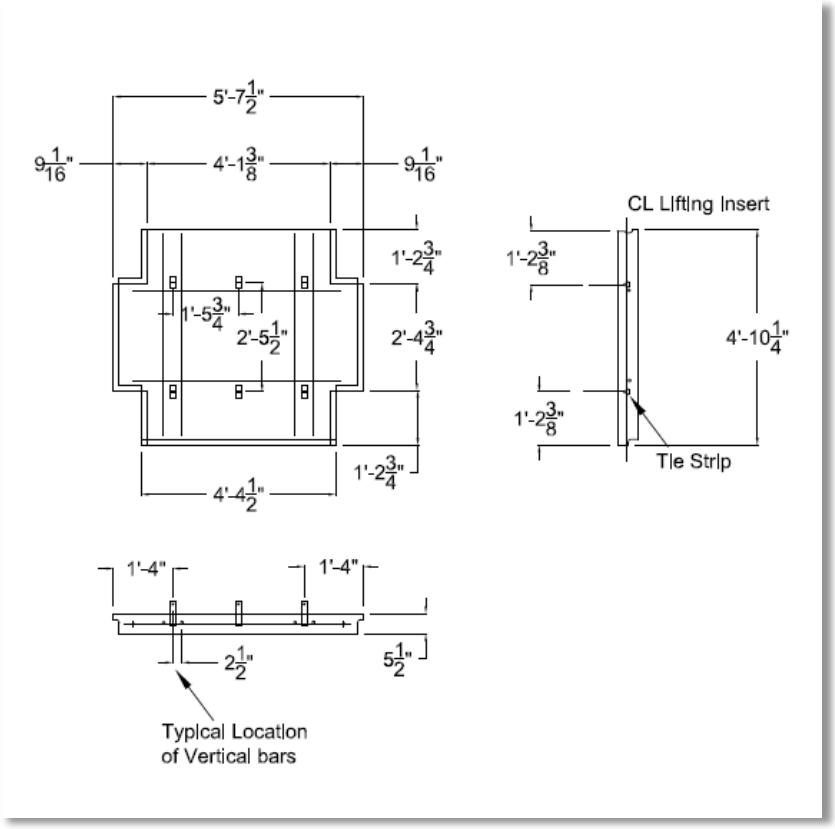

Figure 30. Panel Details.

Backfill Material

The backfill material used in this test program was a fine to medium sand. This sand satisfies the requirements for MSE select backfill specified in AASHTO (2010). Figure 31 shows a particle size distribution curve for the MSE wall backfill material used in the full-scale test.

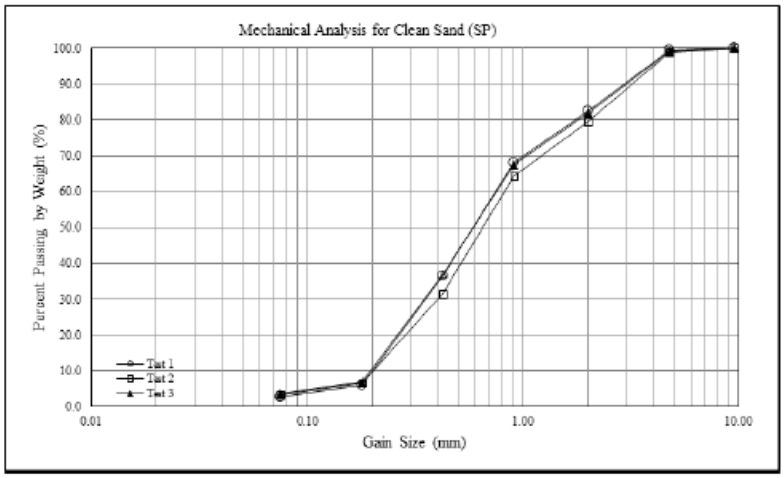

Sample	D_{10}[1]	D_{30}[2]	D_{50}[3]	D_{60}[4]	Perc. Fines	C_c[5]	C_u[6]	w_L	w_P	w_{PI}	Perc. Grav.	Gs	USCS[5]
Clean Sand	0.20	0.36	0.51	0.77	3.1	0.84	3.85	-	-	-	0.7	2.64	SP

Figure 31. Gradation Curve for Backfill Material. Grain sizes in mm (1 inch = 25 mm).

The strength parameters of the backfill material were determined via three Consolidated-Drained triaxial tests. Those tests were performed at three different confining pressures that were selected according to the depth of the instrumented strips adopted in this research. Figure 32 and Figure 33 show test results for a confining pressure ($\sigma_3=\sigma_2$, both horizontals stresses) of 7 kPa. Figure 34 and Figure 35 show results for a confining pressure of 14 kPa, and Figure 36 and Figure 37 present results for a confining pressure of 31 kPa. Figure 38 shows strength envelopes.

To determine the strength properties of the fill, the tests results have been plotted in the s-t space as follows: $s = (\sigma_1+\sigma_3)/2$ and $t = (\sigma_1-\sigma_3)/2$. Figure 39 presents the main results. To determine the friction angle, $\sin(\varphi) = \tan(\alpha)$ and for cohesion $c = a/\cos(\varphi)$.

The friction angle for the backfill material is 27.3°, and the cohesion is 5.45 kPa.

$$\begin{aligned} &\tau = c_{app} + \sigma\tan(\phi') \\ &\tau = \cancel{c}' + (\sigma - \alpha u_w)\tan(\phi') \\ &\Rightarrow c_{app} = -\alpha u_w \tan(\phi') \Rightarrow -\alpha u_w = 10.56kPa \end{aligned} \tag{3.1}$$

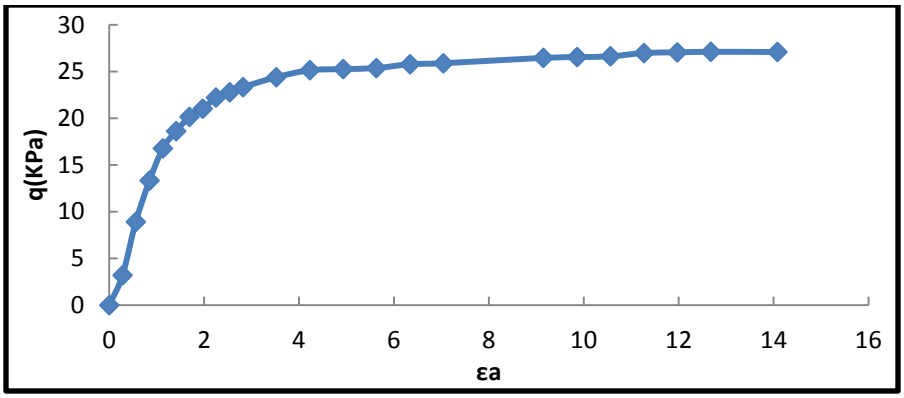

Figure 32. Stress-Strain Curve for σ3=7KPa (100 kPa = 14.5 psi).

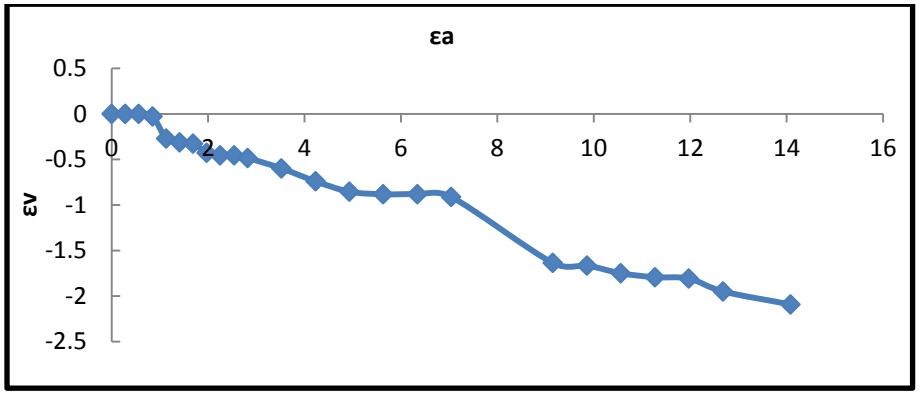

Figure 33. Volumetric Strain vs. Axial Strain for σ3=7KPa (100 kPa = 14.5 psi).

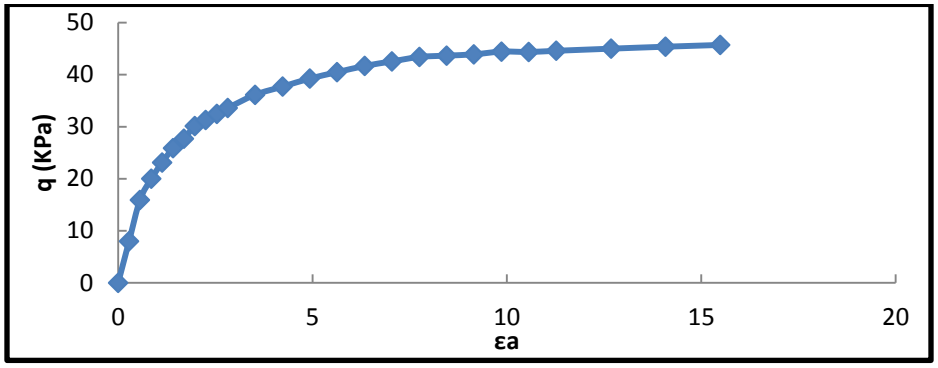

Figure 34. Stress-Strain Curve for σ3=14KPa (100 kPa = 14.5 psi).

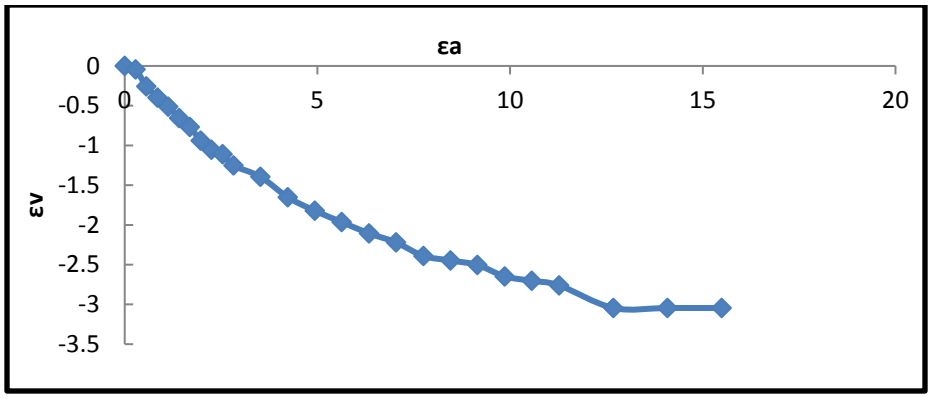

Figure 35. Volumetric Strain vs. Axial Strain for σ3=14KPa (100 kPa = 14.5 psi).

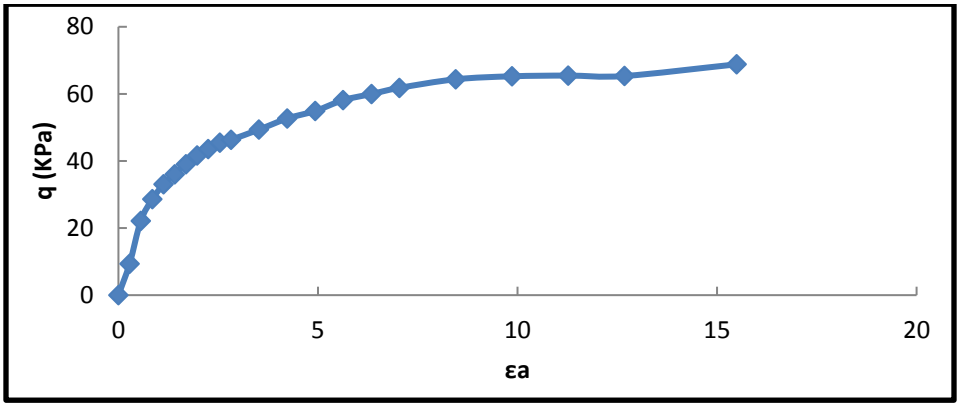

Figure 36. Stress-Strain Curve for σ3=31KPa (100 kPa = 14.5 psi).

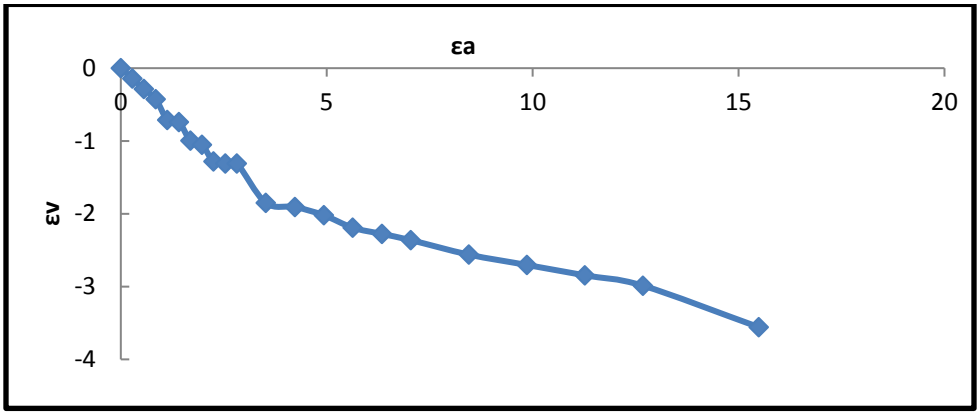

Figure 37. Volumetric Strain vs. Axial Strain for σ3=31KPa (100 kPa = 14.5 psi).

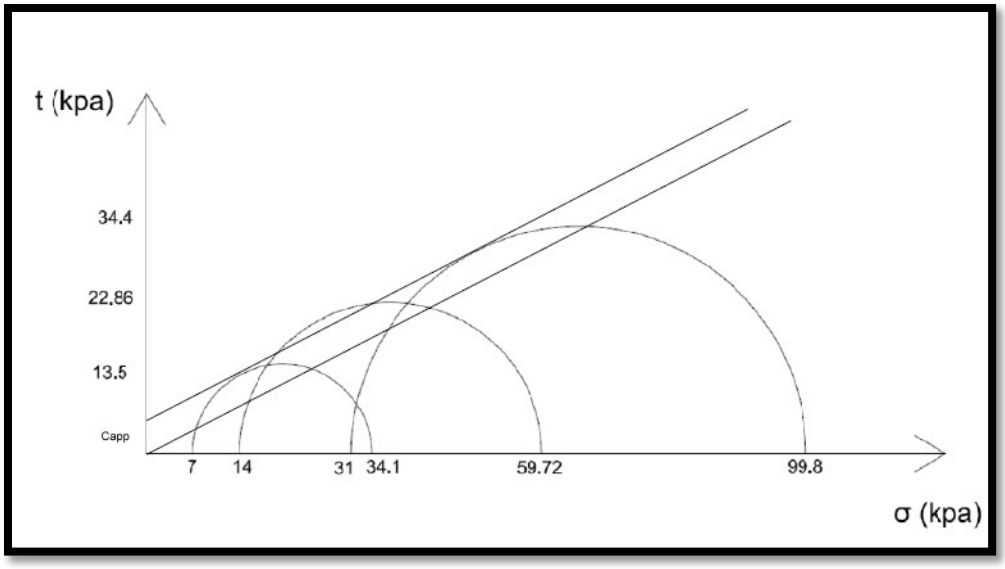

Figure 38. Triaxial Result for Backfill Material (100 kPa = 14.5 psi).

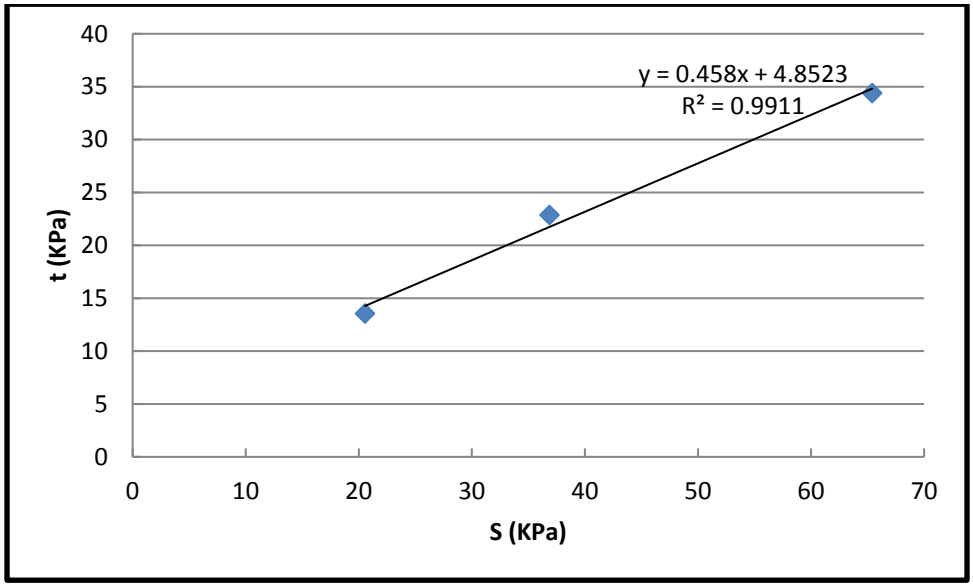

Figure 39. Results in s-t Plain (100 kPa = 14.5 psi).

Wall Reinforcement

RECO provided the metal strips used for the reinforcement used in this study (Figure 40 and Figure 41).

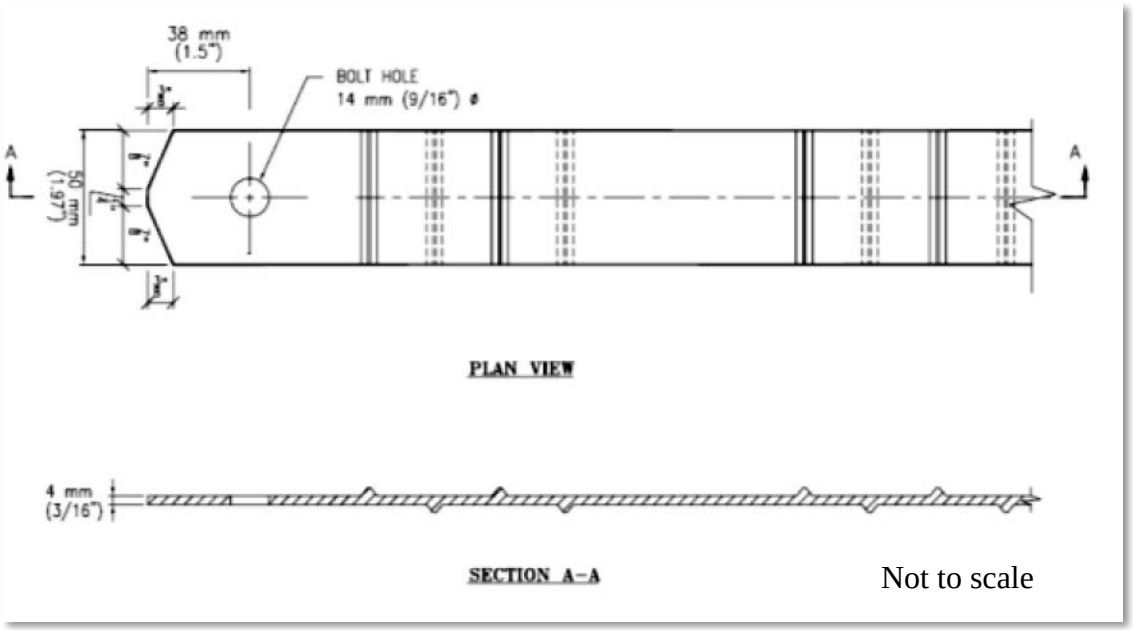

Figure 40. Details of Metal Strip.

Figure 41. Photos of the Strips Provided by RECO.

Drilled Shaft

The length of the drilled shaft is 17.5 ft, where the total length is distributed as follows (Figure 42[a]): 7.5 ft in the natural soil; 7.5 ft in the back fill material, and 2.5 ft above the back

fill level; this portion is necessary to apply the horizontal load. As indicated in Figure 42(b), the diameter of the drilled shaft is 2 ft. The rebar details are shown in the same figure. The drilled shaft was placed to have a full panel on top and a half panel on the bottom in front of the drilled shaft.

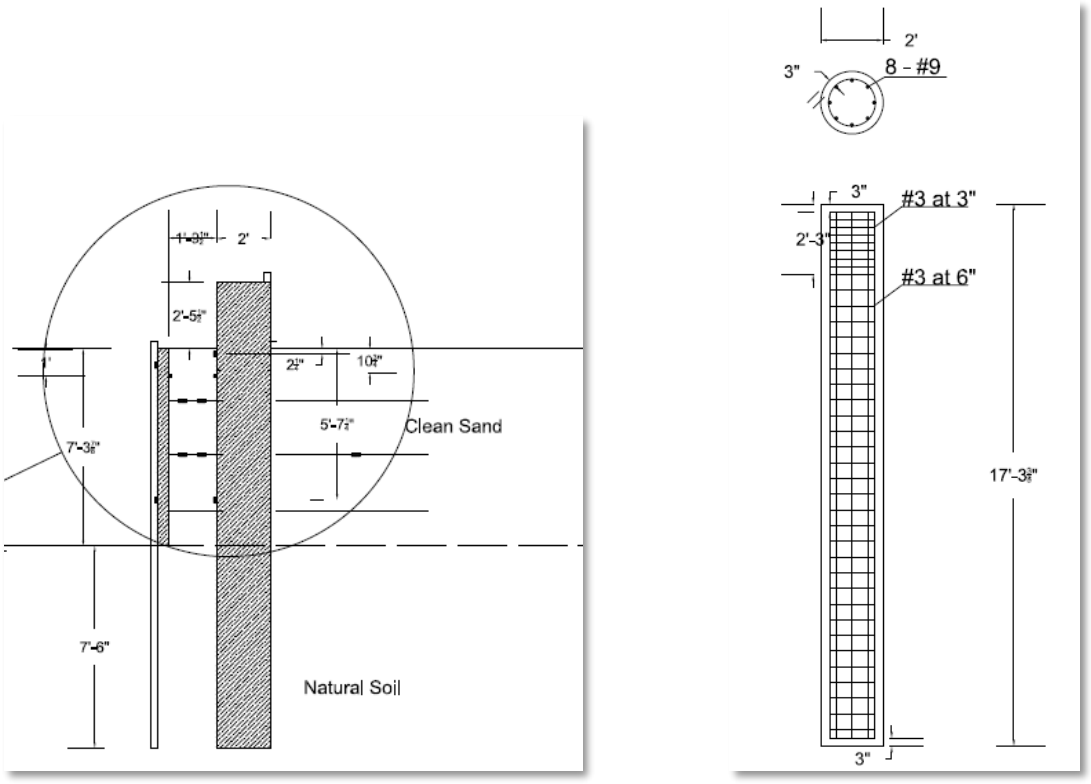

(a) **(b)**

Figure 42. Drilled Shaft Detail.

Instrumentation

To gather all of the information from the test, there were instruments installed on the wall and on the drilled shaft. Table 3 summarizes the instruments used in this project. It also presents the parameters measured and the location of each instrumentation.

Table 3. List of Instruments Used in the Project.

What to Measure	Device	Wall	Drilled Shaft
Horizontal Movement	Photogrammetry	Yes	No
	Survey	Yes	Yes
	Inclinometer	Yes	Yes
	Tiltmeter	Yes	Yes
	String potentiometer	Yes	Yes
Stress	Strain gauge	Yes	No
Earth Pressure	Earth pressure cell	Yes	Yes
Load	Load cell	No	No

Strain Gauge

Strain gauges were installed on the strips to measure the force transferred to them during the application of the horizontal loads. The axial force in the strips was the stress that was measured in the strips. The strain gauges are installed so that the stresses caused by bending and/or temperature changes are compensated. To compensate for these stresses, a full bridge circuit containing the four strain gauges was adopted for each position.

Before installing the strain gauges, the surfaces of the strips were smoothed out at all the places where the gauges needed to be glued. A rotating grinder with sandpaper was used for this purpose (Figure 43). The surface should be clean and shiny, like a mirror (Figure 44).

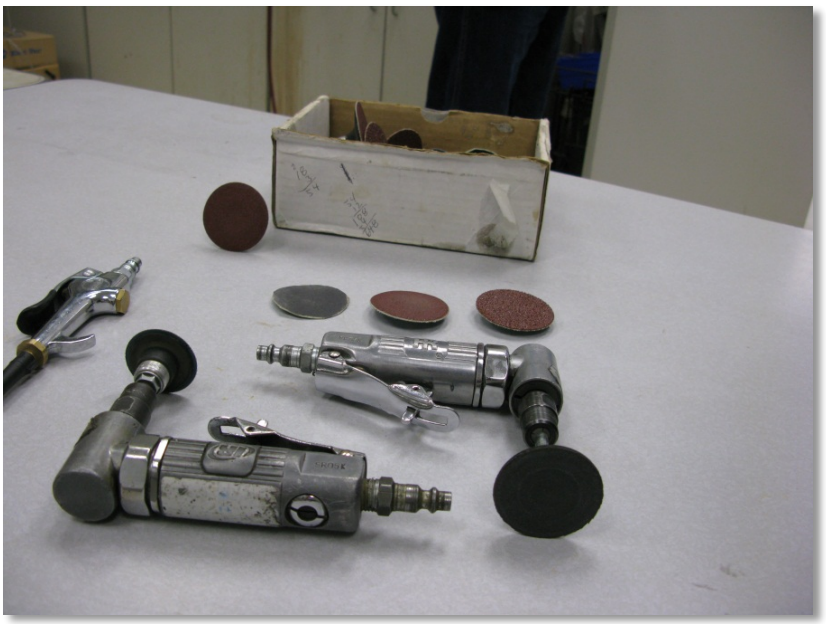

Figure 43. Rotating Grinder with Sandpaper.

Strain gauges and the corresponding connectors were installed using super glue (Figure 45) and were used to extend the wires. To protect the strain gauges and connectors, PVC tape was wrapped around them (Figure 46).

Figure 44. Clean and Shiny Surface.

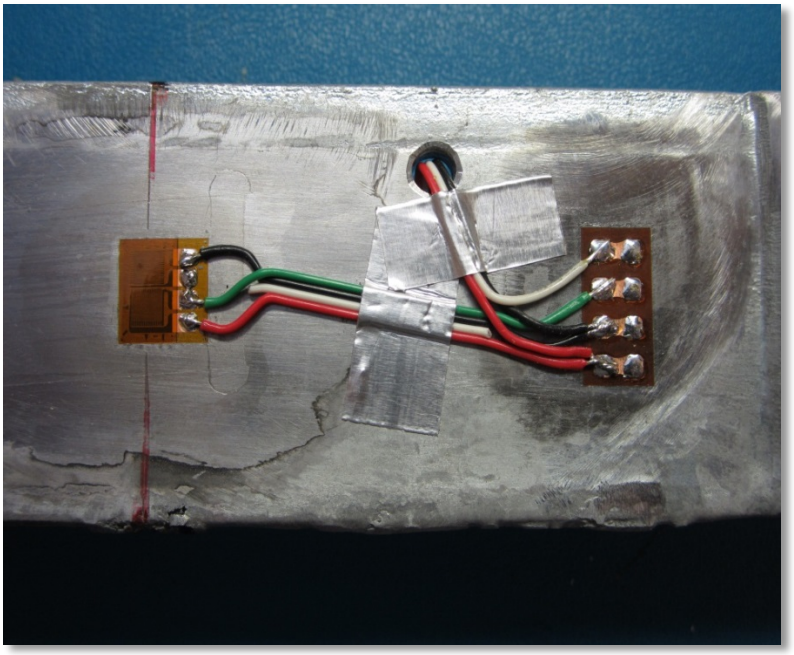

Figure 45. Strain Gauge and Connector Installed Using Super Glue.

Figure 46. Protecting Strain Gauges and Connectors Using PVC Tape.

Tiltmeter

Tiltmeters were used to record the rotation of the wall and drilled shaft (Figure 47). Two tiltmeters were installed on the drilled shaft and two others on the wall. They were installed at the same level in both the drilled shaft and on the wall to enable comparisons of deformation. The tiltmeters were placed inside aluminum boxes to protect them from any damage during wall construction (Figure 48). The tiltmeters were oriented in a way that they could measure the rotation perpendicular to the wall.

Figure 47. Tiltmeter Used in This Project.

Figure 48. Aluminum Box Used to Protect Tiltmeter.

Pressure Cell

Two pressure cells were used in this test. One of them was installed on the wall and the other one on the drilled shaft. These kinds of devices had rarely worked well in previous projects reported in the literature dealing with sand and gravel as fill material. To overcome this problem, two main decisions were taken in this project:

- Relatively larger and more precise pressure cells than the ones generally used in other projects were adopted for this project (Figure 49). They have a big diameter (8 in.) in order to prevent the arching that normally occurs in sand. They were also quite expensive (more than $1600 each cell).
- Special care was taken during the placement and compaction of the soil around the cell. This is to prevent the typical problems observed at the contact between the sand and the pressure cell. To solve this problem, the soil between the two pressure cells was compacted manually in small layers (i.e., around 4 in. each) (Figure 50).

The pressure cells were installed at the top of the wall and of the drilled shaft. The vertical distance between the center of the pressure cells and the top of the wall was 10 in. The maximum pressure occurred induced at the top part of the wall since the load was applied at the top of the drilled shaft.

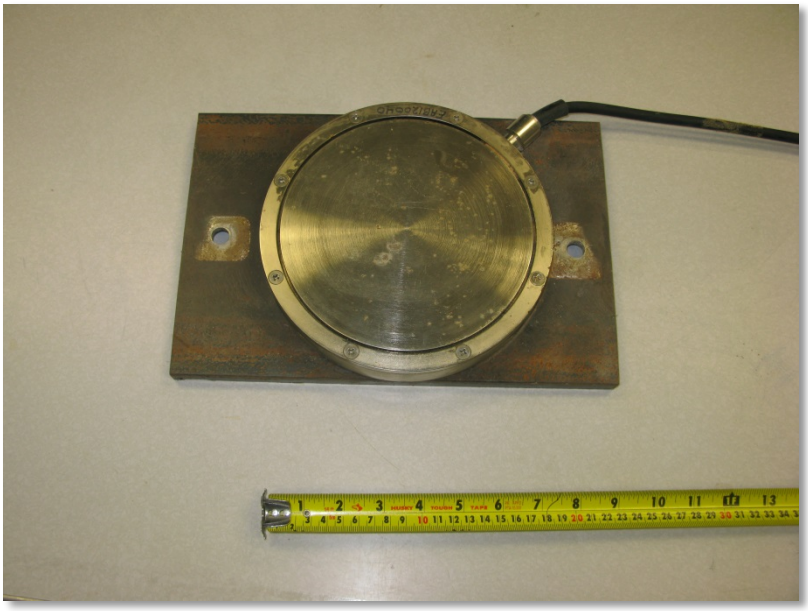

Figure 49. Pressure Cell Used in the Test.

Figure 50. Manually Compacted Area between Two Pressure Cells.

Inclinometer

In addition to the tiltmeters, inclinometers were used in this test for measuring the deformation of the wall and drilled shaft (Figure 51). On one hand, the inclinometer provides the whole profile of deformation (i.e., in the total length analyzed, in the wall or drilled shaft) at given times (e.g., when the measurements with the inclinometer probe took place). On the other hand, the tiltmeters provide continuous information in time, but only for the position where the

device is installed. In order to have complementary information about the deflections in this study and to provide some redundancy, researchers decided to use both.

Figure 51. Inclinometer Probe.

When doing the measurements with the inclinometer, the probe (Figure 51) should go through a plastic casing, and the data are read at pre-established depths. The plastic casings needed to be installed in advance. An important aspect of this technique is to have a good zero (i.e., a reference) reading for the deflections. This is achieved by installing the casing up to a depth where there is no anticipated deflection (i.e., reference for the measurements). In this project, the casing for the wall went into the natural soil (under the wall) to a depth equal to one times the wall height (7.5 ft). The casing went only 3 ft (Figure 52) below the bottom of the drilled shaft. This was due to drilling constraints.

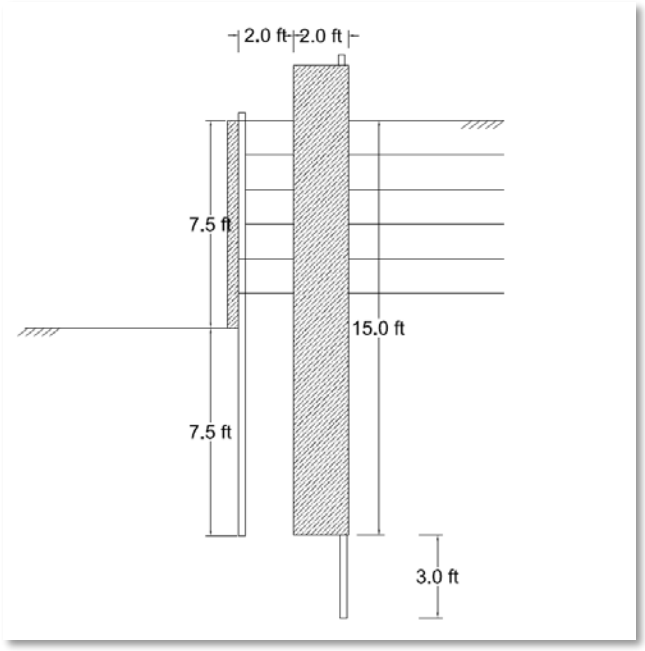

Figure 52. Detail of the Casing.

Photogrammetry

Photogrammetry was used to track the wall deformation. Thirty targets were installed on the wall (Figure 53). On each target a mark of exactly 4 in. (10 cm) in black was included. During the loading test, a camera was used to take pictures of the wall with those signs on the wall face after each load step. A key aspect is that the camera cannot be moved during the test. To ensure that the camera is fixed, a remote device should be used for capturing the photos. This will prevent any small movements that may be caused by the operator while manually capturing the photo from the main camera.

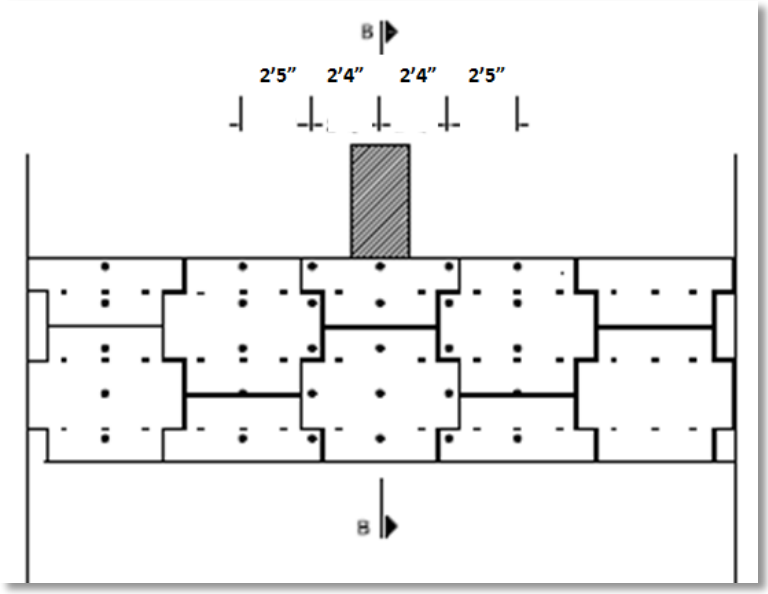

Figure 53. Photogrammetry Signs.

For each load step and each target, two pictures were taken and could be compared with the initial state of the wall to get the deformation of the targets points.

To process the photos, these steps have to be followed:

1. Take the initial picture (t=0) to the CAD program and make it first layer.
2. By using the image processing part of the software (like Photoshop) the target photo can be made transparent.
3. Take that picture to CAD and study a second layer.
4. Measure the movement of the targets.
5. Compare the movements with the known length of the black part (4 in.) and calculate the movements.

The targets were made of 3-in. PVC tubes (Figure 54). To install them on the wall, PVC floor drains were used (Figure 55). Figure 56 shows a sample photo used for the photogrammetry study.

In order to be sure that temperature and sunshine did not affect the targets, a number of control signs, installed at the far end of the wall, were used as reference. The length was measured before and after the test. The length was exactly the same, which indicated that the temperature had practically no impact on the results.

Figure 54. PVC Tube Used for Photogrammetry.

Figure 55. Floor Drain Used to Install PVC Tubes on the Wall.

Figure 56. Sample Photo Used for Photogrammetry.

String Pot

String pots were used to measure the absolute displacement of the top of the drilled shaft with respect to the top of the wall. Figure 57 shows the string pot used in this project. A fixed point was needed to attach one end of the string pot to the wall (i.e., the reference point). A metal rod was installed 14 ft behind the wall facing to make sure it would not move during the test. The other end of the string pot was attached to the drilled shaft. Another string pot was used between the drilled shaft and the wall (Figure 58).

Figure 57. String Pot Used in This Project.

Figure 58. Fixed Point and String Pots.

Loading

To apply the load to the drilled shaft, a hydraulic jack (Figure 59) and pump were used (Figure 60). The jack capacity was 100 kips, and the maximum allowed movement of the piston was 6 in.

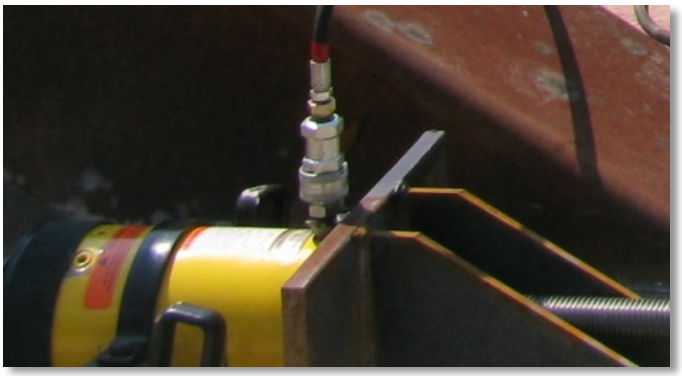

Figure 59. Hydraulic Jack.

Figure 60. Pump for Hydraulic Jack.

For the application of the load, a pulling system was designed. The pulling frame was installed in front of the wall on the pavement (Figure 61[a]). Another loading frame was installed on the drilled shaft (Figure 61[b]).

(a) **(b)**

Figure 61. Load Frame on (a) the Pavement and (b) the Drilled Shaft.

The load frames (both on the drilled shaft and on the pavement) were designed for a maximum force of 100 kips. Figure 61 shows details of the frames and their locations in the test setup.

Construction of the Wall

The first step for constructing the wall was the excavation (Figure 62). As mentioned before, the height of the wall was 7.5 ft; the bottom of the excavation was set in order to achieve the required wall elevation. The slopes for the excavation were 45° in all directions.

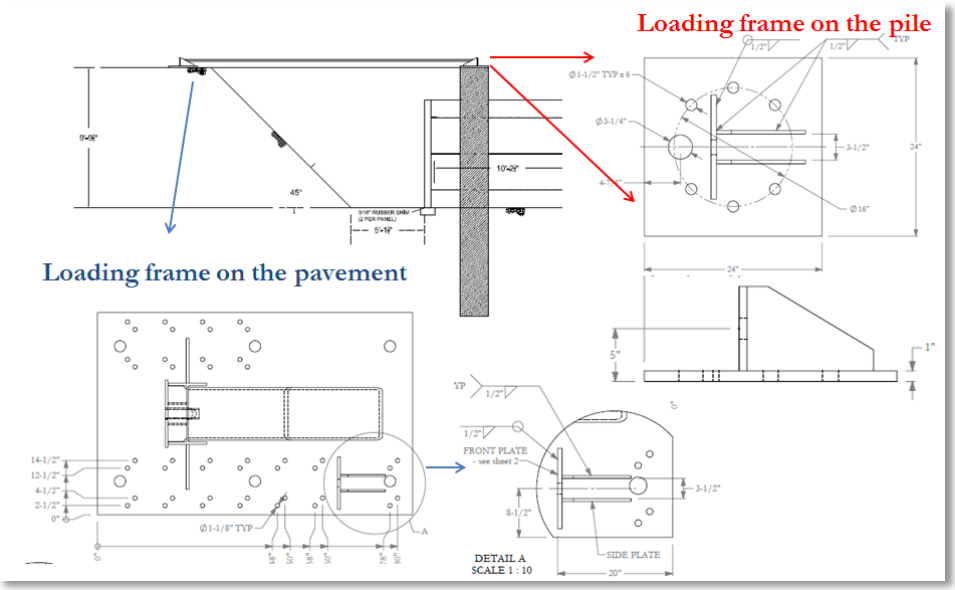

Figure 62. Details of Loading Frames.

Figure 63. Excavation.

Once the excavation had been completed, it was time for constructing the foundation of the wall (Figure 63). Before pouring the concrete, one important aspect for this project was to leave an empty space in the foundation for the inclinometer casing in the exact position where researchers wanted the inclinometer readings to be taken.

Once the foundation was finished, the installation of the panels began. The panels were installed in rows and were held by wooden brackets. Figure 64 presents how the panels remained vertical until the reinforcements and fill were placed.

Figure 64. Wall Foundation.

Figure 65. First Rows of Panels.

The drilled shaft was constructed just after the excavation was completed and before the wall (Figure 65). The casing for the inclinometer in the drilled shaft was attached to the rebar cage (Figure 66).

Once the first row of panels was placed, the backfill material was compacted. The sand was poured behind the panels and compacted until the level reached the first layer of strips (Figure 67). The strips were then placed layer by layer and the installation continued following the same procedure for the other levels of reinforcements (Figure 68).

Figure 66. Drilled Shaft behind the Wall.

Figure 67. First Layer Compaction.

Figure 68. Installed Strips (First Layer).

Compaction

The backfill was compacted in 6 in. (152.4 mm) to 12 in. (304 mm) thick lifts with 6 passes of a 2,176 lb (9.7 kN), 35 in. (890 mm) wide drum roller. The maximum dry density of the backfill was 117.8 pcf (18.5 kN/m^3), as determined by the modified compaction Proctor test (Figure 69).

Two nuclear density tests were conducted at the level of the bottom layer of the strips (Figure 70). The average dry density and water content were 111.7 pcf (17.5 kN/m^3) and 3 percent, respectively. This dry density represents 95 percent of the maximum dry density obtained in the modified Proctor test for the backfill material (ASTM D1557-12 2000).

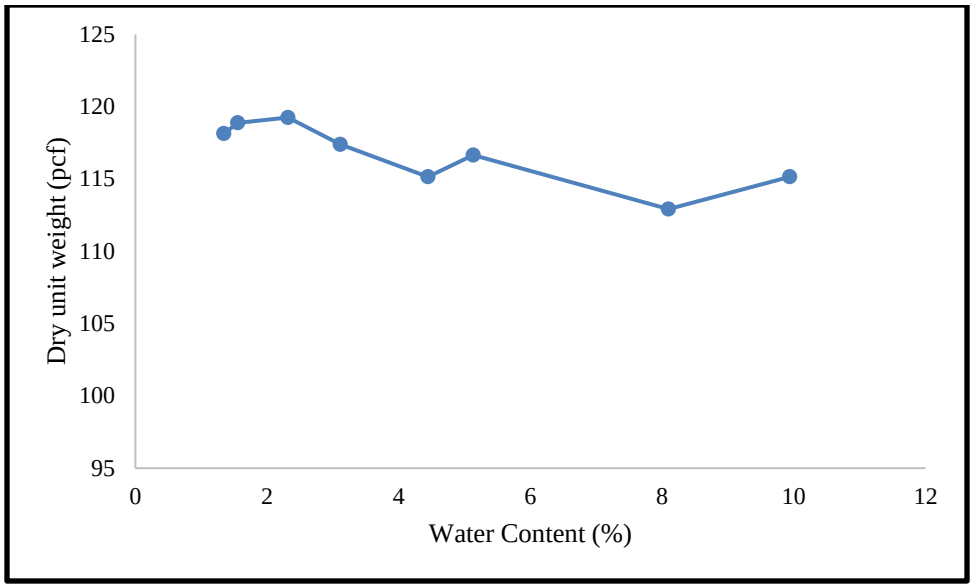

Figure 69. Compaction Curve.

Figure 70. Nuclear Density Test.

Loading Test

The loading test was carried out on Wednesday, August, 22, 2012. It started at 10:45 a.m. and ran for 3 hours (Figure 71).

Figure 71. Photo Taken during the Load Test.

Due to the large amount of data gathered during the loading test, two data loggers were necessary. All of the instruments except the tiltmeters were connected to the main data logger (NGES one). In total, 20 channels were used to read the data collected during the test every 30 seconds. The data associated with the inclinometer was read manually after each load step. Figure 72 shows different key positions associated with the load test.

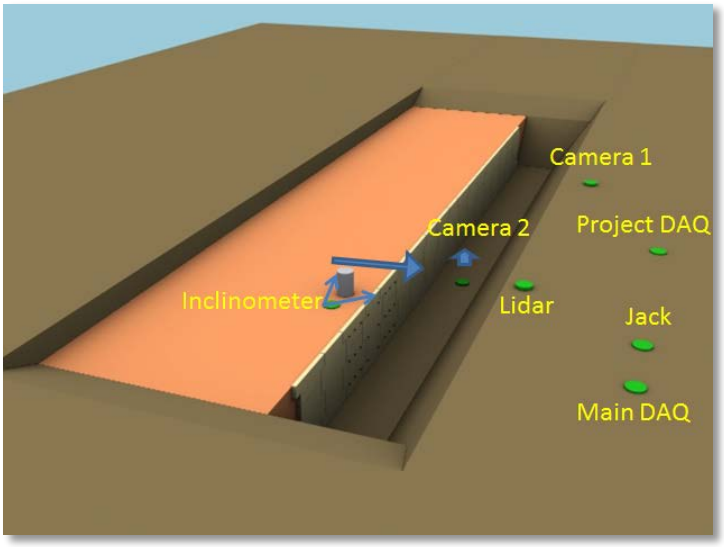

Figure 72. Main Positions Associated with the Loading Test.

Loading Protocol

Some key aspects of the load test are listed as follows:

- It was a static test with load control.
- The horizontal load was applied by pulling the drilled shaft against the wall using a hydraulic jack.
- The data acquisition system recorded the data every 30 seconds.
- The load was applied in steps of 5 kips.
- Each loading step lasted 15 minutes.
- For each loading step, inclinometer readings, LIDAR scanning, and digital photos of the face of the wall were taken.
- An unloading stage took place at a load of 20 kips.
- The unloading was done in steps of 5 kips.
- The duration of each unloading step was around 1 minute.
- The reloading was performed by increments of 5 kips until 20 kips had been reached.
- The duration of each reloading step was around 1 minute.
- Another unloading stage took place at a load of 35 kips.
- As before, reloading after 35 kips was continued until wall failure.
- The failure was at 40 kips.
- At failure, a displacement of 6.13 in. at the top of the drilled shaft was measured.

- At failure, a displacement of 4.15 in. at the top of the MSE wall in front of the drilled shaft was measured.
- At the end of the last loading stage, the unloading was performed.

Figure 73 presents the loading protocol.

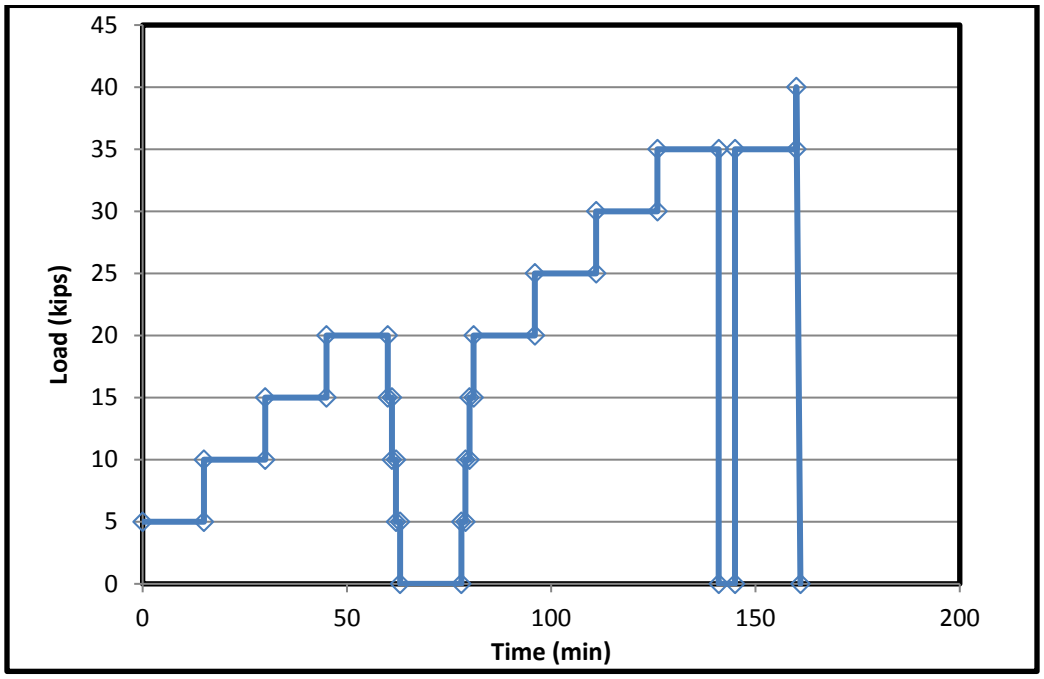

Figure 73. Loading Steps.

Results

In the following sections, some relevant plots combining the more relevant information are presented to assist in the interpretation of the experiment during the load test and to learn about the behavior of the drilled shaft and main components of the wall.

Load-Displacement Curve

One of the main goals of the test was to study the displacement of the wall and of the drilled shaft during the different horizontal load steps. The maximum displacement of the wall occurred in front of the drilled shaft. String pots were used to measure the maximum displacement of both the drilled shaft and wall. Figure 74 shows the load-displacement curve for the drilled shaft. The maximum displacement of the drilled shaft was 6.13 in. and took place at

the horizontal load of 40 kips. At that load, the maximum displacement of the wall was 4.15 in., shown in Figure 75.

Figure 76 shows the displacement of the drilled shaft against the wall displacement. As expected, drilled shaft deformation is greater than wall deformation at every step. The difference between these two movements is related to the soil compression.

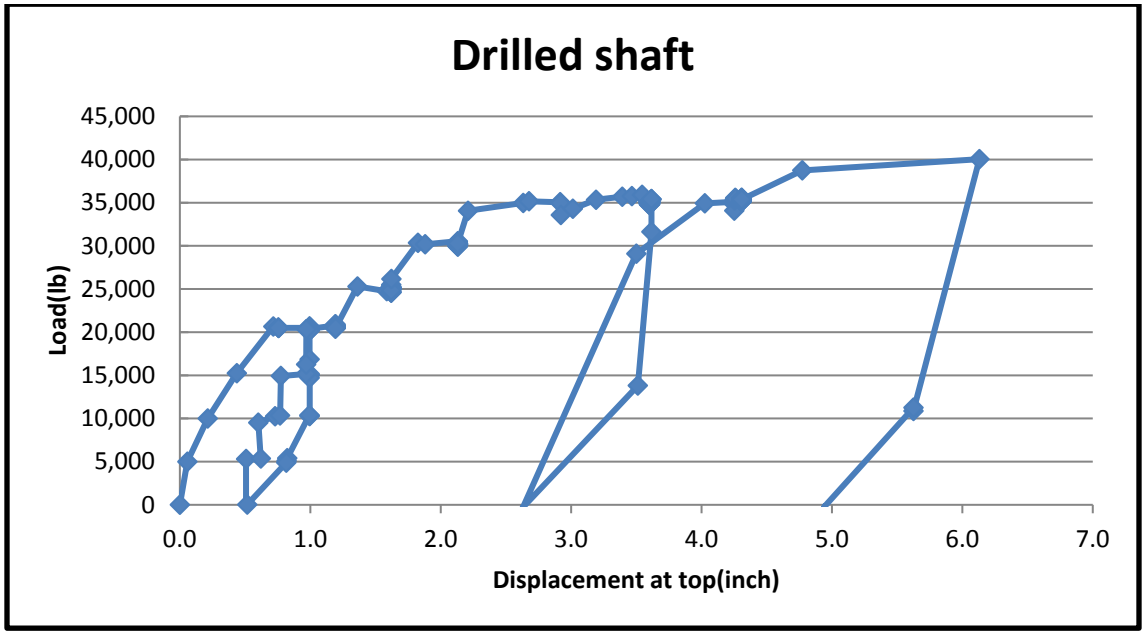

Figure 74. Load-Displacement for the Drilled Shaft.

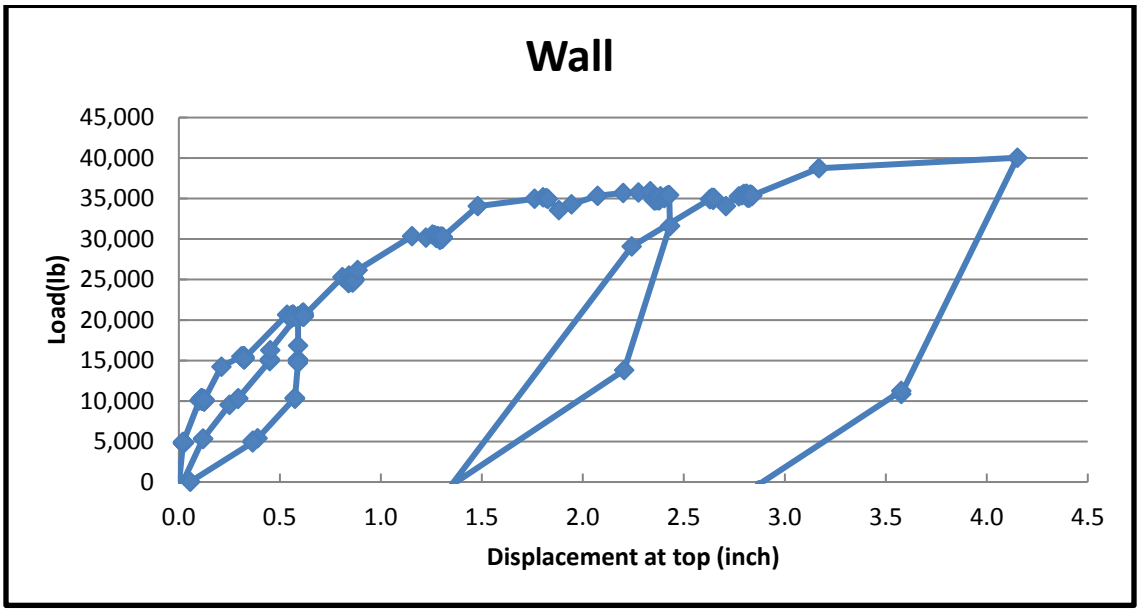

Figure 75. Load-Displacement for the Wall.

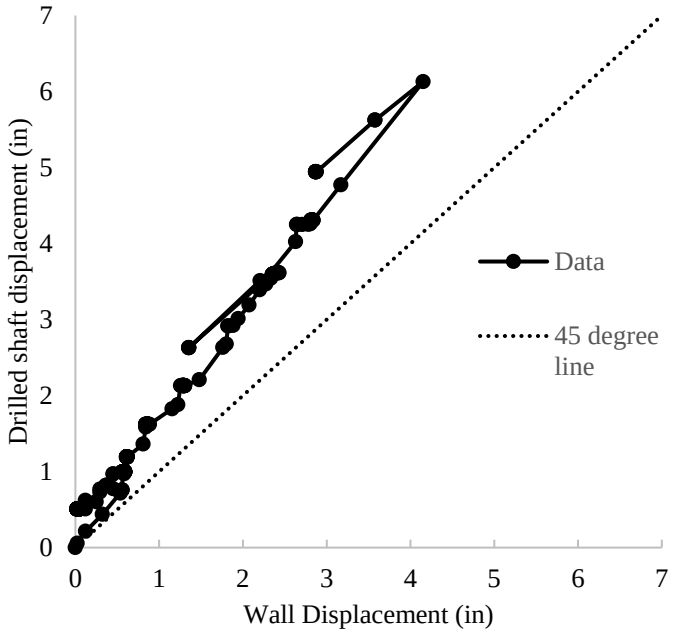

Figure 76. Plot Showing the Drilled Shaft against the Wall Displacement.

Load in Strips

Other very relevant results obtained from the test were the loads developed in the strips during loading. As mentioned before, all of the horizontal loads are taken by the strips in MSE walls. Strain gauges were used to measure the stresses in the strips. There were six instrumented strips in the upper part of the wall. One of the instrumented strips had four strain gauges (S-4-1). Two of them had 2 strain gauges (S-2-1 and S-2-2) and three of them had only 1 strain gauge (S-1-1, S-1-2, and S-1-3). Figure 77 shows the positions of those strips (as coded). The selection of the instrumented strips and the distribution of the gauges along those strips were based on numerical modeling performed before the test and were aimed at designing the instrumentation. For example, the model predicted that the forces in the second layer of strips were higher than the ones in the top layer. Accordingly, the strips with more instruments were located in the second layer. The strip with four gauges was instrumented to learn about the distribution of stresses along the strip.

The results associated with forces in the strips are presented and grouped into two categories: forces in the strips developed due to the geostatic forces only, and forces developed

due to the horizontal load applied by the drilled shaft only (i.e., without geostatic effects). The case without the geostatic forces is used for studying the effect of the lateral load on the strips.

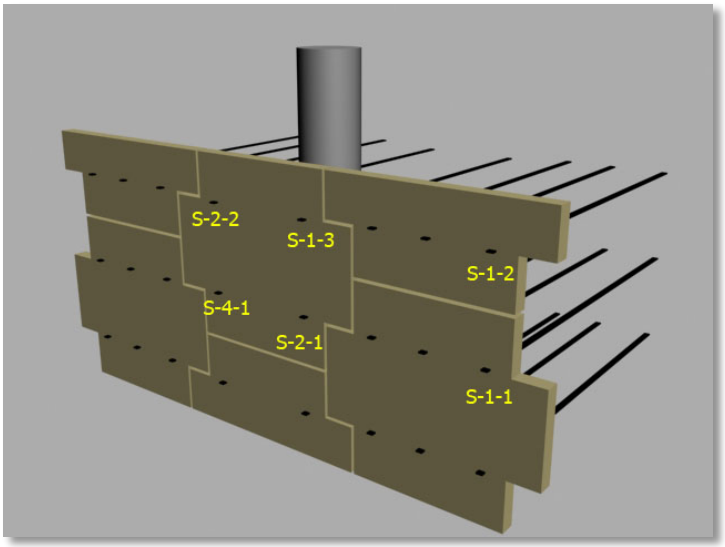

Figure 77. Strips Numbers and Positions.

As mentioned before, the strip with more instruments is the one with four gauges (S-4-1). Figure 78 shows the position of the strain gauges on that strip.

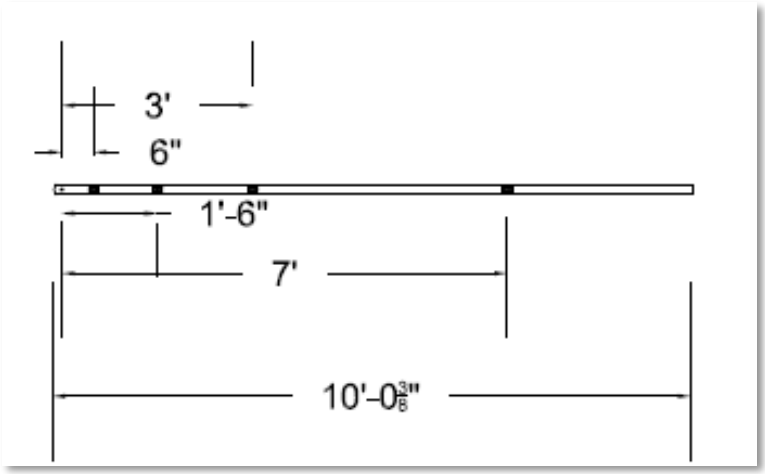

Figure 78. Strip with Four Strain Gauges (S-4-1).

Figure 79 presents the forces developed in strip S-4-1 for the different positions in the strips and load steps considered in the load test. As expected, the force in the strip decreases with the distance from the wall. The maximum force in the strip does not occur at the maximum

horizontal load applied to the drilled shaft. In this case, the maximum force in the strip is 3.86 kips and it occurred at the horizontal load of 25 kips.

Figure 80 presents the forces in the strips, including geostatic forces. In this case, the maximum force in the strip was 4.7 kips.

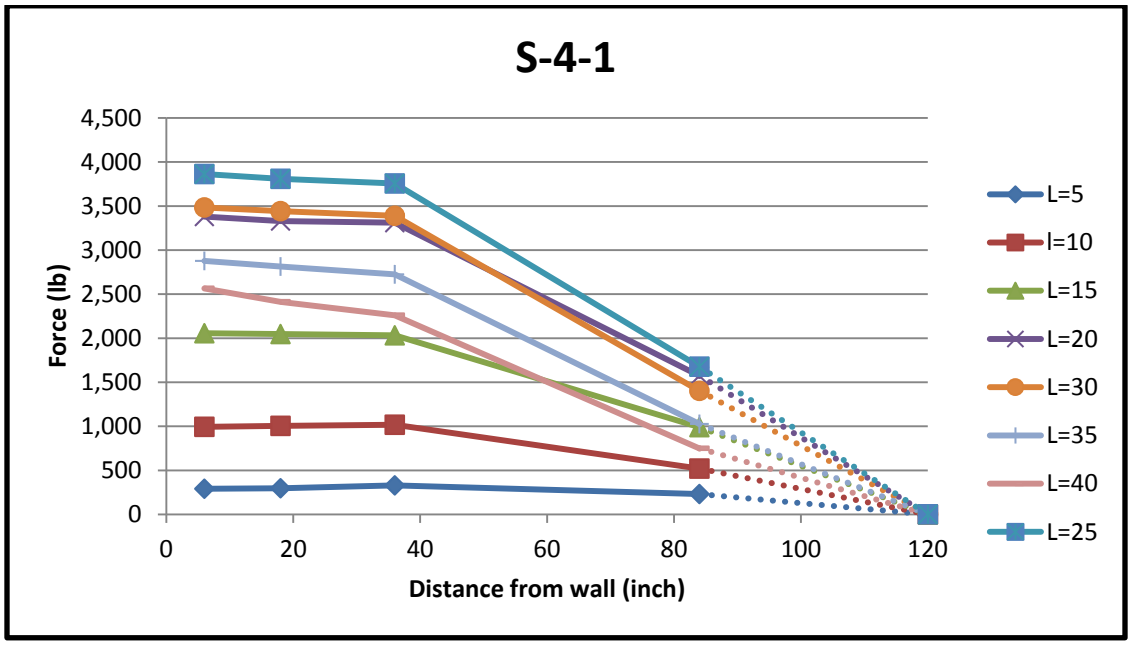

Figure 79. Force in the Strip S-4-1 excluding the Geostatic Force.

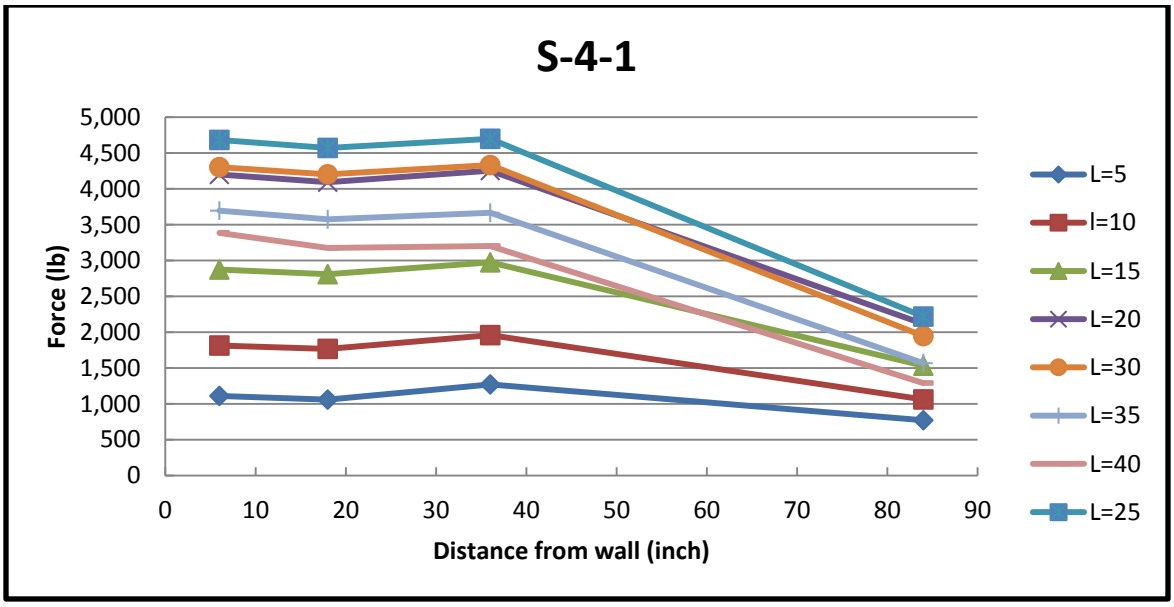

Figure 80. Force in the Strip S-4-1 including Geostatic Force.

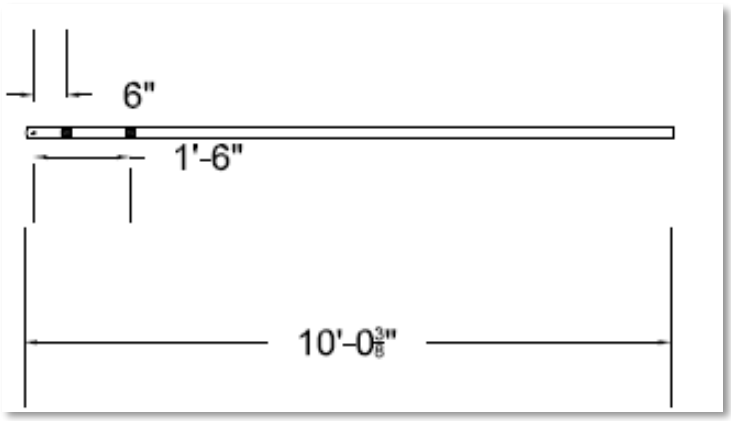

Figure 81. Two Strain Gauge Strip.

As can be seen in Figure 77, there are two strips with two gauges. Strip S-2-1 was installed in the second layer, and strip S-2-2 was installed in the top layer. Figure 81 shows the positions of the gauge in the strip. Figure 82 and Figure 83 present the results for these two strips (i.e., S-2-1 and S-2-2) in the case of no geostatic forces. The maximum force in strip S-2-1 was 3.4 kips, which occurred at a lateral load of 30 kips, and the maximum force in strip S-2-2 was 1.6 kips and occurred at the lateral load of 15 kips. The forces in the second layer of strips are greater than the ones in top layer. These observations confirm the results anticipated by the numerical modeling. When considering geostatic forces, the maximum forces in strips S-2-1 and S-2-2 are 4.1 kips and 1.8 kips, respectively (Figure 84 and Figure 85). Also in this case the maximum force in the strip did not occur when the maximum lateral load was applied.

Note that maximum force in the strip for both the geostatic stresses and the increase in stress due to the horizontal load on the drilled shaft occurred at the level of the second strip and not the top first strip. However the top strip has less ultimate resistance since it is subjected to a smaller geostatic vertical stress.

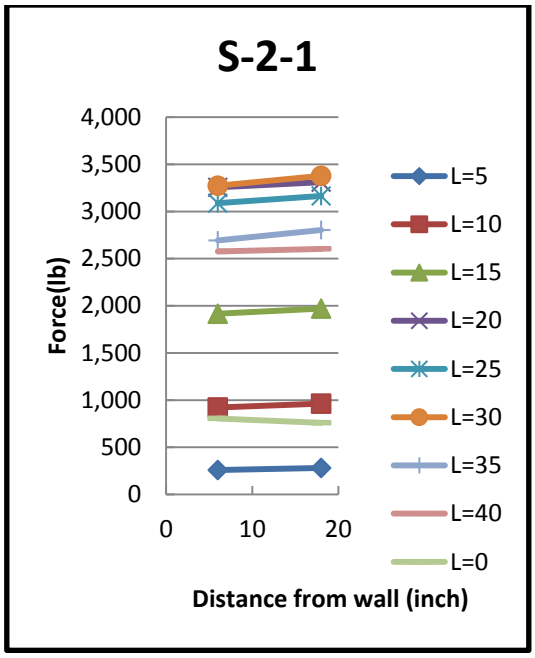

Figure 82. Force in the Strip S-2-1 excluding Geostatic Force.

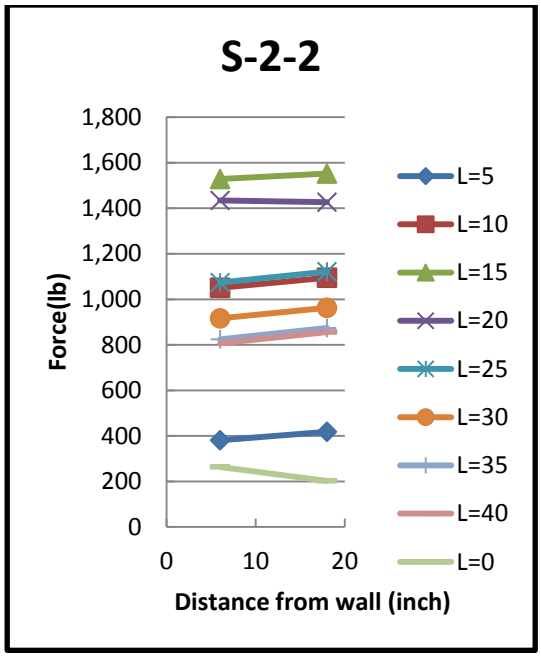

Figure 83. Force in the Strip S-2-2 excluding Geostatic Force.

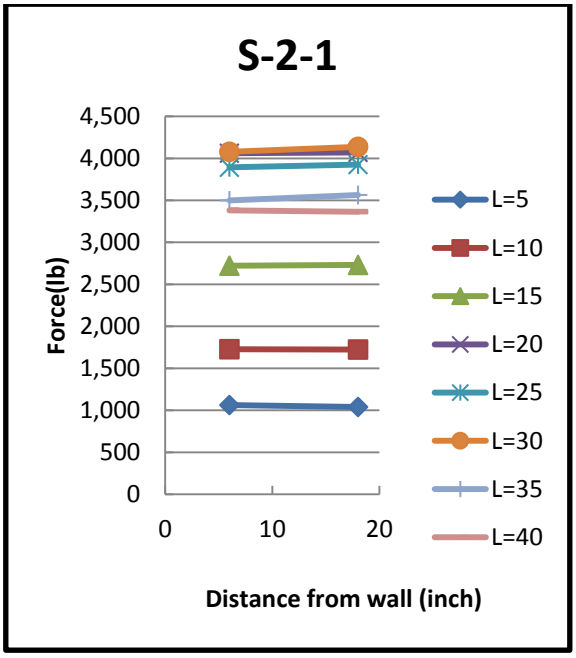

Figure 84. Force in the Strip S-2-1 including Geostatic Force.

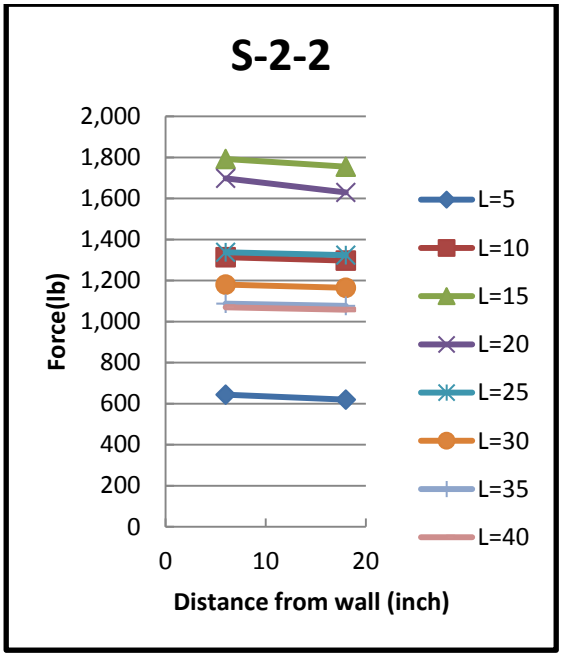

Figure 85. Force in the Strip S-2-2 including Geostatic Force.

Another interesting aspect to study is the relationship between the force measured in each gauge and the lateral load on the drilled shaft. This aspect has been analyzed for two strips, S-4-1 (located in the second layer) and S-2-2 (located in the top layer). The numbering is related to the distance to the concrete panel. Position A is the closest to the panel, and the one identified as D is the farthest. In position A for strip S-4-1, the maximum force measured was 3.86 kips, and it took place when a horizontal load of 25 kips was applied (Figure 86). The force measured in gauge B (in the same strip) is very close to the value observed in position A. In Figure 87, it can be observed that the maximum force was 3.81 kips. If geostatic forces are considered, the maximum force in gauge A is 4.7 kips (Figure 88), and for gauge B maximum force is 4.6 kips. (Figure 89)

As the distance from the panel increases, the force decreases (Figure 90). The maximum force in gauge C is 3.7 kips, and 1.7 kips was measured in gauge D (Figure 91). As shown in Figure 92 and Figure 93, maximum forces in gauges C and D including geostatic force, are 4.6 kips and 2.2 kips, respectively.

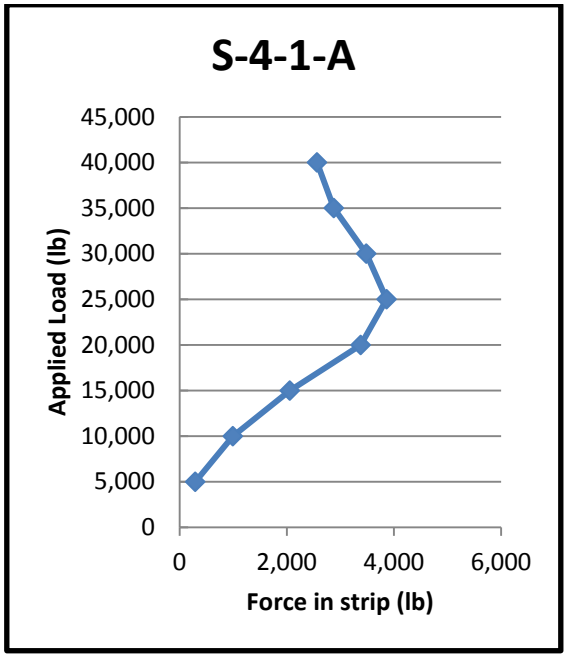

Figure 86. Force in the Strips S-4-1-A.

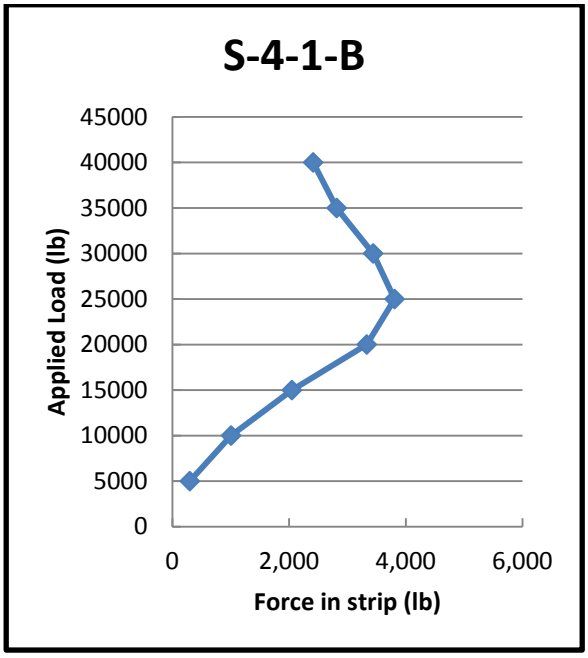

Figure 87. Force in the Strips S-4-1-B.

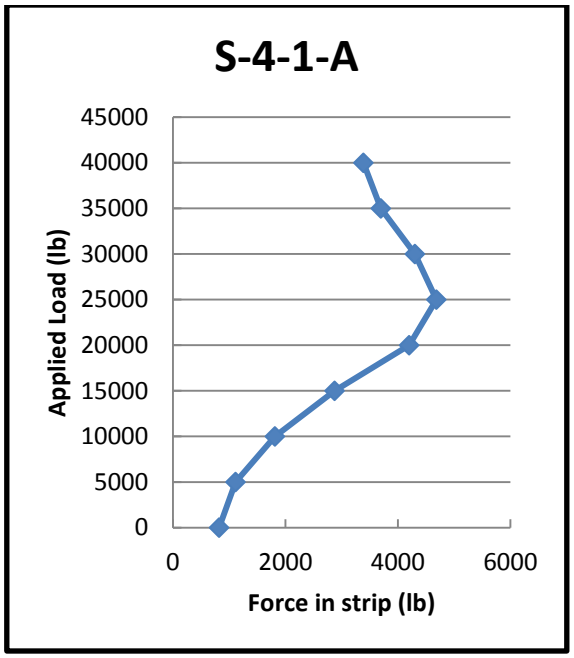

Figure 88. Force in the Strips S-4-1-A including Geostatic Loads.

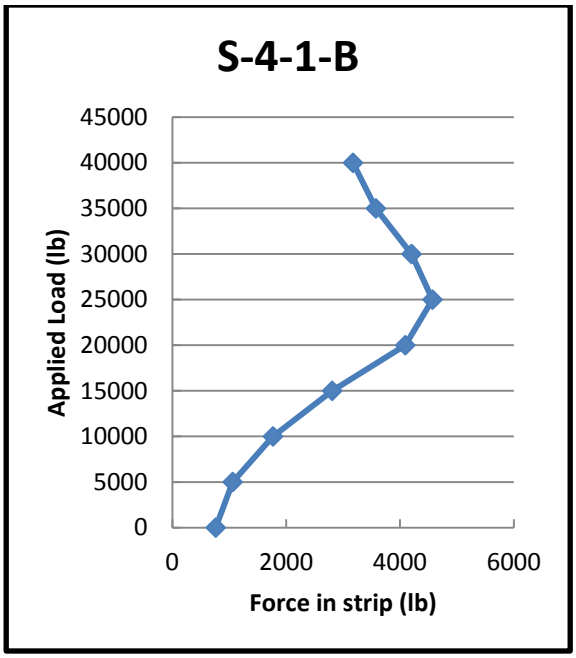

Figure 89. Force in the Strips S-4-1-B including Geostatic Loads.

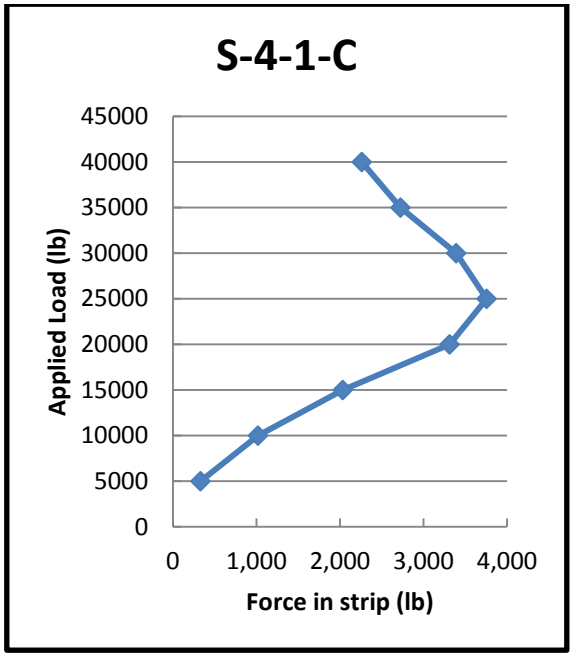

Figure 90. Force in the Strips S-4-1-C.

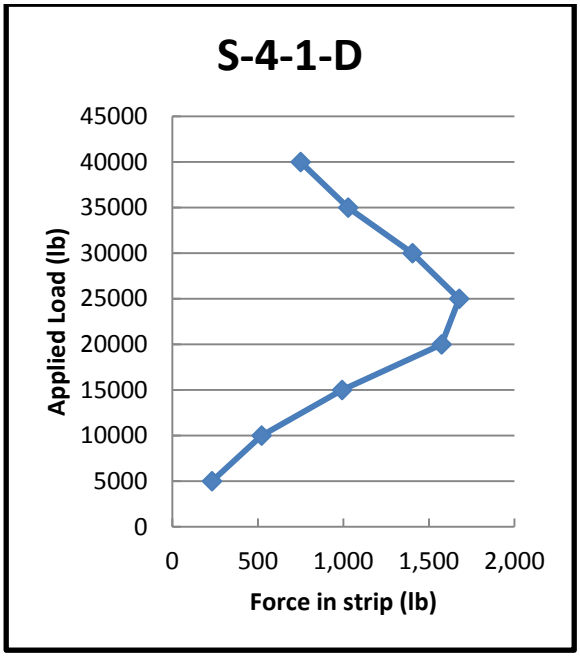

Figure 91. Force in the Strips S-4-1-D.

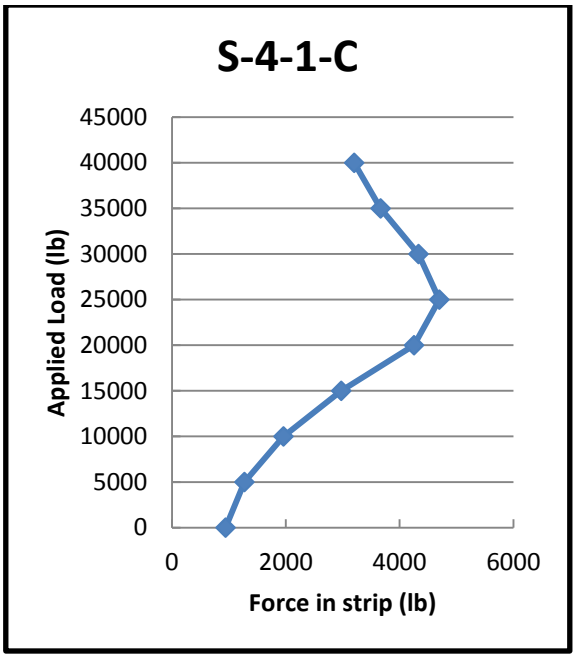

Figure 92. Force in the Strips S-4-1-C including Geostatic Loads.

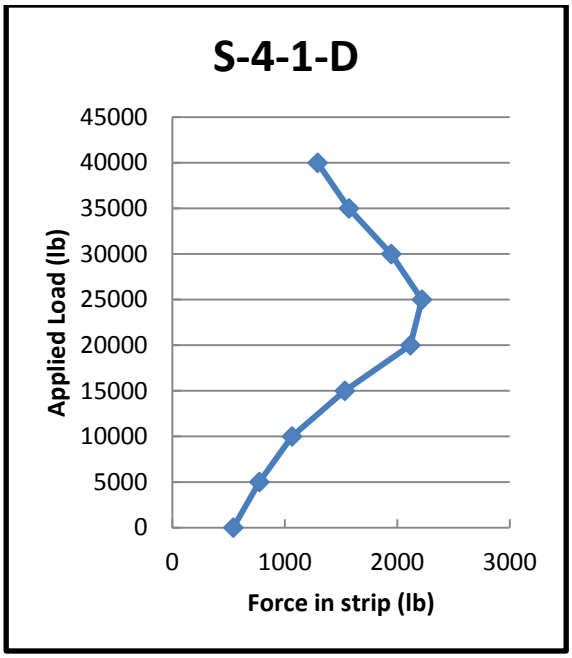

Figure 93. Force in the Strips S-4-1-D including Geostatic Loads.

Strip S-2-2 is the other reinforcement with two gauges studied in this section. It was located in the first layer adjacent to the drilled shaft. In Figure 94, maximum force in gauge A is 1.5 kips, and it occurred when a lateral load of 15 kips was applied. For gauge B, the maximum force is 1.6 kips (Figure 95). Considering geostatic forces, the maximum forces for gauge A and B are 1.8 kips (Figure 96) and 1.7 kips (Figure 97), respectively.

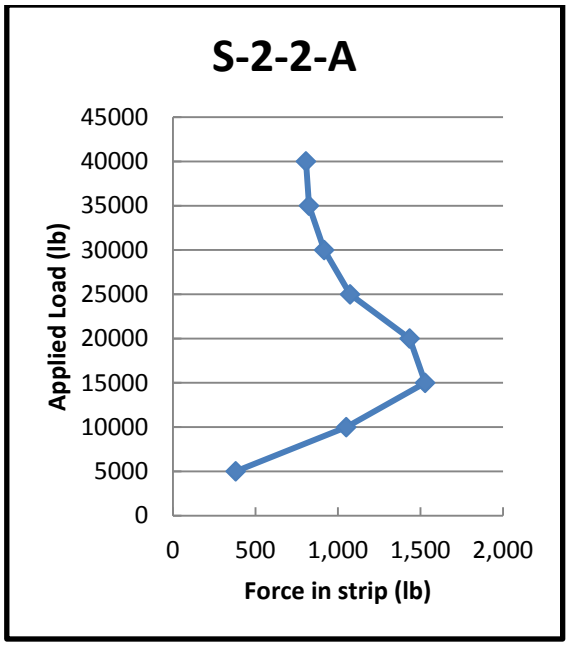

Figure 94. Force in the Strips S-2-2-A.

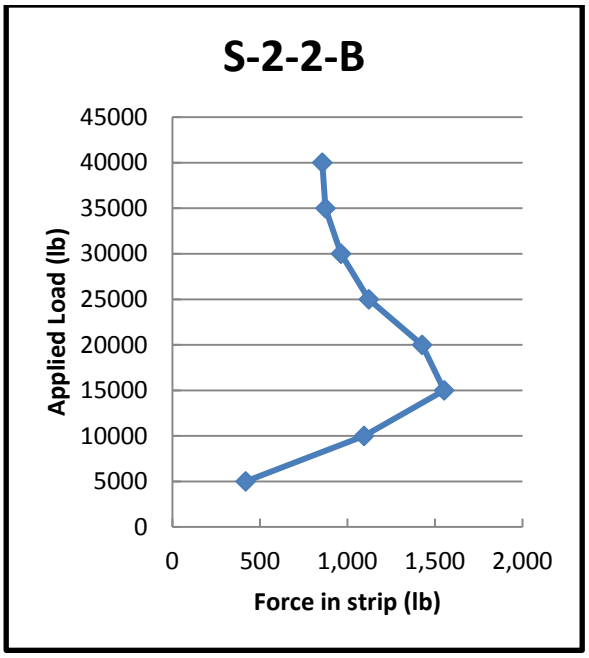

Figure 95. Force in the Strips S-2-2-B.

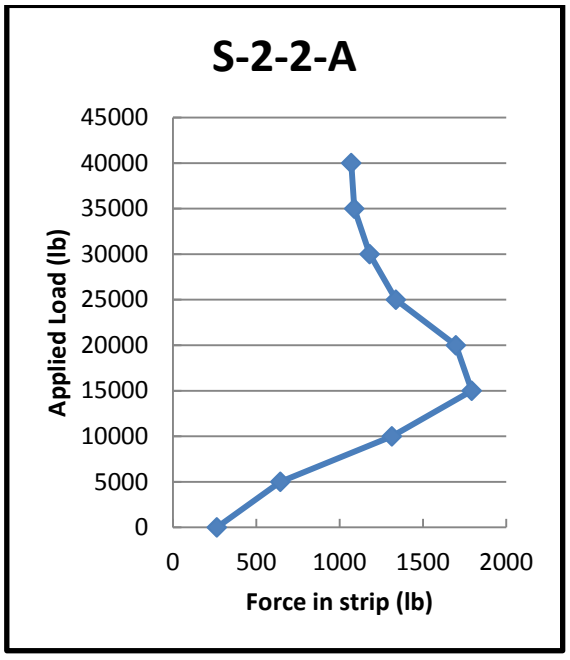

Figure 96. Force in the Strips S-2-2-A including Geostatic Loads.

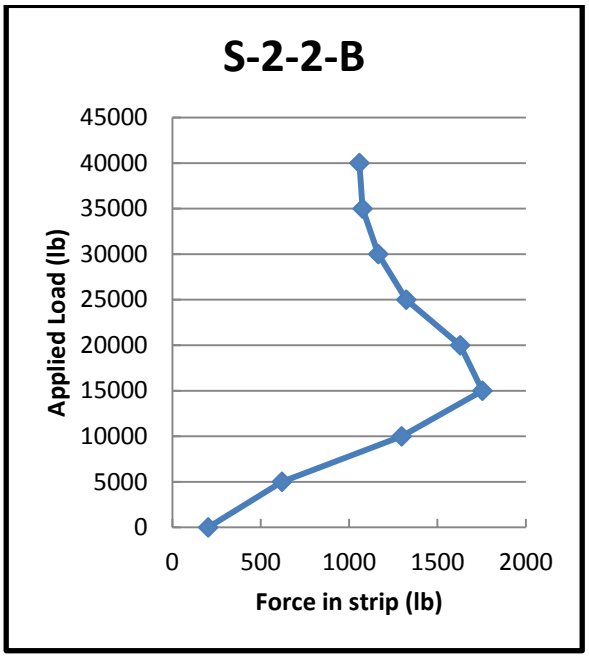

Figure 97. Force in the Strips S-2-2-B including Geostatic Loads.

The force distribution near the drilled shaft is another interesting result obtained from this test. In each layer, there is an instrumented strip at each side of the drilled shaft, one at 18 in.

from the drilled shaft and one at 77 in. from the drilled shaft. The data from these gauges were used to study the variation of forces in the direction parallel to the wall. In Figure 98, forces in the first layer of strips are shown. The 0 corresponds to the position of the drilled shaft. Figure 99 shows the distribution of forces in the second layer. The results for the case with geostatic forces are shown in Figure 100 and Figure 101 for the first and second layers of strips, respectively. As expected, a similar pattern is observed.

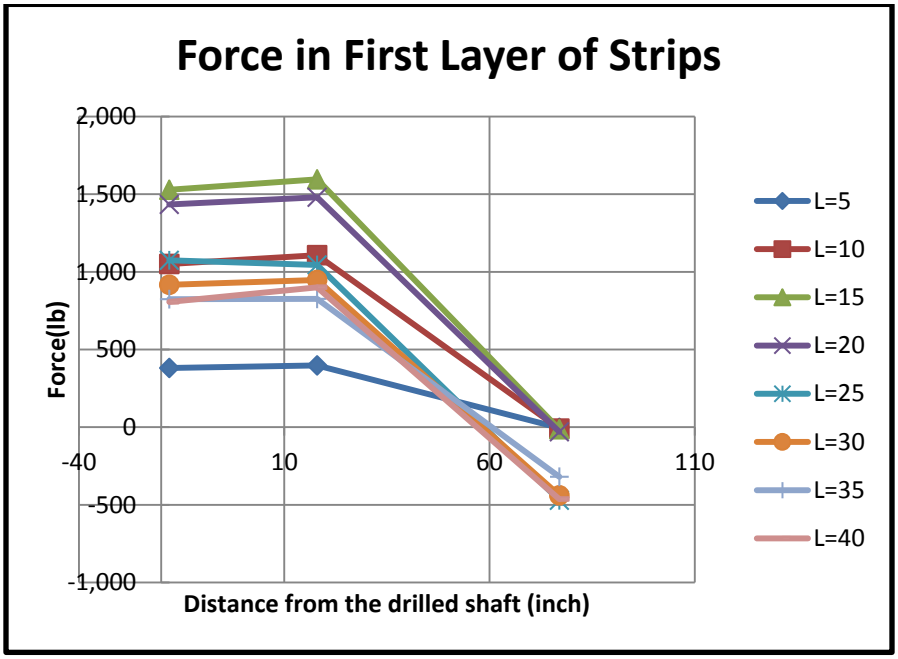

Figure 98. Distribution of Forces at Each Side of the Drilled Shaft in First Layer of Strips.

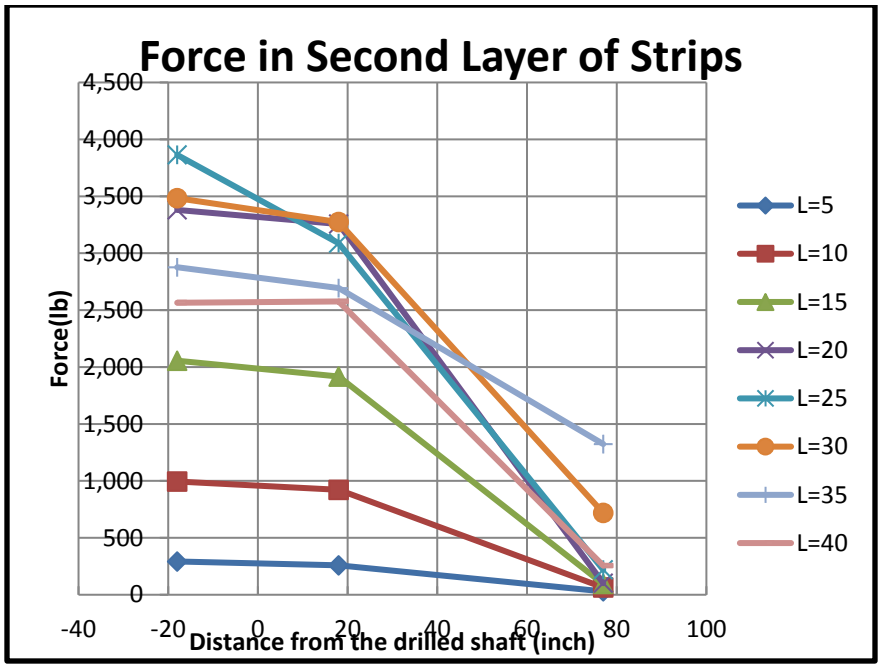

Figure 99. Distribution of Forces at Each Side of the Drilled Shaft in Second Layer of Strips.

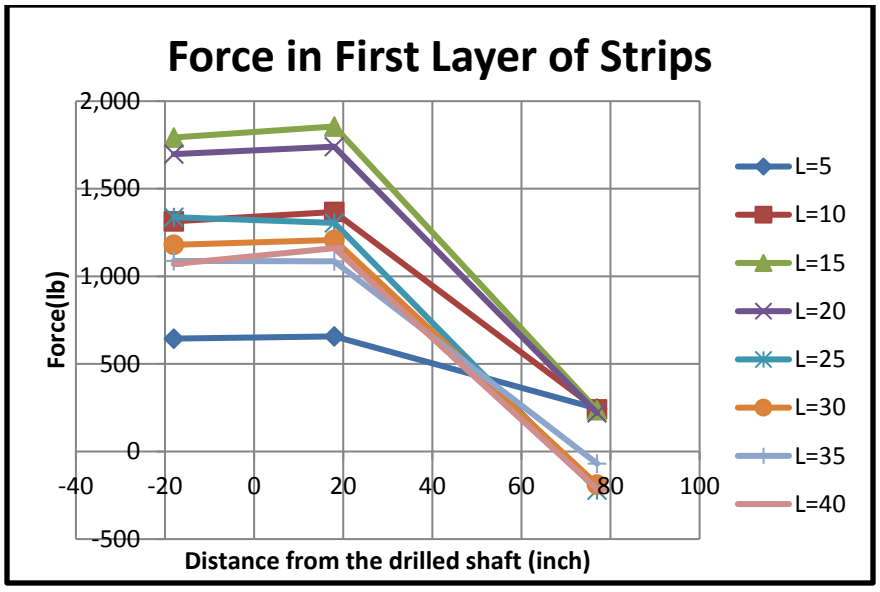

Figure 100. Distribution of Forces at Each Side of the Drilled Shaft in First Layer of Strips including Geostatic Loads.

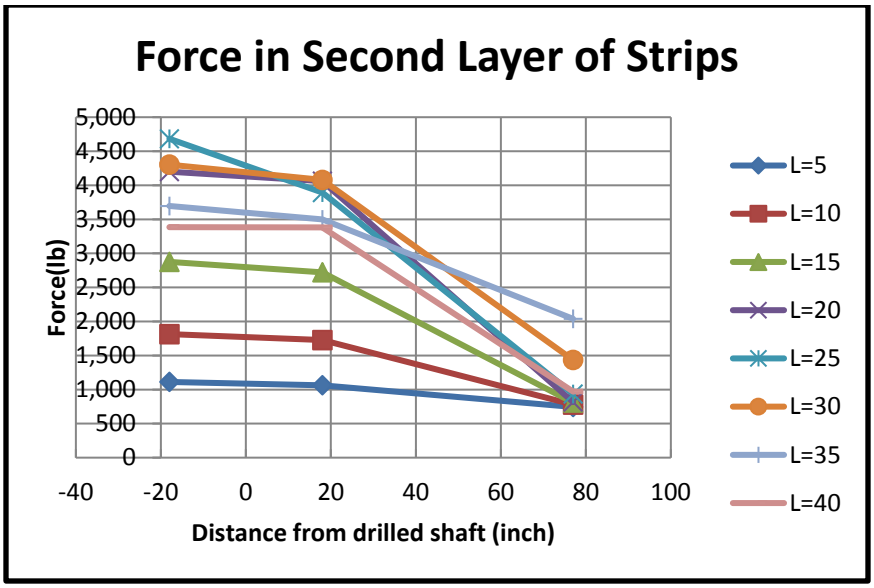

Figure 101. Distribution of Forces at Each Side of the Drilled Shaft in Second Layer of Strips including Geostatic Loads.

Pressure on the Wall and Drilled Shaft

One pressure cell was installed on the drilled shaft and another one on the wall. Figure 102 presents the results in terms of pressure on the drilled shaft against the lateral load. The maximum pressure on the drilled shaft was 17 psi. As seen in Figure 103, the maximum pressure on the wall was 7.8 psi.

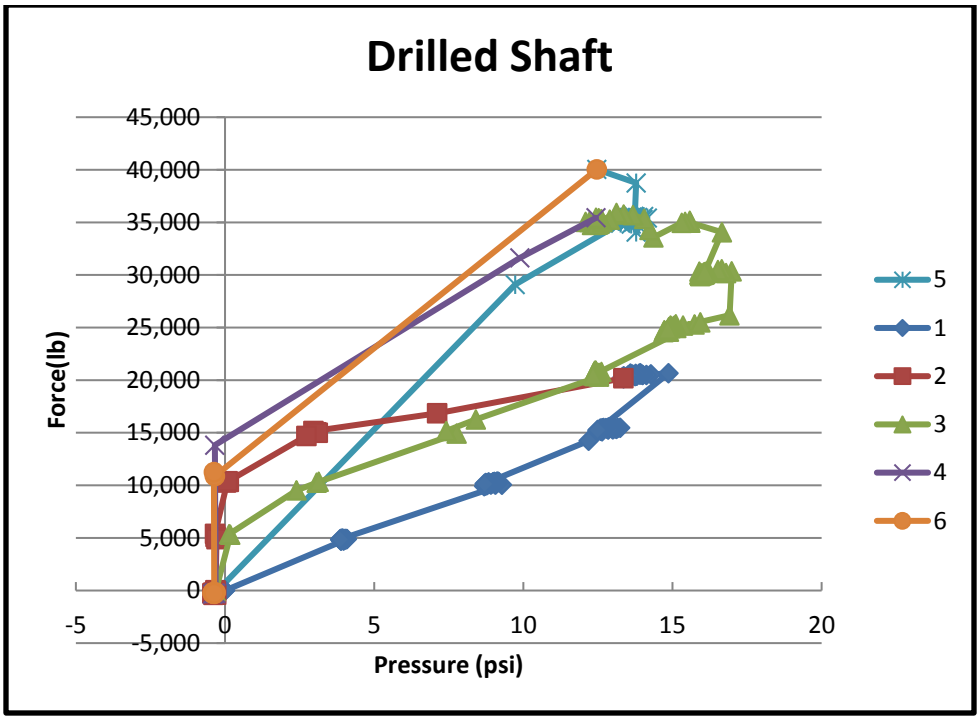

Figure 102. Pressure Measured on the Drilled Shaft with the Load Cell.

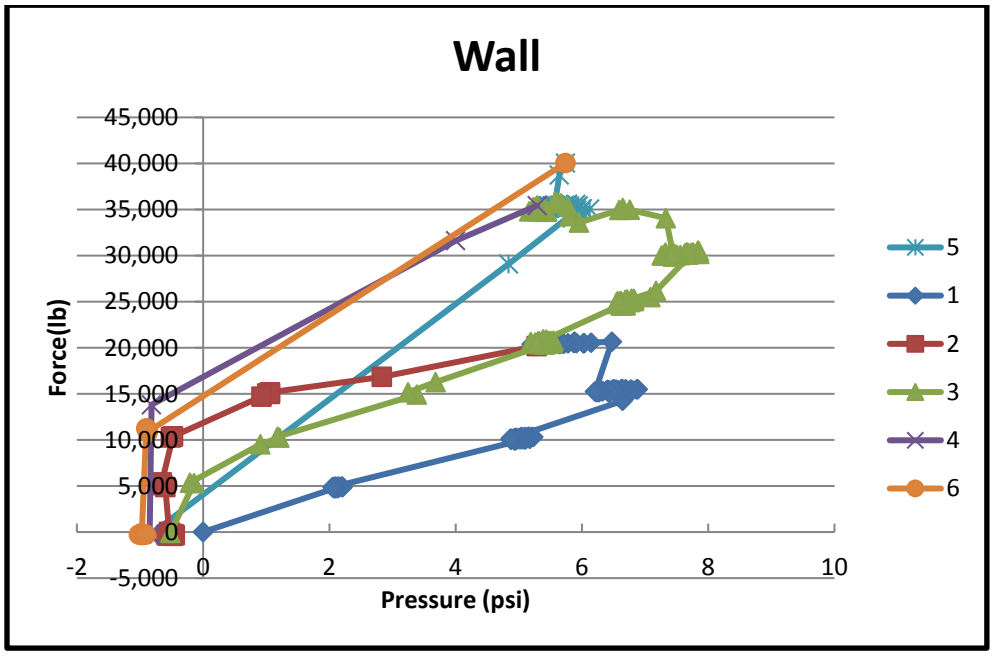

Figure 103. Pressure Measured on the Wall with the Load Cell.

Tiltmeter Results

Figure 104 shows the result for the tiltmeter installed on top of the drilled shaft. The maximum rotation of the drilled shaft at the top is 2.9°. This graph can be compared to Figure

105. Another tiltmeter was installed on the drilled shaft at the depth of 7.5 ft from top of the wall. Maximum rotation of the drilled shaft at that depth was 2.6°, as presented in Figure 106. There was very little bending of the shaft during loading.

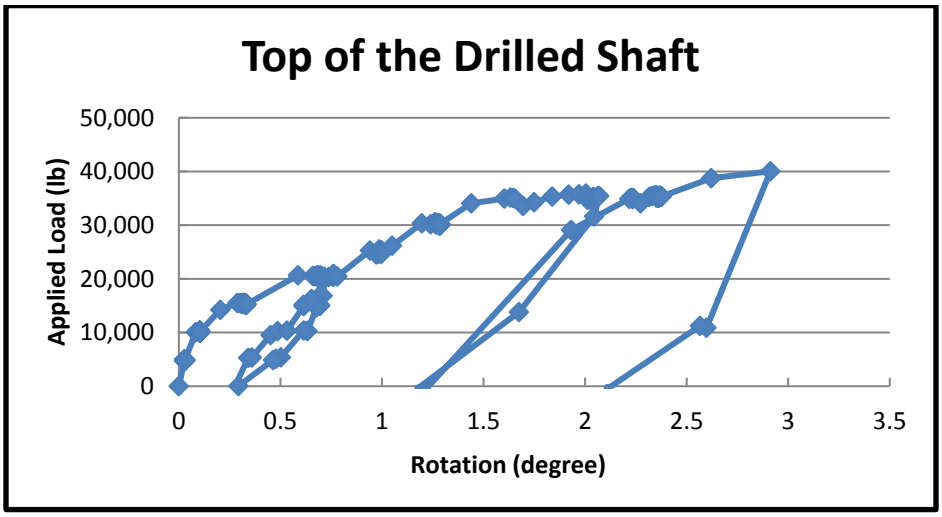

Figure 104. Tiltmeter Result for the Device Installed on Top of the Drilled Shaft.

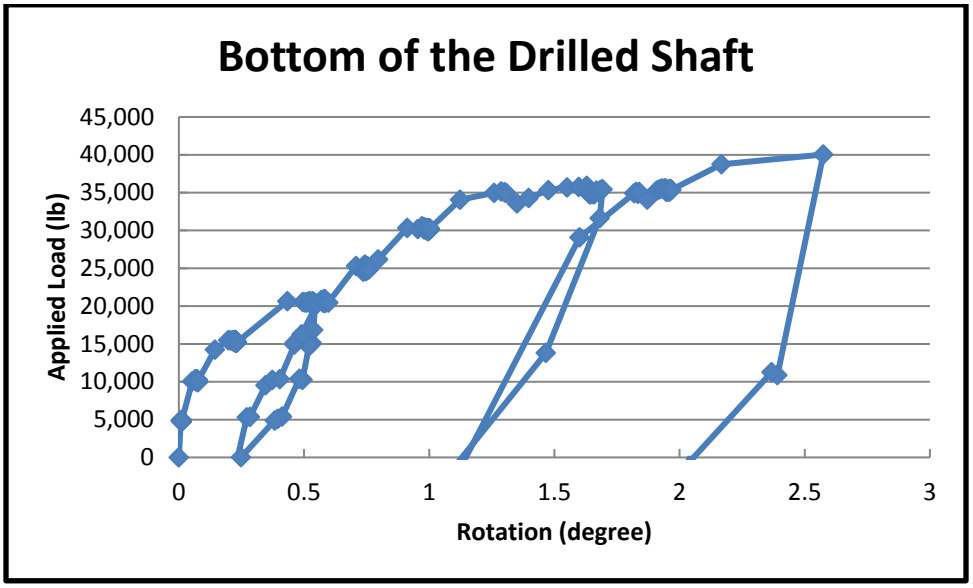

Figure 105. Tiltmeter Result for the Device Installed on Bottom of the Drilled Shaft.

Figure 107 shows the rotation of the top of the wall for different horizontal loads. The maximum rotation on this graph is 2.2°. Figure 108 demonstrates the result for the tiltmeter that was installed on the bottom of the wall. As it can be seen in this graph, rotation in this part of the wall is considerably smaller than the rotation at the top of the wall. There is a lot of distortion in the wall mass.

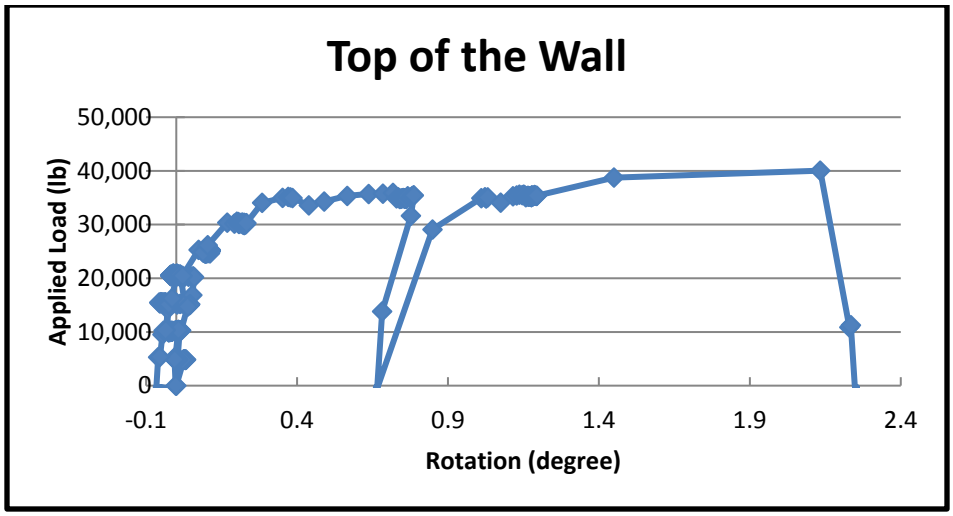

Figure 106. Tiltmeter Result for the Device Installed on Top of the Wall.

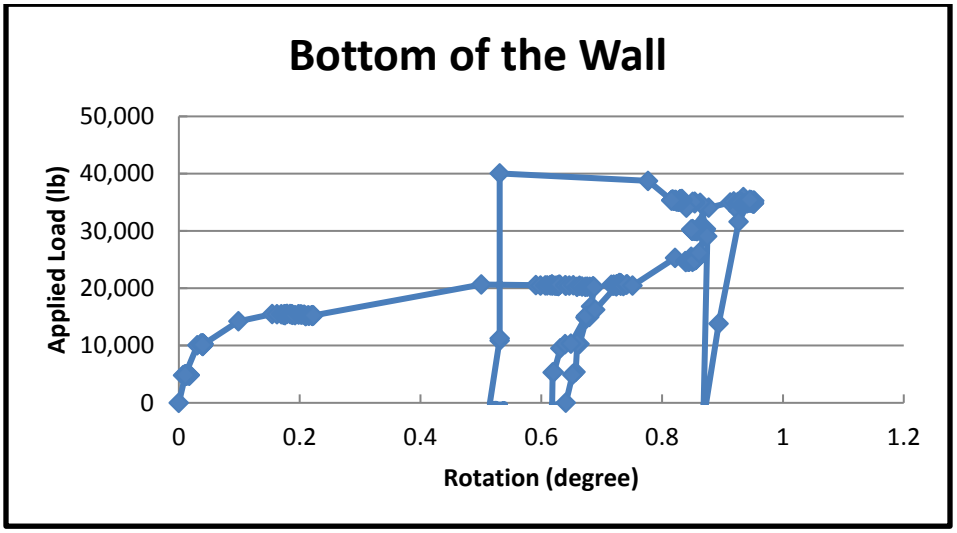

Figure 107. Tiltmeter Result for the Device Installed on Bottom of the Wall.

Inclinometer Results

After each step, it took about 15 minutes to insert the inclinometer probe into the casing in the drilled shaft and the wall and read the results. Data collected by this device were used to calculate drilled shaft and wall displacement in the direction of the load (A-axis) and also the displacement perpendicular to the load direction (B-axis).

The maximum displacement of the top of the drilled shaft according to the inclinometer reading is 5.4 in. (Figure 108). This displacement is smaller than the 6.15 in. measured with the string pot because the inclinometer readings were taken after unloading the 40 kips load back to zero while the deformation from string pot was measured when the load was 40 kips. Under zero

load after unloading, the string pot on the drilled shaft gives 5 in. and the inclinometer gives 5.4 in. The string pot is more reliable. Figure 109 presents a plan view showing the drilled shaft deformation. In this graph, the origin, point: (0,0), is the initial position of the drilled shaft.

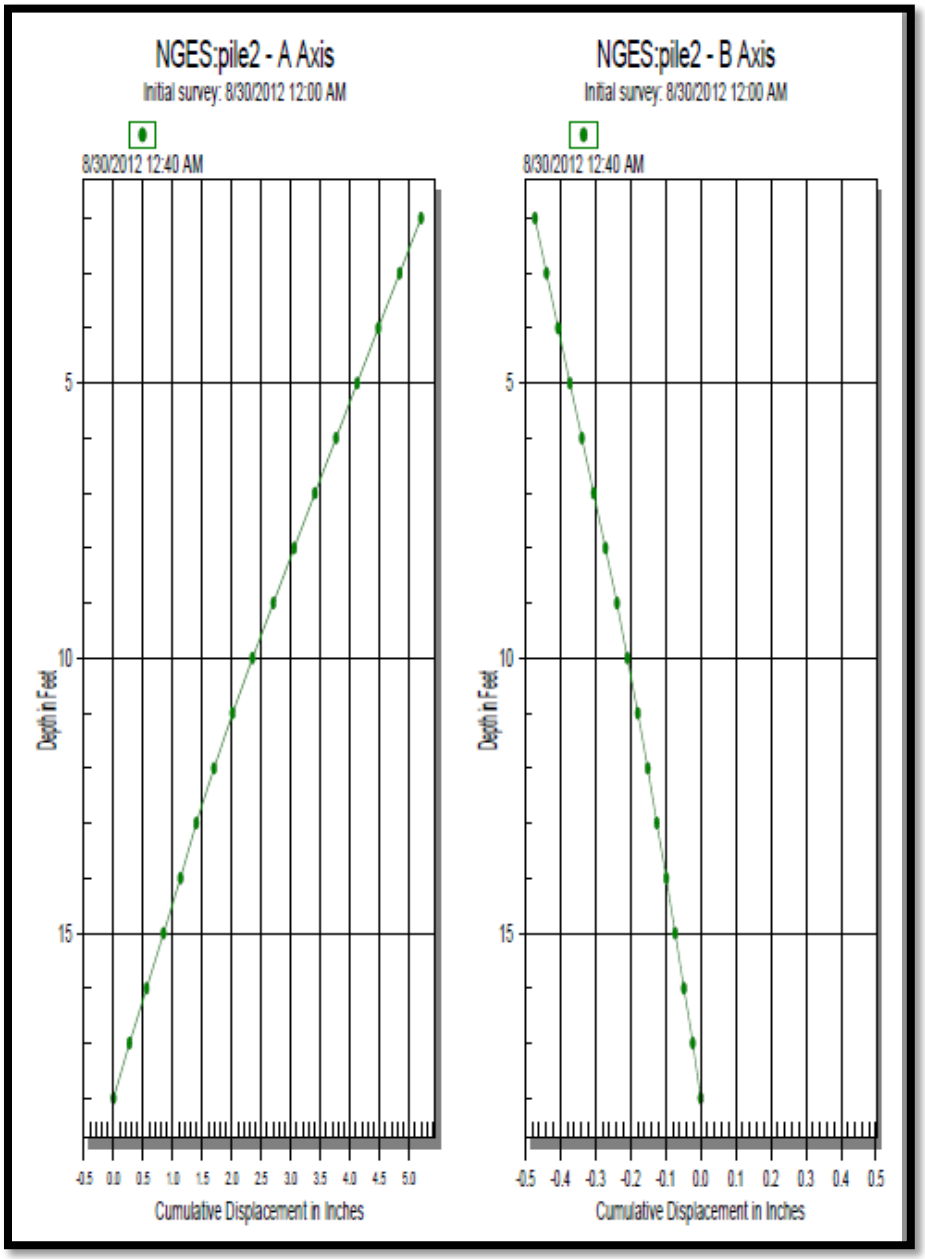

Figure 108. Permanent Drilled Shaft Displacement Profile according to the Inclinometer under Zero Horizontal Load after Unloading from the Horizontal Load of 40 Kips.

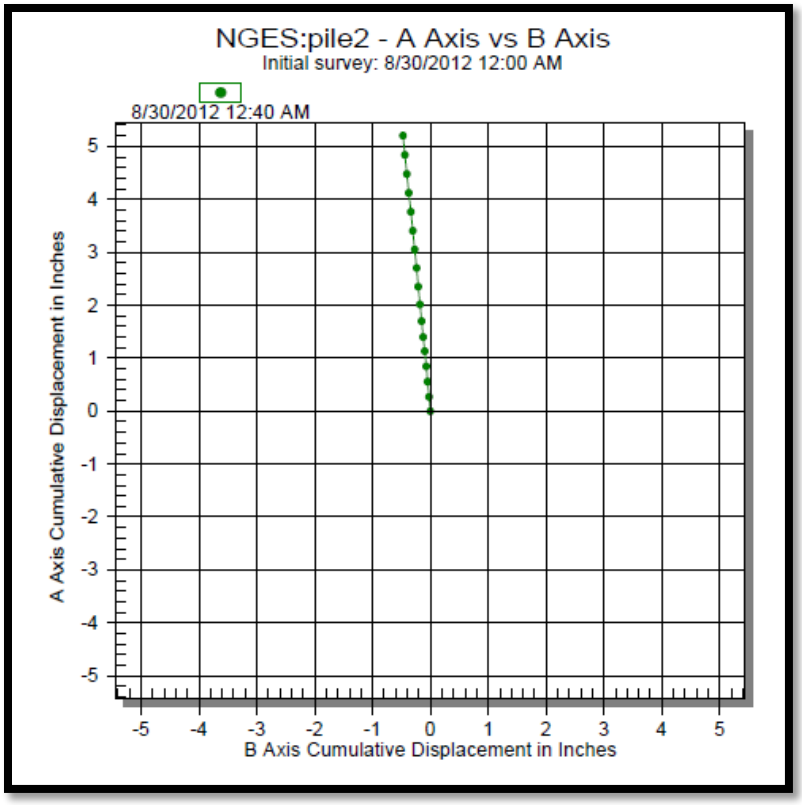

Figure 109. Plan View of the Drilled Shaft Displacement During the Load Test.

The same procedure was applied for the wall. As shown in Figure 110, the maximum deformation of the wall according to the inclinometer is 2 in. The maximum deflection of the wall according to the string pot is 4 in. (Figure 75). The difference is due to the fact that the string pot reading was taken while the 40 kips load was applied. Meanwhile, the inclinometer reading was taken after unloading the load back to zero from 40 kips. Under zero load after unloading, the string pot gives 2.85 in. while the inclinometer gives 2 in. The string pot is more reliable. Figure 111 presents a plan view showing the wall deformation. The initial position of the wall is at the point indicated as (0,0).

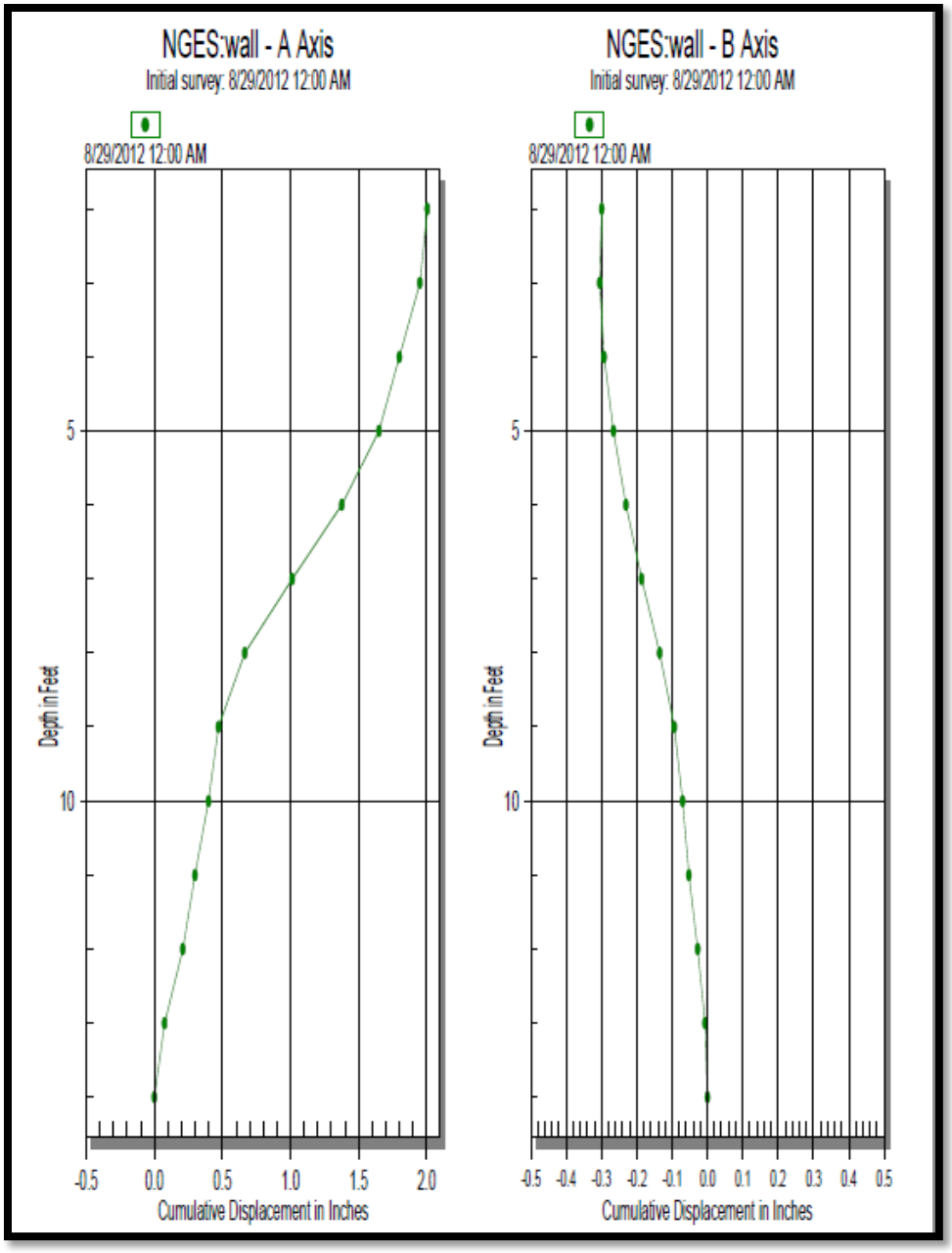

Figure 110. Wall Deformation Profile after Unloading from the Horizontal Load of 40 Kips.

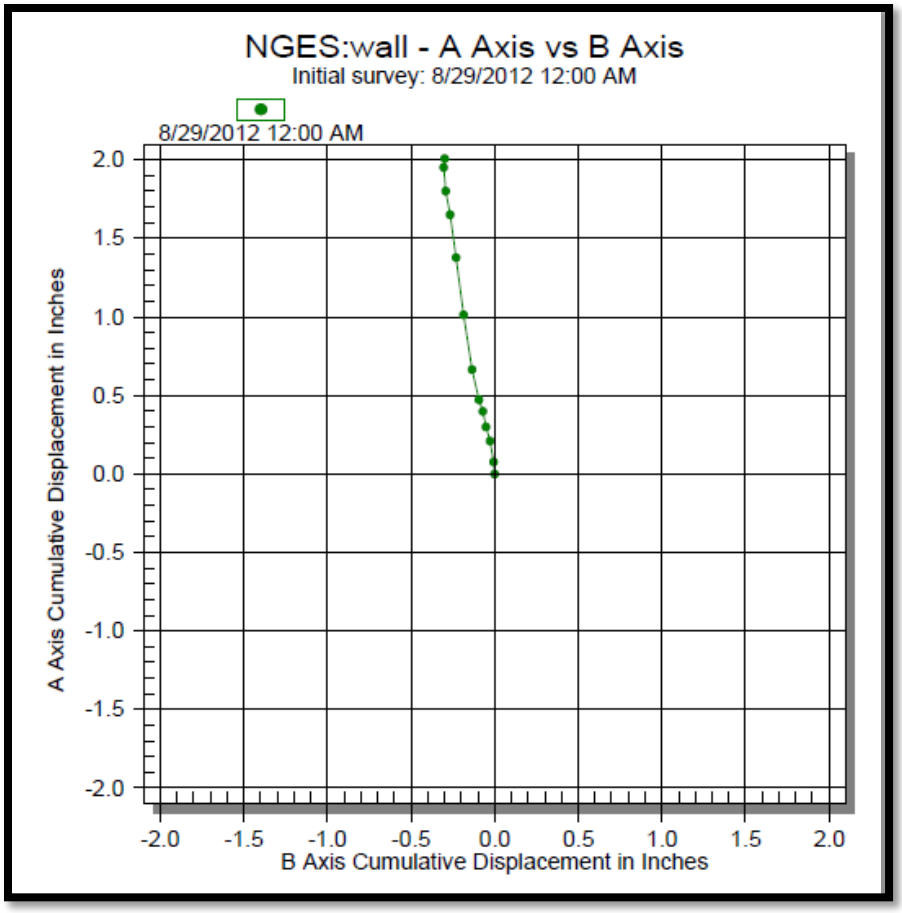

Figure 111. Plan View of the Wall Displacement During the Load Test.

According to the inclinometer, the maximum displacement of the drilled shaft at the horizontal load of 35 kips was 4 in. (Figure 112). The maximum drilled shaft displacement measured with the string pot at that load was 4.03 in. (Figure 74). Figure 113 presents a plan view of the drilled shaft deformation for this step. This procedure was applied for each of the loading steps.

Figure 114 shows the wall displacement profile measured with the inclinometer when the load of 35 kips was first applied. The inclinometer gives a displacement of 1.3 in. while the string pot (Figure 75) gives 1.5 in. Figure 115 presents the plan view of the wall displacement for this step.

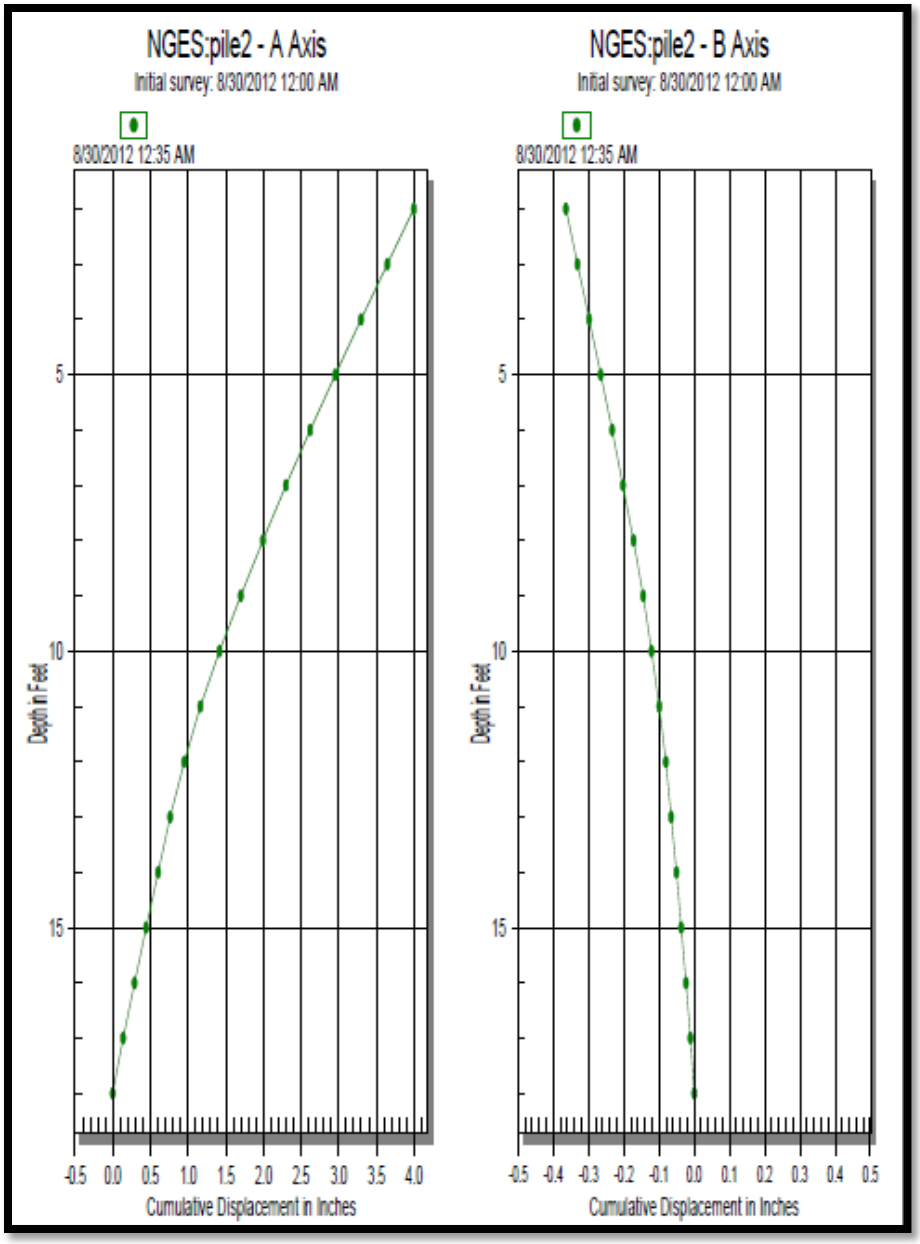

Figure 112. Drilled Shaft Deformation Profile after Unloading and Reloading to a Horizontal Load of 35 Kips.

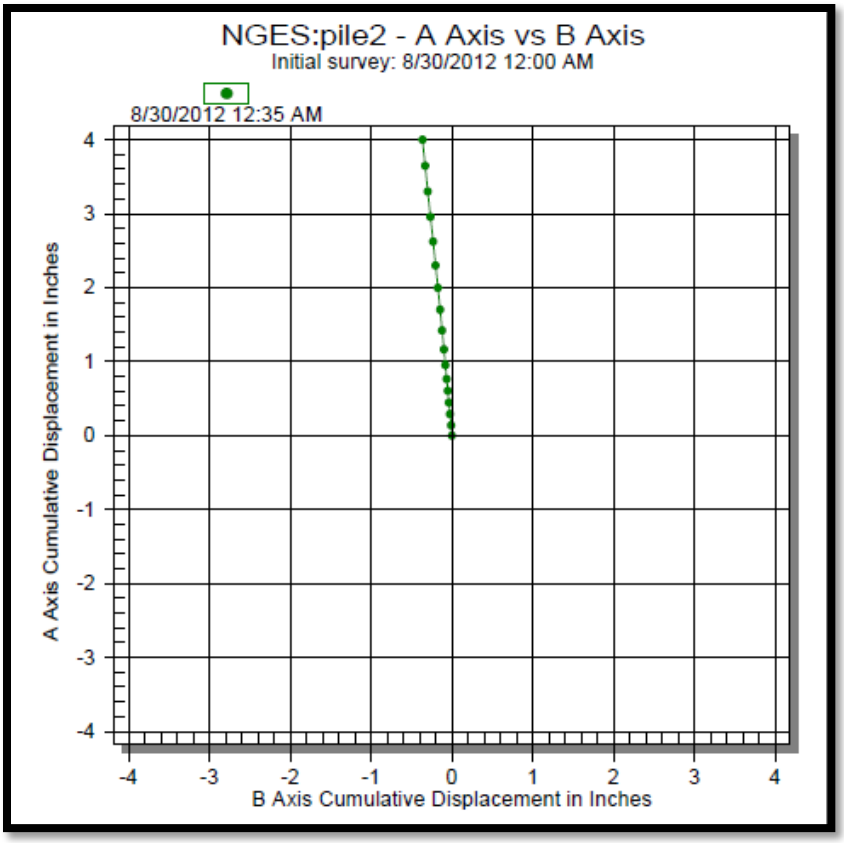

Figure 113. Plan View of the Drilled Shaft Deformation for Horizontal Load of 35 Kips.

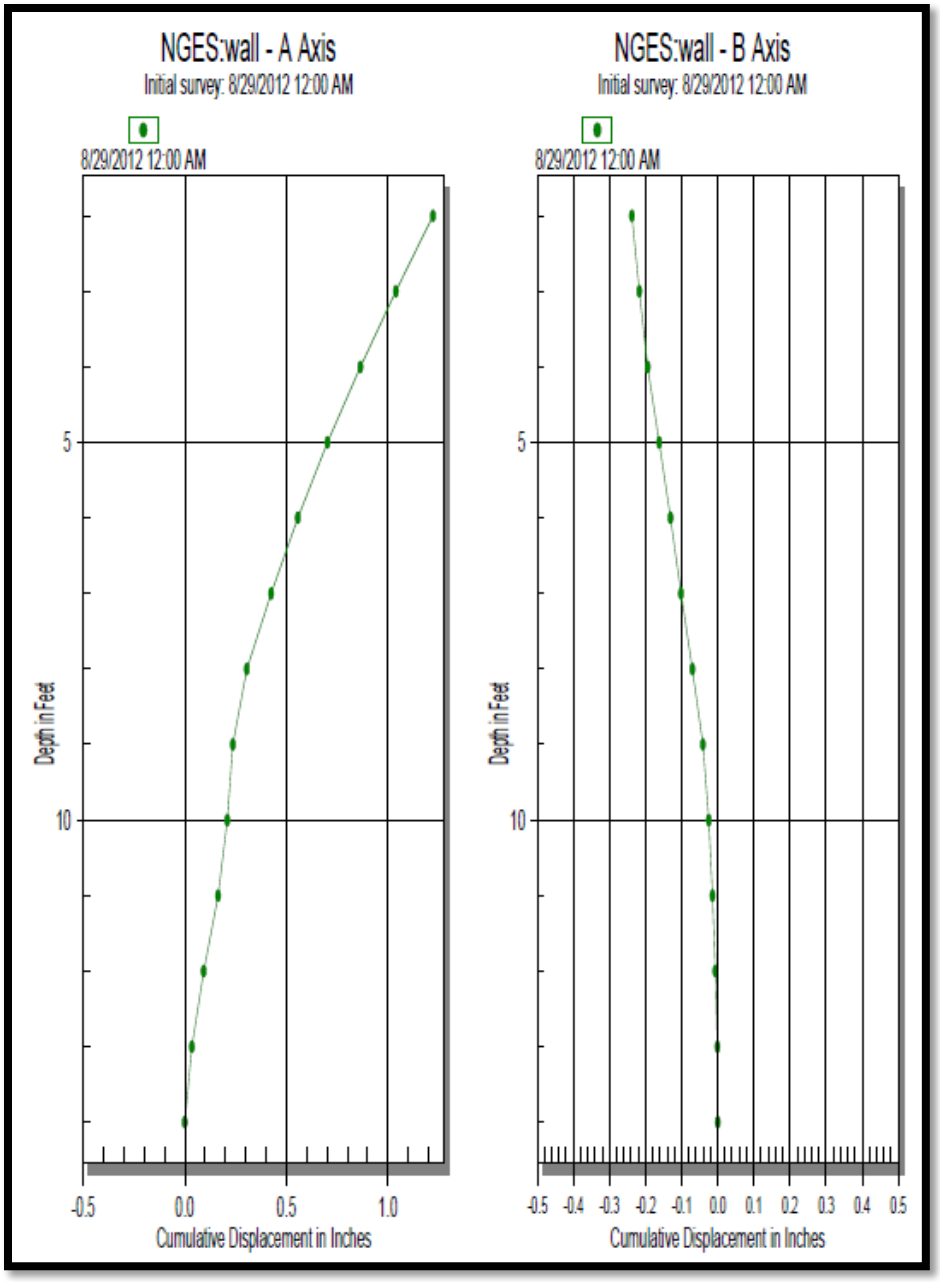

Figure 114. Wall Deformation Profile when the Horizontal Load of 35 Kips Was First Applied.

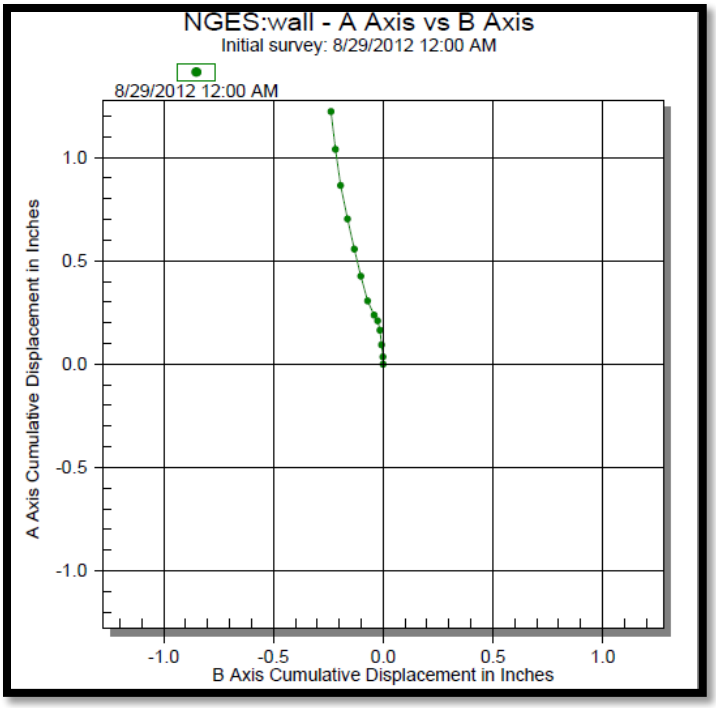

Figure 115. Plan View of the Wall Deformation for Horizontal Load of 35 Kips.

In addition to displacement, the rotation of the drilled shaft and the wall panels can be calculated from the inclinometer readings. The tiltmeters also measured rotation during the test. Figure 116 shows a comparison between the rotation given by the inclinometer and the tiltmeter installed on top of the drilled shaft.

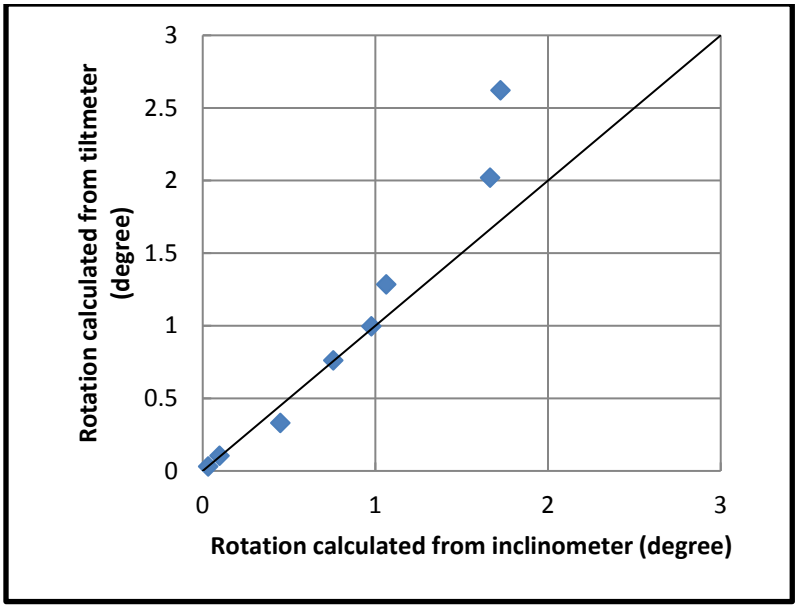

Figure 116. Comparison between Tiltmeter and Inclinometer for Top of the Drilled Shaft.

Figure 117 shows the comparison between the inclinometer and the tiltmeter installed at the bottom of the drilled shaft.

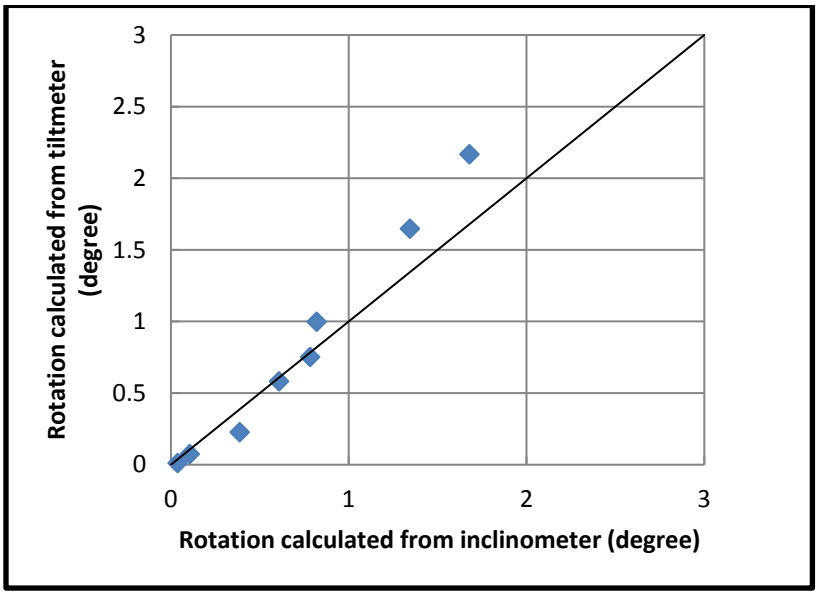

Figure 117. Comparison between Tiltmeter and Inclinometer for Bottom of the Drilled Shaft.

At the two real sites (i.e., projects selected by TxDOT), the inclinometer could not be used in the drilled shaft because the bridge deck was on top of the drilled shaft and prevented the insertion of the inclinometer probe. To get the drilled shaft displacement, more tiltmeters were installed on these projects. As seen in Figure 116 and Figure 117, the results from the tiltmeters match the results from the inclinometer quite well, especially at small displacement.

Results from LIDAR

LIDAR was used to achieve a better understanding of the wall and the drilled shaft deformations. LIDAR scanned the wall surface after each load step. Figure 118 presents the scan related to the initial condition (i.e., before applying the load).

Figure 119 shows the LIDAR plan view of the column at the end of the test. The displacement of the top of the drilled shaft and the top of the wall can be calculated by comparing these two pictures. The final deformation after the unloading of the top of the drilled shaft according to LIDAR is 4.7 in. and the final deformation of the top of the wall is 2.7 in., which matches the results from the string pot (4.94 in. for the top of the drilled shaft and 2.88 in. for top of the wall).

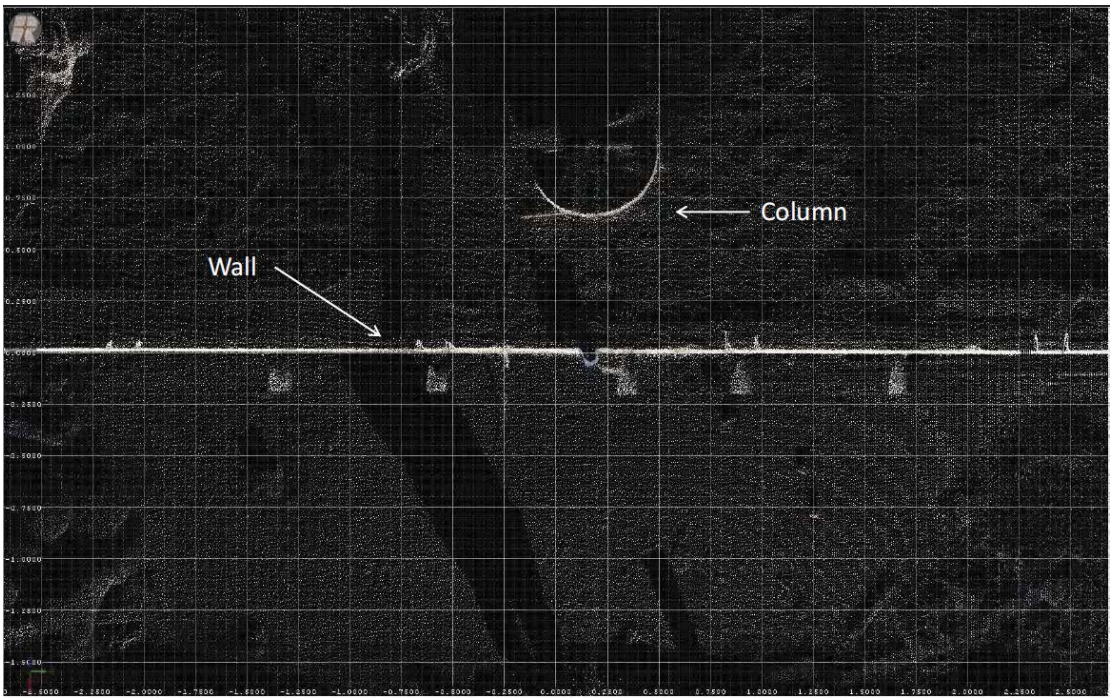

Figure 118. LIDAR Plan Views of the Drilled Shaft and the Wall for Initial Condition.

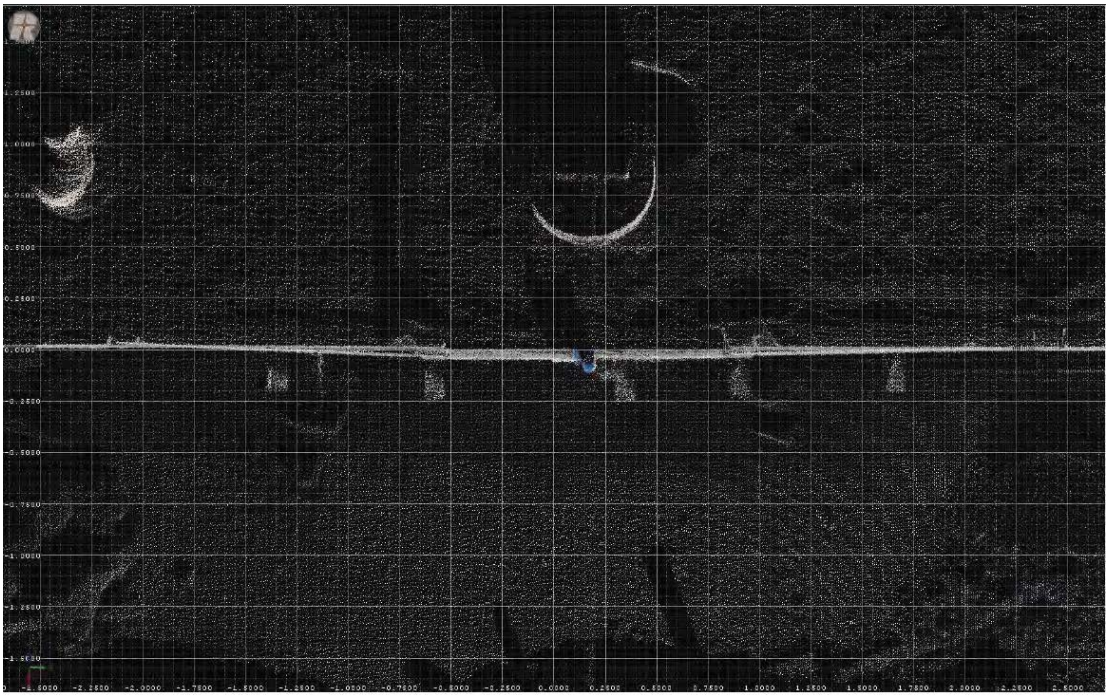

Figure 119. LIDAR Plan Views of the Drilled Shaft and the Wall at the End of the Test.

Wall Deformation

Photogrammetry was used in this research to obtain the deformation contours of the face of the wall at different loading steps. The deformation in the following plots is presented in

millimeters. The zero point on the horizontal axis corresponds to the initial position of the drilled shaft. Figure 120 shows the deformation contour for a horizontal load of 5 kips. The maximum displacement in this step is 0.5 mm. The maximum displacement for the step with a horizontal load of 10 kips is 2.5 mm (Figure 121). The maximum displacement of the wall at 15 kips is 7.6 mm. Figure 123 presents the deformation contour for a horizontal load of 20 kips. The maximum displacement in this step is 13 mm. In subsequent steps, the deformations were concentrated on the top panel in front of the drilled shaft, while the deformation of the other panels was very small. The maximum deformation at 25 kips is 19.5 mm. For the horizontal load of 30 kips, the maximum displacement of the wall is 27 mm (Figure 125). Figure 126 shows the contour of deformation for a horizontal load of 35 kips. The maximum displacement in this step is 50.1 mm. The horizontal load in the last step was 40 kips. Figure 127 shows the associated deformation contour for this step. The maximum displacement in this case is 101.1 mm. The maximum deformations always occurred at top of the wall in front of the drilled shaft. These results confirm the maximum displacement measured by the string pot.

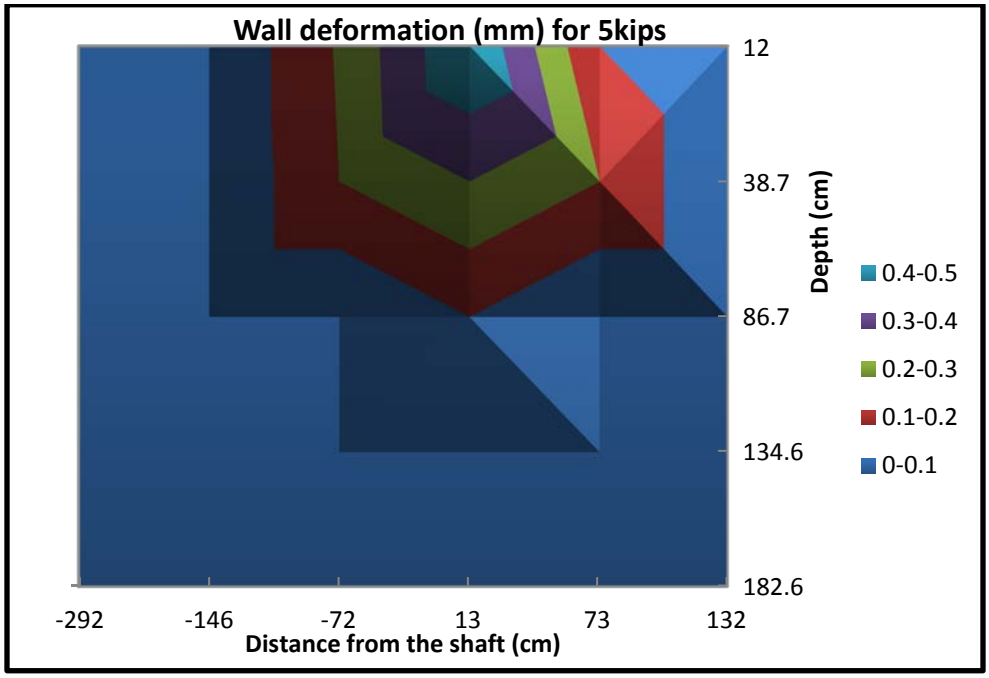

Figure 120. Wall Deformation Contour for Horizontal Load of 5 Kips.

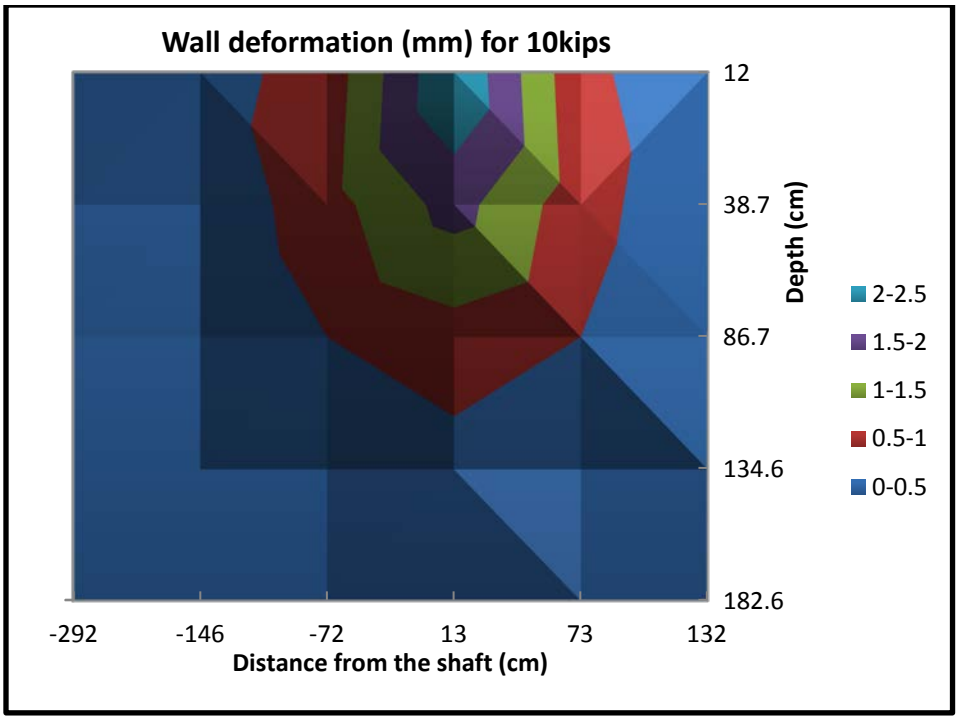

Figure 121. Wall Deformation Contour for Horizontal Load of 10 Kips.

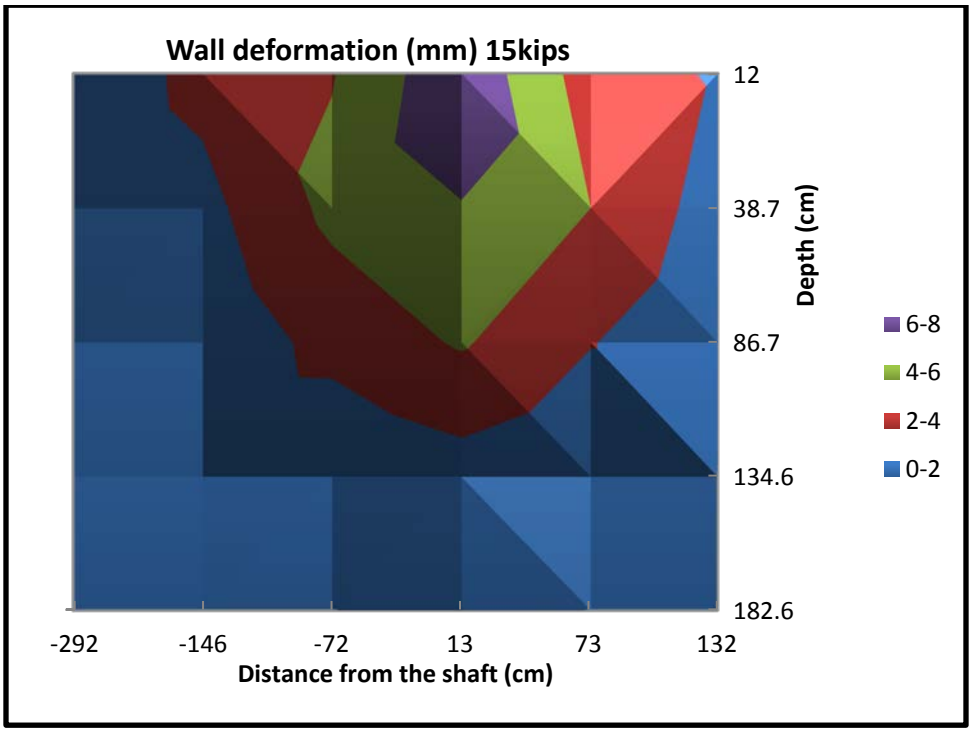

Figure 122. Wall Deformation Contour for Horizontal Load of 15 Kips.

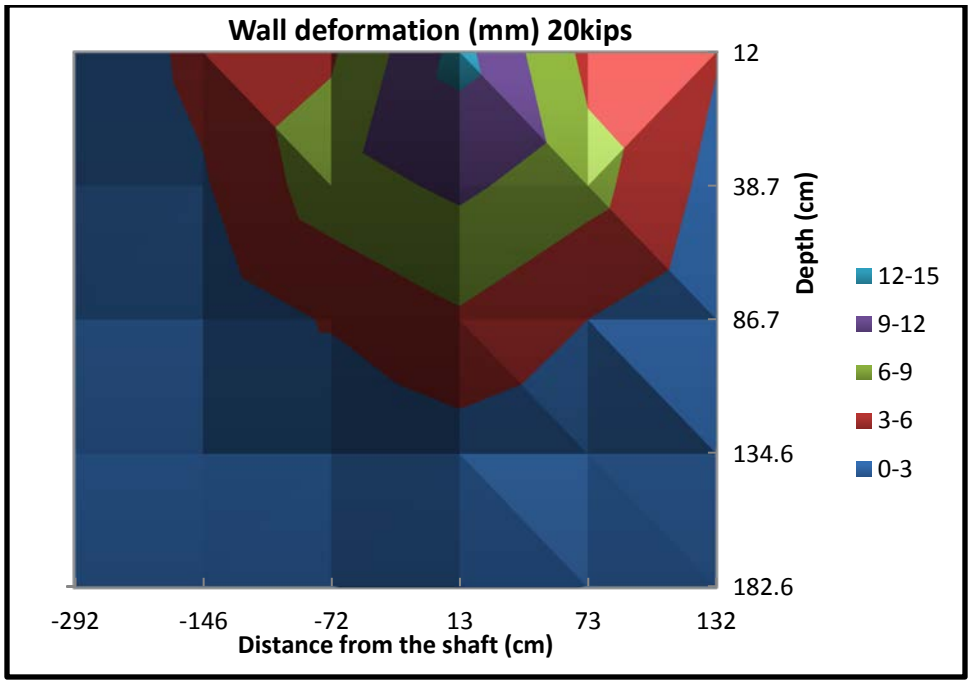

Figure 123. Wall Deformation Contour for Horizontal Load of 20 Kips.

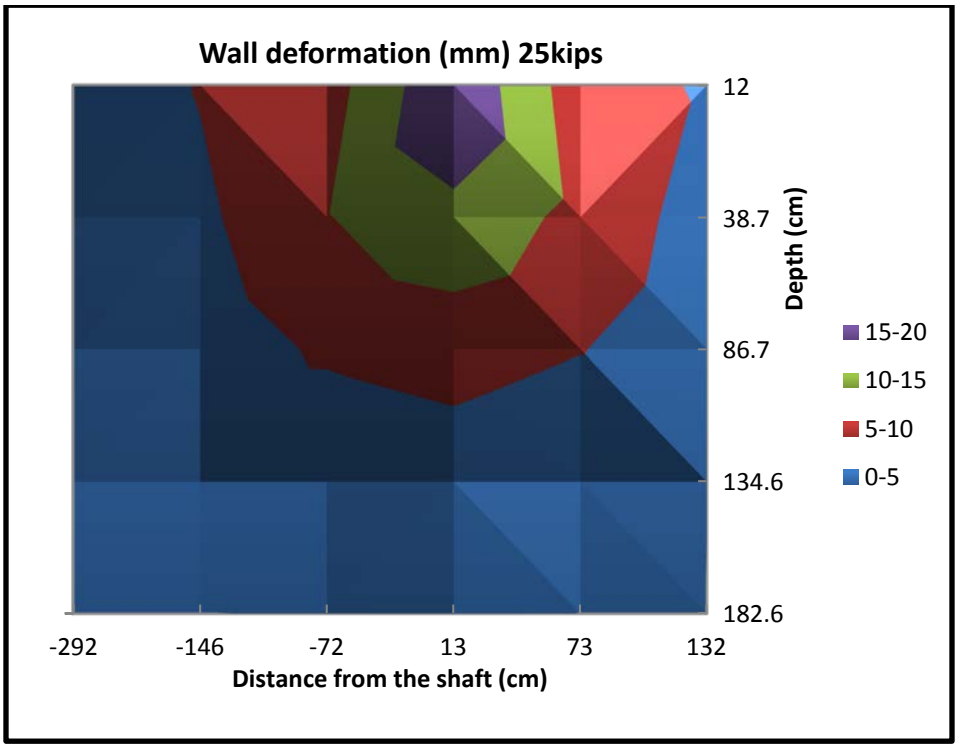

Figure 124. Wall Deformation Contour for Horizontal Load of 25 Kips.

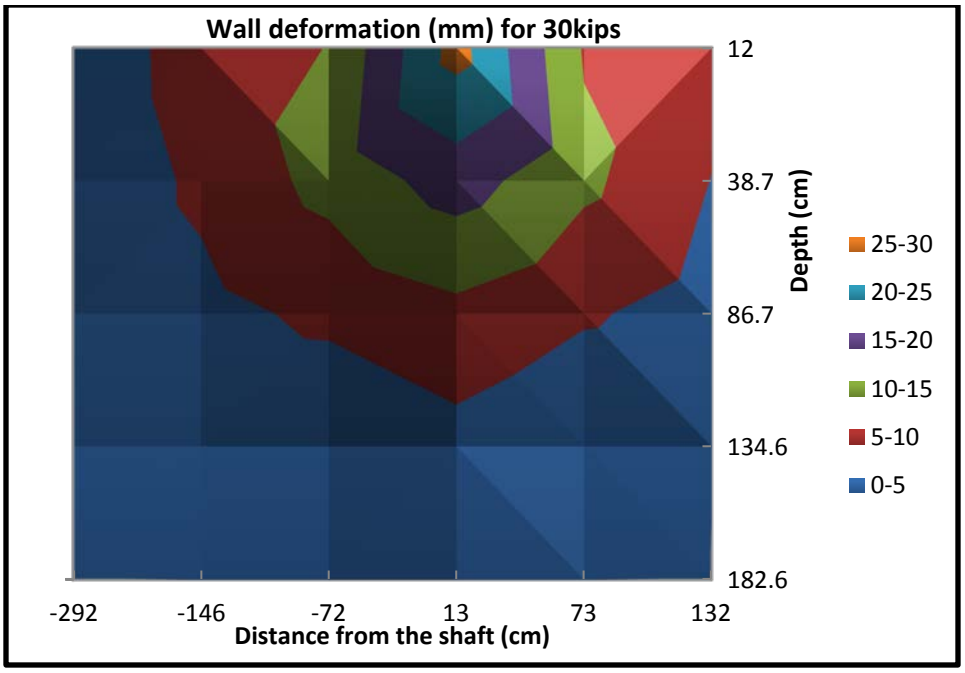

Figure 125. Wall Deformation Contour for Horizontal Load of 30 Kips.

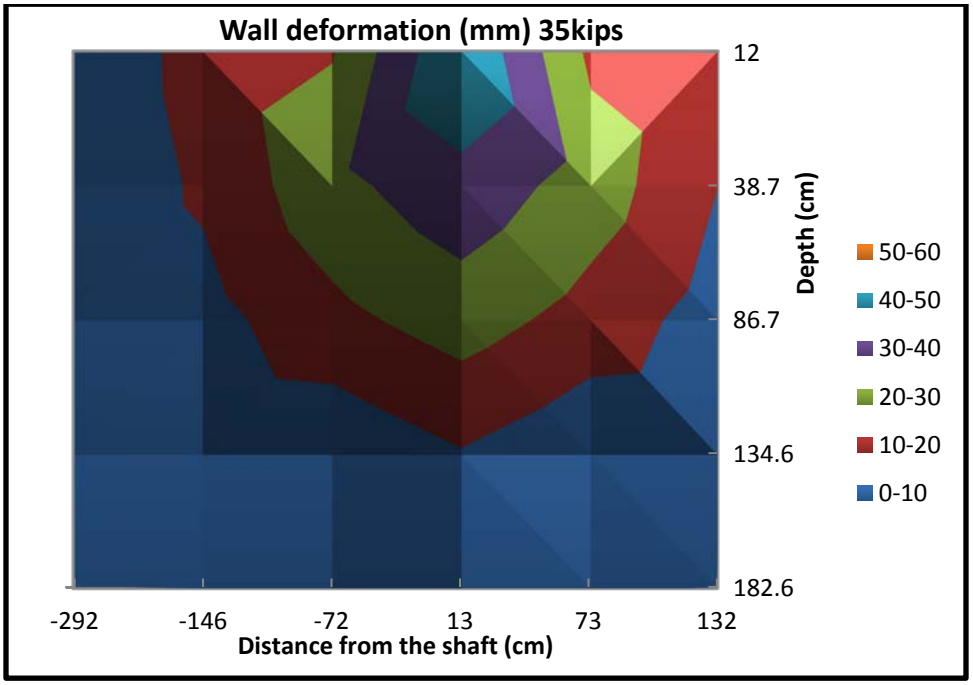

Figure 126. Wall Deformation Contour for Horizontal Load of 35 Kips.

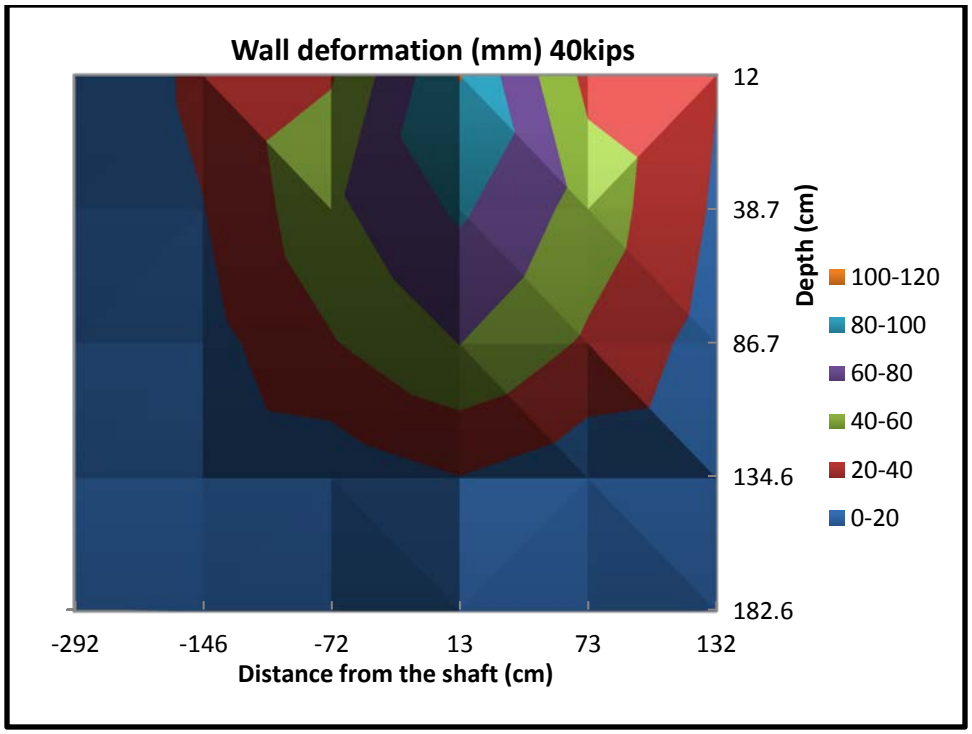

Figure 127. Wall Deformation Contour for Horizontal Load of 40 Kips.

Discussion

Fortunately all of the instruments and devices in this test worked properly and valuable data were collected. These data are useful for calibrating the numerical models. Once calibrated, numerical models can be used to explore the behavior of the wall-shaft system under different loading conditions, geometries, and boundary conditions.

An interesting result obtained in this study is related to the distribution of forces in the strips. The highest force in the strip did not occur at the maximum horizontal load. As seen in Figure 86, the maximum force in the strips happened when a horizontal load of 25 kips was acting on the drilled shaft. Another relevant result is that the force in the second layer of strips is greater than the force in the top layer.

MONITORING AT TXDOT SITE IN BASTROP

Real Project Introduction

The project is an overpass of SH 71 over FM 20 (Figure 128). The overpass is from west of FM 20 to east of FM 969, and the length is 1.354 miles. The project started in September 2012.

Figure 128. Location for Project in Bastrop.

As it is shown in Figure 129, there are two MSE walls in this overpass (i.e., the east wall abutment and the west wall abutment). Based on the construction schedule, the east wall abutment was chosen for this research.

The height of the east wall is 15 ft and its length is 109 ft. The backfill material is crushed rock, and the reinforcement used in this wall is metal grids. The length of the grids varied with depth. For the two top rows of grids, the length is 18 ft. Figure 130 shows the detail of the east wall.

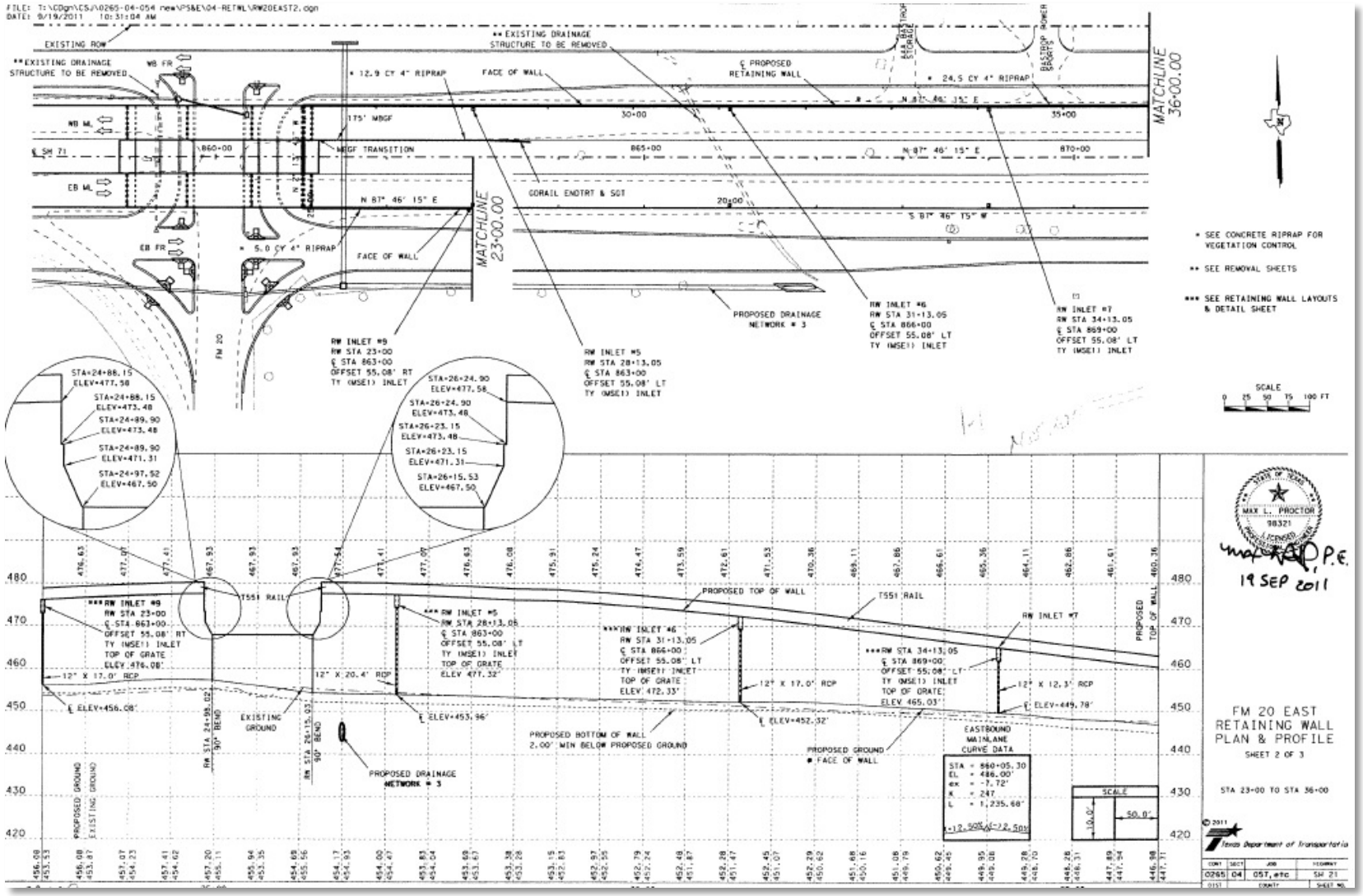

Figure 129. Plan View of the Overpass.

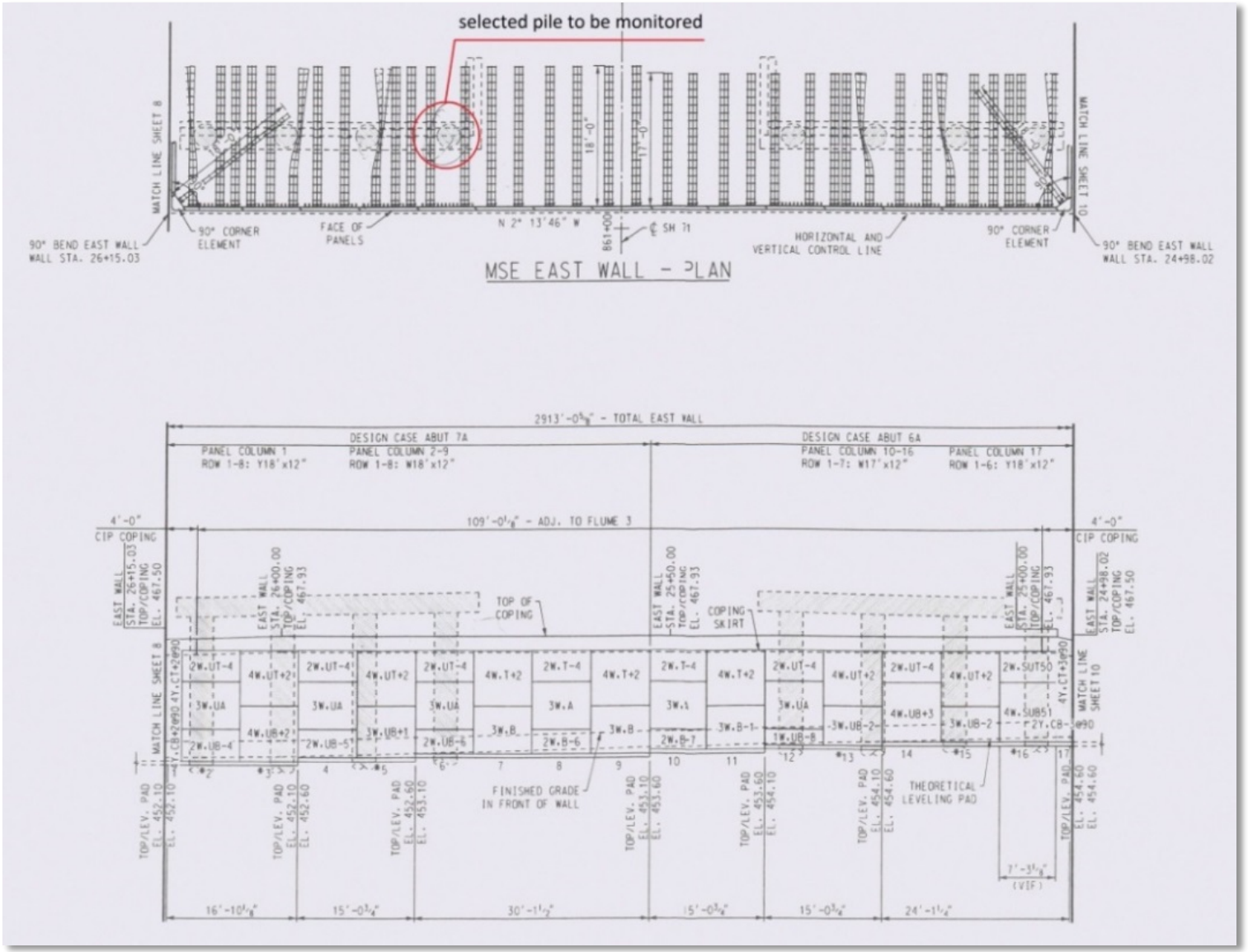

Figure 130. East Wall Detail.

Instrumentation

The instrumentation for this project is similar to the one adopted for the full-scale test at TAMU-NGES. A slight difference is that in the full-scale test most of the devices (e.g., inclinometer casing, tiltmeters) were installed outside the wall but in this project they were installed inside the wall facing. This difference is because this wall is related to an actual bridge and the taskmaster did not want any exposed device on the wall. The instruments (i.e., gauges, tiltmeters) were installed during construction within different layers.

Inclinometer

In this project, the inclinometer is not used for measuring the deflections of the drilled shaft, because the bridge deck is on top of the drilled shaft and there is no room to insert the inclinometer probe in the casing. Three tiltmeters were installed on the drilled shaft and another three tiltmeters were installed on the wall. This was done to have a better understanding of the wall and shaft deformations.

Figure 131. Drilling the Hole for the Inclinometer Casing.

Figure 132. Extended Casing Attached to the Wall.

Figure 133. Casing at Top of the Wall.

Tiltmeter

In the actual projects, three tiltmeters were installed on the drilled shaft and another three were installed on the wall. One tiltmeter was installed at the bottom, one at the middle, and one at top of the wall. Tiltmeters on the drilled shaft were installed at the same positions matching

the ones on the wall. To protect the tiltmeters from compaction and other external actions, metal boxes were used (Figure 134). PVC tubes were used to protect wires (Figure 135).

Figure 134. Tiltmeters Installed on the Wall.

Figure 135. PVC Tubes Used for Protecting Wires.

Strain Gauge

A total of eight full bridge strain gauge circuits were used in this project, four per layer (Figure 136). In order to install the strain gauges on the grids, a first attempt was made to install gauges directly on the bars (Figure 137). After looking at the results of a loading test performed on the bar, this solution would not be acceptable. Another option was to cut the bar at the measurement locations, weld a metal strip with the same section area as the bar, and install the strain gauges on that strip (Figure 138). This was the option that was selected.

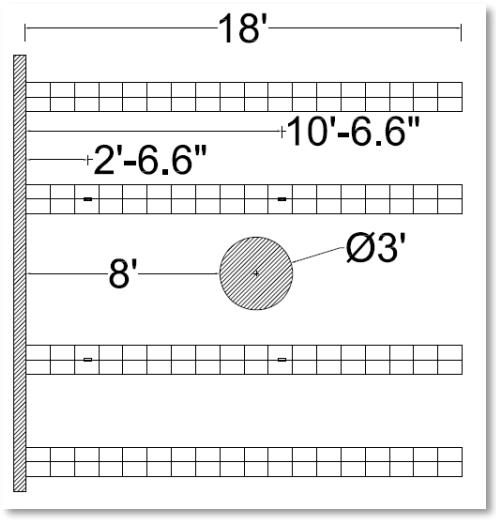

Figure 136. First and Second Layers of Grids.

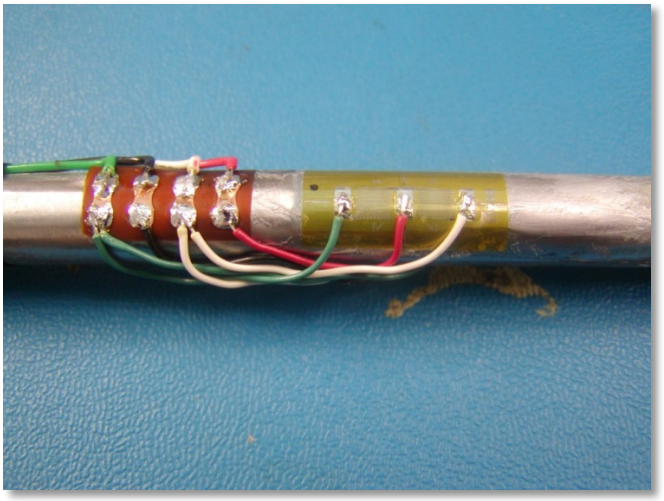

Figure 137. Strain Gauge Installed on the Bar.

Figure 138. Strips Attached to the Bars.

To protect the gauges against moisture and rupture, PVC tape was wrapped around them. In the field, before putting the crushed rock on top of them, a sandbag was placed above and below each gauge to prevent the crushed rock from touching the gauges (Figure 139)

Figure 139. Sandbags for Protecting the Gauges.

Pressure Cell

A pressure cell was used on the inside of the top wall panel. It was installed at the middle of the top panel and was the same as the one used in the full-scale test. To gather good results

from such a pressure cell, it is recommended that a uniform pressure act on it. In crushed rock this is difficult, because this material tends to apply the load to the cell by point loads rather than a uniform pressure; this may lead to imprecise measurements. To solve this problem, a sandbag was installed in front of the cell to help develop a uniform distribution of pressure (Figure 140).

Figure 140. Sandbag Used on Pressure Cell to Uniform the Pressure.

Data Acquisition System

CR1000 was the data logger used at this project site. It was the same as the data logger used to collect data from the tiltmeters in the full-scale test at the TAMU-NGES Riverside Campus. To provide power for the data logger, a solar panel was installed on the site and a battery was used to accumulate power. A Data Acquisition Box was installed on the top of the wall (Figure 141[a]), and the solar panel was installed on top of the riprap so that it would be exposed to sunshine (Figure 141[b]). Figure 142 shows the cross section of the finished wall.

(a) **(b)**

Figure 141. Data Acquisition Installed at Bastrop Site a) Box and b) Solar Panel.

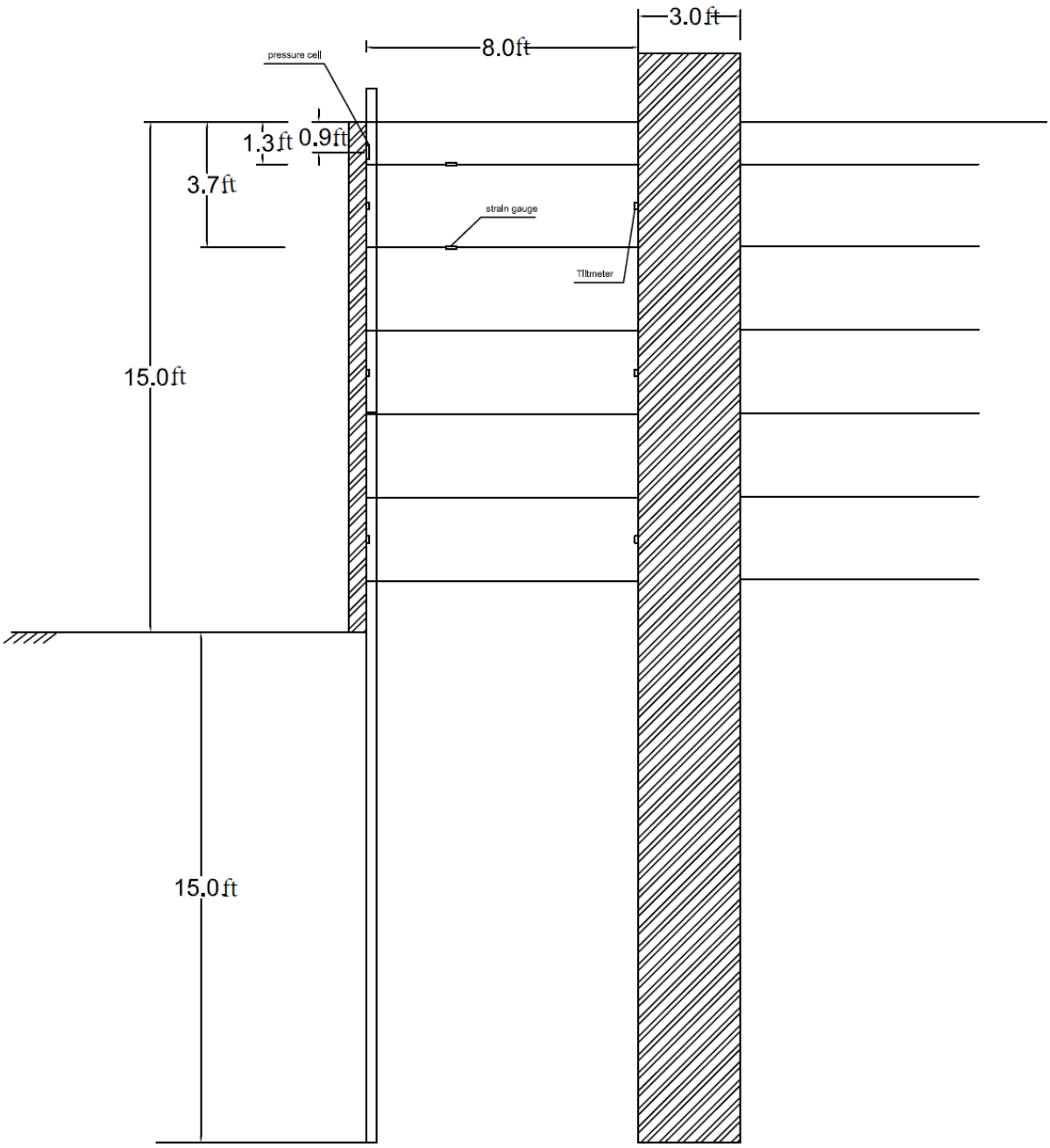

Figure 142. Bastrop Wall Cross Section.

Results

Data from this site were collected from December 2013 until August 2015. Wires were cut and the solar panel was stolen in August 2014. Because of that, the monitoring was not resumed until February 2015 when a new solar panel was purchased and installed.

Strain Gauge Results

A total of eight strain gauges were used in this project site. Four of them were installed on the top layer of metal grids labeled T and four of them installed on the second layer of metal grids from the top labeled B. Figure 143 shows the notation for the strain gauges.

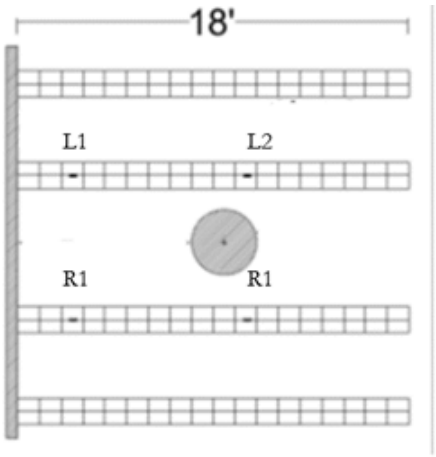

Figure 143. Strain Gauge Numbering.

As shown in Figure 144, from December 2013 to August 2014, there was no change in the forces in the strips. Data were collected after resuming the monitoring. Because of the noise in the data, the relative difference between strain gauge labeled BR2 and the remaining seven strain gauges was plotted in Figure 145. As can be seen, the relative difference is close to constant and validates the observation during the previous period.

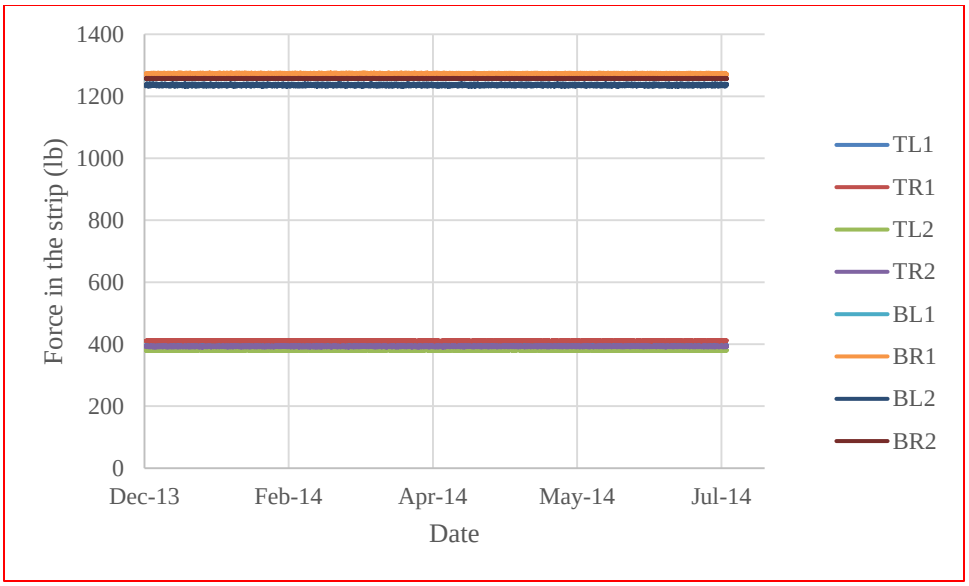

Figure 144. Strain Gauge Data from Bastrop Site.

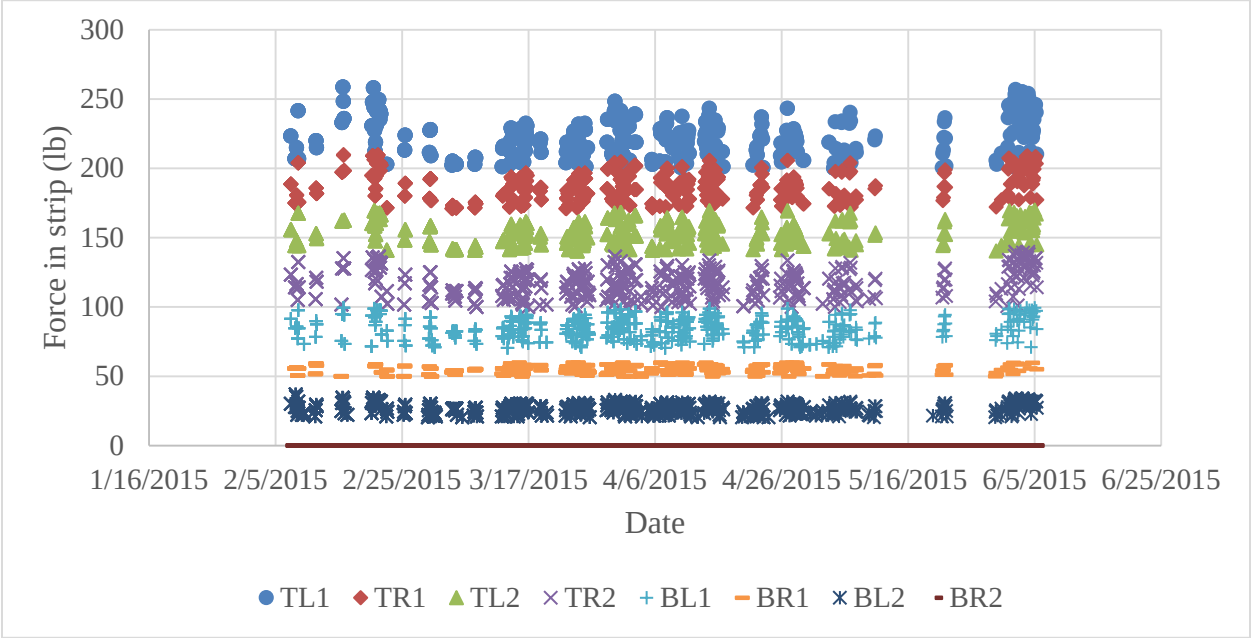

Figure 145. Strain Gauge Data from Bastrop Site after Resuming.

Pressure Cell

At this site, researchers used one pressure cell on the wall at a depth of 9 in. below the top of the wall. Figure 146 shows the data from the pressure cell. Also in this case, no changes were observed.

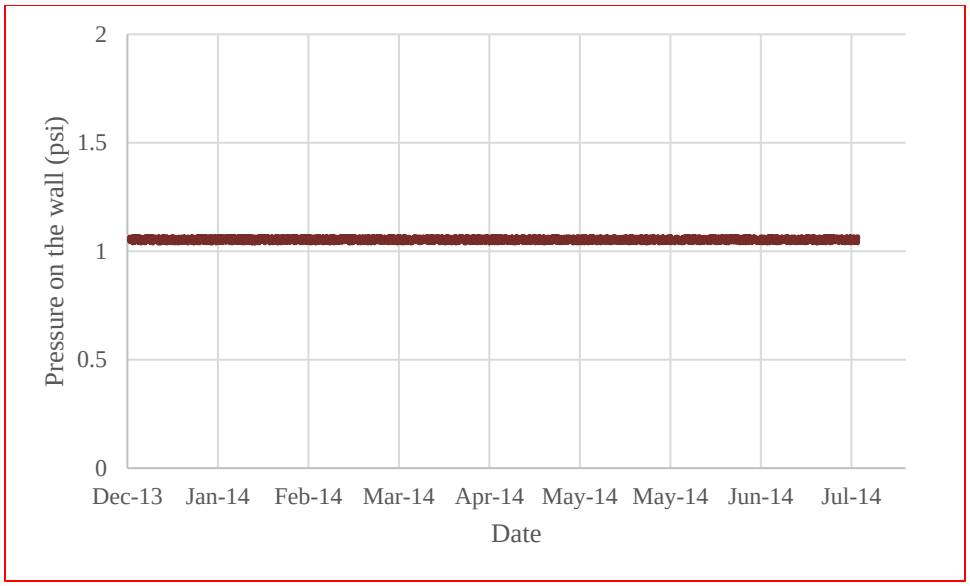

Figure 146. Pressure Cell Data for Bastrop Site.

Data were collected after resuming the monitoring. Figure 147 plots the data. The average is constant during this second period of observation, though there is little variation. The average matches the value during the first period of observation.

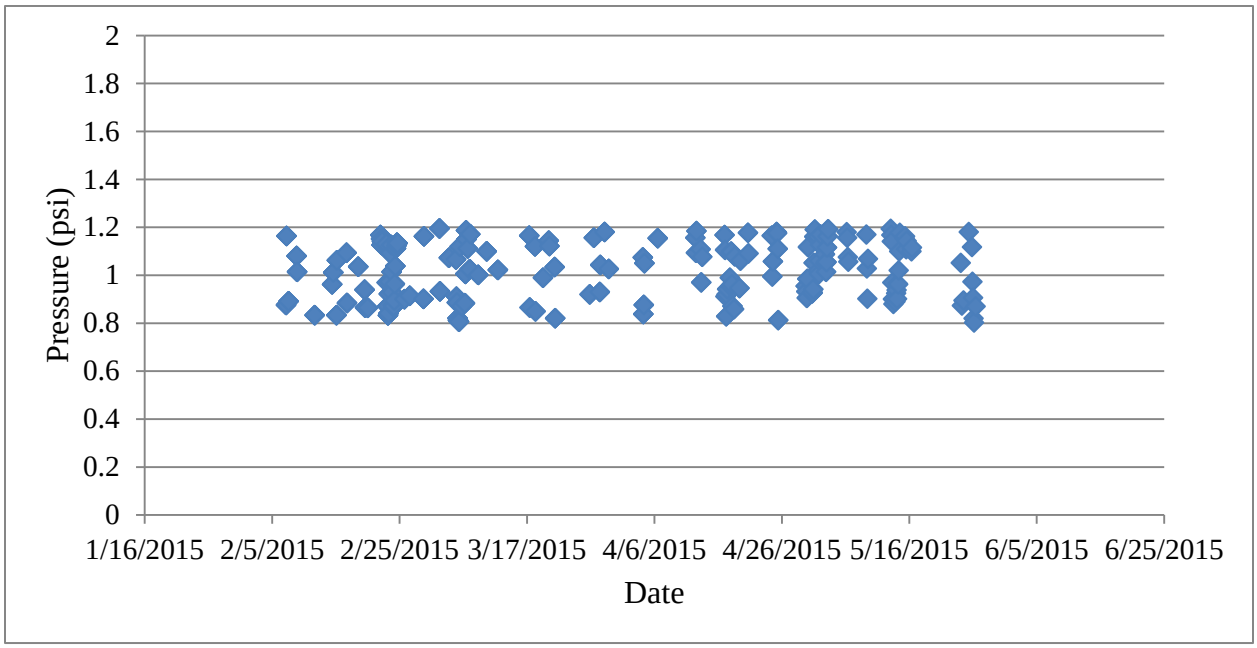

Figure 147. Pressure Cell Data for Bastrop Site after Resuming.

Tiltmeter

A total of six tiltmeters were installed at this site. They were coded as follows: TW at the top of the wall, MW at the middle of the wall, BW at the bottom of the wall, TS at the top of the drilled shaft, MS at the middle of the drilled shaft, and BS at the bottom of the drilled shaft. Figure 148 shows the data gathered for these tiltmeters.

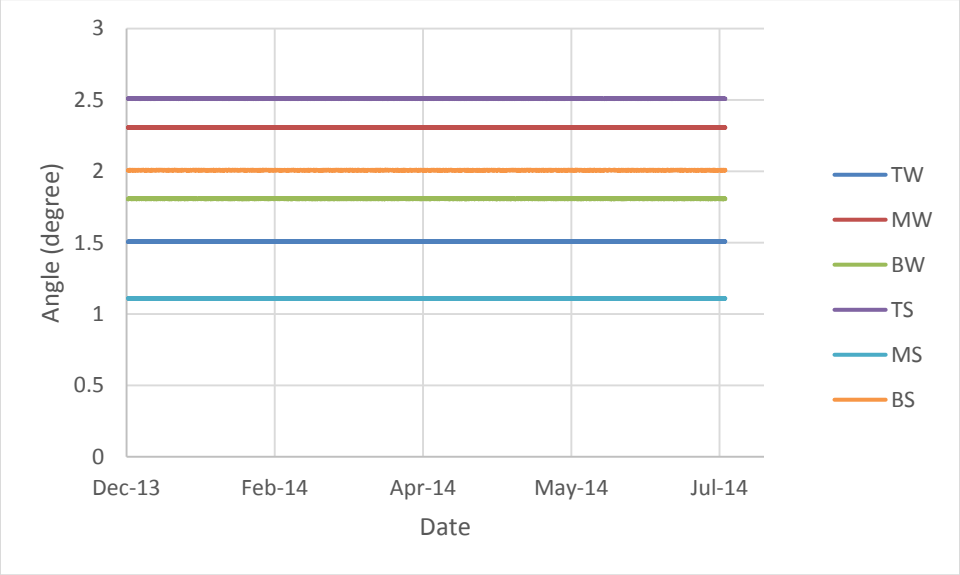

Figure 148. Tiltmeter Data from Bastrop Site.

As shown in Figure 148, there were no changes in the angles over time. Data were collected after resuming the monitoring in January 2015. Because of the noise in the data, the relative difference between the strain gauge labeled BR2 and the remaining seven strain gauges was plotted in Figure 149. The relative difference is constant during monitoring, confirming the data accumulated during the first phase of readings.

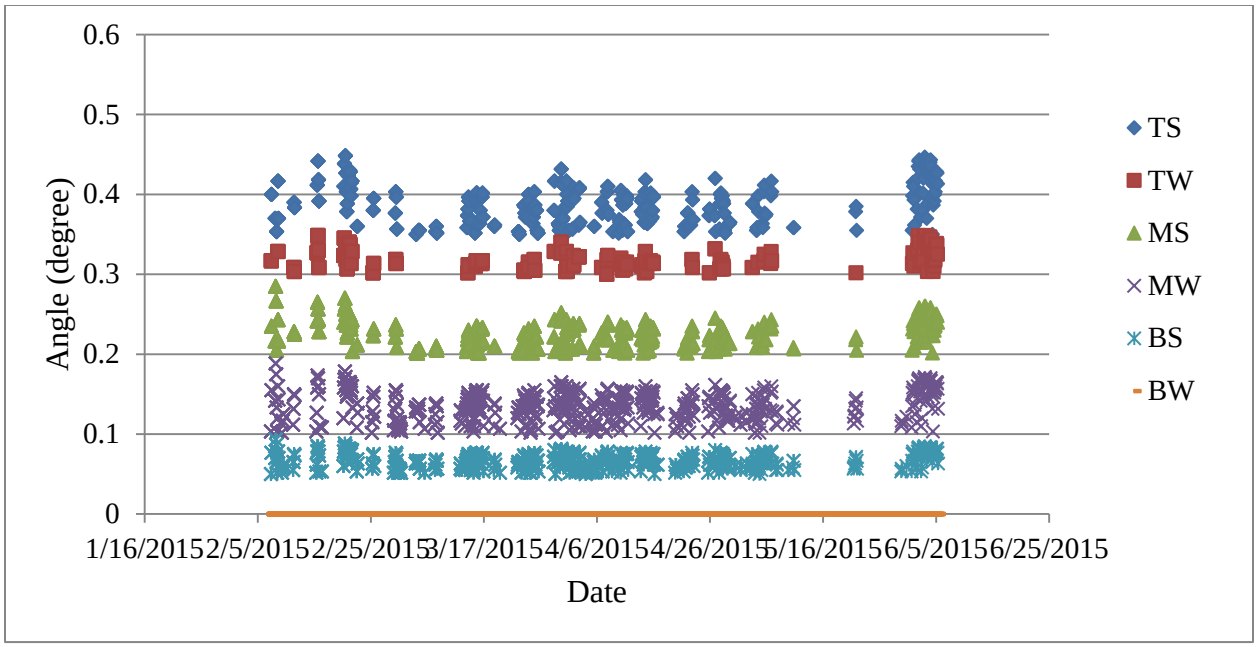

Figure 149. Tiltmeter Data from Bastrop Site after Resuming.

Inclinometer

Figure 150 presents the results after four months. The A-axis is perpendicular to the wall, and B-axis is parallel to the wall. In this case, no changes in the wall deflection were detected with the inclinometer.

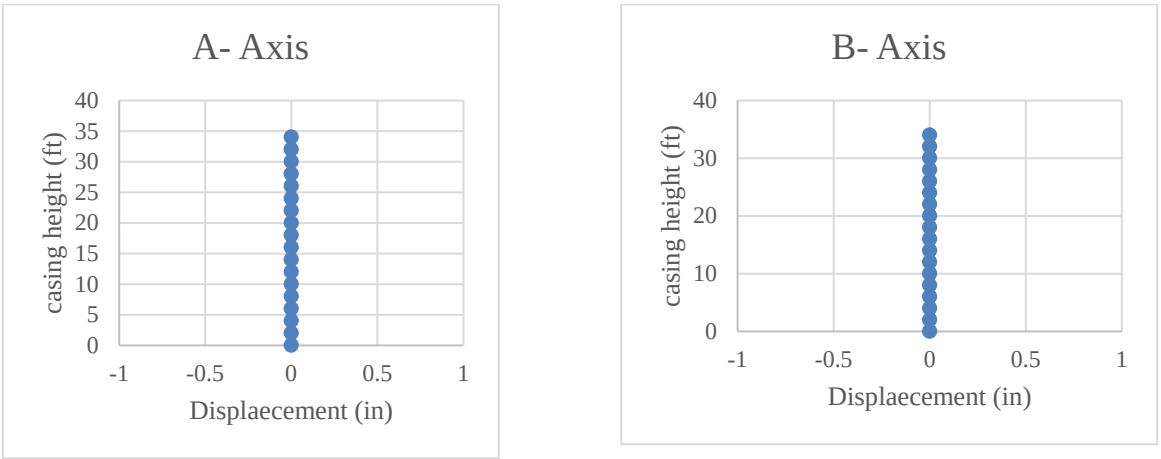

(a) **(b)**

Figure 150. Inclinometer Results for Bastrop Site a) toward the Wall b) Parallel with the Wall.

Data were collected after resuming the monitoring (Figure 151). There is very little change in the wall deflection over time.

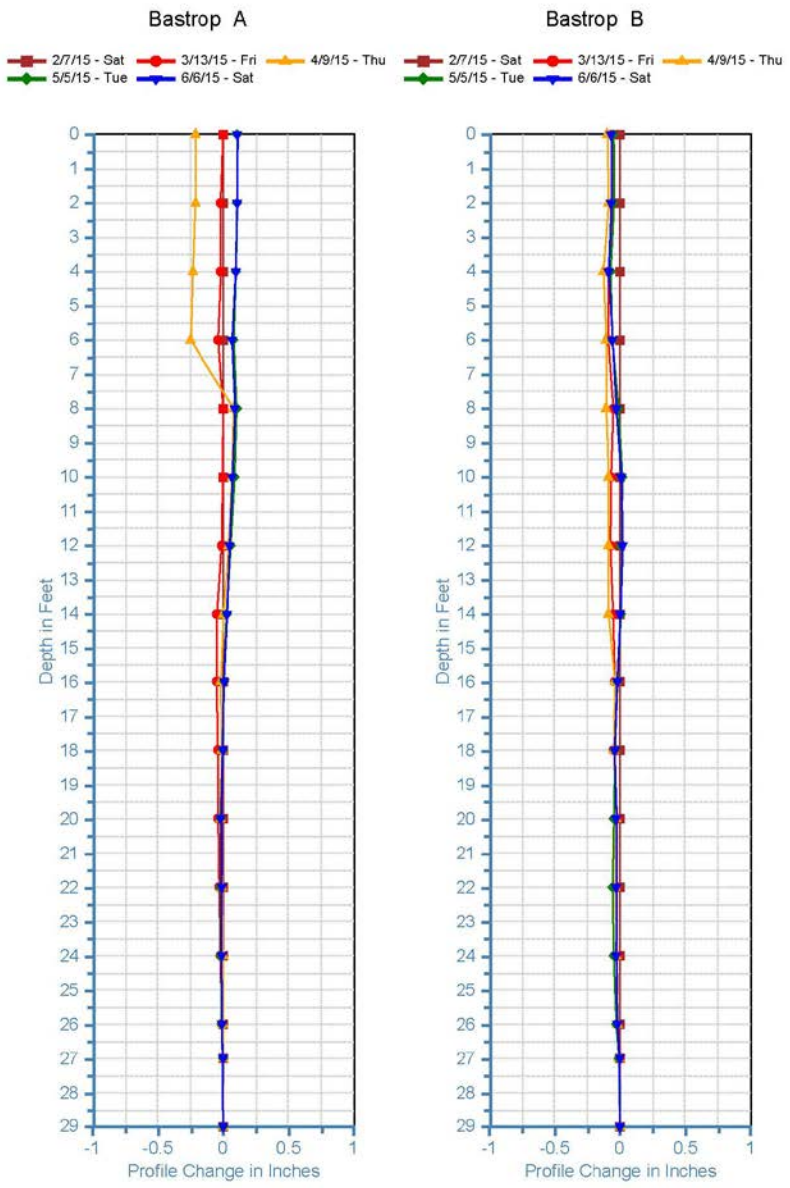

Figure 151. Inclinometer Data from Bastrop Site after Resuming.

MONITORING AT TXDOT SITE AT SALADO

Project Introduction

The second actual site selected in this project for monitoring is a TxDOT project in the Waco District at Bell County. The project is related to a new roadway on IH-35 between FM 2843 and FM 2484 (Figure 152).

Figure 152. Project in Salado.

There are a couple of MSE walls in this project. The wall that was chosen to be monitored in this project is wall AA (Figure 153). Figure 154 presents details of this wall.

The height of the AA wall is 21.5 ft, and the length is 110 ft (Figure 155). The backfill material is crushed rock, and the reinforcement used is metal strips. The length of the strips varied with depth, and for the two top rows of strips was 21 ft.

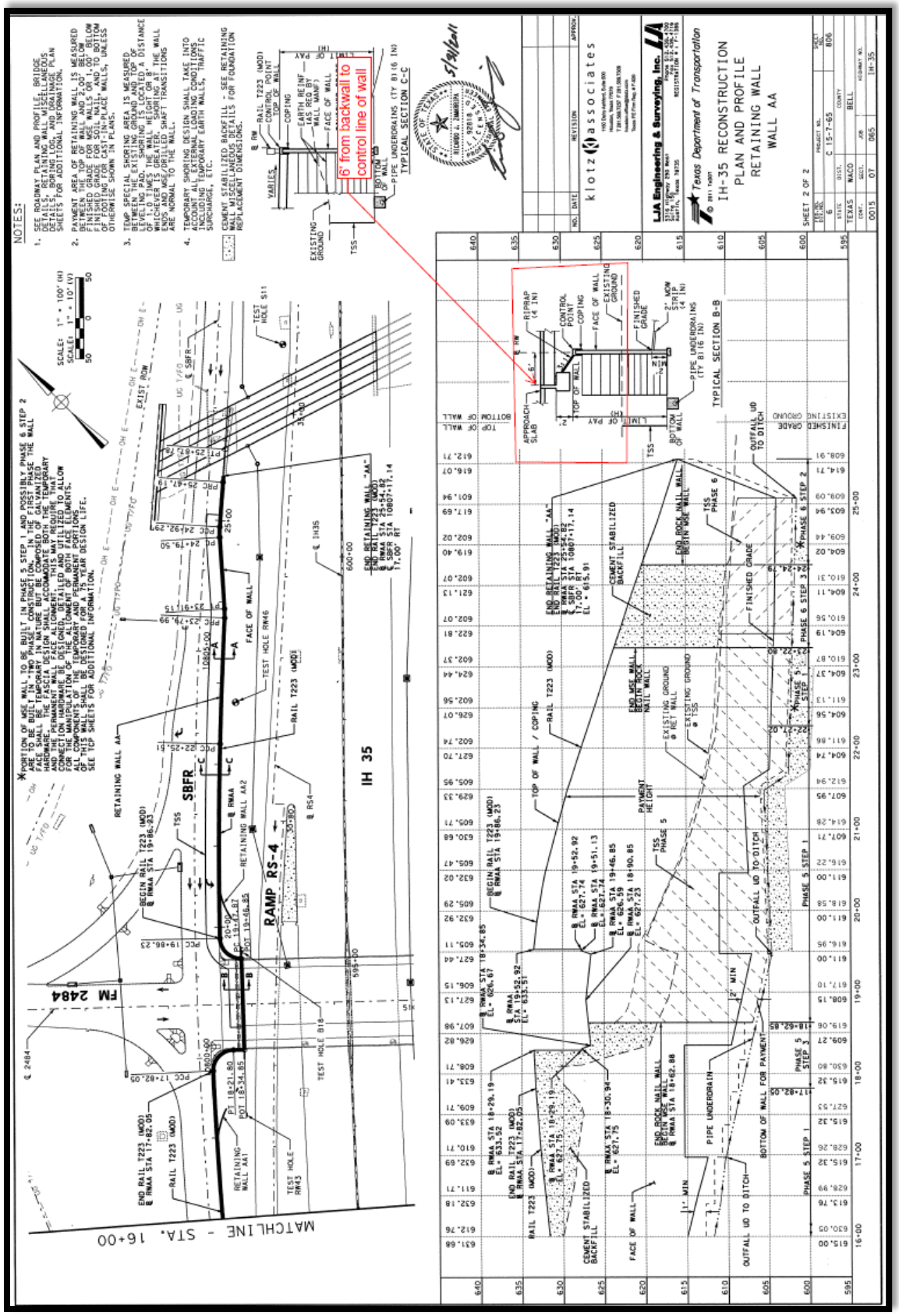

Figure 153. Wall AA Location.

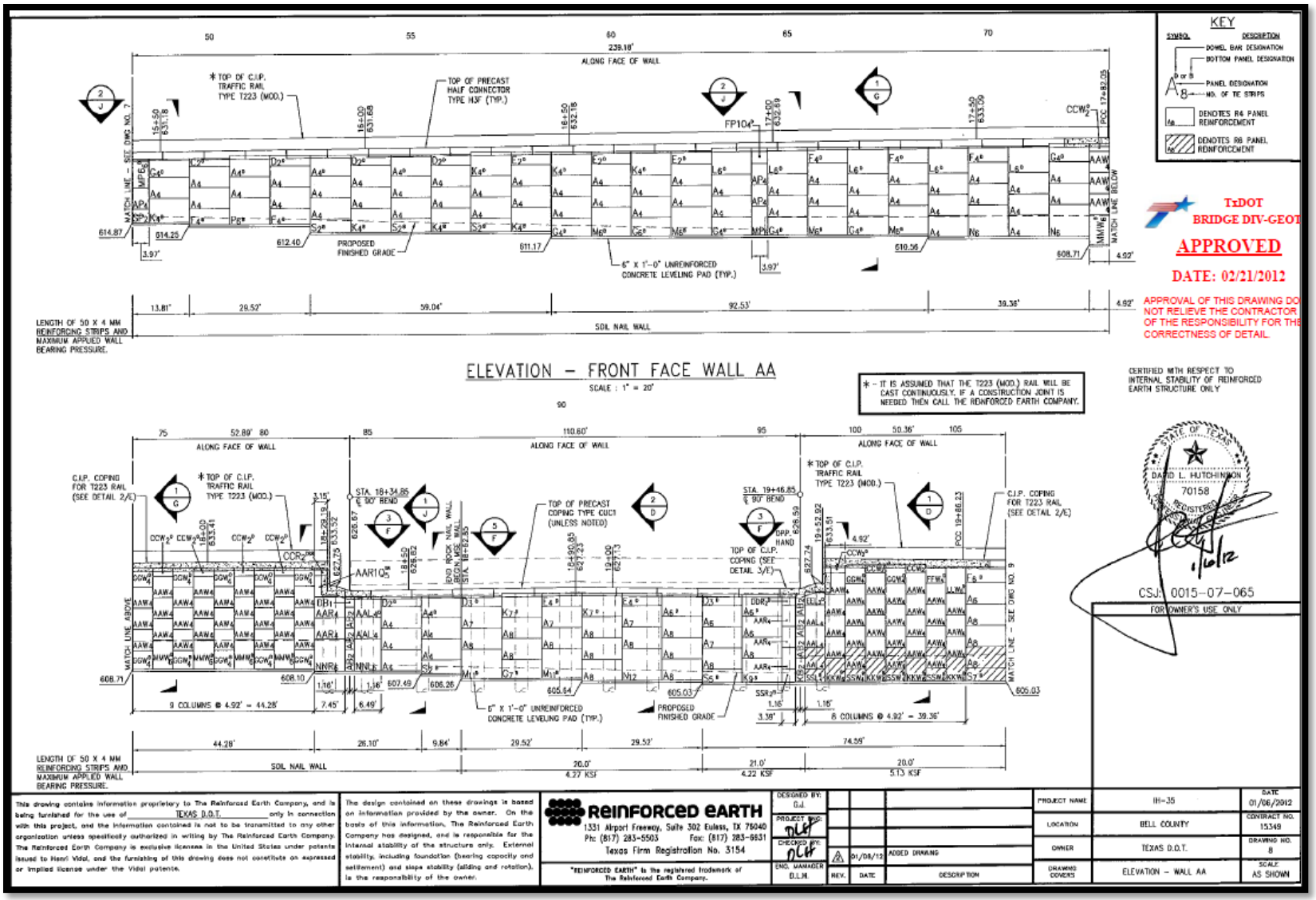

Figure 154. Wall AA Detail.

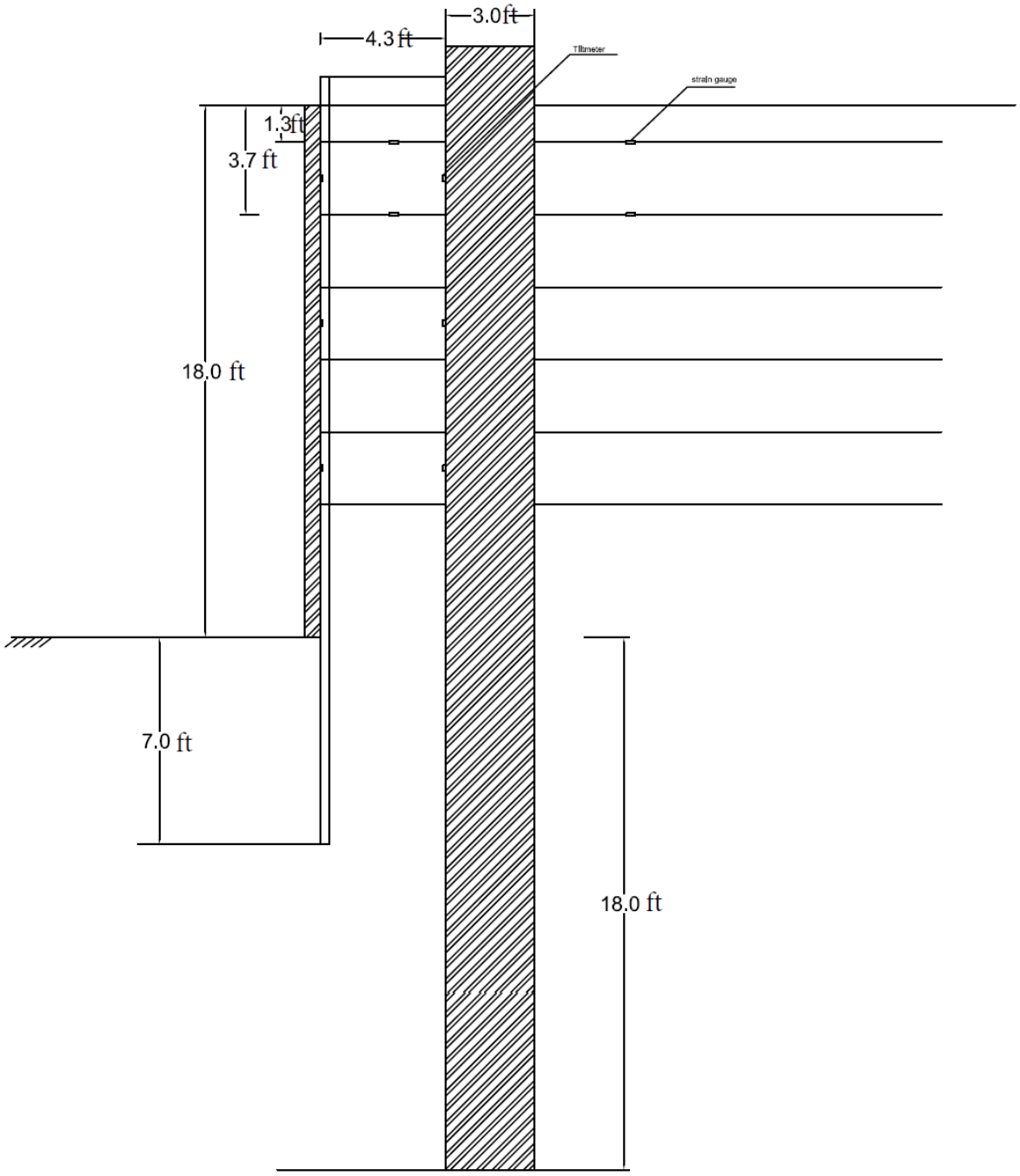

(A)

Figure 155. Cross Section (A) Plan View and (B) of the Salado Wall.

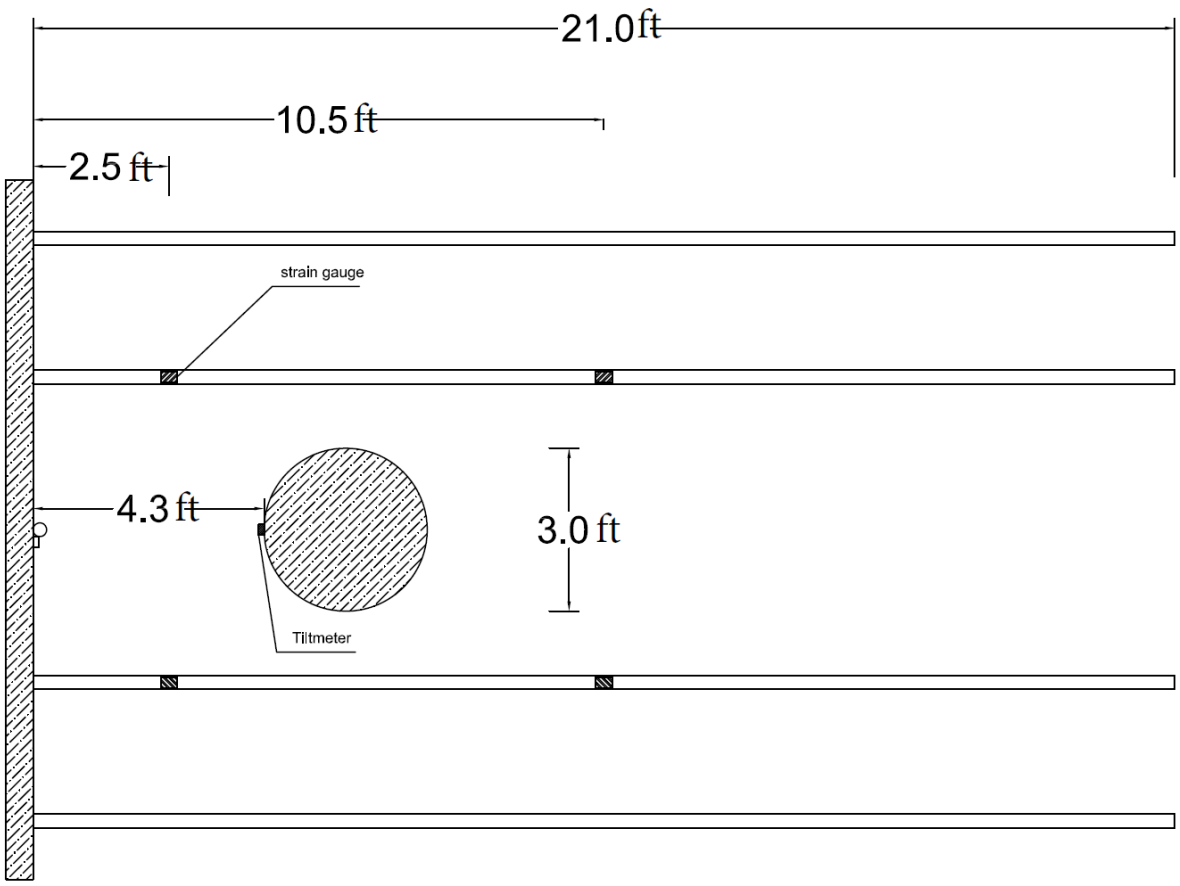

(B)

Figure 155. Cross Section (A) Plan View and (B) of the Salado Wall. (Continued).

Instrumentation

The instrumentation for this project was similar to the one adopted for the Bastrop site, except that this site did not use a pressure cell and the soil reinforcement was metal strips.

Inclinometer

On May 21, 2013, the hole for the inclinometer casing was drilled (Figure 156), the casing was placed in the hole, and then the annulus between the casing and the hole was filled with grout (Figure 157).

Figure 156. Drilling the Hole for the Inclinometer Casing.

The initial plan was to drill the hole to a depth of 21 ft (equal to the wall height) to make sure that the bottom of the casing would have minimal movement. This depth was reduced to 7 ft because hard rock at that depth (i.e., the natural ground) was encountered and drilling a 4-in. diameter hole to a depth of 21 ft was very difficult and expensive. Because of the shallow hard rock, it is unlikely that the bottom of the casing moved.

Figure 157. Final Phase of Hole.

Tiltmeter

A total of six tiltmeters were installed on this project. Three of them were installed on the wall (inside the panels) and three of them were installed on the drilled shaft. They were protected by metal boxes and the wires were protected by metal conduits (Figure 158).

Strain Gauge

Eight full bridge strain gauges were used at this project site. Four of them were installed on the top layer of strips and four were installed on the immediate layer below that. As shown in Figure 159 and in addition to regular protection of the gauges, they were protected by sandbags to prevent any damages from the crushed rock. Wires were protected by PVC tubes and metal conduits.

Figure 158. Tiltmeter Used in Salado Site.

Figure 159. Instrumented Strips in Salado Site.

Results

The bridge opened to traffic in January 2015. The solar panel and data logger were installed on January 15, 2015, and the first data were collected on January 28, 2015. The collection of data took place from January 2015 to August 2015.

Strain Gauge Results

A total of eight strain gauges were used in this project site. Four of them were installed on the top layer of metal strips, which are labeled “T” at the beginning of the reference, and four of them were installed on the second layer of metal strips, which are labeled “B” at the beginning

of the reference. The numbers 2 and 9 refer to the distance from the strain gauge to the wall. Figure 160 shows the numbering of the strain gauges. Figure 161 presents the results for all strain gauges. Because of the noise in the data, the relative difference between the reference strain gauge labeled TL2 and the remaining seven strain gauges are plotted in Figure 161. The averages of the relative difference were constant during monitoring, which is indicative of a stable condition.

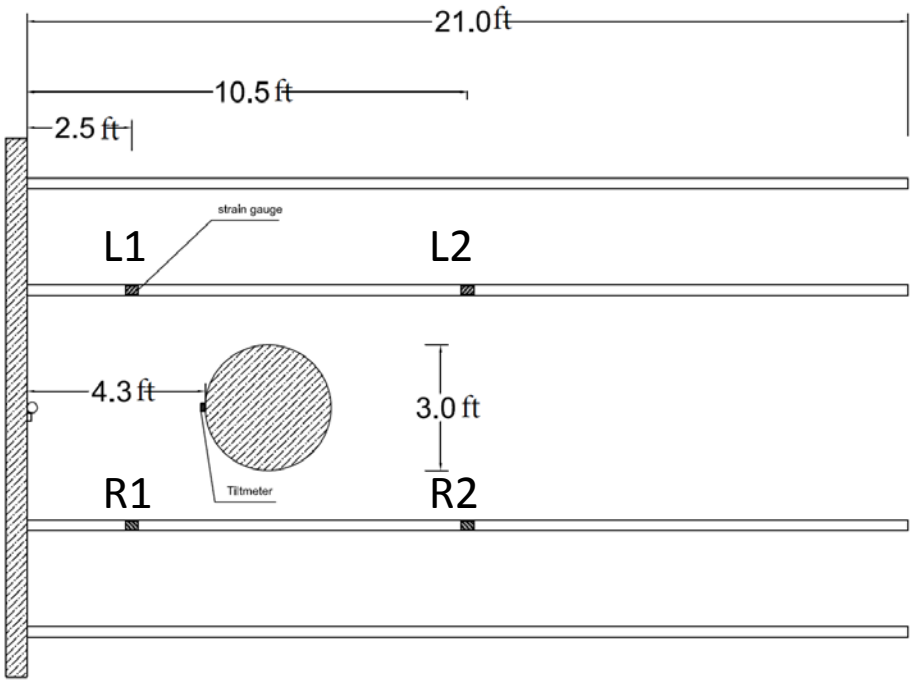

Figure 160. Strain Gauge Numbering.

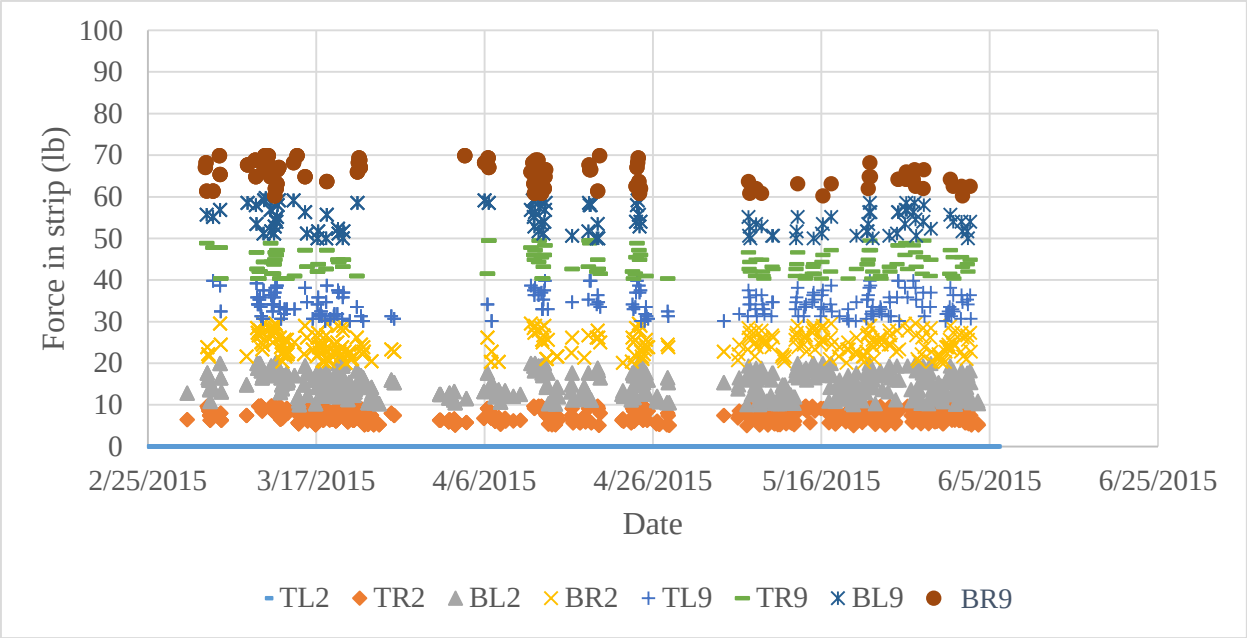

Figure 161. Strain Gauge Data from Salado Site.

Tiltmeter

A total of six tiltmeters were installed in this project: TW at the top of the wall, MW at the middle of the wall, BW at the bottom of the wall, TS at the top of the drilled shaft, MS at the middle of the drilled shaft, and BS at the bottom of the drilled shaft. Figure 162 shows the results for these tiltmeters. Because of the noise in the data, the relative difference between the tiltmeter labeled TS and the remaining seven strain gauges was plotted. The relative difference was constant during monitoring indicating a stable condition. Overall the tilt is very small with a maximum value of 0.1 degree. The rotation is more at the bottom than at the top of the wall and of the drilled shaft, which may point to a very small, deep-seated movement instead of movement created by a top load.

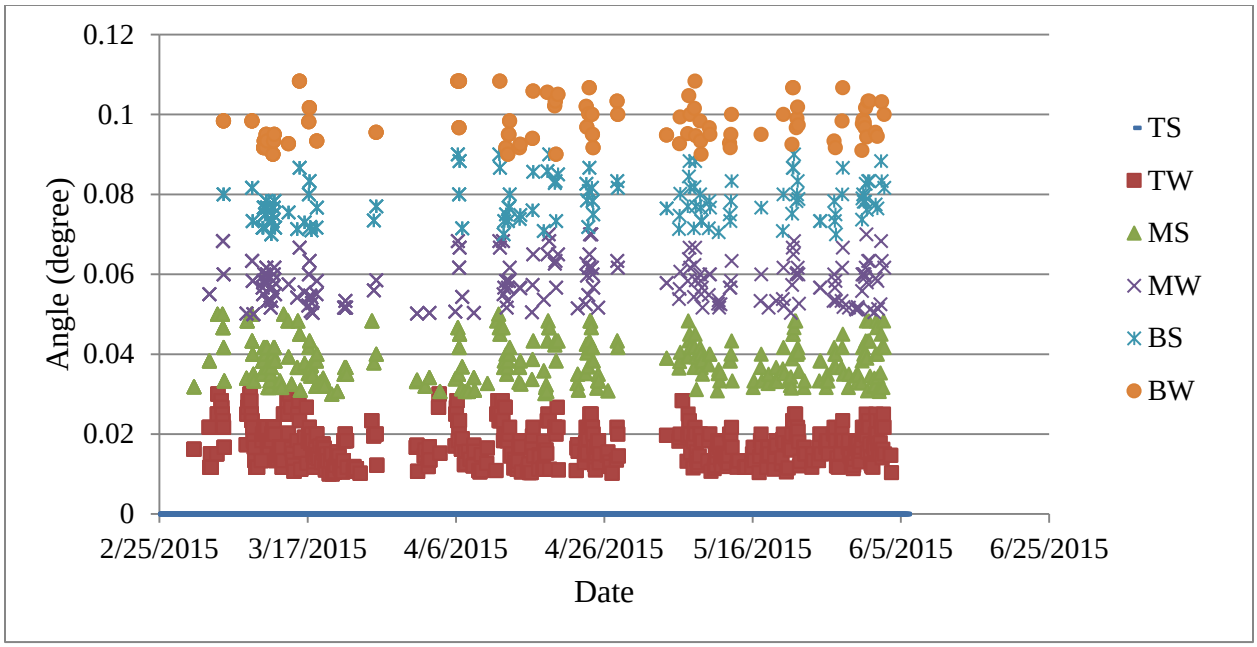

Figure 162. Tiltmeter Data from Salado Site.

Inclinometer

The zero reading of the inclinometer was taken before the bridge was opened to traffic. Figure 163 demonstrates these results. The A-axis is perpendicular to the wall panels, and the B-axis is parallel to the wall panels.

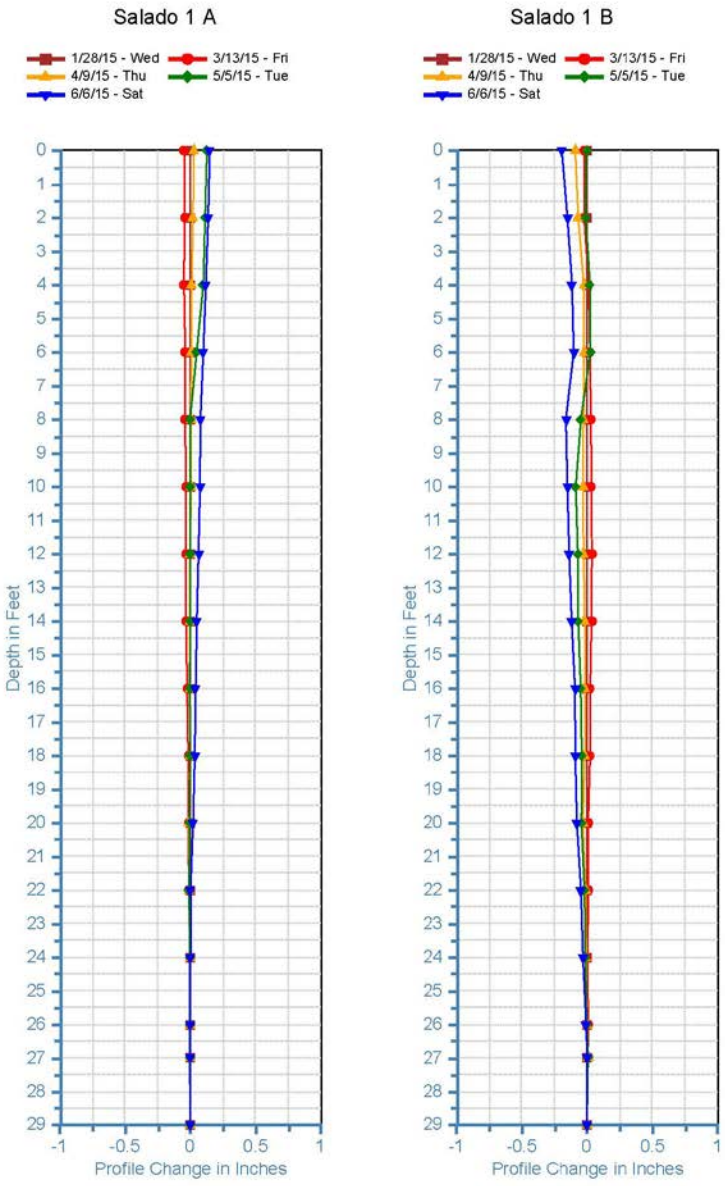

Figure 163. Inclinometer Results for Salado Site a) Perpendicular to the Wall Panels and b) Parallel to the Wall Panels.

CONCLUSION

A full-scale test was performed successfully at the TAMU Riverside Campus. For this test, all of the devices worked perfectly and valuable data were gathered. The real project site in Bastrop, Texas, was monitored from December 2013 to August 2015. All of the devices installed

on the wall and drilled shaft during the construction worked and data collection began when the bridge opened to traffic. The results indicated that no change had occurred in the readings during that entire period of time.

The real project site in Salado, Texas, was monitored from January 2015 to August 2015. All of the devices installed on the wall and drilled shaft were installed during the construction and data collection began when the bridge opened to traffic. The results indicated that no change had occurred in the readings during the observation period.

CHAPTER 5:
NUMERICAL MODELING

INTRODUCTION

This chapter presents the numerical modeling of a drilled shaft built within an MSE wall. It covers the model calibration, a parametric study, numerical results, and a discussion. The model calibration is based on matching the pullout test data and the field test information at the TAMU-NGES at the Riverside Campus. The pullout test data were performed for the TxDOT Project 0-6493 at Texas Tech University, while the field test data were gathered from the test completed at the TAMU Riverside Campus in August 2012, as part of this research. Once calibrated, the numerical model was used to investigate the influence of various factors on the performance of the drilled shaft and the MSE wall. The numerical software FLAC3D (version 4.0) was adopted for this study.

SIMULATION OF THE PULLOUT TEST WITH CABLE ELEMENTS

According to FLAC 3D version 4 manual (Itasca, 2006), the cable elements seem to be most suited to model the strips. Two types of springs are contemplated in FLAC 3D software, shear and normal. Normal springs are mainly used for beam elements, while shear springs are used for cable elements. As the shear spring deforms, the shear force, F_s, per unit length in the spring increases. Deforming the spring implies that the distance between the node of the structural component and the hosting media changes. For a given deformation, the spring shear force increases with increasing spring stiffness (k_s), and it reaches a limiting value of F_s^{max}/L (Figure 164[a]).

The parameters used in the model for the shear spring were Φ_s and C_s. Texas Tech University conducted pullout tests on metal strips (Lawson et al., 2013). The tests were performed at three different depths (i.e., different confining pressure) (Figure 165).

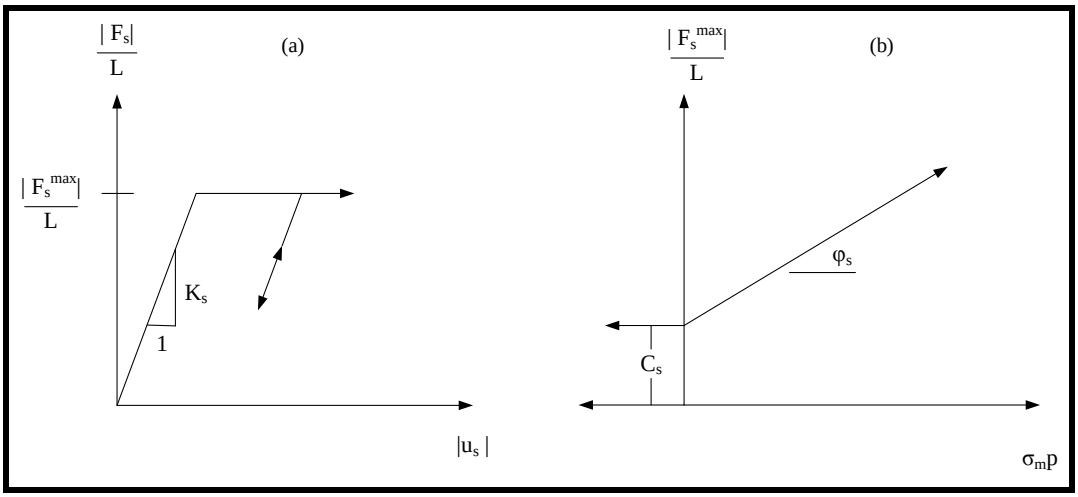

Figure 164. Shear Spring Modulus (Itasca, 2006).

F_s^{max} is defined as the pullout force for a displacement of 0.75 in. The Texas Tech tests (Figure 165) were performed at three different depths, and for each test a point was obtained in the F_s^{max}/L versus $\sigma_m p$ set of axes (Figure 166). The best fitting line was drawn through these three points. According to the FLAC 3D user's guide (Itasca, 2006), the slope of this line is Φ_s and the intercept of the line with the F_s^{max}/L axis is the C_s (Figure 164) (p is the perimeter of the strip). The shear friction angle (Φ_s) was 57.6°, and the shear cohesion (C_s) was 2.64 psi. Note that these parameters are called shear friction angle and shear cohesion, but they do not correspond strictly to the shear parameters of the fill or strips, but rather to the model parameters of the cable related to the shear resistance of the strip-fill interphase back-calculated from the experiments.

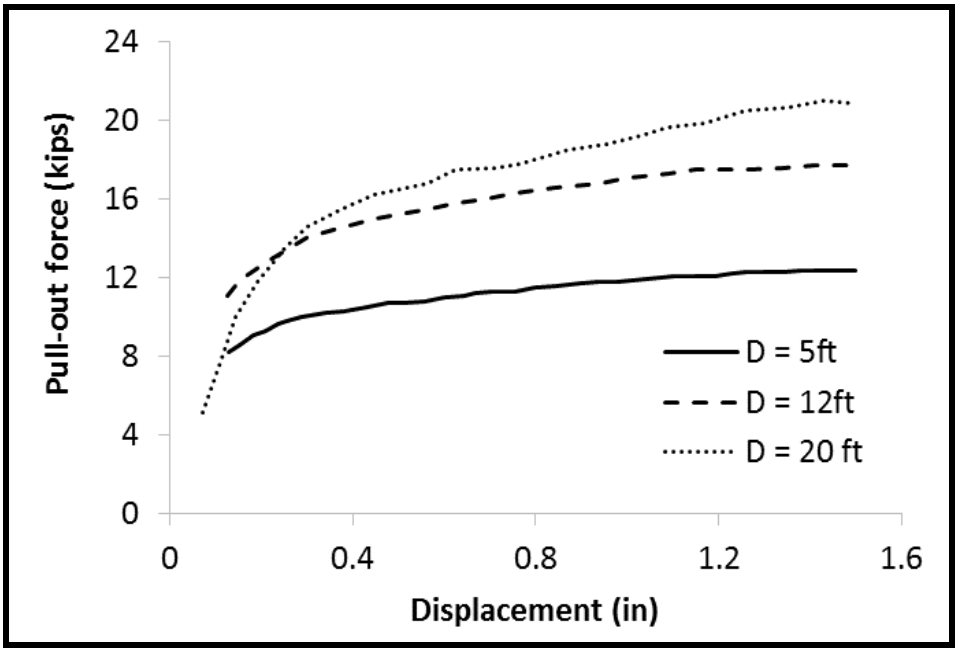

Figure 165. Pullout Test Results for 2.44 m Long Strip at Different Depth (Jayawickrama et al., 2013).

To check if the parameters obtained for the cable elements were correct, the pullout tests were modeled by using FLAC 3D (Figure 167). Figure 168 shows the results of the pullout tests and the model simulations for the 8 ft long strip at a depth of 5 ft. As observed, a very satisfactory agreement between experimental and model results was obtained.

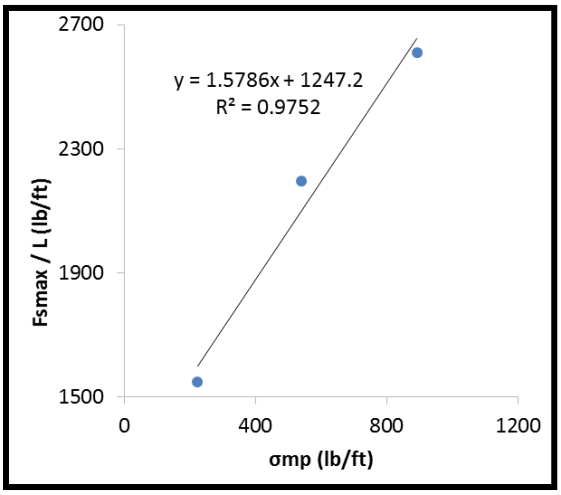

Figure 166. Calibration of Shear Spring for Metal Strips.

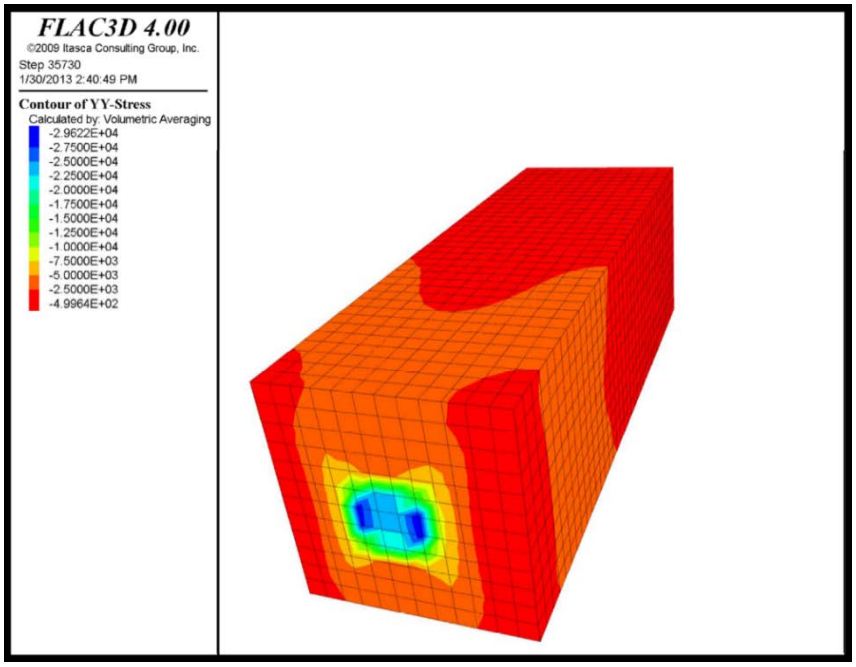

Figure 167. FLAC 3D Model of Pullout Test for 8 Ft Strip in Depth of 5 Ft.

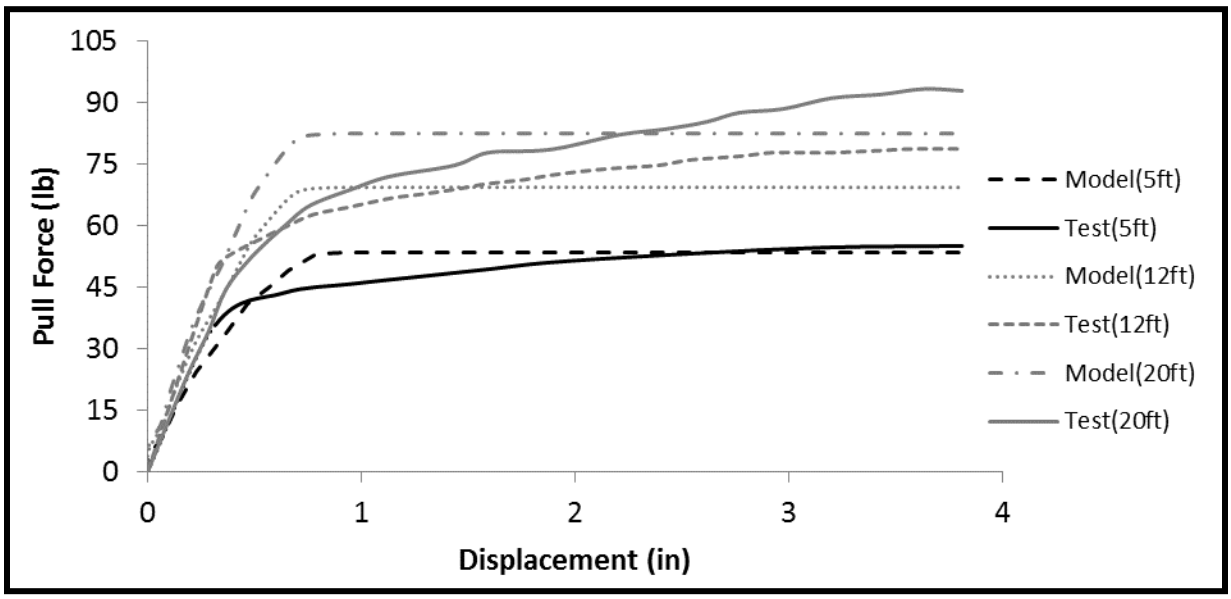

Figure 168. Results for Test and Modeling of Pullout for 8 Ft Strip in Depth of 5 Ft.

MODELING THE PULLOUT TESTS DISCRETIZING THE METAL STRIP IN THE MESH

The interesting point about the use of metal strips as reinforcement for MSE walls is their high friction factor. The friction factor (F^*) is defined as:

$$F^* = \frac{T_{pull-out}}{2\alpha\sigma_v^{'} b L_a} \tag{5.1}$$

where $T_{pullout}$ is the pullout force in the strip for 0.75 in displacement; α is the scale factor, which is equal to 1 for metal strips; σ'_v is the vertical effective stress; b is the width of the strip; and L_a is the length of the strip. For a smooth strip without bumps, F* is taken to be equal to tan(φ), which is about 0.6, but for the actual strip with bumps it can be much higher (up to 6.15). Figure 169 presents the recommended friction factor values by AASHTO (2010), some of the measured values as a function of depth, and the results of the numerical simulations for the 2.44 m long strip.

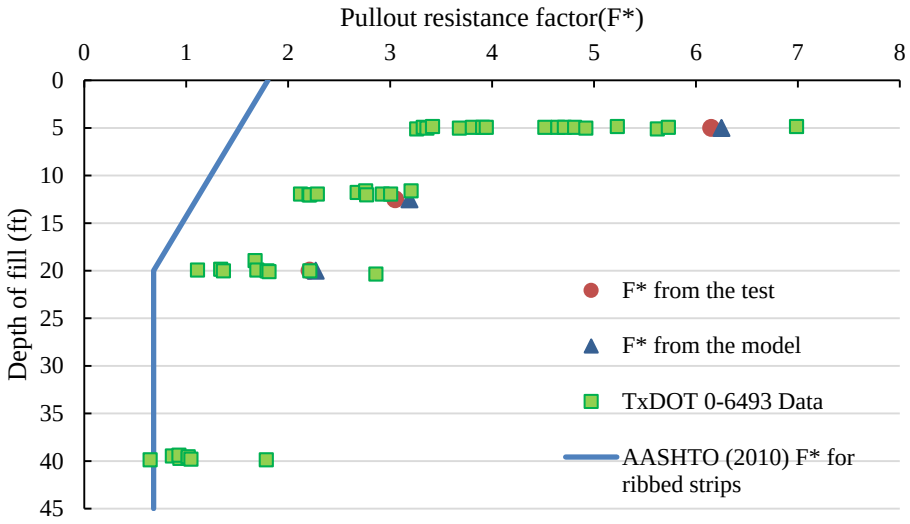

Figure 169. Pullout Resistance Factor vs. Depth.

To study in greater detail the friction factor and to check if high friction factor values are justifiable, an actual strip was modeled in FLAC 3D. Figure 170 shows the details related to the modeling of the strip, and Figure 171 presents the full model. Figure 172 shows the strip with many ribs per foot of length.

Figure 173 plots the results of the pullout modeling of the actual strip. The results from the pullout tests are also plotted on the same graph. The important parameter in this modeling is the number of bumps per foot of the strip. The arrangement of the bumps on the strip is unimportant. Another model prepared for evenly distributed bumps on the strips and the results were the same as the actual strip.

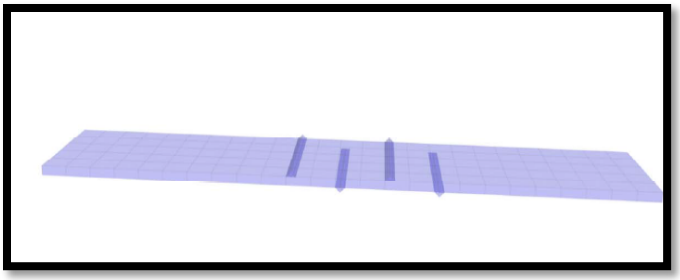

Figure 170. Detail of Modeled Strip (Actual Strip).

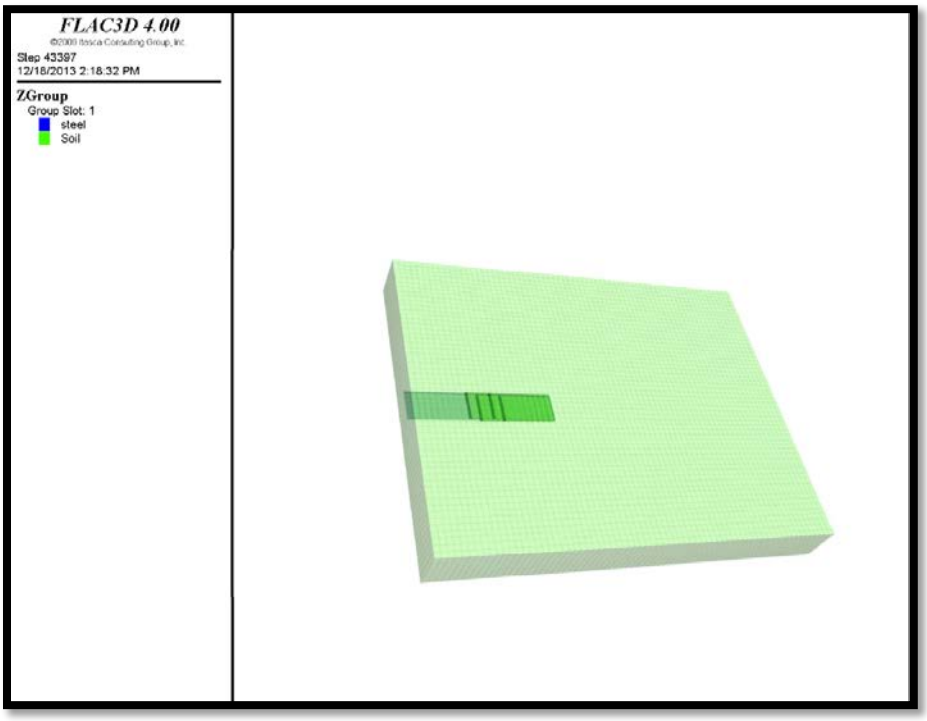

Figure 171. Completed Model of Actual Strip.

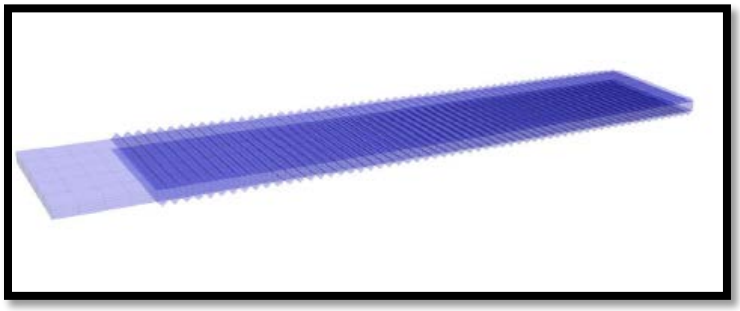

Figure 172. Detail of Modeled Strip with 60 Bumps per Foot.

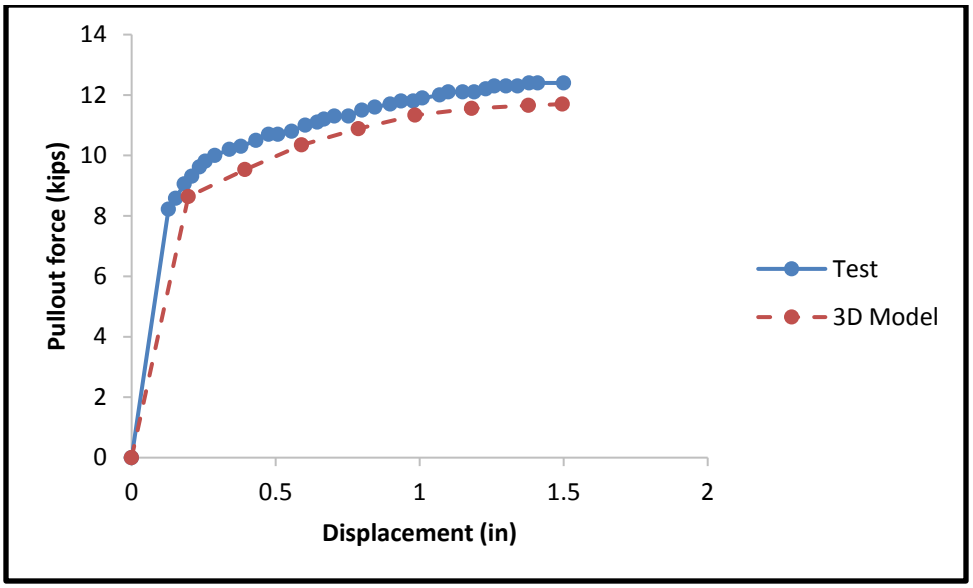

Figure 173. Results of the Modeling the Actual Strip and Pullout Test.

In this part of the research, the effect of the number of the bumps and of their shape was studied. For this purpose, 14 different models were prepared considering different numbers of bumps per foot and using the standard shape for the bumps. Then, this procedure was repeated for four different shapes (i.e., bump angles) and a total of 56 models were prepared. Figure 174 presents the results. These models were developed for a vertical pressure equivalent to a depth of 5 ft. For this depth, the maximum value of the friction factor was 12.5, at which point the steel failed. In order to capture the whole behavior in a unique graph, the strength of the steel was increased in the model to a higher friction value. As can be seen from Figure 174, the number of bumps per foot has a significant influence on the pullout capacity of the strip. This is attributed to the fact that the bumps engage the bearing capacity of the soil in addition to the friction. In other words, the friction factor is more of a bearing capacity/friction factor. Currently, the typical number of ribs is 4 per foot and gives a friction factor of 4, which consistent with the average from pull out tests. It is not possible to place 60 ribs per foot of strip as there would be no room to put all the ribs. However, an increase to 10 ribs per foot is reasonable and gives a friction factor of 12; so the gain in friction factor is very significant as it is 3 times higher than the current value.

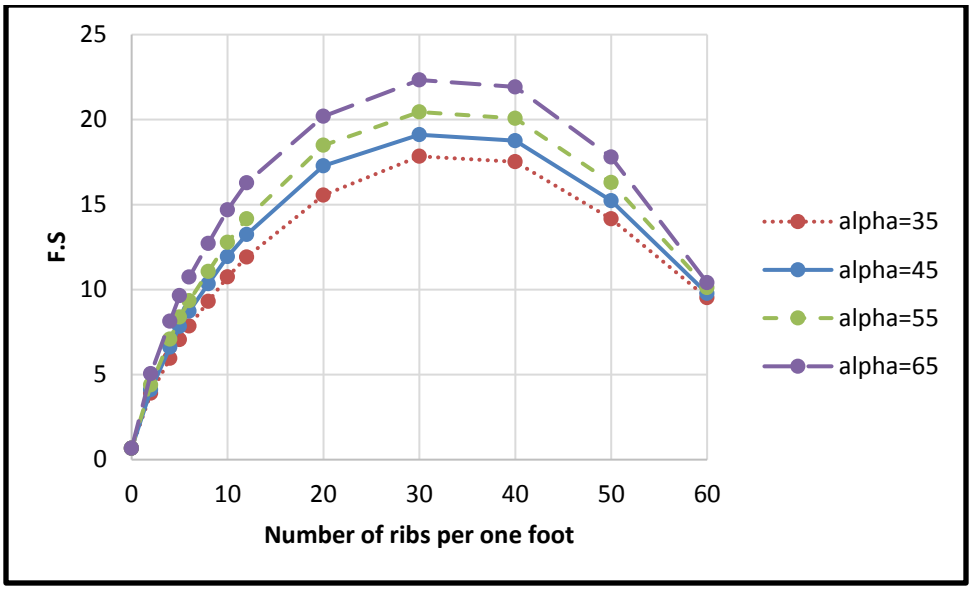

Figure 174. Friction Factor for Different Cases.

SIMULATION OF THE LOAD TEST AT RIVERSIDE CAMPUS

This simulation was conducted while optimizing the two conflicting goals of creating a close representation of the wall and the drilled shaft system on one hand and of keeping sufficient simplicity of representation to be able to make many runs within a reasonable amount of time on the other. The reinforced soil, retained soil, and foundation soil were modeled as linearly elastic-perfectly plastic materials, with Mohr-Coulomb failure criteria (i.e., the so-called "Mohr-Coulomb model"). The Mohr-Coulomb model has been successfully used in other studies to simulate MSE walls (Hatami and Bathurst, 2005; Huang et al., 2009; Huang et al., 2011). Those studies showed that the Mohr-Coulomb model could satisfactorily reproduce the experimental observations. Based on this background information, the Mohr-Coulomb model was adopted in this study.

The reinforcement was modeled as a structural element (i.e., by using the cable element already implemented in FLAC3D). The cable element behaves elastically up to the tensile or compressive strength. The interaction between reinforcement and backfill soil was simulated by Mohr-Coulomb sliders, which are linearly elastic, perfectly plastic springs formulated using the Mohr-Coulomb failure criteria.

The MSE wall facing panel was simulated as a linear elastic material. The contacts between the panels were also modeled by means of Mohr-Coulomb sliders. Considering the interlocking that exists between the panels, the cohesion at the interface was assumed to be equal

to the shear strength of the concrete. The connection between the panel and the reinforcement was assumed rigid (i.e., no connection failure was allowed during the numerical modeling). The drilled shaft was simulated as an elastic material and typical values for concrete were adopted for the Young modulus and Poisson's ratio (Table 4).

The modeling of the wall was carried out in steps. The initial stress field of the foundation soil was first established, and then construction of the MSE wall was simulated by lifts mimicking the actual construction process. A concentrated lateral force was applied at the top of the drilled shaft, and this load was gradually increased by equal increments. The numerical model was calibrated using the data obtained from the field test at the TAMU Riverside Campus.

Table 4. Properties Used in the Numerical Simulation.

Material	Constitutive Model	Properties
Natural soil	Mohr-Coulomb	Φ'=30°, C'=0, ϒ= 114.6 pcf B=1610 psi, G= 536.6 psi
Backfill soil first layer	Mohr-Coulomb	Φ'=27.3°, C'=0.79 psi, ϒ= 114.6 pcf B=680 psi, G= 226.26 psi
Backfill soil second layer	Mohr-Coulomb	Φ'=27.3°, C'=0.79 psi Kpa, ϒ= 114.6 pcf B=475.7 psi, G= 158 psi Mpa
Backfill soil third layer	Mohr-Coulomb	Φ'=27.3°, C'=0.79 psi, ϒ= 114.6 pcf B=455.4 psi, G= 152.3 psi
Drilled shaft	Elastic (isotropic)	B=3.6e6 psi, G=1.2e6 psi, ϒ= 159 pcf
MSE wall facing	Elastic (isotropic)	B=3.6e4 psi, G=1.7e4 psi, ϒ= 159 pcf
Metal Strip	Elastic-perfectly plastic	E=3.04e7 psi , K_s=942 psi, Φ_s=57.6 , C_s=2.64 psi

Natural Soil

The natural soil affects the behavior of the wall and the drilled shaft. At the Riverside Campus, the natural soil is composed of a thin layer of very hard black clay (about 30 cm) overlying a thick layer of clean sand. The sand in the lower layer is a poorly graded sand (classified as SP according to the Unified Soil Classification System, USCS) with a coefficient

of uniformity (C_u) equal to 3.5 and a coefficient of curvature (C_c) equal to 0.88. To obtain the strength parameters of the clean sand layer, PMTs were used. Three PMTs were performed at different depths. The parameters obtained from these PMTs were used to check the bearing capacity of the natural soil. These parameters were also used in the numerical modeling of the test. Figure 175 presents the results of the PMTs for depths of 2.0 ft, 4.4 ft, and 6.9 ft. The vertical axis corresponds to the pressure on the borehole wall (P), and the horizontal axis is the ratio of the change in probe radius to the initial probe radius. The slope of this graph in the elastic region is equal to 2G where G is the shear modulus (Briaud, 1992). The modulus of elasticity obtained from the PMT for the natural sand was 1563.5 psi.

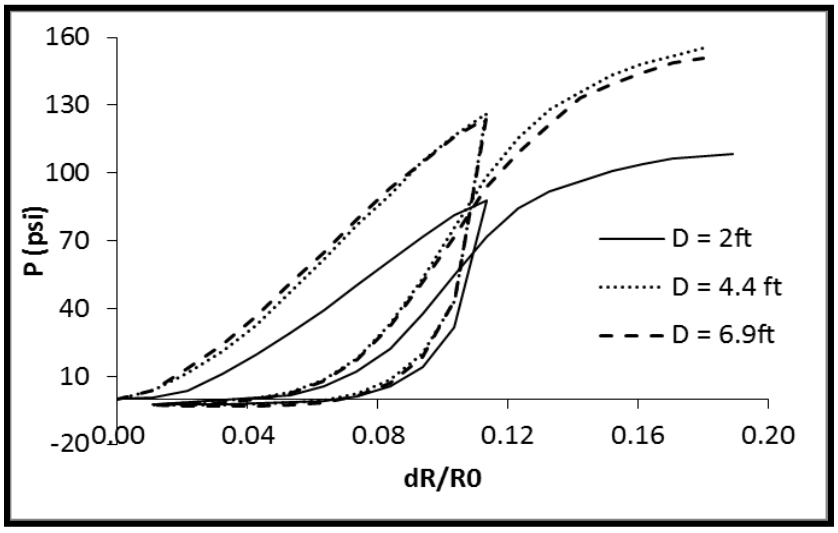

Figure 175. Natural Soil PMT Results at Different Depths.

The natural soil was modeled as a single layer material, and the Mohr-Coulomb constitutive model was adopted in the simulations. Based on existing information related to the site, cohesion was not considered and a friction angle of 30° was assumed.

Backfill Soil

The backfill material used in this investigation was a fine to medium sand. This sand satisfies the backfill requirements for an MSE wall specified in AASHTO Load and Resistance factor design (LRFD) Bridge Construction Specifications, FHWA Publication No. FHWA-10-024 and TxDOT Specification Item N^o 423/Type B select backfill (AASHTO 2010; Elias et al., 1997). The coefficient of uniformity (C_u) for this soil is 4.5, and the coefficient of curvature (C_c) is 0.8. According to the USCS, the soil is classified as a poorly graded sand. The average dry

density and water content are 111.4 pcf and 3 percent, respectively. These values were determined by means of the nuclear density probe (ASTM D6938-10). This dry density represents 95 percent of the maximum dry density obtained in the modified Proctor test for the backfill material (ASTM D1557-12, 2012).

Two types of tests were performed to determine the backfill sand parameters: laboratory tests (triaxial), and in-situ tests (PMT). Triaxial tests were performed at three different confining pressures associated with the different depths of the strips instrumented in this research. The dry density obtained from the nuclear density tests was adopted to prepare the soil samples in the lab. In the triaxial tests, the sand behaved like a loose sand. Figure 176 presents the results of the triaxial tests for backfill material. The friction angle for this material was around 27.3° (i.e., ϕ=27.3°), and the cohesion around 0.79 psi (i.e., c=0.79 psi). The cohesion is likely an apparent cohesion due to a small water content in the sand. PMTs were also performed at depths corresponding to the depths of the strips. The results of the PMTs for the different depths are shown in Figure 177, where the variation of these values with depth can be observed.

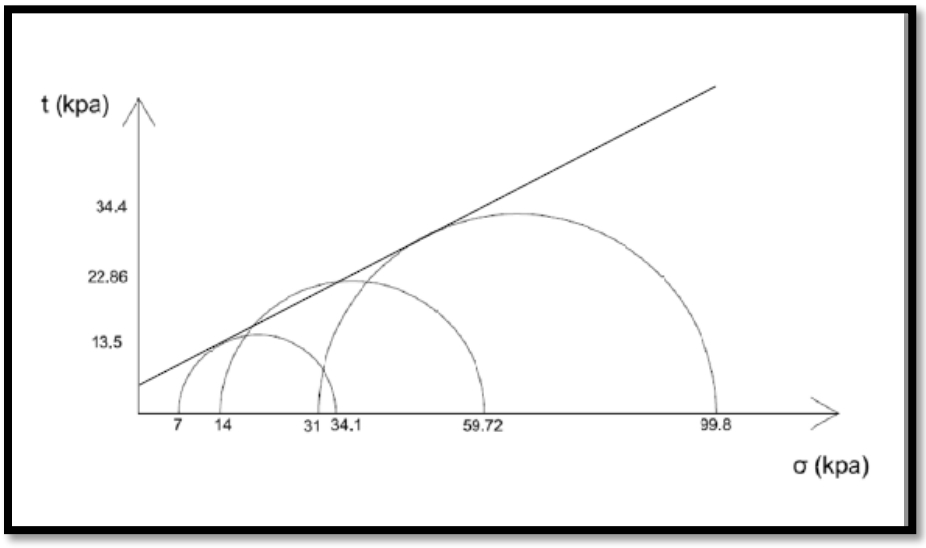

Figure 176. Triaxial Result for Backfill Material.

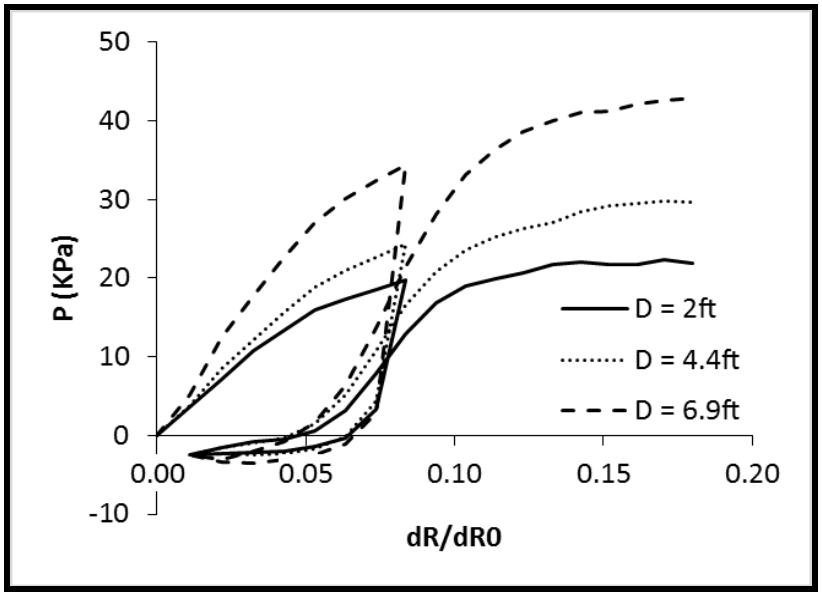

Figure 177. Backfill PMT Results at Different Depths.

In order to mimic the site conditions, the numerical simulation of the backfill soil was also modeled in three layers. Based on the triaxial tests results, a friction angle of 27.3° and cohesion of c=0.79 psi were assumed. The bulk and shear moduli were estimated from the PMT tests for different layers according to Briaud (2013).

Drilled Shaft

There were two options to model the drilled shaft. One of them was to model the pile as a structural element, which did not need to be included in the discretization (i.e., as part of the mesh), but interface elements between the shaft and the soil would be required. The other option was to model the actual shaft as an additional component of the system with the corresponding mesh and then assign the concrete properties to these elements. In this research, the second option was adopted and the shaft was modeled as an actual shaft with elastic properties.

Wall Panels

The wall panels were modeled as actual panels, and concrete properties were assigned to them. The actual wall is not uniform and there are gaps between panels. The panels are connected together by fitting into prepared grooves. There were two options to simulate the panels. One of them was to model actual gaps between panels and grooves. Hatami and Bathurst (2005) concluded that the modeling of the actual panels and the interlocking between them

would not significantly improve the numerical results. They also performed some tests on modular blocks and came to the conclusion that a friction angle of 57° and an apparent cohesion of 6.67 psi were good parameters to model the strength behavior of the MSE wall panels. They mentioned that under this condition, shear failure between the blocks would not happen. The other option was to model the wall as a uniform material but with reduced strength parameters in comparison to concrete. Yoo and Kim (2008) successfully used reduced modulus in their research. They used an elastic modulus of 300 MPa for the wall. Huang et al. (2011) also used the same parameters in their research. In this research, a reduced modulus of 300 MPa was used for the panels.

MSE Wall Model

Once all the necessary parameters to model the MSE wall were defined, the 3D model for the MSE wall was prepared. Table 4 presents all the model parameters adopted to simulate the full-scale test, including: soil parameters (for both natural soil and backfill material estimated from PMTs and triaxial tests), parameters for the drilled shaft, parameters for the panels (based on the manufacturers' specifications), and the parameters for metal strips calculated from the pullout test from Texas Tech.

The parameters mentioned above were used to create the 3D model of the MSE wall in the FLAC 3D program. A total of 22,000 elements were used to model the wall and 5 materials were used to represent the different components of the physical model presented in Figure 179.

Loading Protocol

The loading test was performed statically and under controlled load conditions. The horizontal load was applied using a hydraulic jack that pulled the shaft against the wall. The load was applied by steps of 5 kips (22.24 KN). Each step lasted 15 minutes in order to have enough time to collect data. Two unloading stages were performed. The first one was at a load of 20 kips (88.96 kN), and the second unloading was at a load of 35 kips (155.69 kN). The failure occurred at a horizontal load of 40 kips (177.93 KN). Figure 178 plots the horizontal load versus time. Chapter 4 discusses the loading protocol.

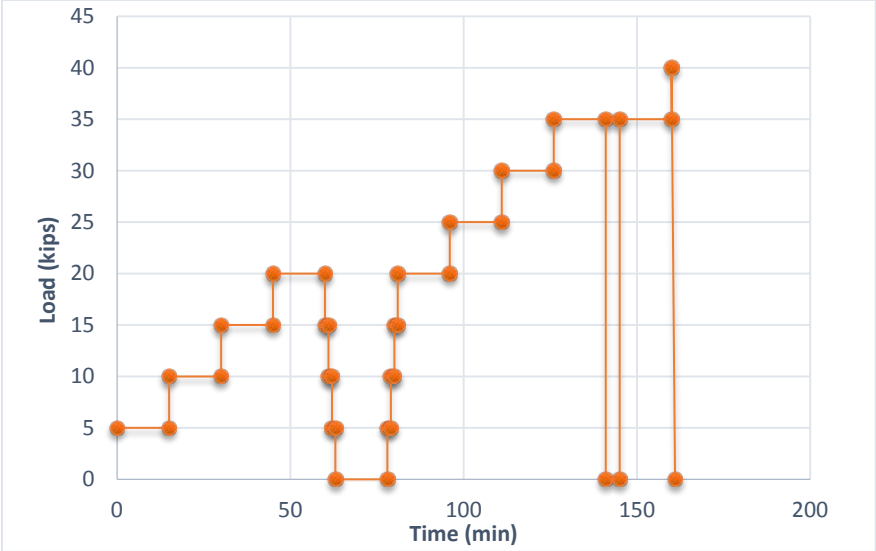

Figure 178. Loading Steps.

The same loading protocol was adopted in the numerical modeling. Figure 180 and Figure 181 depict the horizontal movements of the wall and the shaft after applying 25 kips and 40 kips load, respectively.

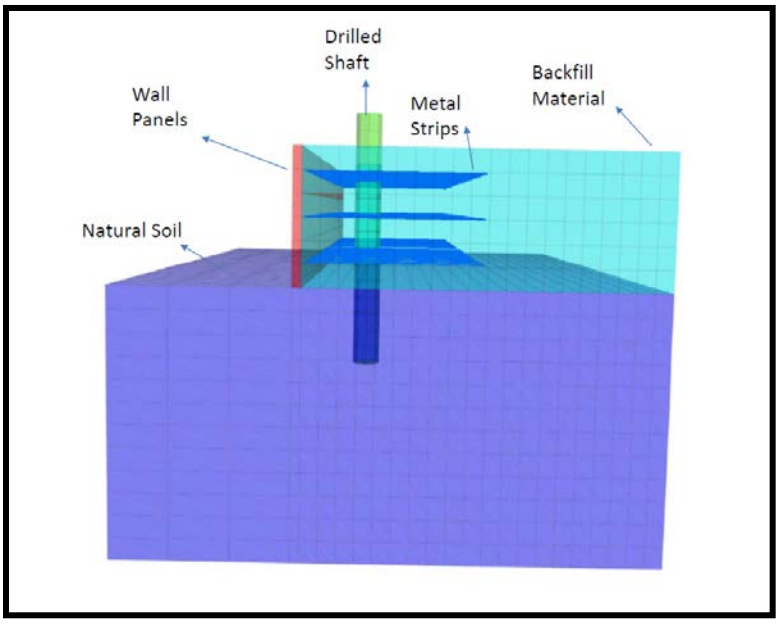

Figure 179. Different Parts of the MSE Wall Model.

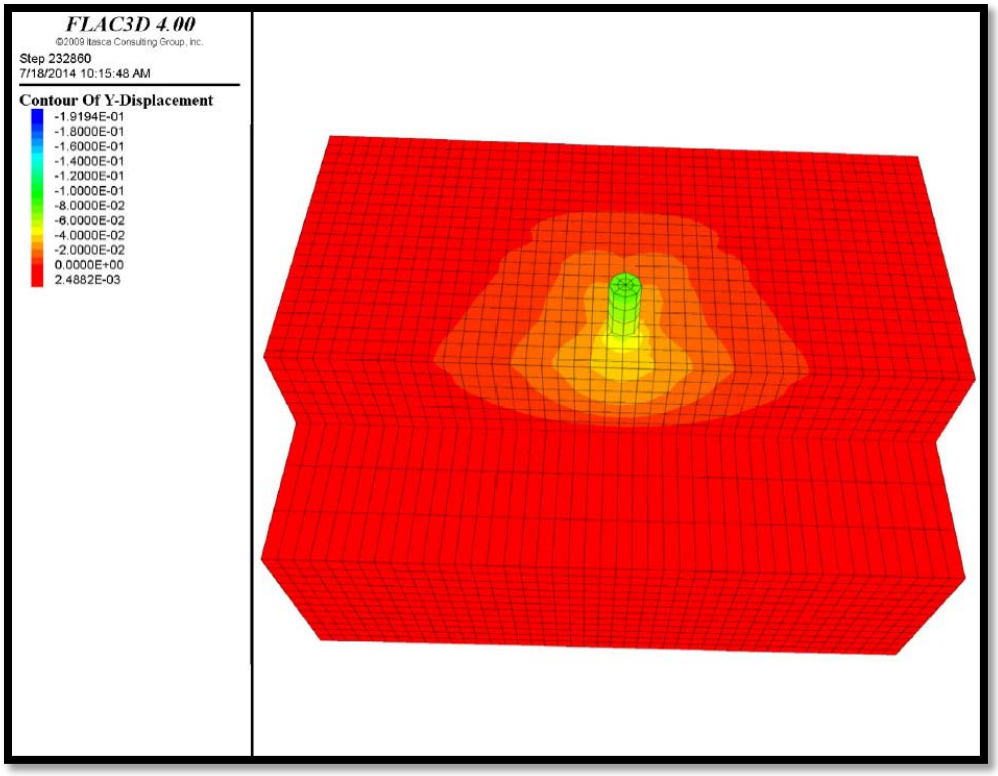

Figure 180. Deformation of the Wall after Applying 25 Kips of Horizontal Load.

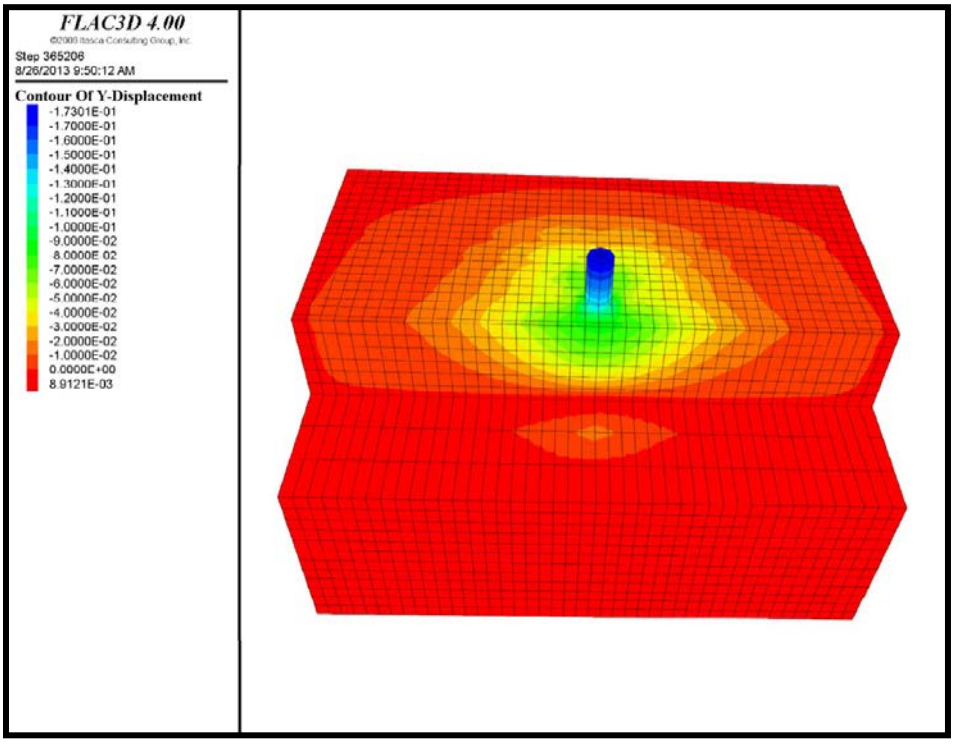

Figure 181. Deformation of the Wall after Applying 40 Kips of Horizontal Load.

Figure 182 presents deformation of the drilled shaft and the MSE wall from the numerical models. Figure 183 shows the displacement at the top of the shaft for both the experiment and the model. The model captures the behavior observed in this test.

(a) **(b)**

Figure 182. Deformation of the Drilled Shaft and the MSE Wall (a) Side View and (b) Top View.

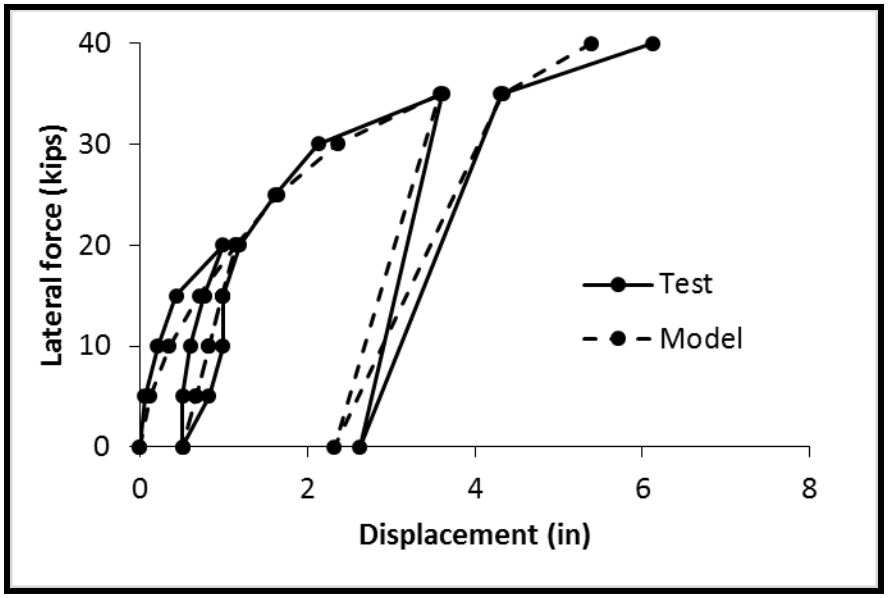

Figure 183. Deformation of Top of the Shaft for the Test and Model.

Figure 184 presents the results for the displacement at the top of the MSE wall for both the test and the model. As discussed before, in order to model the interlocks between the panels in the wall facing, a reduced modulus for the panels was adopted. This could be one of the

reasons for the slight differences observed at the beginning of the tests between experimental and modeling results.

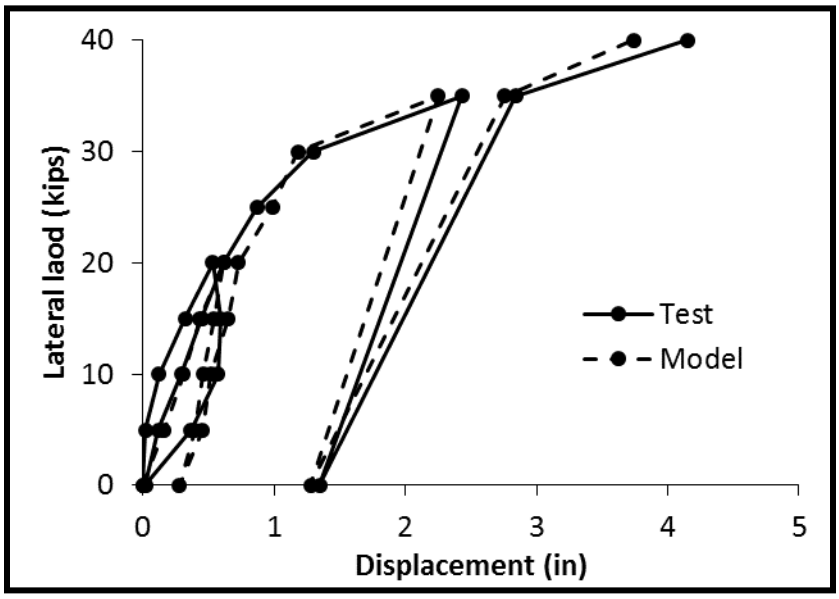

Figure 184. Deformation of Top of the Wall for the Test and Model.

The cable elements (i.e., a type of element available in FLAC-3D) were used to simulate the metal strips. Figure 185 presents the arrangement of strips in the model and the force in the strips when a horizontal load of 25 kip was applied. The force in the strips at the second layer is greater than the top layer. This feature of behavior was also observed in the full-scale test.

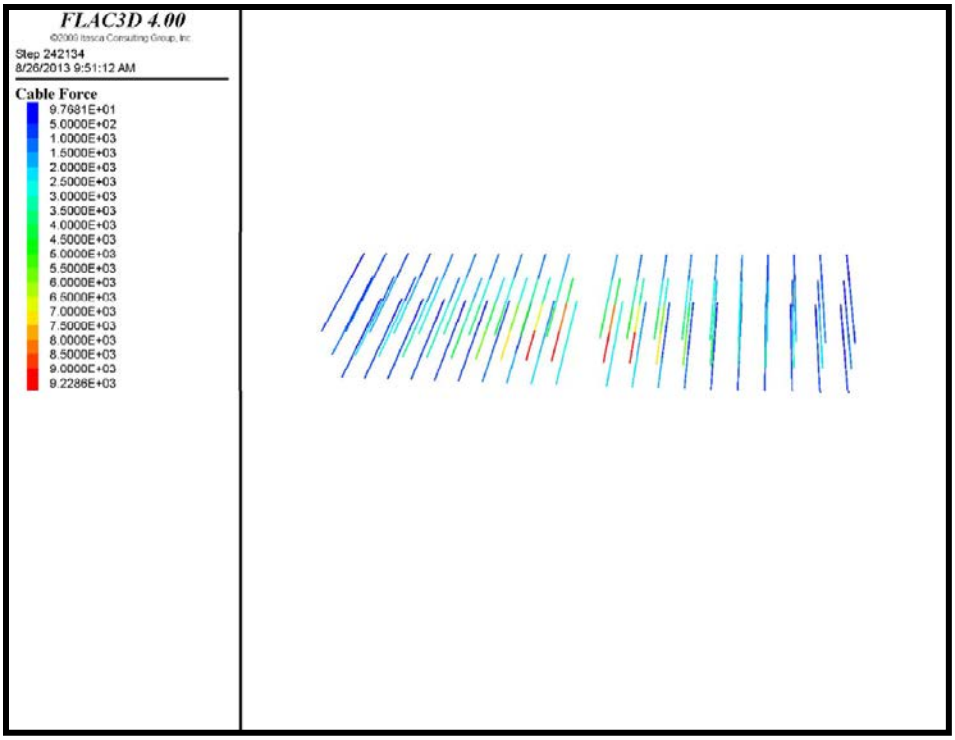

Figure 185. Forces in the Strips after Horizontal Load of 25 Kips.

Figure 186 shows a comparison between the test and the model results for the force developed in the strip located in the second layer near the drilled shaft. The match between the test and the model is not ideal, but the problem associated with this comparison is discussed below.

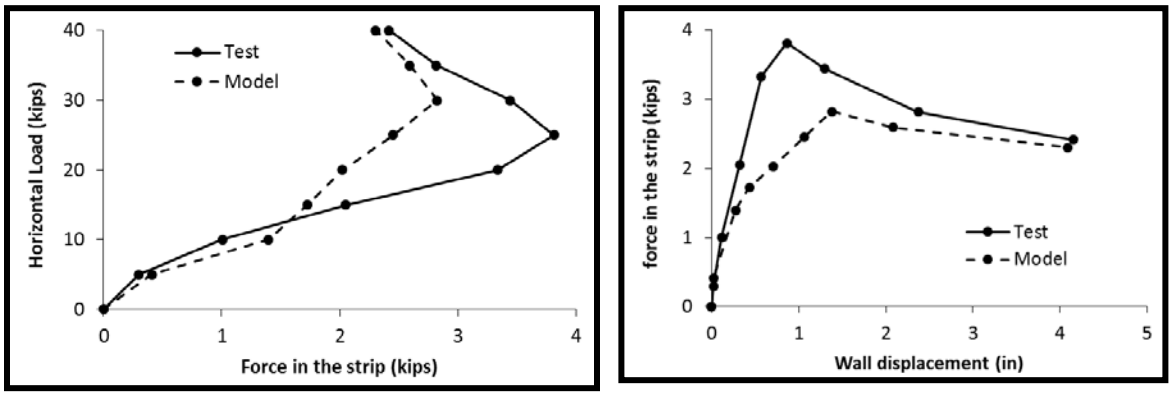

(a) **(b)**

Figure 186. Force in the Strip S-4-1-B according to (a) Horizontal Load on the Shaft and (b) Wall Displacement.

All of the parameters used in numerical modeling were obtained from independent laboratory or in-situ tests. The reference values for the metal strips were obtained from the pullout tests performed at Texas Tech (Lawson et al., 2013). To explore the sensitivity of the model results with respect to the model parameters associated with the cable elements, three different Φ_s for the strips were considered in the numerical analyses. One was obtained from the pullout test (i.e., Φ_s=57.6°, then a higher value Φ_s=70° and a reduced one Φ_s=45°). Figure 187 presents the results showing the response of the strip for these three values.

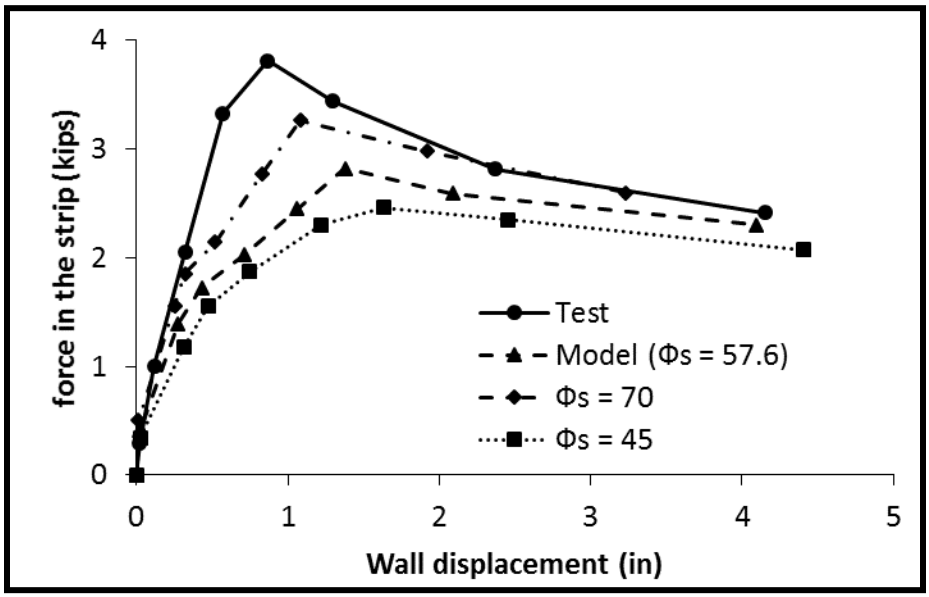

Figure 187. Forces in the Strip for Different Φ_s.

Better results were obtained with the higher value of the friction angle for the strips. The reason is that the ribs on the strips produce a friction factor much higher than 1 because the ribs on the strips engage the bearing capacity of the soil in addition to the friction. Since the ribs are not represented in the simulation, an artificially high friction angle (70°) is necessary to obtain a friction factor much greater 1. Yet this very high friction angle negatively affected other results of the model, such as wall deformation and drilled shaft deformation. In the end, the researchers decided to match the global behavior and accept that the strip forces would be under predicted.

Figure 188 shows a peak in the graph. The reason is that the soil between the drilled shaft and the MSE wall failed in compression after 25 kips of horizontal load on the drilled shaft. The soil in that zone reached its maximum strength, which is the reason for the peak in that graph. Figure 189 presents the plastic zone for different applied horizontal loads on top of the drilled shaft.

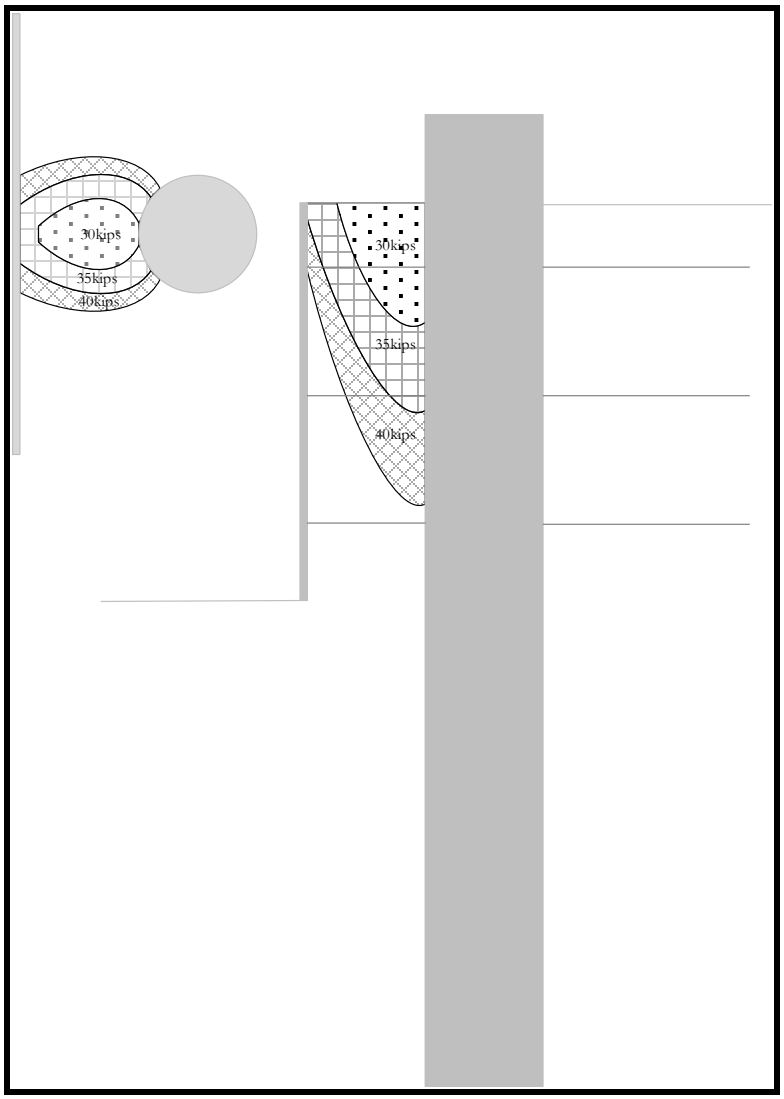

Figure 188. Plastic Zone for Different Values of Horizontal Load on Top of the Drilled Shaft.

A numerical model was prepared for the case without the MSE wall (Figure 189). The aim of this analysis was to study the effect of the MSE wall on the horizontal capacity of the drilled shaft.

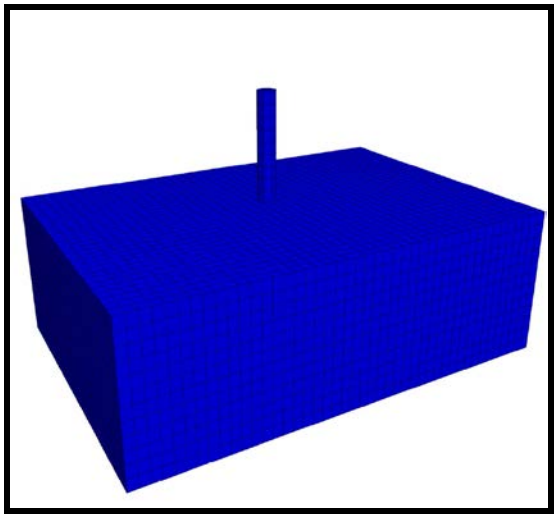

Figure 189. Geometry of the Case without the Wall.

As can be seen in Figure 190, for a displacement of 6 in. at the top of the shaft (which was the maximum observed in the full-scale test), the maximum horizontal load predicted by the model for the case with the wall was 40 kips, while the case without the wall was 10.84 kips. This implies that the horizontal ultimate capacity of the drilled shaft is 75 percent lower in the case without the wall.

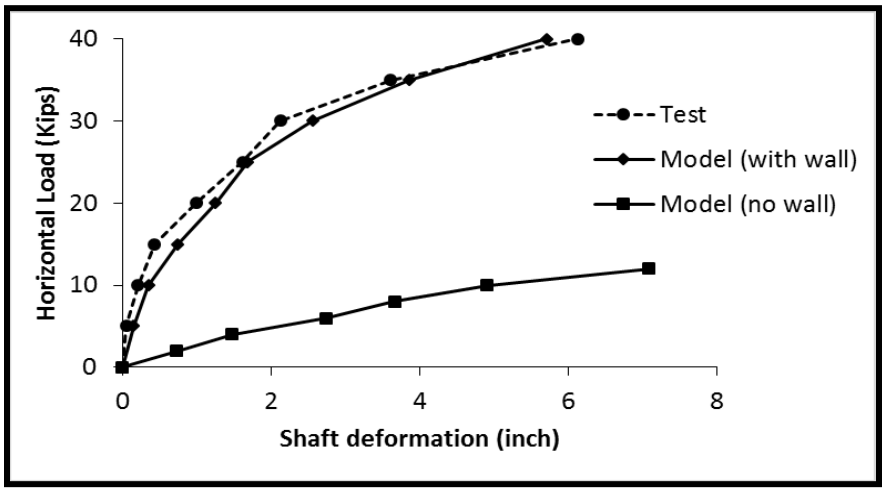

Figure 190. Comparison between the Case with the Wall and the Case without the Wall.

PARAMETRIC STUDY

Outline of the Parametric Study

The parametric study investigated the influence of various factors on the performance of the laterally loaded drilled shaft built within an MSE wall. One case was selected as the baseline

case; for subsequent cases, one parameter was varied at a time with respect to the baseline case to investigate the influence of one particular factor on the performance of the drilled shaft and the MSE wall. The baseline case was determined based on commonly encountered situations in TxDOT practice. Table 5 lists all the cases included in this parametric study. For the baseline case, the MSE wall is 20 ft high (i.e., h=20 ft), the drilled shaft is embedded 20 ft (i.e., d=20 ft) in the foundation soil and extends 3 ft above the top of the MSE wall (i.e., to apply the horizontal load). The total length of the drilled shaft is 43 ft. The drilled shaft is located 4 ft away from the MSE wall (i.e., D=4 ft). The reinforcement length is 0.7 h using FHWA guidelines (Berg et al., 2009). For all the cases, the size of the MSE wall panel is 5×5 ft^2, and the shaft diameter is 3 ft.

The capacity of the drilled shaft with the support of the MSE wall (the model shown in Figure 191) was compared with the capacity of the shaft without the presence of the MSE wall (the model shown in Figure 192). This helped to quantify the effect of the MSE wall on the laterally loaded shaft.

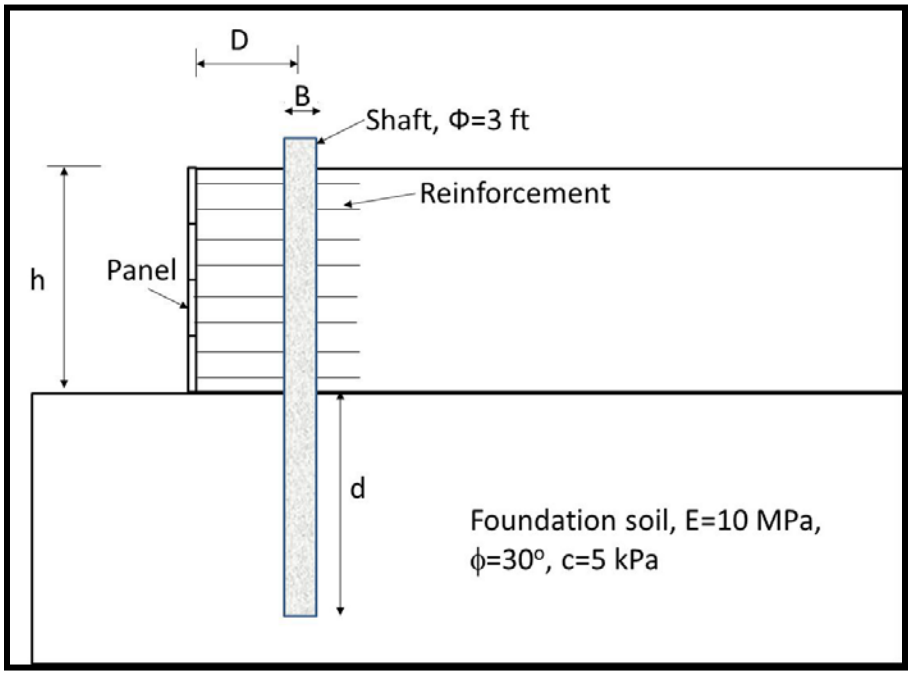

Figure 191. Numerical Model for Drilled Shaft within the MSE Wall.

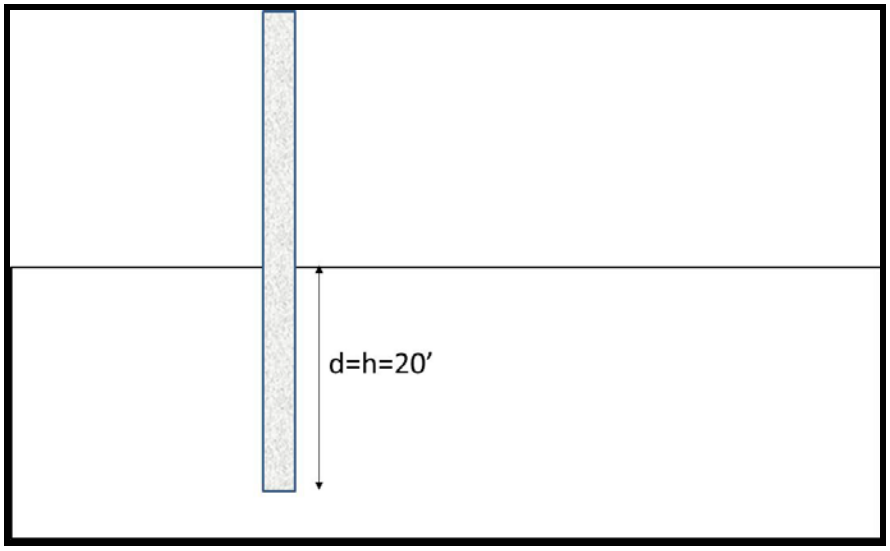

Figure 192. Numerical Model for Drilled Shaft without the MSE Wall.

Table 5. Parametric Study Cases.

Backfill material	Sand: ϕ=30° and E=210 ksf, Crushed rock*: ϕ=40° and E=2.1×10^3 ksf
Diameter of the drilled shaft	2 ft, 3 ft*
Distance between drilled shaft and MSE wall, d (ft)	1.5 ft, 2 ft, 3 ft*, 4 ft, 6 ft, 8 ft, 12, 15
MSE wall height, h (ft)	15, 20*, 25
Embedment depth, d (ft)	10, 15, 20*
Effect the MSE wall	With MSE wall support* (Figure 191), without MSE wall (Figure 192)

Note: *indicates the parameters used for the baseline case.

Baseline Case

Table 6 lists the parameters corresponding to the materials and interface properties of the baseline case.

Table 6. Baseline Material Properties.

Materials	Constitutive Model	Properties
MSE wall panels	Elastic	$E = 4.2\times10^4$ ksf, $\nu = 0.25$, $\gamma = 100$ pcf
Drilled shaft	Elastic	$E = 6.3\times10^5$ ksf, $\nu = 0.3$, $\gamma = 156$ pcf
Backfill material (crushed rock)	Linearly-elastic perfectly-plastic	$E = 2.1\times10^3$ ksf, $\nu = 0.25$, $\phi=40°$, $c = 0$
Foundation soil	Linearly-elastic perfectly-plastic	$E = 210$ ksf, $\nu = 0.25$, $\gamma = 100$ pcf, $\phi = 30°$, $c = 100$ psf
Reinforcement (metallic strip)	Linearly-elastic perfect plastic	$E = 4.4\times10^6$ ksf, $\sigma_t = 2.1\times10^3$ ksf, $\sigma_c = 2.1\times10^3$ ksf

Effect of Different Parameters

Some of the outcomes of the parametric numerical study are presented here to quantify the effect of different parameters on the interaction between the drilled shaft and the MSE wall.

Relative Distance between the Drilled Shaft and the MSE Wall (D/B)

The relative distance between the drilled shaft and the MSE wall (D/B) plays an important role on the interaction between these two structures. The effect of D/B on the load displacement curve at the top of the drilled shaft and on the deflection at the top of the MSE wall is presented in Figure 193 and Figure 194, respectively. As can be seen from these figures, when the drilled shaft is closer to the MSE wall, there is more deflection for both the drilled shaft and the MSE wall.

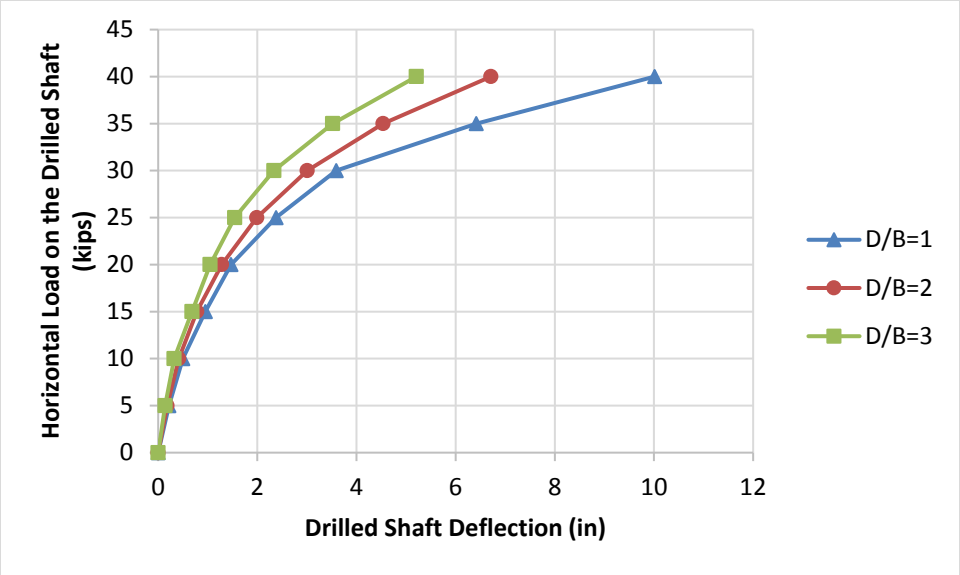

Figure 193. Drilled Shaft Deflection for Different D/B.

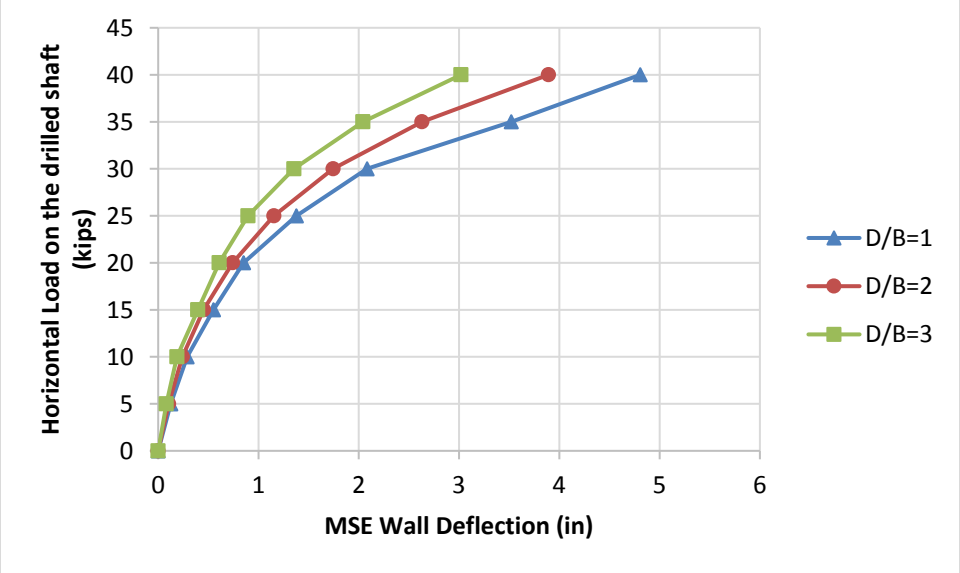

Figure 194. MSE Wall Deflection for Different D/B.

Embedded Depth of the Drilled Shaft (d)

The next parameter to be studied is the embedded depth of the drilled shaft. The common practice is to use an embedment depth equal to the height of the wall. Figure 195 plots the effect of the embedment depth of the drilled shaft on the top deflection of the drilled shaft. The influence is small.

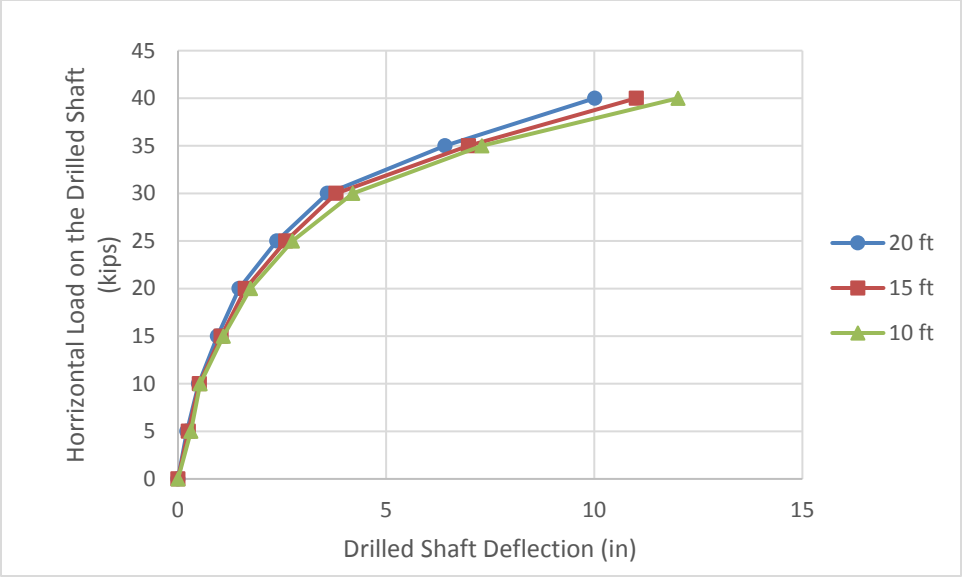

Figure 195. Drilled Shaft Deflection for Different Embedded Depth.

Backfill Material

The most commonly used backfill materials for MSE walls are clean sand and crushed rock. In this research, the effect of these two materials on the interaction between the drilled shaft and the MSE wall was studied.

The deflection of the drilled shaft and MSE wall for the two different backfill materials are presented in Figure 196 and Figure 197, respectively. The deflection for both the MSE wall and the drilled shaft is larger for the sand than for the crushed rock.

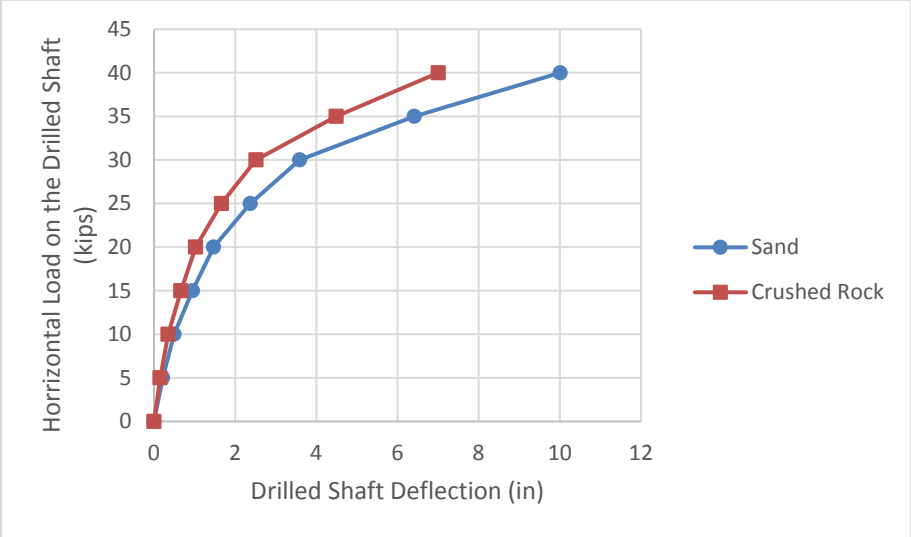

Figure 196. Drilled Shaft Deflection for Different Backfill Material.

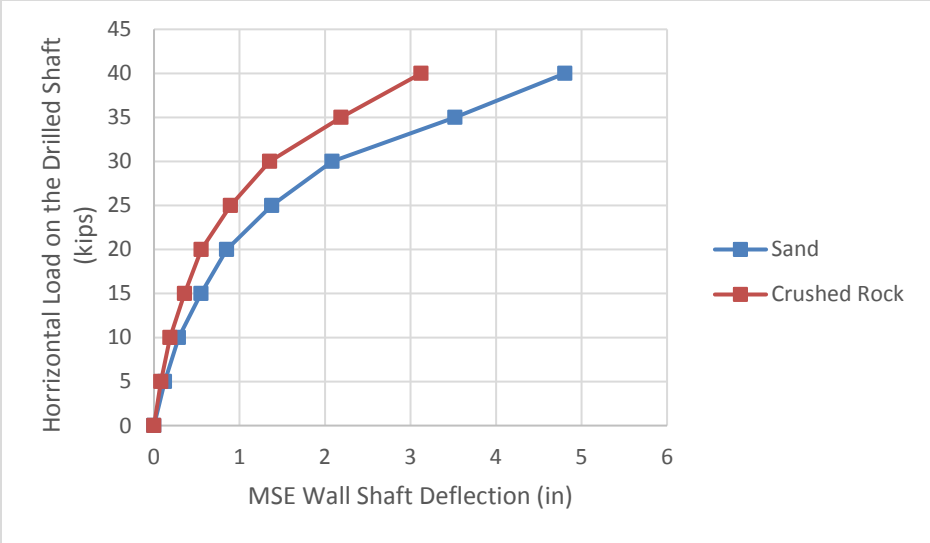

Figure 197. MSE Wall Deflection for Different Backfill Material.

CONCLUSION

Numerical modeling was an important part of this research. A total of 64 3D simulations of the MSE wall, 6 simulations for the pullout test, and 28 simulations for the actual strips were conducted. Wall deformation, drilled shaft deformation, load in the strips at different positions, and pressure on the back of the wall panels were obtained from the MSE wall models. The model parameters for the soil reinforcement were calculated by matching strip pullout tests. The behavior of the metal strips was more closely simulated by modeling the actual strip in 3D.

CHAPTER 6:
PRACTICAL APPLICATIONS

INTRODUCTION

This chapter presents practical applications of this study for the design of horizontally loaded drilled shafts embedded in MSE walls near the front facing. The design methods that are presented in many geotechnical codes and handbooks are for the standard situation where there is no drilled shaft behind the wall. The goal of this chapter is to include the effect of the horizontally loaded drilled shaft on the design of the wall. This proposed design method is based on the results of the full-scale test completed at the TAMU Riverside Campus in August 2012 (Chapter 4), the monitoring of two real project sites (Chapter 4), and numerous numerical models that were calibrated against the test and field data (Chapter 5).

DESIGN METHOD WITHOUT THE DRILLED SHAFT

The internal stability of the MSE wall is addressed by pullout capacity and yield of the reinforcement (AASHTO, 2010).

Pullout Design

One of the possible failure mechanisms for MSE walls is reinforcement pullout. The length of the reinforcement should be long enough to avoid this kind of failure. The reinforcement length is established using the length in the failure zone at the depth of the reinforcement (L_{max}) and the required safe length of the reinforcement (L_a). Figure 198 shows L_{max} for a rigid wall. The design requires the knowledge of L_{max}, which is to be ignored in the length required to resist the maximum tension (T_{max}) in the reinforcement (Briaud, 2013). The force T_{max} is related to the horizontal pressure and is calculated as follows:

$$T_{max} = s_v s_h \sigma_h \quad (6.1)$$

Where T_{max} is the maximum tension resisted by the layer of reinforcement at depth z, s_v is the vertical spacing between reinforcement layers at depth z, s_h is the horizontal spacing between reinforcement at depth z, and σ_h is the total horizontal stress at depth z.

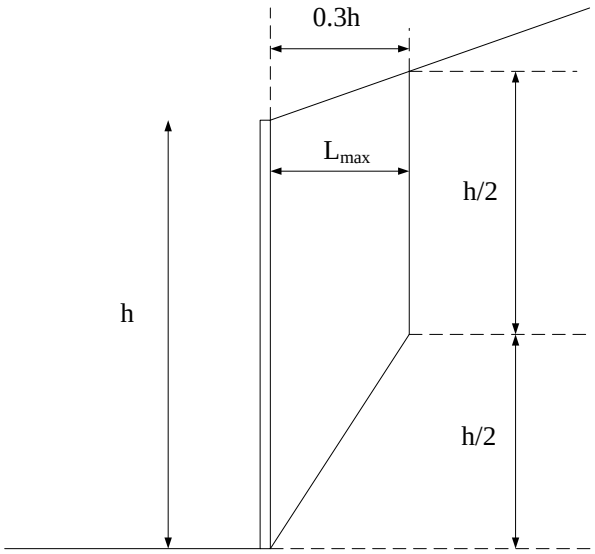

Figure 198. Required Length of Strip in the Failure Zone.

σ_h is calculated as:

$$\sigma_h = k_r \sigma_{ov} + \Delta\sigma_h \tag{6.2}$$

Where k_r is a coefficient of earth pressure, σ_{ov} is the total vertical pressure due to the backfill material, and $\Delta\sigma_h$ is the horizontal pressure due to any surcharge on top of the wall.

The maximum load applied to the reinforcement is T_{max}, which is calculated as mentioned above. The pullout load $T_{pullout}$ for a strip is calculated by:

$$T_{pull-out} = 2 f_{max} b L_a \tag{6.3}$$

Where f_{max} is the maximum shear stress that can be developed at the interface between the reinforcement and the soil, b is the width of the reinforcement, and L_a is length of the inclusion beyond L_{max}. The value of f_{max} is calculated as:

$$f_{max} = F^* \sigma_v' \alpha \tag{6.4}$$

Where F^* is the friction factor proposed by AASHTO (2010), σ'_v is the vertical effective stress on the reinforcement, and α is a scale factor taken as 1 for steel reinforcement, 0.8 for geogrids, and 0.6 for geotextile (Briaud, 2013).

The ultimate limit state for pullout must be satisfied. It is expressed as:

$$\gamma_1 T_{max1} + \gamma_2 T_{max2} = \varphi T_{pull-out} \tag{6.5}$$

Where Υ_1 is the load factor for active earth pressure due to soil weight (Υ_1=1.35), Υ_2 is the load factor for the active earth pressure due to any surcharge on top of the wall (Υ_2=1.5), φ is the resistance factor (φ=0.9), T_{max1} is the part of the load in the reinforcement due to the soil weight, T_{max2} is the part of the load in the reinforcement due to any surcharge on top of the wall, and $T_{pullout}$ is the pullout resistance calculated in Eq. (6.3). The required safe length L_a of the reinforcement is calculated by:

$$L_a = \frac{(\gamma_1 k_r \sigma_{ov}^{'} + \gamma_2 \Delta\sigma_h) s_v s_h}{2\varphi F^* \sigma_{ov}^{'} \alpha b} \tag{6.6}$$

The total length of reinforcement is calculated by:

$$L = L_a + L_{\max} = \frac{(\gamma_1 k_r \sigma_{ov}^{'} + \gamma_2 \Delta\sigma_h) s_v s_h}{2\varphi F^* \sigma_{ov}^{'} \alpha b} + 0.3h \tag{6.7}$$

Yield of the Reinforcement Design

Another possible failure mechanism in an MSE wall is the case where the reinforcement yields. The ultimate limit state for this situation is:

$$\gamma_1 T_{\max 1} + \gamma_2 T_{\max 2} = \varphi T_{yield} \tag{6.8}$$

Where Υ_1 is the load factor for active earth pressure due to soil weight (Υ_1=1.35), Υ_2 is the load factor for the active earth pressure due to any surcharge on top of the wall (Υ_2=1.5), φ is the resistance factor (φ=0.75 for strips, 0.65 for grids and 0.9 for geosynthetics), T_{max1} is the part of the load in the reinforcement due to the soil weight, T_{max2} is the part of the load in the reinforcement due to any surcharge on top of the wall, and T_{yield} is the load corresponding to the yield strength of the reinforcement.

MSE WALL DESIGN WHEN A DRILLED SHAFT IS PRESENT

The main factor in designing an MSE wall is the horizontal pressure to be resisted. Based on this pressure at different depths, the length of reinforcement and their distributions are designed. This pressure needs to be modified when there is a drilled shaft pushing horizontally against the panels of the MSE wall.

Parameters to Be Studied

The additional pressure on the panels due to the horizontal load on the drilled shaft is influenced by different parameters. The parameters that have a significant impact on this additional pressure were discussed in Chapter 5 (shown in Figure 199). These parameters are further discussed in this section.

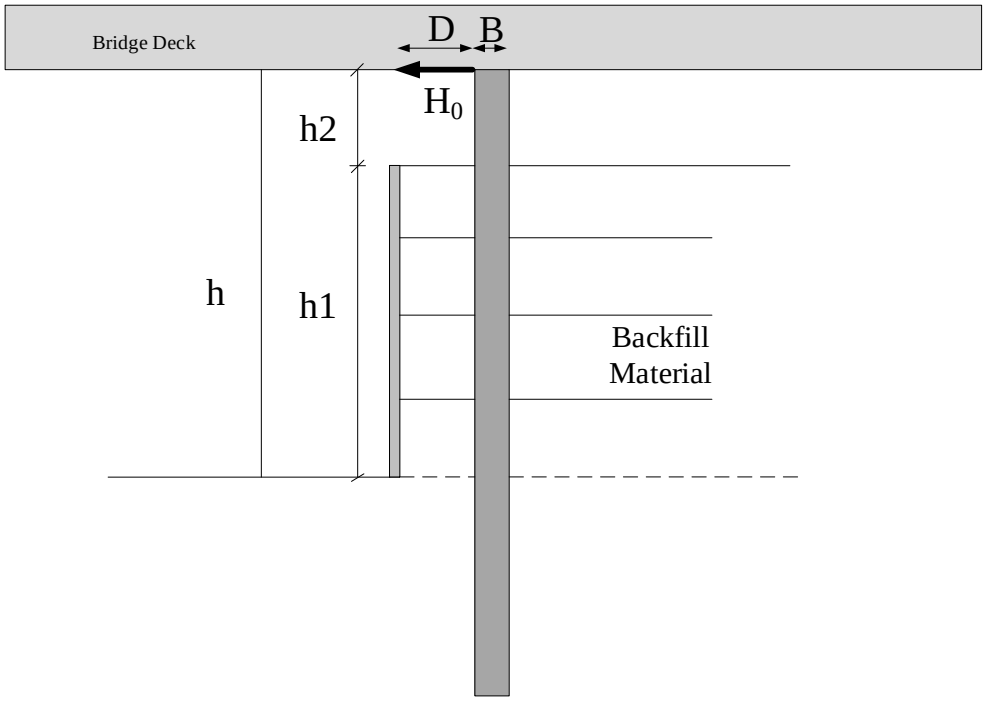

Figure 199. Parameters Affecting on the Pressure on the Panel due to Horizontal Load on the Drilled Shaft.

Horizontal Load on the Drilled Shaft (H_0)

The most important factor is the horizontal load on the drilled shaft, which is called H_0 in this chapter. This load is calculated during the design of the bridge. According to the design procedure provided by TxDOT, an estimate of this load is 13.5 kips. In the full-scale test, the range for the horizontal load on the shaft was between 0 and 40 kips. This range is used to cover many possible load cases in design.

Clear Distance between the Wall and the Drilled Shaft (D)

Another important parameter influencing the additional pressure on the panel is the clear distance between the wall and the drilled shaft (D). When the drilled shaft is far from the wall, there is a smaller pressure on the panels than when it is close.

Diameter of the Drilled Shaft (B)

The diameter of the drilled shaft (B) can have an impact on the pressure on the panel but in real projects, the diameter does not vary significantly. The parameter B is used for normalizing other parameters.

Height of the Wall (h1)

The distribution of the additional pressure on the wall versus depth was found to be a triangle with the largest pressure at the top. The height of the wall plays an important role as the entire height is affected by the pressure increase. The range of wall height studied in this research is 10 to 25 ft.

Backfill Material

The type of backfill material has a minor impact on the pressure on the panels. In real projects, there are two main kinds of backfill materials, crushed rock and clean sand. In this research, the additional pressure on the back of the wall was studied for these two kinds of backfill materials.

Numerical Simulation Cases

In order to study the effect of each parameter on the pressure on the panels, numerous numerical models were prepared in FLAC3D. As was discussed in Chapter 5, the numerical simulation was calibrated with data from the full-scale test at the TAMU Riverside Campus and the monitoring of the real project site at Bastrop. Table 7 shows the parameters used in this research and a total of 64 models were prepared.

Table 7. Parameters Used in Numerical Models.

Horizontal Load on top of the drilled shaft (H_0), kips	0, 5, 10, 15, 20, 25, 30, 35, 40
Diameter of the drilled shaft, ft	2, 3
Clear distance between the drilled shaft and the wall, ft	1, 3, 6, 8, 10, 12, 15
Height of the wall, ft	10, 15, 20, 25
Backfill material	Sand: φ=30° and E=210 ksf, Crushed rock: φ=40° and E=2.1×10^3 ksf

To normalize the parameters that are affecting the additional pressure, two new parameters are defined as follows:

- Relative distance between the drilled shaft and the wall (D/B).
- Equivalent pressure in front of the shaft, calculated as $H_0/(Bh1)$.

The results from the numerical simulations are summarized in four graphs with two of them for the sand backfill and two of them for the crushed rock backfill.

Figure 200 presents the maximum additional pressure on the panels due to the horizontal load on the drilled shaft for the crushed rock and for different relative distances between the drilled shaft and the wall (D/B). As can be seen in this figure, the relative distance between the drilled shaft and the wall plays a significant role on the additional pressure on the panels. As can be expected, the closer the drilled shaft is to the front of the wall, the larger the maximum additional pressure. For all of the horizontal loads in the numerical models, the relationship between the maximum additional pressure on the panel and the equivalent pressure in front of the drilled shaft is linear.

Other interesting data obtained in the numerical study was related to the maximum additional force in the strip around the drilled shaft. Figure 201 shows the results for the crushed rock. This maximum force is due to the maximum additional pressure on the panel.

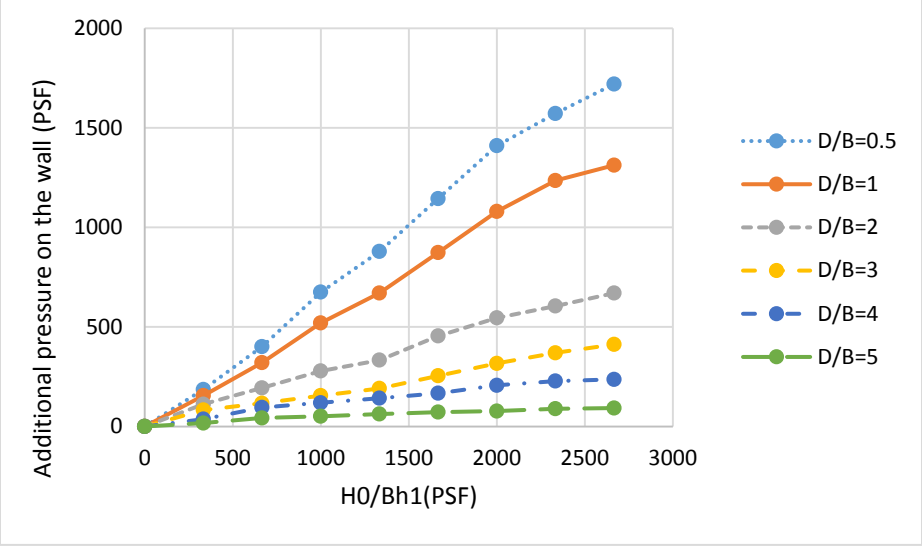

Figure 200. Additional Pressure on the Panels due to Different Horizontal Loads on the Drilled Shaft for Crushed Rock.

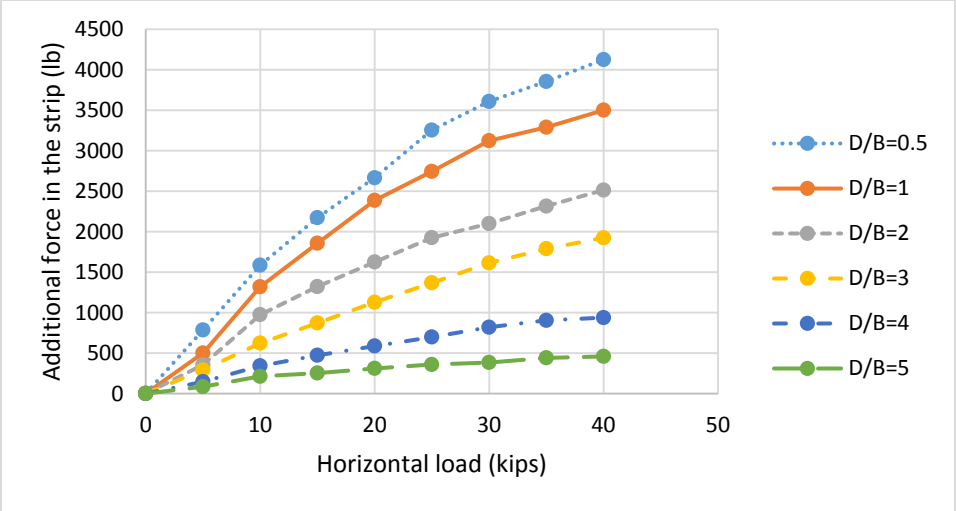

Figure 201. Additional Force in the Strip due to Different Horizontal Loads on the Drilled Shaft for Crushed Rock.

Figure 202 presents the maximum additional pressure on the panels due to a horizontal load on the drilled shaft for the sand backfill and for different relative distances between the drilled shaft and the wall (D/B). As can be seen in this figure, the relative distance between the drilled shaft and the wall plays a significant role on the maximum additional pressure on the panel. As can be expected, the closer the drilled shaft is to the front of the wall, the larger the maximum additional pressure. Also for horizontal loads less than 30 kips, the relationship between the maximum additional pressure on the panel and the equivalent pressure in front of the drilled shaft is linear.

Other interesting data obtained from the numerical study were related to the maximum additional force in the strips around the drilled shaft. Figure 203 shows the results for the sand backfill. This maximum force is due to the maximum additional pressure on the panel.

Note that all of the calculations have been made by assuming that the drilled shaft is loaded in a free head condition. The question is to know if this assumption is correct or not, bearing in mind that the alternative is to consider a fixed head condition where the top of the pile remains vertical. The free head condition is certainly a conservative assumption because it leads to more deflection for the same load, and therefore more pressure on the wall panels. For traffic signs, the free head assumption seems most appropriate. In the case of a bridge abutment, the piles are tied together by a pile cap in the direction parallel to the wall face but this does not prevent the top of the pile from rotating in the direction perpendicular to the front face of the wall, as would be required for a fixed head condition. Any connection to the abutment wing

walls will likely stiffen the response, but it is unlikely that it will create a fixed head condition. This is a complex problem and in the end it will be necessary to choose the right load on the drilled shaft considering the part of the load that can be taken by other parts of the system. A conservative approach was selected with the assumption of a free head condition.

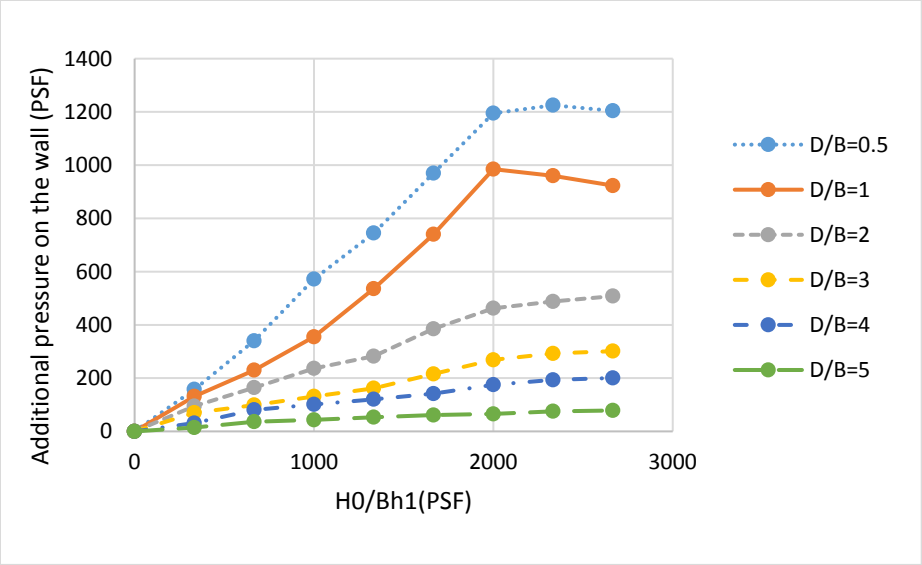

Figure 202. Additional Pressure on the Panels due to Different Horizontal Loads on the Drilled Shaft for Sand.

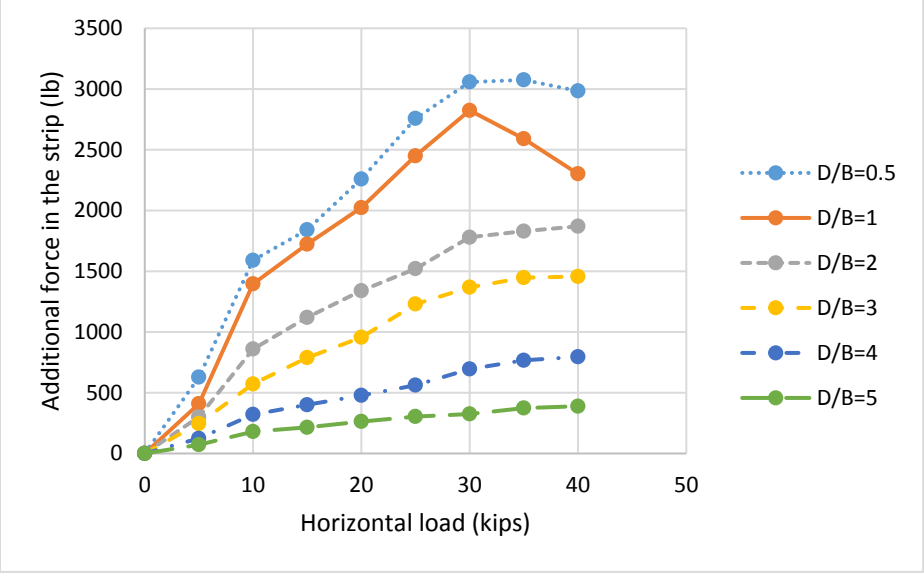

Figure 203. Additional Force in the Strip due to Different Horizontal Loads on the Drilled Shaft for Sand.

Pressure Distribution on the Panels

The maximum additional pressure on the back of the wall due to the horizontal load on the drilled shaft presented above occurs near the top of the wall. To obtain the pressure at any point along the wall, the distribution of pressure should be specified. In order to get the distribution, the pressures on the back of the wall along the wall height are plotted for different cases.

Case 1

Shaft diameter is 2 ft, clear distance between the drilled shaft and the wall is 2 ft (D/B=1), height of the wall is 15 ft, and the backfill material is sand. Figure 204 shows the additional pressure along the wall height. The additional pressure on top of the wall is zero and increases rapidly with depth up to a maximum and then decreases to the bottom of the wall.

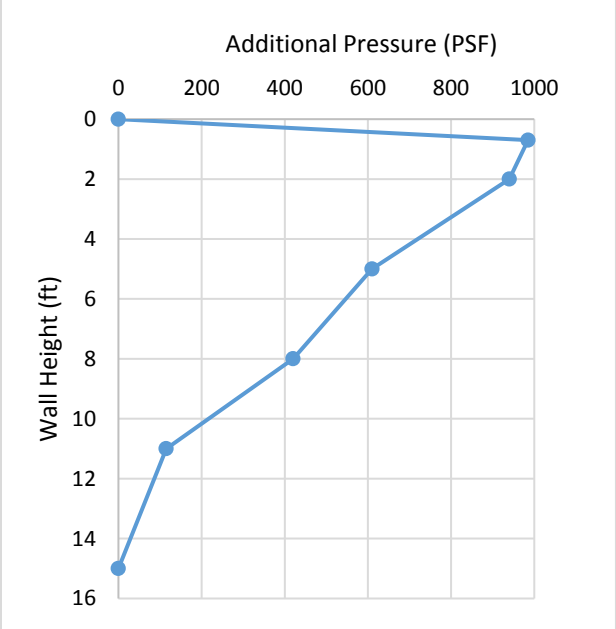

Figure 204. Pressure Distribution along the Wall Height for Case 1.

Case 2

Shaft diameter is 3 ft, clear distance between the drilled shaft and the wall is 6 ft (D/B=2), height of the wall is 20 ft, and the backfill material is crushed rock. Figure 205 shows the additional pressure along the wall height for this case. The shape of the pressure distribution is very similar to that of case 1, yet the maximum value is different. This maximum value can be obtained from the graph presented in the previous section.

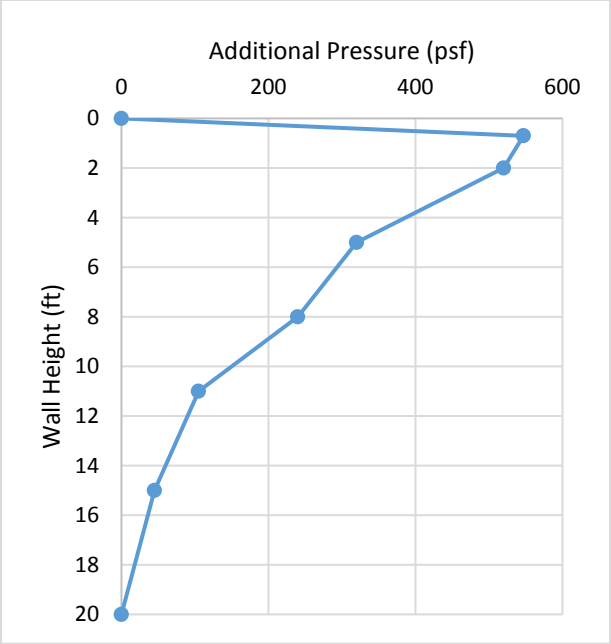

Figure 205. Pressure Distribution along the Wall Height for Case 2.

Case 3

Shaft diameter is 3 ft, clear distance between the drilled shaft and the wall is 9 ft (D/B=3), height of the wall is 25 ft, and the backfill material is sand. Figure 206 shows the additional pressure along the wall height for this case. The shape of the pressure distribution is very similar to that of case 1 and case 2, yet the maximum value is different. This maximum value can be obtained from the graph presented in the previous section.

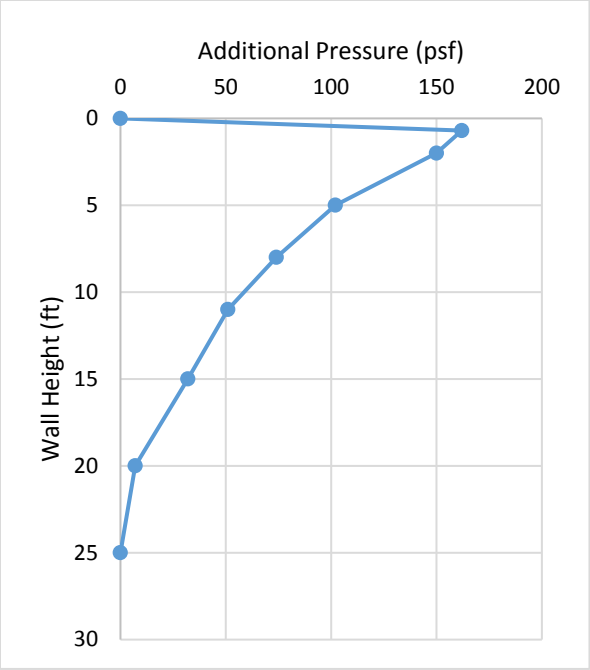

Figure 206. Pressure Distribution along the Wall Height for Case 3.

According to the results of the numerical simulations, the additional pressure along the wall height can be represented by a triangle with the largest pressure at the top (Figure 207). The additional pressure calculated by using this triangular distribution is conservative in some part of the wall, as can be seen by comparing Figure 206 and Figure 207. Accordingly, the diagram shown in Figure 207 is recommended for design. In the diagram, $k_r\sigma_{ov}$ is the soil pressure due to the backfill material, $\Delta\sigma_h$ is the pressure due to any surcharge at the top of the wall, and $\Delta\sigma_s$ is the additional pressure due to the horizontal load on the drilled shaft. In this fashion, the total pressure can be calculated at any depth.

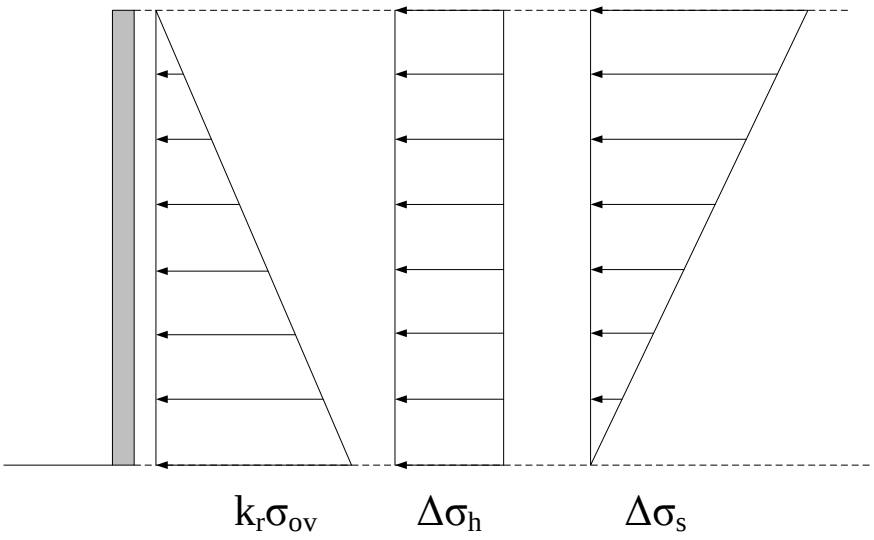

Figure 207. Pressures Acting on the Wall.

PROPOSED DESIGN APPROACH

In the previous section of this chapter, a procedure was recommended to include the additional pressure on the wall due to a horizontal load on the drilled shaft. In this section, this additional pressure is being considered in the design of the wall.

Proposed Design for Pullout

The maximum tension in the reinforcement (T_{max}) is a function of the total horizontal pressure on the wall (σ_h) at the reinforcement depth (z), the vertical spacing between reinforcement layers at depth z (s_v), and the horizontal spacing between reinforcement at depth z (s_h) ($T_{max} = s_v s_h \sigma_h$).

When there is a drilled shaft in the reinforced zone of the wall, the horizontal spacing between the reinforcement (s_h) is usually different in front of the shaft. It can be measured precisely from the wall drawing, but an estimate of s_h in front of the drilled shaft is one and one half times s_h in other parts of the wall.

When there is a horizontally loaded drilled shaft in the wall, a new term is added to the Eq. (6.2) and that new equation is as follows:

$$\sigma_h = k_r \sigma_{ov} + \Delta\sigma_h + \Delta\sigma_s \quad (6.9)$$

Where $\Delta\sigma_s$ is the additional pressure due to the horizontally loaded drilled shaft.

The new equation for calculating the required safe length (L_a) of the reinforcement is:

$$La = \frac{(\gamma_1 k_r \sigma_{ov}^{'} + \gamma_2 \Delta\sigma_h + \gamma_2 \Delta\sigma s) s_v s_h}{2\varphi F^{*} \sigma_{ov}^{'} \alpha b} \tag{6.10}$$

and the total length of reinforcement is calculated by:

$$L = L_a + L_{\max} = \frac{(\gamma_1 k_r \sigma_{ov}^{'} + \gamma_2 \Delta\sigma_h + \gamma_2 \Delta\sigma s) s_v s_h}{2\varphi F^{*} \sigma_{ov}^{'} \alpha b} + 0.3h \tag{6.11}$$

As was shown before, the relationship between the additional pressure ($\Delta\sigma_s$) and the equivalent pressure in front of the drilled shaft (H_0/Bh) is linear. Figure 208 presents the proposed chart to calculate the maximum value of $\Delta\sigma_s$. It is prepared for two main backfill materials used in MSE walls (sand and crushed rock). All of the parameters in the chart can be obtained from the geometry (D, B, h) and design load on the drilled shaft (H_0); then the maximum additional pressure on the panels can be calculated.

One simple way to evaluate the decrease in maximum additional pressure on the wall panels as D/B increases is to use the 2-to-1 method. This 2-to-1 method consists of projecting the average bearing pressure from the drilled shaft on the wall panels with a 2:1 distribution. Figure 208 includes a plot of the maximum additional pressure on the wall according to the 2-to-1 method. For the cases where the drilled shaft is far from the wall, this method is conservative.

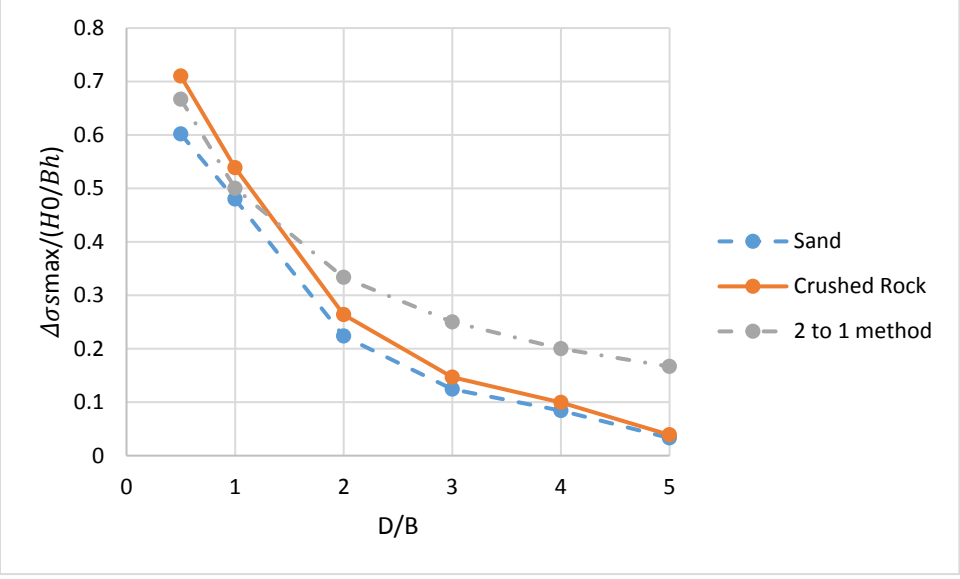

Figure 208. Proposed Chart to Calculate Δσs Based on the Geometry and Applied Horizontal Load on the Shaft.

Proposed Design for Rupture Failure

The governing equation for rupture is $\gamma_1 T_{\max 1} + \gamma_2 T_{\max 2} = \varphi T_{yield}$. Considering the additional pressure due to the horizontal load, the proposed equation for rupture is:

$$(\gamma_1 k_r \sigma'_{ov} + \gamma_2 \Delta\sigma_h + \gamma_2 \Delta\sigma s) s_v s_h = \varphi T_{yield} \tag{6.12}$$

Check Wall Panel for Bending

The additional pressure acting on the panels is due to the horizontal load on the drilled shaft; the panel reinforcement should be checked for the maximum bending on the panel. Figure 209 presents the details of the panel. The additional pressure is largest at the top of the wall, so the most critical panel is the one at the top of the wall.

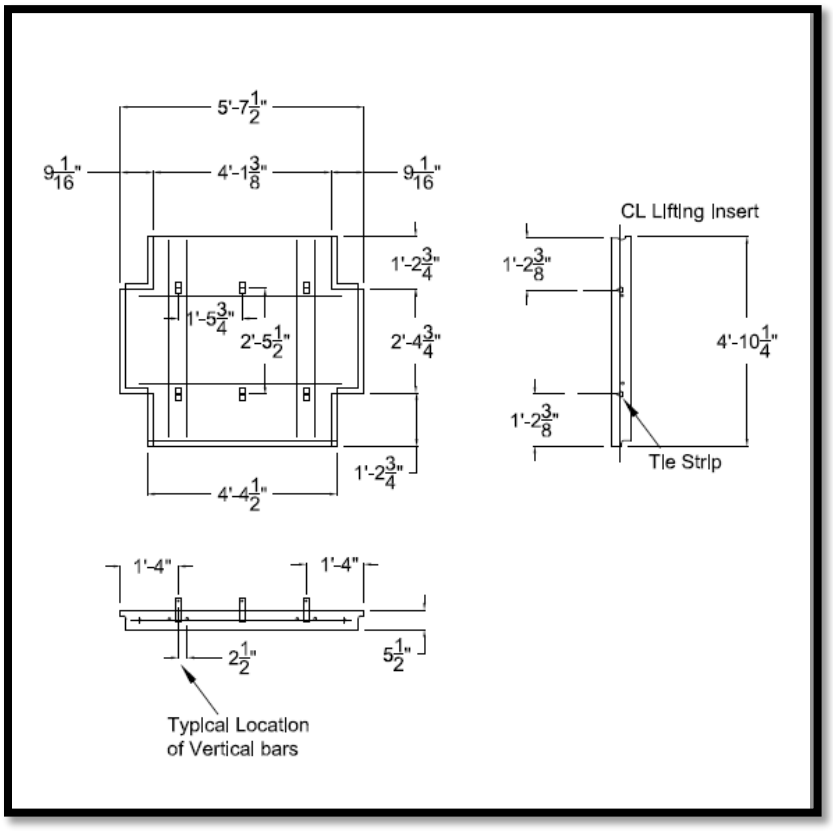

Figure 209. Panel Details.

The design for such a panel for the Bastrop project, including the additional pressure, is presented here:

Maximum span : 2.5 ft

Slab thickness (t) = 5.5in

Additional Pressure : 73.31 psf

Concrete $f_c^{'} = 4000$ psi

Steel $f_y = 60000$ psi

At interior span : $M_{max} = 1/9 \times 1.5 \times 73.31 \times 2.5^2 = 76.4$ lb-ft

Cover of the reinforcement = 1in

$d = t - 1 = 4.5$

$$A_s = \frac{M_{\max}}{\varphi f_y (d - \frac{a}{2})} = \frac{76.4 \times 12}{0.9 \times 60000 \times 4} = 0.0042 in^2$$

Minimum reinforcement used in the panels is:

$$A_{s\min} = 0.0018 \times b \times d = 0.0018(2.5 \times 12) \times 4.5 = 0.243 in^2 \quad (6.13)$$

PRACTICAL APPLICATIONS

The comparison between the current AASHTO design and the new findings for the wall in the Bastrop project is:

- Height of the wall (h) is 18 ft.
- Diameter of the drilled shaft (B) is 3 ft.
- Clear distance between the drilled shaft and the wall (D) is 6 ft (D/B=2).
- Horizontal (s_h) and vertical (s_v) spacing of the reinforcements are both 2.5 ft.
- Backfill material is crushed rock with a unit weight of 120 pcf.

k_r is assumed to be equal to k_a, which is 0.33, F^* at the top of the wall is 1.7, the scale factor (α) is 1.0, and the width of the strip is 0.16 ft. The calculation is for the second row of strips from the top at the depth of 3 ft from the top of the wall.

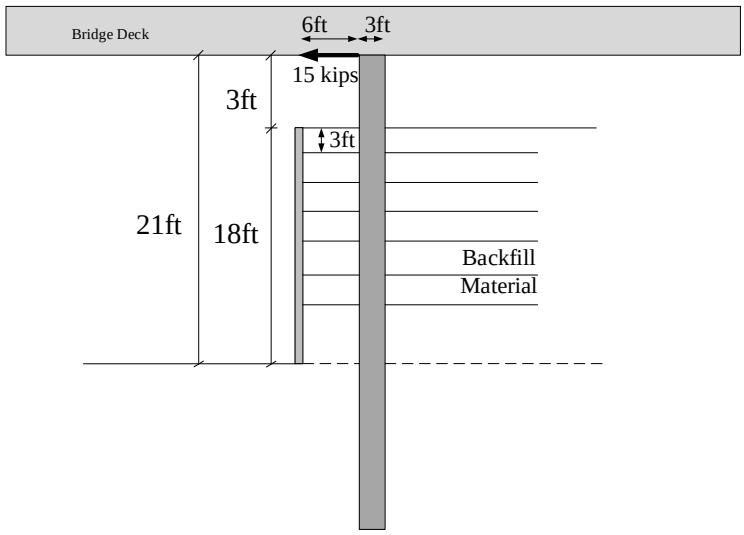

Figure 210. Detail of the Wall.

AASHTO Design Method

The length L_a is given by:

$$L_a = \frac{(1.35 \times 0.33 \times 120 \times 3) \times 2.5 \times 2.5}{2 \times 0.9 \times 1.7 \times 120 \times 3 \times 1 \times 0.16} = 5.7\ ft \tag{6.14}$$

$$L = La + 0.3h = 5.7 + 5.4 = 11.1\ ft$$

The required length of strip is 11.2 ft, and the length of strip used in the project at that level is 18 ft.

Impact of Adding the Pressure due to the Load on the Drilled Shaft

The design horizontal load on the drilled shaft (H_0) for this project is 15 kips.

$$\left\{ \begin{array}{l} \dfrac{H_0}{Bh} = \dfrac{15000}{3 \times 18} = 278 \\ D / B = 2 \end{array} \right\} \Rightarrow \Delta\sigma_s = 73.31 psf \tag{6.15}$$

The additional pressure calculated above is for the top of the triangle, so the additional pressure at the depth of the second row of strips, 3 ft below the top, is $73.31 \times \dfrac{15}{18} = 61.09\ psf$.

The horizontal spacing of the strips in front of the drilled shaft is taken as $1.5 \times s_h = 3.75\ ft$. So the required length of the strip, according to the proposed design guideline, is:

$$L_a = \frac{(1.35 \times 0.33 \times 120 \times 6 + 1.5 \times 61.09) \times 2.5 \times 1.5 \times 2.5}{2 \times 0.9 \times 1.7 \times 120 \times 6 \times 1 \times 0.16} = 11.0\, ft \quad (6.16)$$

$$L = La + 0.3h = 11 + 5.4 = 16.4\, ft$$

In this project, the length of the strips is enough to carry the horizontal pressure on the panel, including the additional pressure due to the horizontal load on the drilled shaft. This project has been monitored since December 2013, and so far there has been no problem. Table 8 presents different lengths of strips for different D/B.

Table 8. Length of Strip for Different D/B.

D/B	$\Delta\sigma s/(H0/Bh)$	$\Delta\sigma s$ (top) (psf)	$\Delta\sigma s$ (at strip level) (psf)	La (ft)	0.3 h (ft)	L (ft)	Increase %
0	0	0	0	5.70	5.40	11.10	0.00
0.5	0.71	197.35	164.46	15.09	5.40	20.49	84.61
1	0.54	149.68	124.73	13.51	5.40	18.91	70.33
2	0.26	73.31	61.09	10.97	5.40	16.37	47.46
3	0.15	40.78	33.99	9.89	5.40	15.29	37.71
4	0.10	27.63	23.03	9.45	5.40	14.85	33.78
5	0.04	10.79	8.99	8.89	5.40	14.29	28.73

GENERAL CONSIDERATIONS

The following are some suggestions to minimize the impact of horizontally loaded drilled shafts on MSE walls.

1. Put the drilled shaft as far as possible from the wall.

As can be seen in Figure 208, there is more pressure transferred to the wall when the drilled shaft is near the wall. The other problem is that when the space between the drilled shaft and the wall is limited, the soil between the panel and the shaft cannot be compacted, which may decrease the friction factor (F^*) of the strips.

2. Compact the soil between the drilled shaft and the wall.

Compaction plays an important role in the friction factor on the strips. The better the compaction is, the greater the load that can be carried by the strips. At the same time, if the soil between the panel and the shaft is not compacted, it will transfer less pressure to the panel. It is difficult to generate a high compaction level in cases where the drilled shaft is very close to the wall in that area.

3. Put the drilled shaft in front of the center of the panel, especially at the top of the wall.

The additional pressure due to the horizontal load on the drilled shaft is largest at the top of the wall. It is preferable to have this pressure resisted by the panel rather than by the shear keys between the panels.

4. If necessary, decrease the spacing of the strips.

Sometimes it is hard to increase the length of the strips due to space restrictions at the site. In these cases, it is likely more economical to decrease the spacing of the strips.

CONCLUSION

The interaction between the drilled shaft and the MSE wall results in an additional pressure on the back of the wall panels. This additional pressure is a function of the geometry of the wall, of the geometry and location of the drilled shaft, and also of the backfill properties.

The additional pressure created by the horizontal load on the drilled shaft has a triangular distribution with the highest pressure at the top of the wall ($\Delta\sigma_{smax}$). By knowing this maximum additional pressure and the depth of the strip, the additional pressure at each level can be found and the required length of the strip at each level can be calculated.

CHAPTER 7:
CONCLUSIONS AND PROPOSAL FOR FUTURE WORKS

SUMMARY AND CONCLUSIONS

The current design guidelines for MSE walls do not consider the interaction between the MSE wall and drilled shafts embedded in the MSE wall. This report addresses this particular problem. Other studies have been conducted on this topic, but they are related to MSE walls using geosynthetics and geogrid as reinforcements. No changes in the design guidelines were proposed after those investigations. In Texas, MSE walls are generally constructed using metallic reinforcements. An investigation that combines laboratory tests, in-situ experiments, monitoring of MSE wall under actual conditions, and numerical modeling was done to advance the current knowledge. The explicit aim was to suggest modifications in the current guidelines and incorporate the interaction between the MSE wall and the drilled shaft into the design of these earth structures.

To study the problem in greater detail, a full-scale test and the monitoring of two actual sites were planned and selected. The design of the instrumentation was done with the aim of gathering the most relevant information from the full-scale loading test at TAMU-NGES and the monitoring from two actual sites. The maximum number of sensors was based on the number of channels available on the data loggers. Durable devices were needed, especially for monitoring the actual TxDOT sites because they were designed to gather data for about 16 months.

The full-scale test was performed successfully at TAMU-NGES. For this test, all of the devices worked perfectly and valuable data were gathered. The test took about 4 hours to perform and 19 people were involved in the test. After the test, it was confirmed that the stress in the second layer of strips (from the top) is greater than the top layer. Also the highest stress in the strip occurred at 25 kips of horizontal load and not at the highest load of 40 kips on the drilled shaft. The reason was that the soil between the shaft and the panel in front of it failed in bearing capacity. The MSE wall and shaft displacement were other important data that were gathered in this test that helped to calibrate numerical models.

The TxDOT project at Bastrop, Texas, was monitored for 20 months. All of the devices were installed on the wall and drilled shaft during the construction phase. The data were gathered

when the bridge was opened to traffic. No significant movement, increase in strip load, nor pressure on the wall panel were observed during the monitoring.

The TxDOT project at Salado, Texas, was monitored for 8 months. All of the devices were installed on the wall and drilled shaft during the construction phase. The data were gathered when the bridge was opened to traffic. No significant movement or increase in strip load was observed during the monitoring.

Numerical modeling was an important component of this research. A number of numerical models were prepared to study the behavior of the drilled shaft and the MSE wall, including the reinforcing strips. A total of 64 simulations for the MSE wall, 6 simulations for the pullout tests, and 28 simulations for the actual strips were conducted. Wall displacement, drilled shaft displacement, load in the strips at different positions, and pressure on the back of the wall panels were obtained from these simulations. The model parameters for the soil reinforcement were calculated from pullout load tests on actual strips. The behavior of the metal strips was studied in more detail by modeling the actual strip in 3D. The influence of each parameter was evaluated, and two main parameter combinations were selected to present the results. The first one is the relative position of the drilled shaft in the MSE wall, which is the clear distance between the drilled shaft and the wall divided by the drilled shaft diameter (D/B). The second one is the equivalent pressure in front of the drilled shaft, which is the horizontal load on the shaft divided by the diameter of the shaft times the height of the MSE wall ($H_0/(Bh1)$).

The effect of a horizontally loaded drilled shaft behind the MSE wall creates an additional pressure on the back of the wall panels and increases the load in the reinforcement. This additional pressure is a function of the geometry of the wall, of the geometry of the drilled shaft, and of the properties of the backfill material. This pressure has a triangular distribution with depth with the larger pressure at the top ($\Delta\sigma_{smax}$). It is shown how, by knowing this maximum pressure and the depth of the strip, the additional pressure at each level can be found. From this additional pressure the required length of the strip at each level can be calculated. A design procedure is outlined.

PROPOSAL FOR FUTURE WORKS

Some aspects that could contribute to a better understanding of the interaction between the drilled shaft and the MSE wall and its design are:

- **Isolate the drilled shaft from the wall:** To avoid the additional pressure due to the drilled shaft on the wall panels, the drilled shaft can be isolated from the backfill material. This can be achieved by using a compressible type of material between the drilled shaft and the MSE wall to reduce the amount of pressure transmitted to the panels.
- **Redesign the metal strips:** Metal strips are a very interesting kind of soil reinforcements because of their high friction factor. This friction factor is related to the bumps on the strips, and is a function of the number of bumps and their geometry. The combination of the bump numbers and geometry can be optimized in order to obtain a much higher friction factor by performing pullout tests and numerical modeling. This will result in either shorter strips or fewer strips in the wall, as well as a more economical design.

REFERENCES

Abdelouhab, A., Dias, D., and Freitag, N. (2011). "Numerical Analysis of the Behaviour of Mechanically Stabilized Earth Walls Reinforced with Different Types of Strips." *Geotextiles and Geomembranes, 29*(2), 116–129.

Ahmadabadi, M. and Ghanbari, A. (2009). "New Procedure for Active Earth Pressure Calculation in Retaining Walls with Reinforced Cohesive-Frictional Backfill." *Geotextiles and Geomembranes, 27*(6), 456–463.

American Association of State Highway, and Transportation Officials. Subcommittee on Bridges. (2010). *AASHTO Load and Resistance Factor Design Movable Highway Bridge Design Specifications*. Washington, D.C.: AASHTO.

Anderson, P. L. and Brabant, K. (2005). "Increased Use of MSE Abutments," Proceedings of the 22nd Annual International Bridge Conference, Pittsburgh, PA, paper 5-10.

Arenas, A. E. (2010). *Thermal Response Of Integral Abutment Bridges With Mechanically Stabilized Earth Walls.* (No. Vctir 13-R7). Charlottesville, VA: Virginia Center for Transportation.

ASTM (2012). *Standard Test Methods.* West Conshohocken, PA: American Society for Testing and Materials.

Bathurst, R. J., Nernheim, A., and Allen, T. M. (2009). "Predicted Loads in Steel Reinforced Soil Walls Using the AASHTO Simplified Method." *Journal of Geotechnical and Geoenvironmental Engineering, 135*(2), 177–184.

Berg, R. and Vulova, C. (2007). "Effects of Pile Driving through a Full-Height Precast Concrete Panel Faced, Geogrid-Reinforced, Mechanically Stabilized Earth (MSE) Wall." *Proc., Sessions of Geo-Denver 2007, ASCE Geotechnical Special Publication No, 159.*

Berg, R. R., Christopher, B. R., and Samtani, N. C. (2009). *Design of Mechanically Stabilized Earth Walls and Reinforced Soil Slopes–Volume II.* (No. FHWA Gec 011-Vol Ii). Washington, D.C.: FHWA.

Bergado, D. T., Lo, K., Chai, J., Shivashankar, R., Alfaro, M. C., and Anderson, L. R. (1992). "Pullout Tests Using Steel Grid Reinforcements with Low-Quality Backfill." *Journal of Geotechnical Engineering, 118*(7), 1047–1062.

Bergado, D. T. and Teerawattanasuk, C. (2008). "2D And 3D Numerical Simulations of Reinforced Embankments On Soft Ground." *Geotextiles and Geomembranes, 26*(1), 39–55.

Briaud, J. (1992). *The Pressuremeter*. Rotterdam: Taylor & Francis/Balkema.

Briaud, J. (2013). *Geotechnical Engineering: Unsaturated and Saturated Soils*. Hoboken, New Jersey: John Wiley & Sons.

Chen, D., Nazarian, S., and Bilyeu, J. (2007). "Failure Analysis of a Bridge Embankment with Cracked Approach Slabs and Leaking Sand. *Journal of Performance of Constructed Facilities, 21*(5), 375–381.

Christopher, B. R., Gill, S. A., Giroud, J., Juran, I., Mitchell, J. K., Schlosser, F., and Dunnicliff, J. (1990). *Reinforced Soil Structures Volume I. Design and Construction Guidelines.* (No. FHWA-Rd-89-043). Washington, D.C.: FHWA.

Elias, V., Barry, P., and Christopher, R. (1997). *Mechanically Stabilized Earth Walls and Reinforced Soil Slopes Design and Construction Guidelines: FHWA Demonstration Project 82, Reinforced Soil Structures WSEW and RSS.* Washington, D.C.: Us Department Of Transportation, Federal Highway Administration.

Gerber, T. M. and Cummins, C. R. (2009). *Modeling and Analysis to Quantify MSE Wall Behavior and Performance.* (No. UT-10.03). Salt Lake City, UT: Utah Department Of Transportation.

Hatami, K. and Bathurst, R. J. (2005). "Development and Verification of a Numerical Model for the Analysis of Geosynthetic-Reinforced Soil Segmental Walls under Working Stress Conditions." *Canadian Geotechnical Journal, 42*(4), 1066–1085.

Hossain, M., Kibria, G., Khan, M., Hossain, J., and Taufiq, T. (2011). "Effects of Backfill Soil on Excessive Movement of MSE Wall." *Journal of Performance of Constructed Facilities, 26*(6), 793–802.

Huang, B., Bathurst, R. J., and Hatami, K. (2009). "Numerical Study of Reinforced Soil Segmental Walls Using Three Different Constitutive Soil Models." *Journal of Geotechnical and Geoenvironmental Engineering, 135*(10), 1486–1498.

Huang, J., Han, J., Parsons, R. L., and Pierson, M. C. (2013). Refined Numerical Modeling of a Laterally-Loaded Drilled Shaft in an MSE Wall. *Geotextiles and Geomembranes, 37*, 61–73.

Huang, J., Parsons, R. L., Han, J., and Pierson, M. (2011). Numerical Analysis of a Laterally Loaded Shaft Constructed within an MSE Wall. *Geotextiles and Geomembranes, 29*(3), 233–241.

Itasca. (2006). *Fast Lagrangian Analysis of Continua In 3-Dimensions, Version 4.0, Manual.* Minnesota: Itasca.

Jayawickrama P., Surles J. G., Wood T. D., and Lawson W. D. (2013). *Pullout Resistance of Mechanically Stabilized Reinforcements in Backfills Typically Used in Texas: Volume 1*. Report 0-6493-1.Texas Tech University. Texas Department of Transportation. Lubbock, TX.

Jewell, R. A. (1980). *Some Effects of Reinforcement on the Mechanical Behaviour of Soils.* (Doctoral, University Of Cambridge).

Johnson, A. P. (2013). *Pullout Resistance Of Mechanically Stabilized Earth Reinforcements Embedded In Coarse Backfill And Measured In A Large Scale Test System.* Lubbock, TX: Texas Tech University.

Khodair, Y. A. and Hassiotis, S. (2005). "Analysis of Soil–Pile Interaction in Integral Abutment." *Computers and Geotechnics, 32*(3), 201–209.

Kibria, G., Hossain, M., and Khan, M. (2014). "Influence of Soil Reinforcement on Horizontal Displacement of MSE Wall." *Int. J. Geomech*., 14(1), 130–141.

Koerner, R. M. and Soong, T. (2001). "Geosynthetic Reinforced Segmental Retaining Walls." *Geotextiles and Geomembranes, 19*(6), 359–386.

Laefer, D. F., Fitzgerald, M., Maloney, E. M., Coyne, D., Lennon, D., and Morrish, S. W. (2009). "Lateral Image Degradation in Terrestrial Laser Scanning." *Structural Engineering International, 19*(2), 184–189.

Lawson, W. D., Jayawickrama, P. W., Wood, T. A., and Surles, J. G. (2013). "Pullout Resistance Factors for Inextensible MSE Reinforcements Embedded in Sandy Backfill." Paper Presented at the *Transportation Research Board 92nd Annual Meeting* (13-2684).

Leshchinsky, D., Vahedifard, F., and Leshchinsky, B. A. (2012). "Revisiting Bearing Capacity Analysis of MSE Walls." *Geotextiles and Geomembranes, 34*, 100–107.

Miyata, Y. and Bathurst, R. J. (2012). Measured and Predicted Loads in Steel Strip Reinforced< I> C−< I> Φ Soil Walls In Japan. *Soils and Foundations, 52*(1), 1–17.

Pierson, M. (2008). *Behavior of Laterally Loaded Shafts Constructed behind the Face of a Mechanically Stabilized Earth Block Wall*. Ann Arbor, MI: Proquest.

Pierson, M. C., Parsons, R. L., Han, J., and Brennan, J. J. (2010). "Laterally Loaded Shaft Group Capacities and Deflections behind an MSE Wall." *Journal of Geotechnical and Geoenvironmental Engineering, 137*(10), 882–889.

Pierson, M. C., Parsons, R. L., Han, J., Brown, D., and Thompson III, W. R. (2009). *Capacity of Laterally Loaded Shafts Constructed behind the Face of a Mechanically Stabilized Earth Block Wall.* (No. K-Tran: Ku-07-6). Topeka, KS: Kansas Department of Transportation.

Rollins K., Price J. S., Nelson K. R., (2013). *Lateral Resistance of Piles near Vertical MSE Abutment Walls.* Report No. UT-13.04 submitted by Brigham Young University to Utah Dpt. of Transportation, 433 pages.

Stuedlein, A. W., Bailey, M., Lindquist, D., Sankey, J., and Neely, W. J. (2010). "Design and Performance of a 46-M-High MSE Wall." *Journal of Geotechnical and Geoenvironmental Engineering, 136*(6), 786–796.

Suksiripattanapong, C., Chinkulkijniwat, A., Horpibulsuk, S., Rujikiatkamjorn, C., and Tanhsutthinon, T. (2012). "Numerical Analysis of Bearing Reinforcement Earth (BRE) Wall." *Geotextiles and Geomembranes, 32*, 28–37.

Tanchaisawat, T., Bergado, D., and Voottipruex, P. (2008). "Numerical Simulation and Sensitivity Analyses of Full-Scale Test Embankment with Reinforced Lightweight Geomaterials on Soft Bangkok Clay." *Geotextiles and Geomembranes, 26*(6), 498–511.

Yoo, C. and Kim, S. (2008). "Performance of a Two-Tier Geosynthetic Reinforced Segmental Retaining Wall under a Surcharge Load: Full-Scale Load Test and 3D Finite Element Analysis." *Geotextiles and Geomembranes, 26*(6), 460–472.

Zhou, W., Yin, J., and Hong, C. (2011). "Finite Element Modelling Of Pullout Testing on a Soil Nail in a Pullout Box under Different Overburden and Grouting Pressures." *Canadian Geotechnical Journal, 48*(4), 557–567.